Ministry of Higher Education and Scientific Research

Hassiba Benbouali University of Chlef

Faculty of Technology

Department of Mechanical Engineering

THESIS

Submitted in fulfillment of the requirements for the degree of:

DOCTORATE (LMD)

Field: Mechanical Engineering

Specialty: Mechanical Construction

By

Ghania HABBAR

Title:

PREDICTION OF THE MECHANICAL BEHAVIOR OF A SANDWICH TUBULAR STRUCTURE BASED ON NATURAL FIBERS UNDER QUASI-STATIC AND FATIGUE LOADING

Defended on: **23/05/ 2024**, in front of the committee members:

KHELIL ALI	Professor	UHB-Chlef	President
HOCINE Abdelkader	Professor	UHB-Chlef	Supervisor
RIBEIRO João	MCA	Institute Polytechnic of Bragança -IPB-	Co-Supervisor
DEHMOUS Hocine	MCA	Mouloud Mammeri University - Tizi Ouzou	Examiner
BELALIA Azzedine	MCA	UHB-Chlef	Examiner
MEDJDOUB Sidi Mohamed	MCA	University of Sidi Bel Abbes	Examiner
BEZAZI Abderrezak	Professor	University of Guelma	Invited

ACKNOWLEDGEMENT

Initially I would like to thank almighty ***Allah*** that gave me the opportunity to carry out this outstanding experience, where I grew professionally and personally. Always giving me the strength necessary and accompanying me along the way through the completion of this stage of my studies. I thank the Almighty for giving me the strength and patience to work through all these years so that today I can stand proudly with my head held high.

This thesis marks the end of an arduous but insightful journey in scientific research. It would have never been completed without the tireless assistance, guidance, motivation, and constant support from my supervisor, **Pr. HOCINE Abdelkader**. His wisdom, patience, stimulating suggestions, and encouragement gave me the energy to complete what at times seemed to be an unattainable goal. I would like to thank him for his invaluable advice and guidance throughout the course of this study. I will be forever indebted to him.

I would like to extend my appreciation to **Pr. JOAO Ribeiro** as my co-supervisor from the Institute Polytechnic of Bragança (IPB) Portugal for his valuable support, advice, and assistance.

I would also like to extend my sincere appreciation to the Chairman **Pr. KHELIL Ali**, and committee members: **Associate Pr. DEHMOUS Hocine, Associate Pr. BELALIA Azzedine**, and **Associate Pr. MEDJDOUB Sidi Mohamed** for giving me the honor and agreed to review this doctorate thesis. Thank you very much for the time and efforts that you devoted to reviewing, evaluating and commenting on my thesis. Furthermore, I would like to thank **Pr. BEZAZI Abderrezak** as an invited committee member in the defense ceremony.

Pr. KHELIL Ali the Head of the Controls, Tests, Measurements, and Mechanical Simulations research laboratory deserves my heartfelt gratitude for providing me with all of the resources that I need to successfully complete this research project.

My sincere thanks also go to the people in charge of doctoral formation (CFD), **Pr. ZIDANE Ibrahim** and all the members of CFD, for their efforts during the doctoral formation.

Gratitude is extended to **Pr. ZAHLOUL Hamou** for his invaluable contributions to my success in the doctoral examination to realize my dream. I am sincerely thankful for his support, and encouragement. He was one of the few people who believed in me.

I would also like to thank all the teachers and staff of the faculty of technology and department of mechanical engineering at Hassiba Benbouali University of Chlef for their patience, assistance, support, administrative collaboration, and everything they have done for me in order to complete this work.

To all the professors who imparted me lessons and constituted a fundamental part of my higher education and professional formation since my primary school till my higher education in UHBC.

I am grateful for the professional advice I have been fortunate to receive from so many people. In particular, I would like to thank: **Dr. MAIZIA Abdelhakim, Pr. BEZAZI Abderrezak,** and **Dr. BOULEDROUA Omar**. Your patience, kindness, and passion for research are a real inspiration. Our research collaboration and friendship are something I look forward to continuing.

My earnest thanks to **Pr. Zied Driss**, director of the Electromechanical Systems Laboratory (LASEM) of the National Engineering School of Sfax (ENIS) and all the team members.

I would like to express my deep gratitude to all my family members for their moral and personal support, and for their encouragement in every step of my life.

Finally, my huge thanks and appreciations to everyone who has helped, supported, and guided me through this period of my academic life.

Ghania

DEDICATION

This thesis is the culmination of my journey to a Ph.D., which was just like climbing a high peak step by step, accompanied by encouragement, hardship, trust, and frustration. When I found myself at the top, experiencing the feeling of fulfillment, I realized that, though only my name appears on the cover of this dissertation, a great many people, including my supervisors, my family members, well-wishers, my friends, colleagues, have contributed to accomplishing this huge task.

I acknowledge the people who mean a lot to me, my parents, **Ali** and **Zohra Zerguerras**, for showing faith in me and giving me the liberty to choose what I desired. I salute you all for the selfless love, care, pain, and sacrifice you made to shape my life. Although you hardly understood what I researched, you were willing to support any decision I made. I would never be able to pay back the love and affection showered upon me by my parents.

To the one whom God has crowned with awe and reverence, to the one whose name I carry with pride, my support in this life, and the source of security from which I draw my strength, to my dear who wanted this the most: **My Father**.

To the one whom God placed Paradise under her feet, whose heart embraced me before her hand, and made adversity easy for me with her prayers. To the compassionate heart and the bright candle who was for me on the nights, the secret of my strength and success: **My Mother**.

I express my thanks to:

My sisters: **Atika, Soria, Fadhila, Khadidja** and especially my little sister: **Khalida: *'My soul mate'*** Thank you for your support and patience. You have been the support that never tires. You treated me like a princess who was only devoted to studying.

My three dear brothers: **Mohamed, Hamid**, and **Fethi**, who believed in me and surrounded me with their care and love and to whom I wish a successful life.

My brothers in laws: **Bensaadia Youcef, Erasem Sid Ahmed** and **Tellab Mustapha.**

My sisters in laws: **Medah Aicha, Bensaadia Fatima** and **Maaouch Leila.**

My nieces: **Faiza** 'The first of the family and ***My little sister***', **Nada, Rahaf; Maram, Lydia, Farah** and **Bassma.**

My nephews: **Mahmoud, Anis, Seyf El Islam, Dhyae eddine, Nadhir, Maemoun, Zakaria, Abd elmalek, Abd elmoumen,** and **Tamim** for their support and valuable prayers.

My deepest gratitude goes to all them for their unflagging love and unconditional support throughout my life and my studies.

All the members of my big family and anyone bearing the name*:* ***HABBAR*** and ***Zerguerras.***

My friends: *Guendouz Elghoul Mohamed Amine, Bouchrit Zohir, Djahafi Slimane, Tekfa Oussama, Bouchakour Abdallah, Sahraoui Mohamed Amine, Bachir Ismail, Seddar.Y Abdelnour, Damou Ali, Belkacemi Mohamed Amin and Bouraada Fouâd. For girls: Bouchakour Bouchra, Gribi Fatma, Didouh Hadjer, Abdazzi Zohour, Dahmani Kaouther, and Belkacemi Nafissa.*

My colleagues: *Louza Abdelkader, Ghouaoula Abdelhamid, Hamida Halmi, Kara Achira Fouad. S, Fellague Chebra Abdelhak, Belguebli Amina and all the UHBC PhD students of mechanical engineering: 2019/2020 and 2020/2021.*

My Tunisian family: *all the members of Graja family, Anissa Toutache and her husband kamel.*

My Portuguese family: *Younes M. Della, Outman Lachgar, Ferial Khaldi, Racha Mansouri, Ariana Busellato and Wassim Lacheb.*

All the individuals I encountered during my academic years, whose presence enriched my experience with memorable and enjoyable moments.

Those who wished for our downfall, may God make them a bridge for us to cross for the best.

I dedicate this humble work to all the students and especially to those from Third World countries who, despite their often-difficult working conditions, try to cling to the progress of technology.

I dedicate this PhD thesis to all those who love to learn.

To me and all my personalities.

And finally, to you: ***Dearest Reader.***

GHANIA Kimou

*Dedicated to **my niece** memory:*

HABBAR Hiba Zahret El Batoul

I will never, ever get to touch, smell, and hug you again,

My little angel, but at least I know you will always be present in this thesis.

This thesis is dedicated to the loving memory of

***My Dearest Grandparents**:*

HABBAR Mohamed** and **BENABOURA Khedidja

ZERGUERRAS Mohamed** and **SEFFOUH Aouda

*Dedicated to the memory of my colleague: **DJAHBAR Ahmed**, who battled cancer.*

Wherever a beautiful soul has been, there is a trail of beautiful memories.

'Life is what happens to you while you're busy making other plans'

John Lennon

ABSTRACT

To provide a new solution for hydrogen transportation that is lightweight and less expensive, the current contribution concentrates on the mechanical behavior of eco-sandwich pipes constructed of biocomposite materials under static and cyclic loads, using three-dimensional elasticity theory.

To achieve the sizing of the tubular eco-sandwich pipelines, a multiscale characterization is performed, beginning with the micro- and macro-mechanical scales. The micromechanical approach is used to predict the mechanical properties of bio skins before analyzing the whole cylinder sandwich structure under different loadings. The second step focuses on understanding the behavior of a sandwich element in the tubular structure through a macro-mechanical model.

The analytical and 3D numerical models are developed through this contribution to investigate the mechanical behavior of sandwich pipe under static and cyclic internal pressure loading. The suggested models provide an exact solution for stresses, strains, and displacement of sandwich pipe, which is made of epoxy material for the core layer and reinforced materials with an alternate layer for the skin layers. The main aim of this work is to evaluate the potential applications of bio-fibers in order to replace glass synthetic fibers generally employed in sandwich pipes. In this subject, a failure analytical analysis was developed using the Tsai-Wu criterion for skins and Von-Mises for the core.

In order to increase the rigidity of a biocomposite sandwich and reduce the gap compared with a synthetic sandwich, the main results show that a gradual reinforcing of layer numbers was chosen, which permitted the best behavior. On the other hand, the ultimate pressure and safety factors obtained by increasing biocomposite layers are significant for composite transportation pressure pipelines and can play the same role at this stage of analysis.

Keywords:

Biocomposite; Natural fibers; Eco-sandwich; Pipelines; Hydrogen; Transport; Multiscale; Micro; Macro; Mechanical behavior, Internal pressure; Static; Cyclic, Failure.

ملخص

تم إنجاز هذه الأطروحة لغرض تطوير حل جديد لنقل الهيدروجين خفيف الوزن والأقل تكلفة، تركز هذه الدراسة على السلوك الميكانيكي لأنابيب الساندويش البيئية المصنوعة من مواد مركبة هجينة طبيعية تحت حمل ساكن ودوري، باستخدام نظرية المرونة ثلاثية الأبعاد.

لتحقيق تحجيم خطوط أنابيب الساندويتش البيئية، يتم إجراء توصيف متعدد المقاييس، بدءًا بالمقاييس الميكانيكية المجهرية (الميكرو ميكانيكية) والدقيقة . يتم استخدام النهج الميكرو ميكانيكي للتنبؤ بالخواص الميكانيكية للجلود الحيوية قبل تحليل هيكل شطيرة الأنبوب بالكامل تحت أحمال مختلفة، الخطوة الثانية تركز على فهم سلوك عنصر الساندويتش في البنية الأنبوبية من خلال نموذج ماكر وميكانيكي (دقيق).

تم تطوير النماذج التحليلية والعددية ثلاثية الأبعاد من خلال هذه الاطروحة لاستكشاف السلوك الميكانيكي لأنبوب الساندويتش تحت تأثير تحميل الضغط الداخلي الساكن والدوري . تقدم النماذج المقترحة حلاً دقيقًا للضغوطات والتشوهات والإزاحات لأنبوب الساندويتش، الذي يتكون من مواد الإيبوكسي للطبقة الجوهرية ومواد معززة بطبقة بديلة للطبقات الخارجية. الهدف الرئيسي من هذا العمل هو تقييم التطبيقات المحتملة للألياف الحيوية لاستبدال ألياف الزجاج الاصطناعية المستخدمة عادة في أنابيب الساندويتش. في هذا السياق، تم تطوير تحليل فشل تحليلي باستخدام معيار Tsai – Wu للطبقات الخارجية ومعيار Von-Mises للطبقة الجوهرية.

لزيادة صلابة الساندويتش الحيوي المركب وتقليل الفجوة مقارنة بالساندويتش الاصطناعي، تشير النتائج الرئيسية إلى أنه تم اختيار تدعيم تدريجي لعدد الطبقات، مما سمح بالسلوك الأفضل. من ناحية أخرى، فإن الضغط النهائي وعوامل السلامة التي تم الحصول عليها عن طريق زيادة طبقات الساندويتش الحيوي ذات أهمية بالغة لأنابيب المركبة لنقل الضغط ويمكن أن تلعب نفس الدور في هذه المرحلة من التحليل.

الكلمات المفتاحية:

مركب حيوي هجين؛ ألياف طبيعية؛ ساندويتش بيئي؛ خطوط الأنابيب؛ نقل؛ متعدد القياسات؛ مجهري؛ دقيق؛ سلوك ميكانيكي؛ ضغط داخلي؛ ساكن؛ دوري؛ فشل.

INDEX

INDEX OF FIGURES

INDEX OF TABLES

INDEX OF FLOWCHARTS

NOMENCLATURE

Latin lower-case letters

n_c	Number of core layers.
n_s	Number of skin layers.
R	Radial direction.
$r_{ext}^{(k)}$	Outer radius of the layer k [mm].
r_f	Radius of the cylindrical fiber.
r_i	Inner radius of skins [mm].
r_o	Outer radius of skins [mm].
T	Time [min].
v_{12}	Major Poisson's ratio.
v_F	Poisson's ratio of fiber.
v_M	Poisson's Ratio of matrix.
W	Number of composite layers.

Latin upper-case letters

C	Stiffness tensor.
C_{ijkl}	Stiffness constants.
$D^{(k)}, E^{(k)}$	The integration constants.
E_{11}	Longitudinal young's modulus [GPa].
E_M	Young's modulus of matrix [GPa].
E_F	Young's modulus of fiber [GPa].
E_{22}	Transverse young's modulus [GPa].
$F_{11}, F_{12}, F_{22}, F_{66}$ F_1, F_2	The standard Tsai-Wu parameters.
$G_{TT'}$	Transverse shear module.
G_{12}	Longitudinal shear modulus.
G_F	Shear modulus of fiber.
G_M	Shear modulus of matrix.
K_F	Lateral compression module of fiber.
K_M	Lateral compression module of matrix.
K_L	Lateral pressure module.

P_a	The amplitude pressure.
S_{ijkl}	Flexibility or compliance constants.
T_a	Temperature amplitudes.
T_i	The initial temperature at $t = 0$.
T_σ	Deformation basis change matrices.
T_ε	Constraint base change matrices.
U_r	Radial displacements [mm].
U_z	Axial displacements [mm].
U_θ	Circumferential displacements [mm].
U_r	Radial displacements [mm].
V_f	Volume fraction of the fiber.
Z	Axial direction.

Greek letters

γ_0 and ε_0	The integration constants.
ΔT	Temperature deviation [°C].
ε_r	Radial strain vector.
ε_z	Axial strain vector.
ε_θ	Circumferential strain vector.
ε'	Deformation vector in the coordinate system.
ε_{kl}	Strain tensor.
Θ	Circumferential direction.
σ_{ij}	Stress tensor.
σ_{xu}	The tensile strengths of the composite material [MPa].
σ_{yu}	The compressive strengths of the composite material [MPa].
σ_{yxu}	In the layer plane shear strength [MPa].
σ'	Stress vector in the coordinate system [MPa].
σ'_{xu}	In the direction of the fibers [MPa].
σ'_{yu}	In the transverse direction [MPa].
σ_L	Longitudinal stress in fiber plan [MPa].
σ_T	Transverse stress in fiber plan [MPa].
τ_{LT}	Shear stress in fiber plan [MPa].

τ_{zr}	Shear strain vector in the plan z − r [MPa].
$\tau_{z\theta}$	Shear strain vector in the plan z − Θ [MPa].
$\tau_{\theta r}$	Shear strain vector in the plan Θ − r [MPa].
$\emptyset$	The winding angle (°).

List of Acronyms and Abbreviations

AL	Aluminum.
BV	Bauhinia Vahlii.
CFRC	Carbon Fiber Reinforced Composite.
CLT	Classical Lamination Theory.
CLPT	Classical Laminated Plate Theory.
CSC	Compressive Strain Capacity.
CSM	Chopped Strand Mat.
DMA	Dynamic Mechanical Analysis.
DOF	Degrees Of Freedom.
DSC	Differential Scanning Calorimetry.
EP	External Pressure.
ESEM	Environmental Scanning Electron Microscopy.
FF	Functional Failure.
FE	Finite Element.
FEA	Finite Element Analysis.
FEM	Finite Element Method.
FRP	Fiber-Reinforced Plastic.
FTIR	Fourier-Transformed Infrared spectroscopy.
FW	Filament Winding.
GRP	Glass Reinforced Plastics.
HDPE	High-Density Polyethylene.
IP	Internal Pressure.
IROM	Inverted ROM.
IVI	Intermediate-Velocity Impact.
L	Layer.
LNFC	Long Natural Fiber Composites.
MLF-WC	Multi Layered Filament Winding Composite.

OHC	Over-expanded Honeycomb Cylinder.
P	Pipe.
PALF	Pineapple Leaf Fiber.
PE	Polystyrene.
PU	Polyurethane.
R	Round.
ROM	Rule Of Mixture.
RVE	Representative Volume Element.
S	Flexibility tensor.
Sq	Square.
Seq	Sequence.
SLPT	Sandwich Laminated Plate Theory.
TCP	Thermoplastic Composite Pipe.
TGA	Thermo Gravimetric Analysis.
TSC	Tensile Strain Capacity.
UHMWPE	Ultra-High-Molecular-Weight Polyethylene.
UD	Unidirectional.
V	Vessel.
XPS	X-ray Photoelectron Spectroscopy.
XRD	X-Ray Diffraction.
3D	Three Dimensions.

GENERAL INTRODUCTION

GENERAL INTRODUCTION

The drawbacks of synthetic composites predominantly revolve around their adverse environmental impact, reliance on non-renewable resources, and the challenges associated with their difficulty in degradation once they are discarded. These composites, which are often derived from synthetic polymers such as plastic, contribute significantly to plastic pollution and ecosystem degradation. These issues underscore the pressing need for more sustainable alternatives in material choices, such as the adoption of biocomposites, which offer a more sustainable and environmentally friendly alternative. Biocomposites are materials made of biological polymers (biopolymers) and natural reinforcements such as cellulose fiber, flax fiber, hemp fiber, or other organic materials. These materials are characterized by their renewability, their degradability, their low environmental impact, and their technical performance.

However, it is important to note that the transition from synthetic composites to bio-composites can present challenges, such as the limited availability of specific raw materials, initial production costs, and performance apprehensions in particular applications. Nevertheless, with continued advances in research and technology, bio-composites are increasingly seen as a promising solution to the environmental challenges associated with synthetic composites.

It is in this context that the present thesis proposes to replace the synthetic fibers used in the design of sandwich tube skins with natural long fibers. It is important to note that sandwich tubes can play an important role in the transport of hydrogen if they are properly designed and manufactured. Sandwich tubes are structures composed of two external skins and an internal core, which is generally lighter. These structures are often used in industry to provide an optimal combination of strength, rigidity, and lightness. When it comes to hydrogen transportation, sandwich tubes can be an attractive option for the safe and efficient storage and transportation of hydrogen gas. They allow design flexibility, meaning they can be tailored to the specific needs of hydrogen transport based on weight, volume, and safety requirements. This recourse will also depend on the hydrogen storage technology chosen, as there are different approaches, such as gaseous, liquid, or solid storage.

It's important to note that the area of hydrogen storage and transportation is an active research topic, and new technologies and innovations continue to emerge to address the challenges associated with hydrogen as an energy vector.

In order to reach this goal, the main focus of this thesis is to study how eco-sandwich structures behave mechanically under both static and dynamic hydrogen transport test pressures. The multiscale nature of composites requires micro, macro, and structural analysis.

This work proposes a dimensioning of eco-sandwich tubular structures with a comparison of results with tubes based on synthetic fibers. The developed model is carried out analytically in MATLAB and numerically in ANSYS. The developed model takes into account two loading modes, static and dynamic cyclic, in order to simulate the fatigue phenomenon.

Before reaching this, an estimation of the material properties of the biocomposites is carried out, followed by the mechanical behavior of a sample of the tubular structure, called the macro-mechanical scale, using the theory of laminates.

The first chapter centers on a comprehensive review of the integration of natural fibers in the design of sandwich and multilayered composite pipes and vessels, where several studies have been exploring alternative options of synthetic materials, such as environmentally friendly materials, in the design of highly reliable systems of gas transportation and storage structures. Therefore, it is necessary to understand the behavior of cylindrical sandwich pipes made of natural fibers compared to synthetic fibers under various quasi-static and dynamic loads, such as internal fluid pressure, changing temperatures, and occasional loads. This state of the art focuses on the influence of several factors, including material type, winding angle, stacking sequence, core thickness, and skin thickness, on the behavior of biosandwich pipes under static and dynamic loading. It also covers experimental methods used to study the response of multilayer and sandwich pipes. This is followed by attention to their analytical and numerical formulations under different loads. Furthermore, the main challenge in this area is to enhance the use of natural fibers in pipe and vessel construction to promote more sustainable and environmentally friendly practices.

The interest of the second chapter is to present the mathematical and numerical formulation of multiscale modeling approaches for composite structures, namely micro, macro, and structure. Models have been developed based on advanced analytical and numerical formulations to determine the stress and strain fields through the thickness of laminated elements and tubular sandwich structures.

The third chapter of this contribution aims to predict the mechanical properties of skin layers made of PALF (Pineapple Leaf Fiber), date palm, and Alfa fibers, which are considered

Algeria's most plentiful plant resources, at different volume fractions. To this end, micromechanical analytical and FEM models were developed using the MATLAB 8.3 and ANSYS 18.1 software programs. The effect of reinforcement volume fraction on Young's, shear modulus, and Poisson's ratios is investigated. Four theories: (Hashin vs. Rosen, Halpin-Tsai, Chamis, and ROM) form the basis of the analytical models. In order to identify an appropriate theory between them that is in satisfactory agreement with the experimental data collected by Rakesh [1], a comparison has been conducted for the composite made from PALF fibers. The appropriate theory is combined with the FEM model to predict the mechanical properties of skin layers made of PALF, date palm, and Alfa fibers, where the combined findings are inefficient. The FEM used four RVEs, corresponding to the volume fraction of natural fibers.

The fourth chapter of our contribution focuses on the development of an analytical model for the analysis of the behavior of a sandwich element with natural skins. The stacking sequence of the item in question is $[+\emptyset/-\emptyset/$ core $/+\emptyset/-\emptyset]$. The stratified laminated plate theory (SLPT) is the basis of the analytical model.

The last and fifth chapter uses the three-dimensional anisotropic elasticity model to investigate the stress and strain of sandwich pipes subjected to static and cyclic internal pressure. It is assumed that the pressure loading is independent of the axial coordinate and symmetrical about the cylinder's axis. The core layer of sandwich pipes is made of an isotropic material with linearly elastic behavior, while each layer of the skins —internal or external— is made of a homogeneous, anisotropic material. The anisotropic skin and isotropic core of the sandwich are both addressed to an analytical failure using Tsai-Wu and Von-Mises, respectively. The principal goal of this chapter is to analyze the probable applications of bio-fibers to substitute glass synthetic fibers that are usually employed in sandwich pipes under static and cyclic loadings.

This work is concluded with a general conclusion that includes the main results and comments from the work carried out, as well as points that were not covered by this contribution and which may be the subject of future work.

CHAPTER I:

LITERATURE REVIEW

CHAPTER I: LITERATURE REVIEW

I.1- INTRODUCTION

Even though metallic materials have been the subject of in-depth research for many years, which has given scientists a great deal of confidence in their behavior, corrosion remains a formidable obstacle. New materials and unconventional technologies have been developed as a result of the current technological advancement, the metallic material crisis, and rising environmental aggression. Composites are gradually substituting metallic materials in lightweight structures, including aircraft, oxygen and hydrogen gas storage structures, vessel construction, and a variety of other engineering applications, due to the advantages they provide over metallic materials in terms of lightweight, low cost, recycling, sustainability capacity, rigidity, fatigue strength, and corrosion resistance [2]–[15].

Synthetic fibers are artificially produced fibers designed to fulfill specific purposes. Glass [16]–[22], steel [23]–[27], Kevlar (aramid) [16]–[18], [28], plastic, and carbon fibers [16]–[18], [29]–[32] are among them. The Synthetic fibers have numerous serious drawbacks, including: high density [16], [33], [34], Non-biodegradable nature [16], [32]–[37], they have high energy consumption [16], [33], [37], [38] , high cost of production [16], [33], [37], [39], [40], also non recyclability [16], [32], [34], [35], [37], [41], the fact that synthetic fibers burn more quickly [42], CO2 emission [16], [37], and can have a negative influence on human health and the environment.[16], [32], [33], [37], [41]. Understanding the serious drawbacks of synthetic fibers helps you recognize why engineers have been searching for an alternative.

In recent years, the needs for environmentally friendly materials and worries about the risks of synthetic fibers have inspired significant interest in the development of alternative materials to substitute synthetic fibers in future industry sectors.

Natural fiber-reinforced composites are already garnering the attention of researchers and designers for a wide range of industrial applications. The use of natural fibers rather than synthetic fibers minimizes the amount of carbon released into the environment [43], [44]. Natural fibers are gradually replacing synthetic fibers due to their: Bio-degradable nature [16], [35], [45]–[51], high abundance in nature [16], [47], [50], [52], Natural fibers are currently gaining popularity as a low-cost engineering material. [16], [46]–[52] and renewability [16], [35], [47], [49], [50], [52], they offer low density [16], [38], [44], [46], [49], [50], high energy consumption [16], [46], in addition to their lightweight [16], [46], [51], [52] and Recyclability

[16], [35], [44], furthermore, these natural fibers are environmentally friendly [44], [48], [49], [51], [53] , because of these characteristics, natural fibers have become an appealing alternative material that can replace the application of synthetic fibers in a variety of engineering applications, as shown in Table 1, where a comparison is made.

Table 1. Comparison of Glass fiber and Natural fiber.

Properties	***Glass fiber***	***Natural fiber***	***References***
Cost (US$/ton)	1200–1800	200–1000	[54]–[56]
Energy (GJ/ton)	30	4	
Density (g/cm3)	2.4	1.2–1.6	[57]
Renewability	Non renewable	Renewable	[19], [49], [58]–[60]
Recyclability	No	Yes	
Energy consumption	High	Low	
Disposal	Non-biodegradable	Biodegradable	
Health risk when inhaled	Yes	No	
CO2 emission	High	Low	

Fiber types, applications, and manufacturing costs all have an impact on fiber choices. Natural fibers are classified into two types: Animal fibers (such as silk [47], [57], [61]–[63], which is mostly used in biomedical applications, especially sutures [60], hair ,wool [47], [51], [64]–[66] and feather) and plant fibers such as: Pineapple Leaf Fiber (PALF) [1], [44], [56], [67], [68], Alfa [36], [69], palm [52], [70]–[72], hemp [73]–[77], kenaf [76], [78]–[82], jute [80], [83]–[85], bamboo [48], [53], [86] is known as natural glass fiber due to the fibers' longitudinal orientation also flax [76], [87], banana, cotton, sisal, agave, ramie, coconut, and many others.

Natural fibers are proposed in a variety of applications to substitute for or join synthetic fibers as hybrid materials. To accomplish this, some research focused on determining their mechanical properties under different loading tests.

Table 2 presents the most often treated natural fibers and their applications in various industries such as automotive, civil engineering, biomedical engineering, aerospace engineering, pipe and vessel manufacturing, agriculture, textiles, and cosmetics.

It has become essential to evaluate the performance of the composites before employing them since natural fiber-based composites are being applied in more and more domestic and industrial applications. It is possible to choose the most appropriate composite for a certain application by characterizing these composites. To characterize the mechanical, thermal, and

microstructural characteristics of the composite materials, a variety of tests, including tensile, flexural, impact, and durability tests, environmental scanning electron microscopy (ESEM), X-ray diffraction (XRD), X-ray photoelectron spectroscopy (XPS) , Fourier-transformed infrared spectroscopy (FTIR), dynamic mechanical analysis (DMA), differential scanning calorimetry (DSC), and thermos-gravimetric analysis (TGA), must be performed.

Sgriccia et al. used XPS, FTIR, and ESEM to characterize the surfaces of treated and untreated natural fibers (flax, kenaf, hemp, and henequen), to determine water absorption in natural fiber composites. The chemical treatments include alkali and Silane. Sodium hydroxide (NaOH) is one of the chemical agents used for this process [76]. Research by Mahjoub et al. aims to characterize and evaluate the physical and mechanical properties of the unidirectional kenaf fiber epoxy composite with various fiber volume fractions and compare them to the results of the analytical model, the rule of mixture (ROM) [88]. Djebloun et al. carried out an experimental study In order to compare the mechanical characteristics of the Lif date palm tree fibers from the south of Algeria, exactly in the Biskra region-which is considered to be an isotropic material-to other synthetic and plant fibers previously studied [52]. To evaluate the flexural, compressive, and tensile mechanical characteristics of jute/epoxy composites and compare their results to those of FEA simulations, Sangamesh et al. performed experimental research [89]. Boria et al. studied the reaction to low-velocity impacts on green sandwich panels containing unidirectional flax fiber-reinforced epoxy laminate skin faces and a high-density agglomerated cork panel core [90]. Among the fibers with the potential to replace synthetic fibers is bauhinia vahlii (BV) bast fiber. In India, Pakistan, and Nepal, BV fiber is gaining prominence as a renewable resource. Sahu et al. conducted a nearly identical experiment to that of Sgriccia et al. To characterize the structural and chemical changes of the treated and untreated BV fibers, they applied XRD, FTIR analysis, and ESEM [4].

The entire world is becoming increasingly interested in gas and oil, which are definitely the most important sources of energy on Earth. The heart of the world’s energy market is the oil and natural gas industries. Because the efficiency of gas and oil storage and transportation processes relies on compliance with the demands of related equipment and relevant technologies, there will undoubtedly be an increase in the demand for innovation, research, and development activities. The utilization of composite structures in transportation and storage systems such as flowlines, gathering pipes, vessels, storage cylinders, and distribution pipelines is expanding. According to the studies done by Verijenco [14] and Hwang [15], composite

materials present a strong alternative to metallic materials due to their great rigidity and resistance. As a result, fiber-reinforced composites are widely used in structural composition.

Fiber-reinforced composite materials are more adaptable than some types of metal materials, which make them preferable in applications like the transportation and storage of gas and oil. According to Wang [91], multilayer composites are suitable for both static and dynamic structures.

The use of multilayered composite materials and laminates with thin or thick walls has been favored in various works for cylindrical tubes used in transportation and storage due to their combination of lightweight and resistance [92]–[107].

The numerous synthetic fibers used in the design and fabrication of the composite transport and storage structures listed above include: carbon, glass, aramid and Kevlar fibers [2], [108], [109].

Natural fibers have their own value- added and are seen as a potential replacement for synthetic fibers [110]. Bio-composite materials derived from natural, renewable sources such as bio-fibers and bio-resin have received significant interest in recent years, mainly due to the increased awareness of environmentally sustainable technologies, the weight reduction they offer, the added functionality and the occupational health benefits [8].

Table 2. Mechanical properties of different natural fibers.

Fiber	*Density [g/cm^3]*	*Elongation at break [%]*	*Tensile Strength [MPa]*	*Moisture absorption*	*Young's modulus [GPa]*	*Applications*	*References*
Abaca	1.5	3-10	400 - 980	5 - 10	3 - 12	- Several industrial applications exist: automotive and packaging, shipping, building construction, aeronautics, international-grade furniture, and crafts.	[9], [16], [41], [42], [51], [62], [111]–[114]
Alfa	0.89 - 1.52	5.8	35 - 900	-	18 - 25	- Structural applications: sport, automotive industries, textile applications, and papermaking applications.	[16], [69], [114]–[118]
Bagasse	1.2 - 1.25	1 - 3	20 - 290	-	17 - 28	- Lightweight structures and textile applications.	[9], [16], [41], [51], [112], [114], [119]–[123]
Bamboo	0.6 - 1.41	1.1 - 5.8	140 - 1150	1.4 - 8.5	11 - 46	- Structural, furniture, and engineering applications like sliding panels, bearings, linkages, and bushings, the papermaking industry, civil engineering applications, aerospace engineering, automotive applications, the textile industry, the construction industry, and sound engineering applications.	[9], [16], [41], [42], [51], [62], [69], [86], [112], [114], [122]–[127]
Banana	0.71 - 1.35	1.5 - 53	54 - 914	7 - 12	7 - 33.8	- Automotive, textile, and civil engineering applications.	[9], [16], [42], [62], [111], [114], [128]–[130]
Coir (coconut)	1.15 - 1.5	15 - 51	95 - 593	8 - 49	3.3 - 17.3	- Building panels, projector covers, voltage regulator covers, vessels, flush door shutters, roofing sheets, safety helmets, post boxes, brushes, and brooms.	[9], [16], [41], [42], [49], [55], [111], [112], [114], [118], [124], [125], [130]–[132]
Cotton	1.5 - 1.6	3 - 10	250 - 800	7.85 - 8.5	3.7 - 13	- Textile industry, self-cleaning applications, semi-structural or non-structural applications, construction, and automobile fields.	[9], [16], [41], [42], [49], [51], [55], [62], [111], [112], [114], [118], [131], [132]

Flax	1.4 - 1.5	1 - 4	343 - 2000	1.2 - 12	27 - 100	-Window frames panels, decking, railing systems, fencing, tennis rackets, bicycle frames, forks, seat posts, snowboarding, laptops, and the textile industry.	[9], [16], [41], [42], [49], [51], [55], [62], [69], [111], [112], [114], [118], [124]–[126], [131]–[133]
Hemp	1.35 - 1.6	0.8 - 4	270 - 1110	2.3 - 12	23.5 - 90	- Construction materials, textiles, cordage, geotextiles, paper and packaging, electrical, manufacture of bank notes, manufacture of pipes, aerospace applications, food and beverages, automotive sector, furniture, luxury market, cosmetics, and personal care items.	[9], [16], [41], [42], [51], [55], [57], [69], [74], [111], [112], [114]–[116], [118], [124], [125], [131], [134]
Jute	1.23 - 1.6	1 - 9	114 - 860	11 - 13.7	8 - 78	- Civil engineering applications, building panels, roofing sheets, door frames, door shutters, transport, packaging, geotextiles, and chipboards.	[9], [16], [42], [49], [55], [57], [111], [112], [114]–[116], [118], [119], [121], [123]–[125], [130], [132], [135]
Kenaf	0.6 - 1.65	1.3 - 6.9	157 - 983	6.5 - 12	12 - 66	- Automotive industry, civil engineering, sports and leisure, furniture, consumer goods, pipes and tanks, packaging material, mobile cases, bags, insulations, clothing-grade cloth, soilless potting mixes, animal bedding, as well as material that absorb oil and liquids.	[16], [41], [42], [49], [51], [62], [82], [88], [111], [112], [114]–[116], [119], [121], [123], [125], [126]
Okra	1.15 - 1.45	2.5 - 8.6	68 - 380	4 - 6	5 - 16.55	- Lightweight insulating materials, transportation applications, building, and architectural sectors.	[9], [136], [137]
Palm	0.7 - 1.2	2 - 19	97 - 773	-	2.5 - 80	- Hot-dry construction and building, automotive applications, textile industry, traditional applications such as burlap sacks and ropes, construction and building, and wood substitutes.	[9], [16], [51], [138], [139]
PALF	0.8 - 1.6	0.8 - 14.5	126.6 - 1627	11.8 - 12	4.405 - 82.5	- Decoration, fabric, furniture, aerospace, sports, composite, and automobile industries, textiles, cosmetics, and medicine.	[16], [41], [44], [51], [57], [114]–[116], [119], [121], [125], [130], [131]

Ramie	1 - 1.55	1.2 - 4	220 - 1000	3.6 - 17	23 - 128	- Industrial sewing thread, fishing nets and filters, cloths, household furnishings, and clothing.	[9], [16], [41], [42], [51], [55], [57], [69], [111], [112], [114]–[116], [119], [121], [124], [126], [130], [131], [138]
Silk	1.3 - 1.37	18 - 34	100 - 1500	-	5 - 25	- Biomedical and industrial applications, textiles and apparel, clinical applications: from braided suture threads for surgical options to porous, reinforced-composite scaffolds for cartilage and bone repair, automobile, house building, and art craft applications.	[16], [55], [112], [115], [118], [140], [141]
Sisal	1.2 - 1.6	2 - 8	507 - 855	10 - 22	9 - 41	- Construction industry, such as panels, doors, shutting plates, and roofing sheets; also, manufacturing of paper and pulp.	[9], [16], [41], [42], [49], [51], [55], [57], [69], [111], [112], [114]–[116], [119], [121], [125], [126], [130], [131], [138]
Wool	1.3 - 1.32	0.9 - 35	120 - 3000	-	2.3 - 17	- Cosmetics, pharmacotherapy, medical area, textile engineering, building insulation, agriculture sector.	[9], [55], [112], [115], [118], [142], [143]

I.2- RESEARCH IDENTIFICATION OF COMPOSITE PIPE CONFIGURATIONS BASED ON NATURAL FIBERS

This part concentrates on demonstrating the two pipeline configurations used in the design, which are multilayered and sandwich. The first composite pipelines were based on synthetic fibers, which improved the strength of the structure under different loadings. For several years, there has been considerable interest in the substitution of synthetic fibers for natural fibers, notably in the construction of pipelines. In this context, different investigations are analyzed in Table 3.

They are based on composite materials (natural or hybrid), manufacturing processes, stacking sequences, winding angles, the specimen's geometry (circular or square tube), and mechanical testing.

I.2.1- Multilayered configuration pipe

The pipeline manufacture employed various processes, including filament winding, laminates, extrusion, and hand layup using synthetic fibers, natural fibers, or hybrid composites with different geometrical parameters.

I.2.1.1- Filament wound process

The filament winding technique includes dragging continuous fibers into a container of resin mixture or bath and wrapping the continuous resin-impregnated fibers over a rotating mandrel to obtain the required form. This process provides persistent quality in geometrical accuracy, high fiber volume fractions, and load stresses compared to other fabrication processes.

The use of bio-composites in tube manufacturing using filament winding technology is a significant challenge for engineering designers. The cylindrical composite structure production process with filament winding technology offers constant quality in geometrical correctness, considerable fiber volume fractions, and load stresses as compared to alternative fabrication methods. In order to increase collapsing behavior and other enhancements that have an impact on energy absorption effectiveness, the filament winding process structures may be tailored or modified.

Mahdi et al. used the filament winding technique to produce circular, cylindrical, and conical shells from oil palm frond fiber, glass, and carbon with epoxy composites. They explored how material and geometry affected the crushing behavior of composites [144]. In order to study the

mechanical properties of composite tubes reinforced with flax fiber yarn, Lehtiniemi et al. used the filament winding method to produce the composite tubes. The results were compared to those of composite tubes made of polymer reinforced with glass fiber [145]. The tensile, flexural (three-point bending), and impact strength properties of filament-wrapped tubes made of basalt, kenaf, and hybrid kenaf/basalt composites with a blend of ultra-high-molecular-weight polyethylene (UHMWPE) and high-density polyethylene (HDPE) matrix were studied by Mokhtar et al [59]. Alkbir et al. experimentally investigated the influence of geometry on energy absorption capability and load-carrying capacity of natural fiber kenaf hexagonal tubes with various angles [146]. Misri et al. conducted research on the filament winding technique used for manufacturing kenaf green composites in 2015 [147]. Supian et al. conducted an experimental study of Kenaf/glass fiber-reinforced epoxy hybrid composite tubes manufactured with three winding orientation parameters (±30, ±45, and ±70). The filament winding technique is used to make hybrid composite tubes out of distinct continuous kenaf and glass fibers combined into a single fiber band intra-ply [148].

I.2.1.2- Hybrid materials “tube” (bio + synthetic)

For structural applications, natural reinforcing fibers are mostly investigated in combination with stiffer fibers (carbon, glass, and basalt). The use of natural fiber hybridization as a replacement for existing bulky synthetic materials has attracted attention in a variety of engineering applications where the aim is to protect the environment and minimize reliance on synthetic materials. First, the hybridization approach employs the filament winding technique, allowing for the merging of several continuous fibers composite bands into a single hybrid fiber composite band in a tubular construction. In sandwich constructions, created by De Rosa et al., a mixture of synthetic and natural fibers is used for the skins and the core [149]. Many researchers have studied the mechanical behavior of hybrid composites as well as the effect of hybridization on their mechanical properties. Albahash and Ansari [7] as well Ricciardi et al. [150], as investigated the hybridization of natural/synthetic fiber-reinforced epoxy composites, with the discovery of natural/synthetic hybrid composites tubes having potential crashworthiness performance equivalent to a synthetic tube in order to protect the environment and reduce dependency on synthetic materials.

Table 3. Research identification of composite tubes based on natural fibers.

Year	*Researchers*	*Research objective*	*Bio material/hybrid*	*Process of fabrication*	*Design and experiments parameters*
2002	Mahdi et al. [144]	The impact of structure geometry and reinforcement type on crushing behavior and energy absorption.	Carbon/epoxy, glass/epoxy and oil palm frond fiber/epoxy	Filament wound, laminated, and hand layup.	-Specimen's geometry: Cylindrical and conical composite shells. -Material: Natural and synthetic composite.
2009	De Rosa et al. [149]	Inter-laminar shear strength tests and four-point flexural tests of laminates impacted with different energies.	Glass/jute hybrid	Laminates	-Hybrid material: 14 glass fiber layers + 4 jute fiber layers.
2013	Mokhtar et al [59]	Investigate the performance of UHMWPE/HDPE-reinforced kenaf, basalt and hybrid kenaf/basalt composites.	UHMWPE/HDPE-reinforced kenaf, basalt and hybrid kenaf/basalt composites	Extrusion	-Mechanical testing: tensile, flexural (three-point bending) and an impact test (Charpy). -Material: Natural and hybrid composite.
2014	Alkbir et al.[146]	The crashworthiness effect of geometry on energy absorption capability and load-carrying capacity.	Natural kenaf fiber reinforced composite hexagonal tubes	Hand layup	-Mechanical testing: Quasi-static axial compressive load. -Material: Natural composite -Winding angle: 40–60 º.
2017	Albahash And Ansari [7]	The potential of natural fiber investigations in the application of crash energy absorption.	Three types of fiber (Jute, hybrid Glass and Jute fiber, hybrid Kevlar and Jute fiber).	Hand layup	-Specimen's geometry: Circular and square tube. -Winding angle: 0/90º. -Material: Natural, synthetic and hybrid composite
2020	Supian et al. [148]	Crash worthiness of energy absorption tube for vehicles.	Kenaf fiber yarn -glass fiber/Epoxy	Filament winding	-winding orientations: ±30°, ±45°, ±70°. -Material: Natural and hybrid composite.
2021	Kari et al.[83]	The influence of the winding angle on the properties of the tubes.	Jute/Epoxy tubes	Filament winding	-Stacking layers. -Winding angles :50 °, 55 °, 60 °, 65 °, 75 °, and 90. -Mechanical testing: Circumferential tensile and stiffness tests.

I.2.1.3- Experimental characterization of tubes

According to an intermediate-velocity impact (IVI) load, Supian et al. investigated the hybrid composite tube's capability to absorb energy. The tube Kenaf/glass fiber specimens were evaluated using pneumatic impact load equipment to determine the dynamic impact response [148]. Misri et al. tested, reported, and proved the composites' good tensile characteristics in split-disk and torsion tests [147].

I.2.2- Sandwich configuration pipe

Over conventional materials, sandwich composites have a low overall density, a high strength-to-weight ratio, and a high stiffness-to-weight ratio, can provide excellent thermal and acoustical insulation, and ultimately have uniform energy absorption capacity. According to the literature, some of the research presented below concentrated on analyzing the materials of sandwich pipeline manufacturing based on metallic materials known as traditional pipe-in-pipe, multilayered, and honeycomb materials.

Pipe-in-pipe and sandwich pipes transporting oil and gas are subjected to the internal pressure of the content and to the loading of environments with high external water pressure in deep-water or sub-sea applications. [151].

I.2.2.1- Sandwich metallic

Sandwich pipe in pipe are used in the offshore oil and gas industry, according to the literature. They are long, circular, cylindrical structures composed of two concentric steel pipes with an annular core layer.

For various degrees of adhesion between the core layer and the exterior pipe, Castello and Estefen studied the ultimate strength of sandwich pipe in pipe under coupled external pressure and bending [152], [153].

In order to capture the real response of sandwich pipe in pipe under external pressure capacity, Arjomandi et al [154]. Created a numerical model based on the finite element (FE) approach.

I.2.2.2- Sandwich composite

In 2023, a nonlinear finite element model was created to investigate the dent rebounding behavior of submarine sandwich pipes under the impact of a low-velocity falling object by Xianming Liu et al. The pipe specimen consisted of two concentric steel tubes as skins and the

cement-based composite filled as a core. This model investigated the differences in dent characteristics between sandwich pipes' inner and outer tubes exposed to lateral loads. The dent depth and strain of the outer tube and the inner tube were investigated in relation to the effects of material qualities, geometrical factors, and interlayer interaction [155].

Existing research focuses mostly on isotropic pipes but rarely on anisotropic pipes such as filament-wound or honeycomb sandwiches.

The sandwich pipe is considered one of the most promising underwater pipelines for deep-water oil and gas transmission because of its high strength and thermal insulation [151].

I.2.2.3- Honeycomb sandwich

Honeycombs and polymer foams are common core materials for composite sandwich panels, both of which offer low density and reasonable shear properties, while the face sheets are stiffer and offer high strength.

Honeycomb sandwich structures are one of the earliest architected cores.

Sandwich structures are used for dynamic loading events. The typical applications reported in the literature are for low-velocity impact (perforation), shock wave, and crashworthiness applications. For sandwich structure face sheets, typical materials used are either metals (stainless steel/aluminum) or fiber composites.

Sandwiched cylindrical shells with honeycomb cores have great potential for pipeline applications. Existing research mostly focuses on isotropic pipes, with little attention paid to composite pipes, particularly honeycomb sandwich pipes.

A novel carbon fiber reinforced composite CFRC over-expanded honeycomb cylinder OHC were revealed by Compression behaviors and free vibration experiments by Zhu and Fan [156].

Wang et al. created a new approach for analyzing the dynamic response of a honeycomb sandwich pipe to moving pressure. This contribution is founded on love shell theory and equivalent single-layer theory [157].

I.2.2.4- Multilayered sandwich

The design of fiber-reinforced cylindrical composite structures is currently gaining interest. Because filament-wound pipes constructed of fiber-reinforced polymers have various potential

benefits over pipes made of conventional materials, they have already attracted a lot of interest in the fields of mechanical industry and civil infrastructure. Several research investigations have been conducted to characterize the failure processes of filament-wound pipes. Multilayered sandwich pipes constructed from lightweight multiply Fiber-Reinforced Plastic (FRP) skins entirely bonded to a polymeric core are an exceptionally appealing concept due to their excellent strength- and stiffness-to-weight ratios, as well as their corrosion resistance. By changing the fiber volume, reinforcement angle, and other factors in the manufacturing of FRP skins using automated filament winding, the designer has access to unparalleled tailor-ability. The behavior and analysis of composite pipes made up of several filament-wound layers are more complicated than their conventional homogeneous counterparts.

The literature reveals that thick-walled sandwich tubes comprised of FW skins and an isotropic core are less treated than thin-walled multilayer composite cylindrical structures. As a result, there is a greater concentration on understanding and optimizing the efficiency of sandwich tubes for practical industrial applications.([97], [158]–[162]).

I.3- INVESTIGATIONS RESEARCH ON DIMENSIONING COMPOSITE PIPE

The current state of the art consists of identifying a wide range of research topics dealing with the dimensioning of multilayer composite tubular structures or laminates for the transport of oil and gas products. These works have been categorized in this contribution based on factors related to pipeline and vessel dimensioning. Throughout the literature, there is a litany of parameters that must be considered while designing a composite tubular structure in order to ensure its reliability and improve its lifespan. The research carried out focuses first on a better understanding of the behavior of composite structures under varied loads using a so-called deterministic approach, and then on the impact of variations in a set of variables on structural reliability. Table 4 highlights a range of investigations and categorizes them into seven categories. This categorization allows for the presentation and discussion of the literature studied. The principal category of this classification provides two model output approaches: deterministic and reliable.

I.3.1- Deterministic model output based on conception

According to the literature, the deterministic models used in the design provide two types of outputs: stress and strain. The failure of a pipeline is defined by the equivalent stress exceeding

the elastic limit for isotropic materials and the expression of a stress threshold for anisotropic materials using stress-based design or stress capacity. The strain concept, also known as strain capacity, is defined as the maximum strain that a pipeline with a certain set of characteristics can withstand before failing. The type of failure varies depending on which strain capacity is being calculated: tensile strain capacity (TSC) or compressive strain capacity (CSC).

I.3.2- Reliability model output based on conception

Due to the uncertainties of material parameters, geometrical characteristics, and loads, a reliability approach is a key tool in the design and maintenance decision-making process. As a result, various research studies evaluated pipeline failure probability for composite tubular structures in order to understand the influence of uncertainties on their design and, as a result, obtain more analytical data compared with deterministic computations.

Table 4. Classification of state of art related to pipeline and vessel design.

Literature	Pipelines/Vessels configuration		Analysis type		Model parameter		Methodology			Analytical approach		Law behavior	Output model
	Multilayered	*Sandwich*	*Deterministic*	*Reliability*	*Loading*	*Structure parameters*	*Analytical*	*FEM*	*Experimental*	*Elasticity*	*CLT*		
Rosenow [163]	P	-	X	-	Biaxial, hoop pressure and tensile loading.	Winding angle Layer sequence	X	-	X	-	X	Non-linear	-Stress and strain capacity -Failure analysis
Varga et al. [164]	V	-	X	-	Cyclic IP	Thickness and winding angle	X	-	X	X	-	Linear	-Strain capacity -Failure analysis
Wild and Vickers [165]	P	-	X	-	IP, EP and Axial force.	Winding angle	X	-	-	-	X	Linear	-Stress and strain capacity -Failure analysis
Xia et al. [166]	-	P	X	-	IP	Winding angle	X	-	-	-	X	Linear	-Stress and strain capacity
Xia et al.[97]	P	-	X	-	IP	Winding angle Stacking sequence	X	-	-	X	-	Linear	-Stress and strain capacity
Xia et al.[158]	-	P	X	-	IP and thermomechanical loading	Winding angle	X	-	-	-	X	Linear	-Stress and strain capacity
Xia et al.[159]	-	P	X	-	Pure bending	Winding angle	X	-	-	-	X	Linear	-Stress and strain capacity -Deflection
Parnas and Katrici [167]	V	-	X	-	Combined mechanical and hygrothermal loading.	Wall thickness and winding angle	X		X	-	X	Linear	-Failure analysis -angular velocity
Chapelle and Perreux [168]	V	-	X	-	IP	Winding angle Stacking sequence	X	-	X	X	-	Non-linear	-Failure analysis

Kobayashi et al. [169]	P	-	X	-	IP	Materials properties Stacking sequences	X	X	X	X	-	Linear	-Stress and strain capacity
Zheng and Liu [170]	V	-	X	-	IP and thermal residual stress.	Winding angle Number of the composite layers	X	X	X	-	X	Non-linear	-Failure analysis.
Hocine et al. [12]	V	-	X	-	IP and thermomechanical loading	Winding angle and layer sequence	X	-	-	X	-	Linear	-Stress and strain capacity
Arjomandi and Taheri [154]	-	P	X	-	IP and/or EP	Skins and core thickness	-	X	-	X	-	Non-linear	-Stress and strain capacity
Ghouaoula et al.[171]	V	-	X	-	IP	Winding angle and Stacking sequence	X	-	X	X	-	Non-linear	-Failure analysis.
Chapelle et al. [172]	V	-	X	-	IP	Stacking sequence	-	X	-	X	-	Non-linear	-Stress and strain capacity
Guz et al. [95]	P	-	X	-	EP	Stacking sequence	X	-	-	X	-	Linear	-Stress capacity
Misri et al. [173]	P	-	X	-	Compression	Winding angle	-	-	X	X	-	Non-linear	-strain capacity
Hocine et al. [174]	P	-	-	X	IP	Winding angle	X	-	-	X	-	Linear	-Stress and strain capacity -Failure Probability
Sulu & Temiz [175]	P	-	X	-	IP	Stacking sequence	-	X	X	X	-	Non-linear	-stress capacity -Failure analysis.
Maizia et al. [11]	P	-	-	X	Hygro-thermo-mechanical loading	Thickness and winding angle	X	X	-	X	-	Linear	-Failure probability
Ghouaoula et al. [176]	P/V	-	X	-	-IP; Tension and IP with end effect	-	X	-	-	X	X	Non-linear	-Stress and strain capacity
Hocine et al. [177]	P	-	-	X	IP	Ply thickness and Winding angle	X	X	-	X	-	Non-linear	-Failure analysis. -Failure Probability

Maizia et al. [178]	V	-	-	X	IP	Winding angle and layer thickness	-	X	-	X	-	Failure behavior	-Failure probability
Wang and Han [179]	-	P	-	X	IP and external hydrostatic pressure	-	-	X	X	X	-	Non-linear	-Failure analysis
Ghouaoula et al. [180]	V	-	-	X	IP	Thickness and winding angle	X	-	-	X	-	Linear	-Failure probability
Wang et al. [98]	P	-	X	-	Torsional load	Layer thickness	X	X	-	X	-	Linear	-Stress and strain capacity
Hocine et al. [181]	V	-	-	X	Creep and IP	Winding angle	X	-	-	X	-	Non-linear	-Service life
Zubail et al. [182]	P	-	-	X	Thermomechanical loading with corrosion effect	Thickness and winding angle	-	X	-	X	-	Linear	-Life cycle assessment
Hastie et al. [162]	-	P and V	X	-	IP and thermal load	Thickness and winding angle	-	X	-	X	-	Linear	-Stress and strain capacity -Failure analysis.
Kari et al. [83]	P	-	X	-	Circumferential traction Compression	Winding angle	-	-	X	X	-	Linear	-The influence of mechanical properties
Nghiep et al.[183]	V	-	X	-	Thermomechanical loading	Stacking sequence	-	X	-	X	-	Non-linear	-Failure analysis
Patel et al.[184]	V	-	X	-	IP	Shape of the meridian. vessel	X	X	-	X	-	Linear	-Stress at the junction
Jasion and Magnucki [185]	-	V	X	-	IP	Shape of head vessels	-	X	-	X	-	Linear	-Stress distribution in head vessels
Luo et al. [186]	V	-	X	-	Ultrasonic impact treatment	impacting velocity	-	X	X	-	-	Non-linear	-Residual stress

-: Not defined, **X**: defined, **P**: Pipe, **V**: Vessel, **IP**: Internal Pressure, **EP**: External Pressure.

I.4- MODELS BEHAVIOR OF CYLINDRICAL COMPOSITE STRUCTURE

Several studies have been carried out analytically, statistically, and experimentally in order to characterize and analyze the behavior of composite structures under varied mechanical, thermal, or combined loads [187].

A major focus on developing tool behavior models has been investigated to develop composite cylindrical structures. Nowadays, an impressive amount of research is concentrated on the stress and failure analysis of multilayered and sandwich cylindrical structures.

The state-of-the-art demonstrates that two theoretical approaches have been used to analyze the behavior of composite structures, namely the classical theory of laminates and the so-called theory of elasticity. The first one produces no stress in the direction of thickness. The second illustrates that the stress created through radial thickness has a considerable impact on the selection of stacking sequences of multilayered or skin layers of a sandwich.

I.4.1- Multilayered structures (pipes and vessels)

Multilayered cylindrical structures as shown in Figure 1 are playing a growing and necessary role in structures because of their extraordinarily great flexural stiffness-to-weight ratio in comparison to monolithic structures and other systems. Rauf and Gürgen obtained that multilayer structures offer high energy-absorbing characteristics without compromising flexibility, in contrast to monolithic systems [188].

Based on three-dimensional (3D) anisotropic elasticity, Xia et al. established an analytical tool for investigating the mechanical behavior of multilayered pipes under internal pressure. The current analytical model provides a precise elastic solution to stresses and deformations [97].

Parnas and Katrici formulated an analytical approach that utilized classical lamination theory to design and predict the behavior of multilayered composite vessels under pressure through the formulation of the elasticity issue [167].

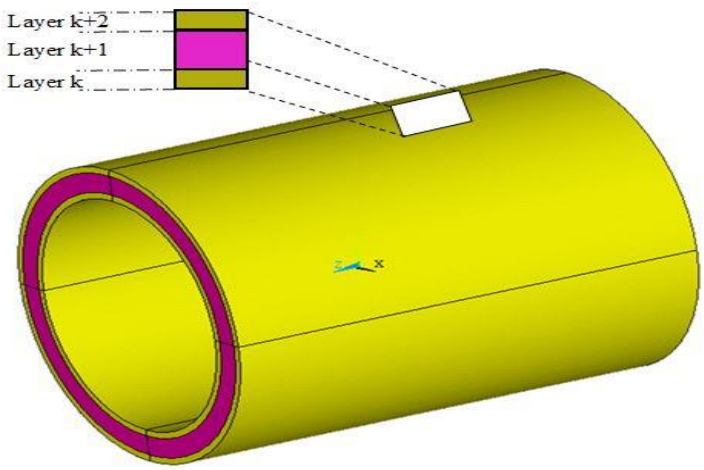

Figure 1. Multilayered cylindrical structure under internal pressure.

Chapelle and Perreux [168], as well as Hocine et al. [189], developed an analytical technique. In order to estimate the behavior of a type 3 vessels cylindrical section for hydrogen storage applications. Figure 2 illustrates that the suggested analytical model gives a precise solution for stresses and strains on the cylindrical structure subjected to mechanical static loading in different cases, such as traction loading, pure internal pressure (pipe), and internal pressure with end effects (vessel).

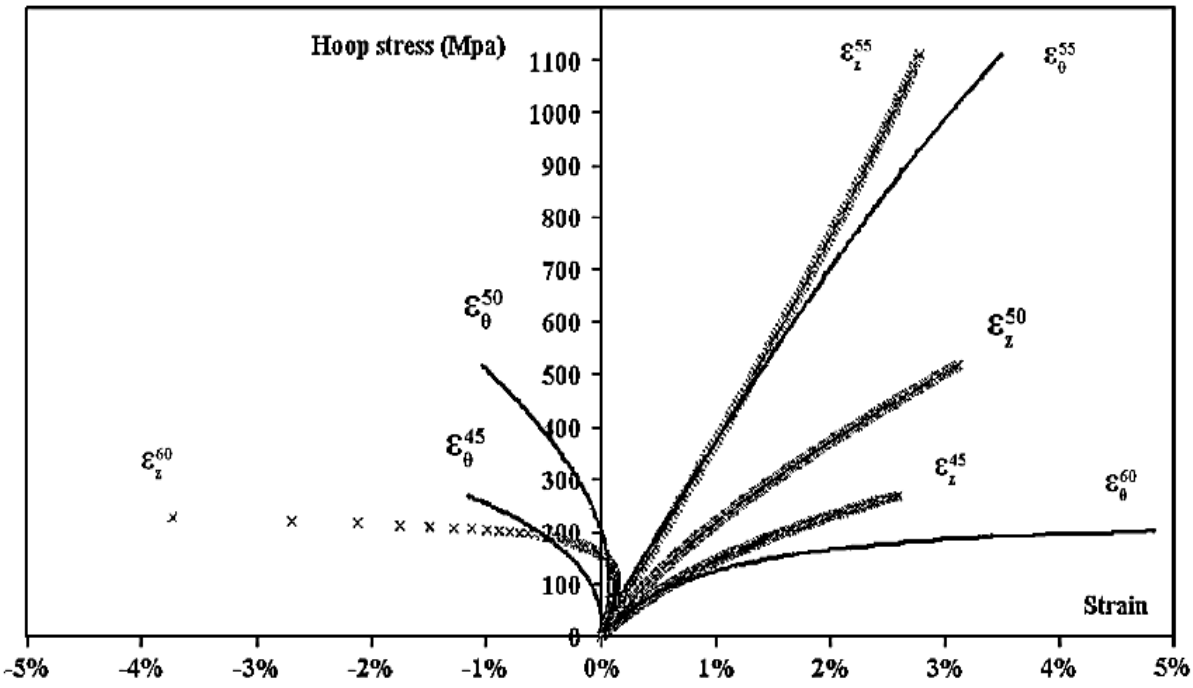

Figure 2. Based on the modeling, simulated hoop and axial stresses versus hoop stress for a G/E composite with 6 layers. The winding angles considered are : 45°,50°,55°,60° [168].

A research conducted by Zheng and Liu on the elasto-plastic stress analysis and damage progression of type III vessels under internal pressure and thermal residual stress included elastic stress analysis of composite laminates [170].

The stress analysis of multilayered composite cylinders exposed to bending loads to determine how the material properties, thickness, and winding angle of the composite layers affect the stress variation of the composite cylinders was studied by Menshykova and Guz [94].

Wang et al. created a three-dimensional elasticity solution and Finite Element Method model for predicting the failure of multilayered, thick-walled, fiber-reinforced composite pipes under torsional load. For the purpose of computing the failure coefficients, anticipating the pipe failure, and formulating the design suggestions, the Tsai-Hill failure criterion was applied. [98].

In addition to developing an analytical method to determine stresses, strains, and displacements across the wall thickness of a multilayered composite cylinder composed of orthotropic material, Elgohary et al. also developed a numerical analysis to investigate a composite cylinder exposed to an internal pressure load with a tensile axial load [190]. The findings collected revealed the influence of the ratio of the anisotropy of the material E_1/E_2 on the stress variation with the winding angle. [190].

Using the finite difference approach, Ansari et al. created a numerical elastic analysis of multilayered filament-wound composite pipelines exposed to cyclic internal pressure and temperature loading. Some concerns, such as homogenous, anisotropic, and linearly elastic materials, are taken into account in this tool design, and it is assumed that the properties of the material do not vary with rising temperature [191].

I.4.1.1- Discussion of multilayered composite pipe

- ***Stacking sequence and thickness effects***

According to Xia et al., the stacking sequence and wall thickness play an important role in the design of thin multilayered pipes under internal pressure and affect their response. According to Figure 3, there are noticeable discontinuities in the hoop and axial stresses depending on the angle-ply [97].

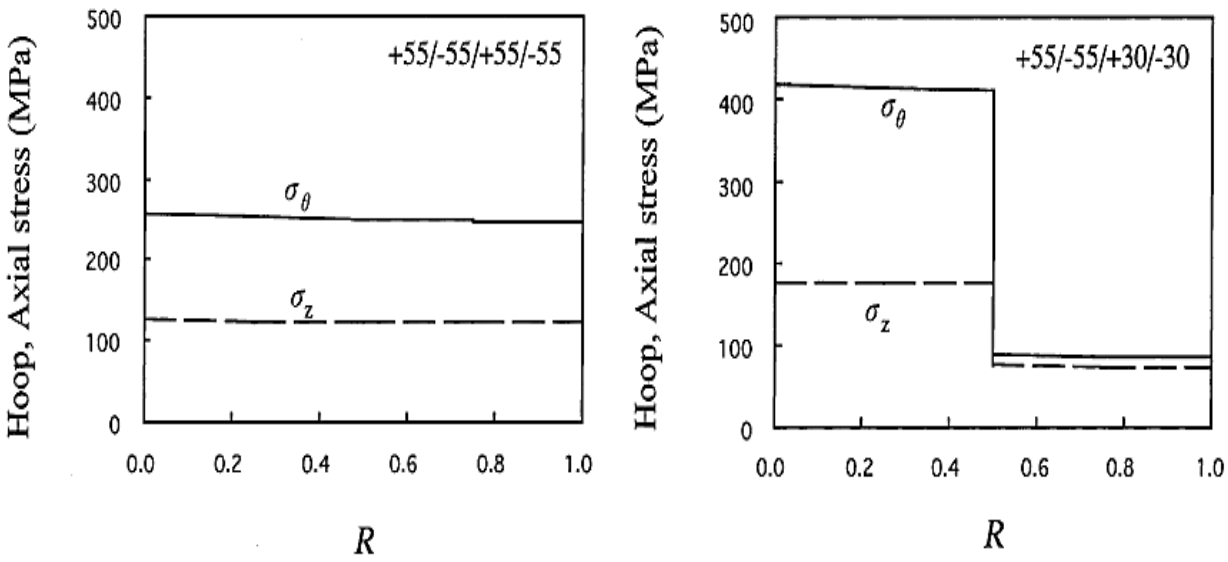

Figure 3. The variation of hoop and axial stresses across the non-dimensional radial distance [97].

- ***Thin and thick wall approach effects***

The two methods produce identical results in terms of the optimal winding angle and burst pressure for the cylindrical pressure vessel for outer to inner radius ratios up to 1.1. The thick wall analysis is required as the ratio increases. The selection of thin or thick approaches, where the deviation is substantial, influences the optimization of the filament wrap angle. When the wall thickness increases, a difference in burst pressure of the order of 30% is observed. This finding calls into question the thin-wall analysis but remains reliable for an interval of thickness.[167].

The analysis of a thick composite pipe demonstrates how stresses vary depending on the material of the inner layer and its thickness when exposed to a bending load. [94].

- ***Winding angle effect***

Regarding hydrogen composite vessel type III, responses such as displacement, stress, and strain rely on the rising of the winding angle, where the radial displacement and shear-stress decrease while the radial stress increases. The hoop and axial stresses decline in the liner and increase in the winding layers of the composite parts [170].

Ansari et al. demonstrated that for multilayered composite pipe subjected to cyclic loading, hoop and axial stresses depend on fiber orientation, extremely near the circumferential (90°) and longitudinal (0°) windings [191]. It has been shown that there is an inverse relationship

between the axial stress and the absolute magnitude of the ply angle. It can be demonstrated that when fiber orientation moves to circumferential, the quantity of axial stress reduces (Figure 4).

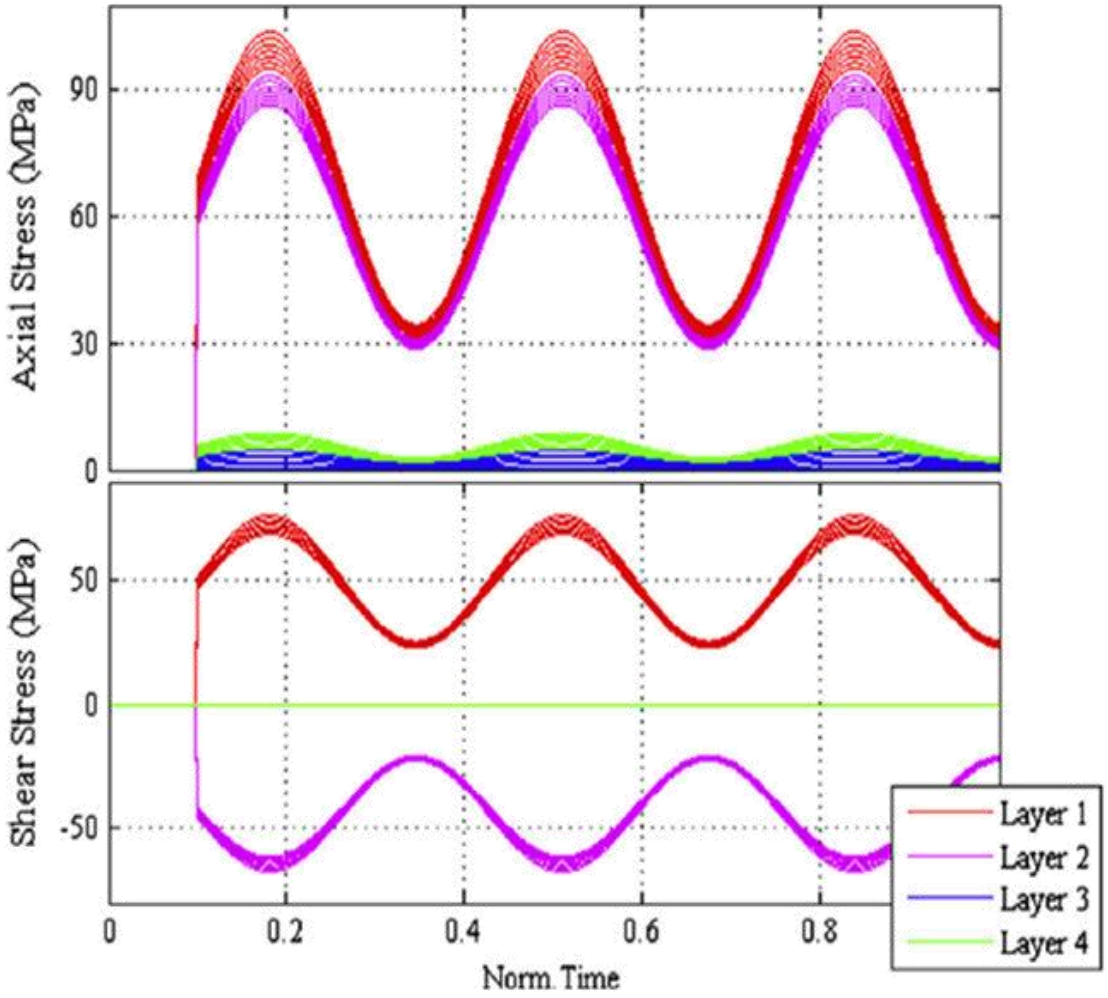

Figure 4. The distribution of axial and shear stresses under pure cyclic internal pressure [191].

The winding angle optimization provided the safest choice for the multilayered composite cylinders subjected to various loadings, when a range of 50°–55° is appreciated. Using different failure theories, the winding angle can vary relatively or significantly depending on the material properties and different loading conditions [190], as shown in Table 5.

Table 5. Optimal winding angles based on failure criterion [190].

Optimum winding angle	***Carbon / Epoxy E_1/E_2=14.27***	***Graphite / Epoxy E_1/E_2=12.81***	***E-Glass / Epoxy E_1/E_2=3.94***
Netting Theory	54.74 °		
Tsai Wu Tsai Hill	51.3 °	52.8 °	54.6 °
Netting Theory	53.3 °	54.4 °	55.3 °

I.4.2- Sandwich pipes

Sandwich pipes are versatile and provide the industry with new high-performance materials and they are typically lightweight, have an excellent stiffness-to-weight ratio, and are easy to manufacture [192]. Figure 5 presents the components of sandwich pipe used in gas and oil transport.

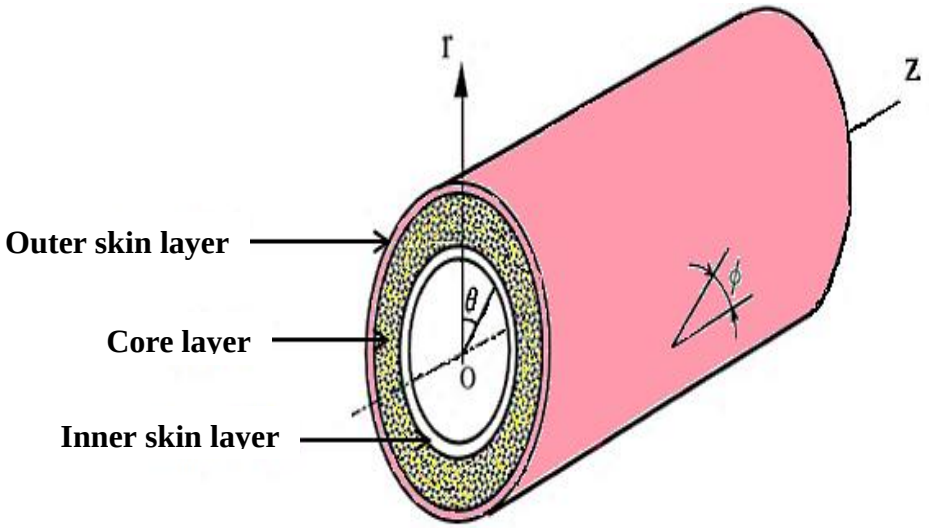

Figure 5. Components of sandwich cylindrical pipe.

In order to investigate stresses and strains via thickness under various loading conditions such as internal pressure, thermal loading [158] and pure bending [159], Xia et al. created a computer model for thick-walled filament winding sandwich pipes using the conventional laminated plate theory. Previously, Xia et al. subjected the sandwich pipe to a combination of a 100 K temperature rise and an internal pressure of 10 MPa, with the skin layers (inner and outer layers) made of the same material. They contrasted carbon fiber/epoxy (T300/934) with E-glass/epoxy [158].

The main purpose of Rafiee and Reshadi's research was to investigate the influence of core thickness, winding angles, and boundary conditions on the functional failure pressures of GRP mortar pipes with skins made of FW layers. To determine the functional failure pressures of those pipes when they are subjected to internal hydrostatic pressure, a progressive damage modeling approach was developed [160].

Due to the hot compressed fluid that moves into pipes, a thermo mechanical examination has been conducted by Bakaiyan and Ameri. They provide an elastic solution for two lamination schemes [±55°/Core/±55°] and [±60°/Core/±60°] based on three-dimensional anisotropic

elasticity. Using the quadratic Tsai-Hill criteria, they studied the optimum winding angles with the lowest failure coefficient [161].

Hastie et al. [193], [194] investigated a Thermoplastic Composite Pipe (TCP) for a deep water riser application consisting of a fiber-reinforced thermoplastic laminate entirely bonded between inner and outer thermoplastic liners, which are known as sandwich pipe in pipe. They studied the influence of different pressure and heat gradient combinations on stress and strain outcomes [193], local TCP failure response, and various laminate ply stacking sequences for the TCP, applying the Maximum Stress and Tsai-Hill failure criteria [194]. In 2020, Hastie et al. carried out a Hashin failure investigation of the TCP structure [195].

In the case of a long pipe, Hastie et al. created a 3D FE model able to evaluate the stress state in a section of FW sandwich pipe under internal pressure mixed with identical or gradient thermal loads for closed and axially restrained (open) ends. By selecting a stacking sequence layout $[-\emptyset/+\emptyset$ / core $/+\emptyset/-\emptyset]$. the performance of various configurations with thicker cores or an increased number of skin plies is also evaluated by estimating the layer failure coefficients of pipes through the components of the sandwich configuration (see Figure 6) [162].

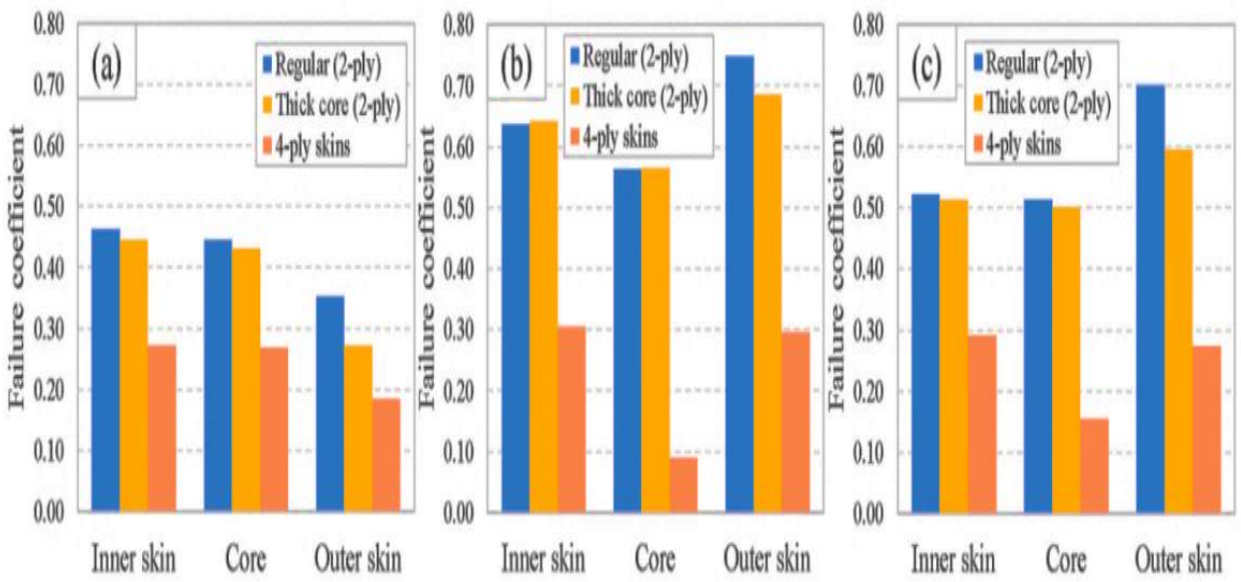

Figure 6. Layer failure coefficients for pipes with φ = 55◦ and closed ends: P0 = 30 MPa; ΔT = 0°C (a), ΔT = 100 °C (b), ΔT0 = 100 °C (c) [162].

I.4.2.1- Discussion:

The 3D modeling approach of the FW sandwich pipe developed in various research studies makes it possible to take into account several design parameters, such as:

- Filament winding angle of skins.
- Stacking sequence and number of skin layers.
- Core sandwich thickness.
- Materials used for multilayer skins and core.
- Material defects (delamination, damage, etc.).
- Multilayer and core skin behavior laws (elastic, viscoelastic, viscoelastic-plastic with damage).
- Thermomechanical loading effect.
- Load combinations: variable biaxial load ratios.
- Influences of geometric imperfections (ovalization, deviation of the axis of the cylinder from the line etc.)

➢ ***Materials properties***

According to Xia et al., the materials' anisotropic characteristics significantly influence how stress variation affects them [158].

➢ ***Core stiffness***

For sandwich composite pipe construction with low core stiffness, Xia et al. demonstrate that the impact of the core material on the pipe's strength is quite significant [158].

➢ ***Core thickness***

The pressures for First-Ply Failure (FPF) and Functional Failure (FF) enhance linearly with core thickness; however, the relative difference between FPF and FF pressures decreases [160].

➢ ***Skin thickness***

Hastie et al. examined the effects of altering the liner thickness, which performed the function of skins regarding the central laminate [193]. When the thermal gradient rises, Hastie et al. conclude that the variation in the thickness of the metallic coating produces a compromise between the safety factors of the metallic liner, obtained using the Von-Mises criterion, and that of the multilayer body part, achieved by the Tsai-Hill criterion. Here, the Tsai-Hill coefficient is unaffected by the heat gradient for equally thin layers; nevertheless, the von Mises fracture coefficient increases significantly in the inner coating.

According to Hastie et al., increasing the number of FW skin plies produces a trade-off between decreasing and raising the failure coefficient for skins and cores under hoop-dominated loads [162].

- ***Winding angle***

According to Xia et al., the effect of stress variations greatly depends on the winding angle [158].

The influence of winding angle on FPF and FF pressures for three common boundary conditions was examined. It is discovered that the interval of 50° - 60° for the winding angle is a key range for two sets of boundary conditions due to the decreasing of Functional Failure pressures versus the rising winding angle [160].

The performance of the closed-ended FW sandwich pipe is largely dependent on the angle of the fiber and is optimal at the traditional angle of 55° [162].

- ***Boundary conditions***

Three distinct boundary condition configurations for GRP pipes exposed to internal hydrostatic pressure experiments are investigated. Both ends of the pipe are free, with no bottom effect, indicating a hoop/axial stress ratio of (1:0). For the second boundary condition (b), the pipe ends are blocked with zero axial strain. Third boundary condition setup, the pipe ends are sealed but not constrained. In a parametric investigation, the impact of boundary conditions on functional failure pressures is explored, and it is also discovered that the particular boundary condition influences the optimal winding angle [160].

The failure coefficient for the core of an optimal high-angle design while operating under low pressure depends significantly on the temperature of the sandwich pipe with axially restrained ends under combined internal pressure and thermal load. [162].

- ***Loading***

Depending on load and end conditions, the greatest failure coefficient for the filament-wound sandwich pipe might appear in different layers of skin, which must be carefully examined during the design phase. [162].

The effects of various pressure and heat gradient loading combinations on failure distributions based on the Von-Mises criteria for isotropic liners and interactive Tsai-Hill for fiber-reinforced

laminate were investigated. Failure predictions for high-pressure transmission are not affected by the evolution of heat gradients during the lifespan of TCPs. This gives the designer a greater range of internal fluid temperatures [194].

Under high pressure, the skins are further stressed, as demonstrated by Hastie et al. The core and skins of the restrained FW sandwich pipe are less and more temperature-sensitive, respectively. [162].

I.4.3- Conclusion of discussions

It is mentioned that the failure analysis approaches for FW sandwich pipes presented in the state of the art have been globally modeled analytically. To carry out local failure analysis, the use of the finite element approach is needed in conjunction with the global modeling of the pipeline.

I.5- CHARACTERIZATION OF COMPOSITE PIPE BASED ON NATURAL FIBERS

The introduction of bio-composites in the fabrication of tubes using the filament winding method poses a genuine challenge for engineering designers. Research studies enumerate the use of long natural fiber composites (LNFC) in the manufacturing of composite tubes using the filament winding process [83].

To minimize mass, cost or maximize some aspect of the performance of the tube, no single material may be found or be able to support different loadings. So the combination of different materials is the goal of some recent research in order to make a combined composite structure in much structural geometry. To protect the environment and minimize dependency on synthetic materials, there has been a rise in the exploration and use of hybrid composite natural and synthetic fibers in the production of multiple shapes of tubes, such as square, circular, or hexagonal [83], [196].

Natural and synthetic fibers are combined using various processes. The initial manufacturing configuration involves stacking bio-composite layers with synthetic layers, which is known as a hybrid composite interlayer (See Figure 7).

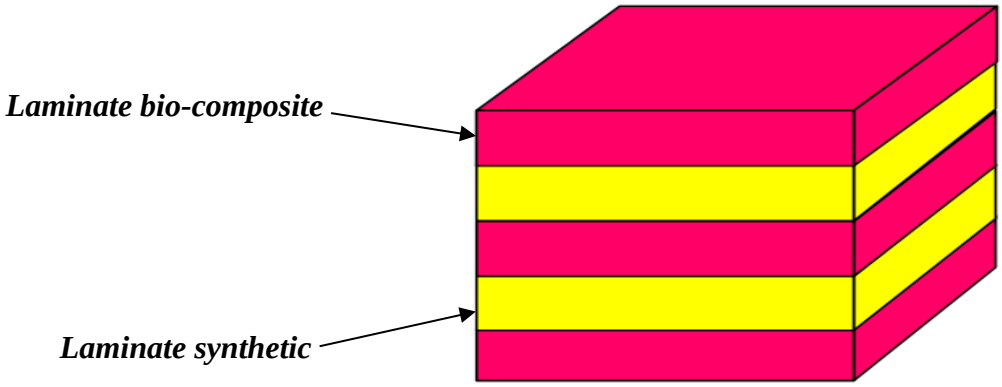

Figure 7. Stratified composite with bio and synthetic layers.

For the second technique, there are different configurations to obtain a hybrid sandwich form. The first one, the biocomposite layers, is considered the core, and the synthetic layers are skins. This is illustrated in Figure 8 [196].

Another form is presented in which the biocomposite and synthetic layers are joined as skins and the syntactic foam is used as a core. As shown in Figure 9 [197].

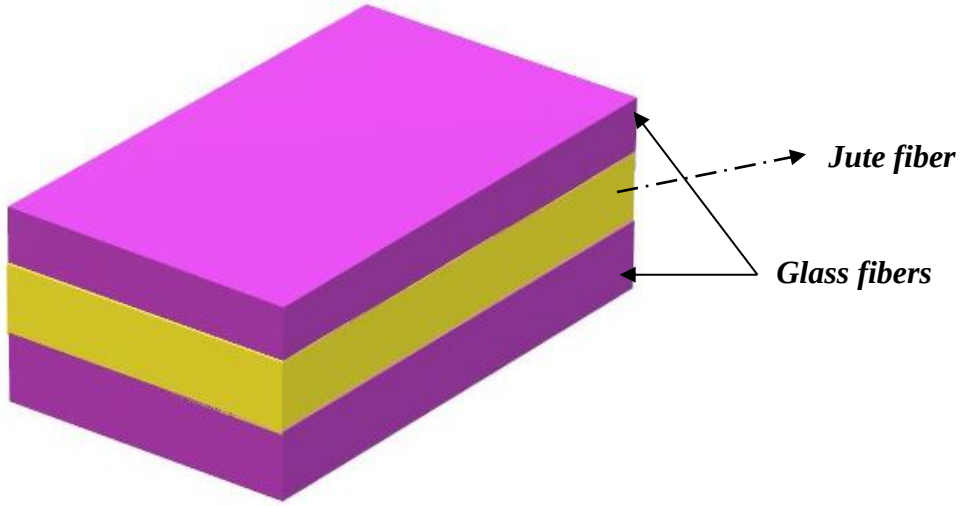

Figure 8. Sandwich panel with bio-core.

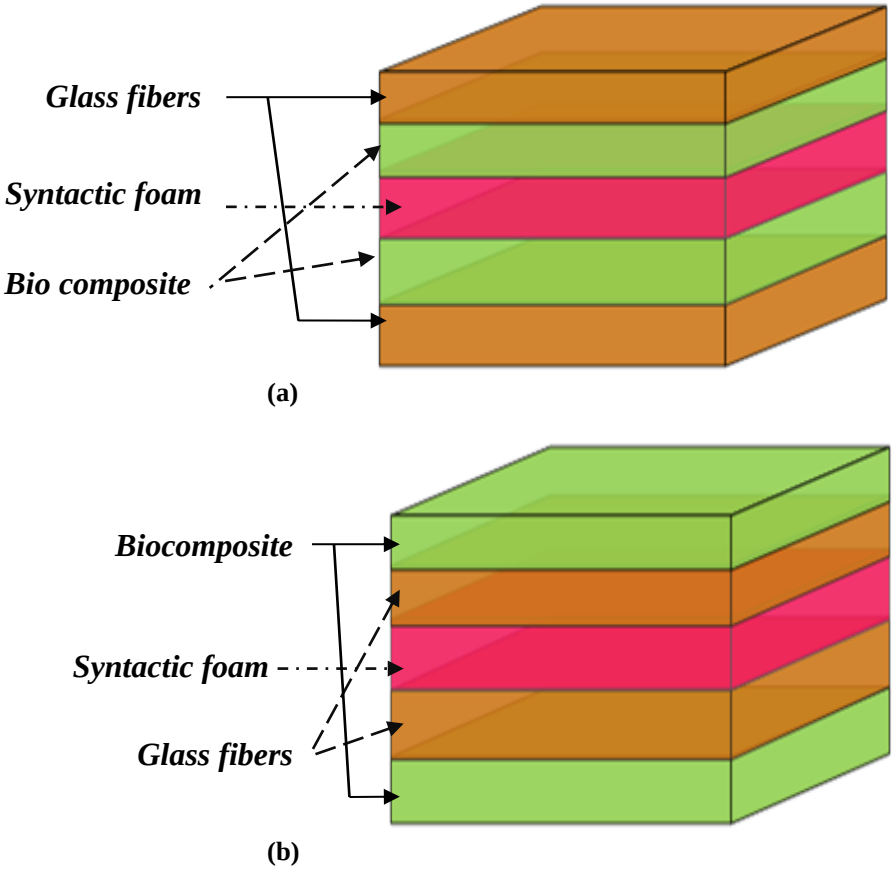

Figure 9. Sandwich panel with hybrid skin layers.

Another approach is hybridization, which involves combining multiple continuous fiber composites into a single hybrid fiber composite band in a tubular structure. (see Figure 10) [148]. In automotive applications, Othman and Ismail recommended this technique [198].

The current literature review indicates that researchers are interested in two types of experimental tests: quasi-static loading and crushing behavior.

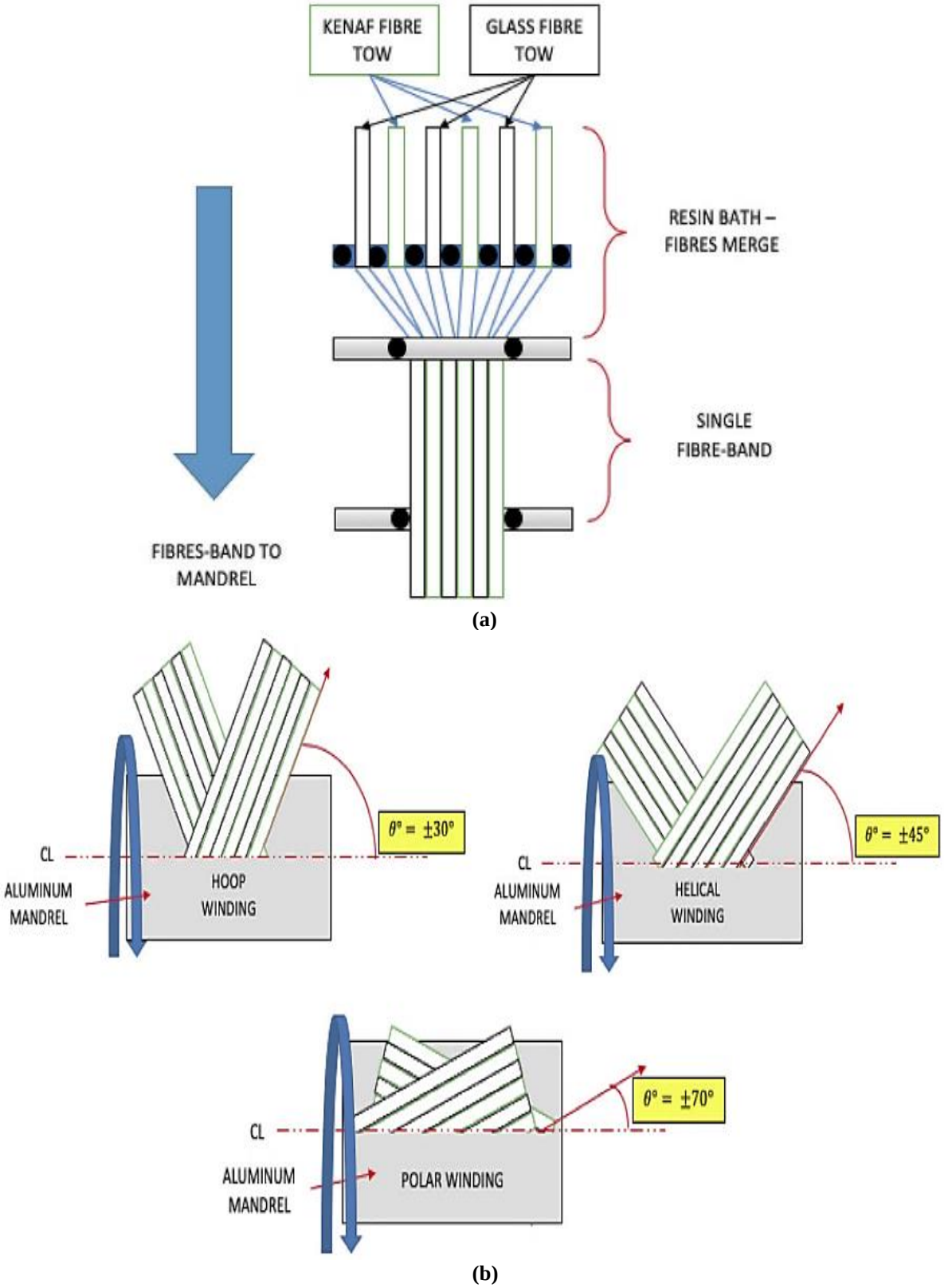

Figure 10. Filament winding phases for a hybrid kenaf/glass fiber-reinforced epoxy composite tube (a) Initial phase-Hybrid composites in a resin bath (Kenaf and glass fiber tows merged) wrapped over a mandrel. (b) Intermediate phase - Hybrid fiber band interplay process with winding passage on $\pm\theta$ fiber orientation [148].

I.5.1- Quasi-static loading

Under quasi-static axial loads, Othman and Ismail examined the behavior of jute and polyester wrapped on an aluminum alloy 6063T52 thin-walled tube fixed with four layers of jute of ±45° square and round tube profiles, where the aluminum alloy was selected as a core material. Six composite tube specimens were tested, including ALR-4L, ALR-4L-PU, ALR-4L-PE, ALS_q-4L, ALSq-4L-PU, and ALS_q-4L-PE. AL, R, S_q, L, PE, and PU are abbreviations for Aluminum, Round, Square, Layer, Polystyrene and Polyurethane. In terms of quasi-static loading, a comparison of square and round tube profiles revealed different initial load contacts. When it came to energy absorption, polystyrene foam outperformed polyurethane foam [198].

The study conducted by Kari et al. aims to examine the mechanical properties of jute-epoxy tubes with varied winding angles (90° /±α /90°) where α namely: 50°, 55°, 60°, 65°, 75°, and 90° are under stiffness and hoop tension as specified in ASTM D2412 and ASTM D2290 respectively [83]. The six configurations of eco-multilayered pipes tested show the same linear pattern of stiffness. This is illustrated in Figure 11.

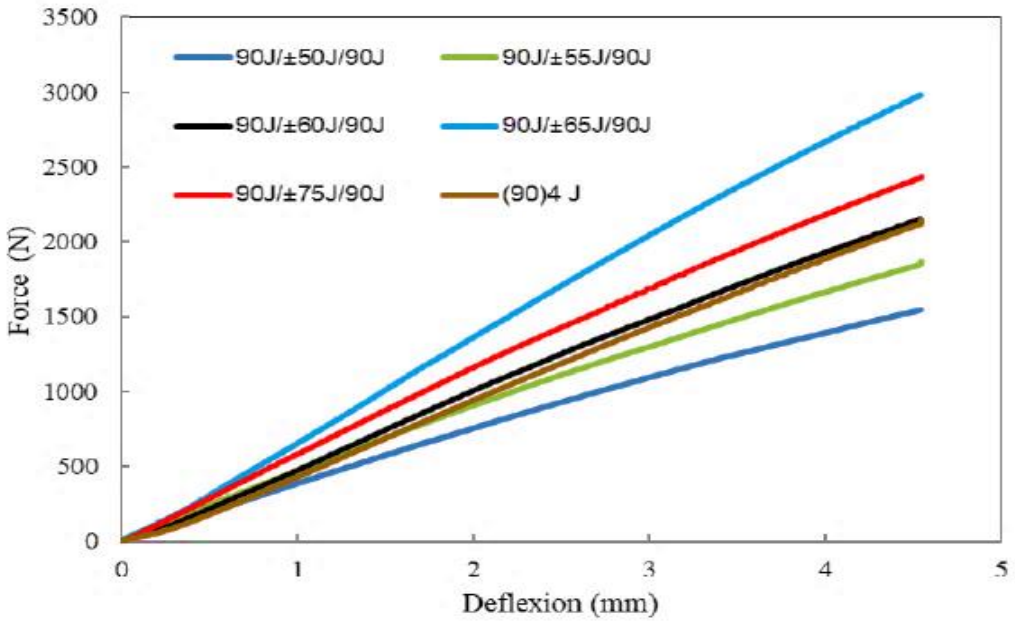

Figure 11. The load-deflection graph depicts the behavior of jute/epoxy tubes when subjected to parallel-plate loading [83].

I.5.2- Crushing behavior

Moyo and Velmurugan evaluated the axial crushing behavior of jute/glass hybrid [Glass/Jute/Glass] sandwiched tubes in quasi-static conditions with the aim of determining the possibility of their usage as energy absorbers during an impact. The jute yarn was being woven

at an angle of ± 45°. A filament winding machine was used to create four variants of hybrid tube configurations: 2CSM/4Jute/2CSM, 3CSM/6Jute/3CSM, 4CSM/6Jute/4CSM, and 4CSM/8Jute/4CSM [196].

Supian et al. evaluated the influence of winding orientations of ±30°, ±45° and ±70° on two specimens of kenaf/glass fiber-reinforced epoxy hybrid composite filament-wound tubes and glass-reinforced epoxy filament-wound tubes. The effects of intermediate-velocity impact (IVI) loads have been identified on the two specimens stated previously. The kenaf/glass hybrid composite tube specimens outperformed the synthetic glass composite tube in terms of crashworthiness. [148].

I.5.3- Cyclic loading

The literature review shows that the exact and analytical solutions for multilayered and sandwich pipes under mechanical and thermal loads are limited to static studies. Some contributions employed analytical and numerical methods to investigate the dynamic behaviors of multilayered composite pipes under time-deponent mechanical loadings.

Many studies have carried out quasi-static and dynamic analyses of thick or multilayered composite pipes exposed to thermal, thermomechanical [158], [191], [195], [199], [200], as well as hygrothermal loads [201]–[207] in the recent past.

When analyzing the dynamic behavior of multilayered filament wound composite pipes under cyclic thermal loading and cyclic internal pressure, Soleimani et al. precisely solve the problem while taking the influence of humidity into account [206]. The main thing they found was that the winding angle changed the amplitude of the axial and hoop stresses (Figure 12), especially when the stresses were close to the circumferential and axial directions.

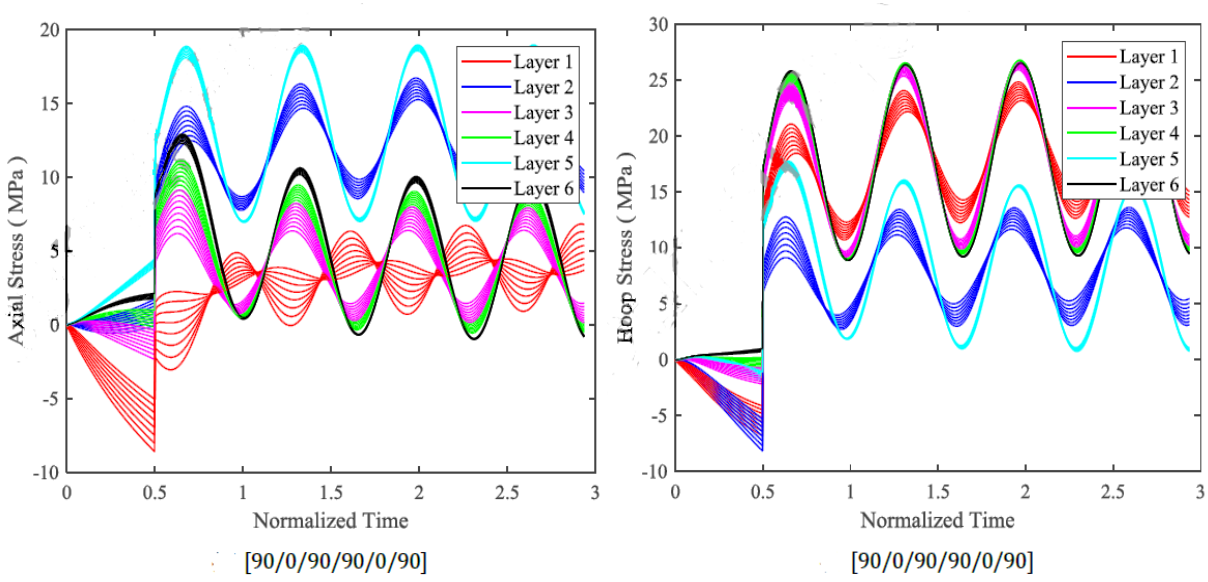

Figure 12. The time history of axial and hoop stresses across the pipe thickness, under cyclic internal pressure and temperature [206].

Moreover, there is no exact or analytical solution procedure for the dynamic analysis of sandwich pipes under the cyclic mechanical and thermal loading based on the three-dimensional elasticity theory.

I.5.4- Discussion:

I.5.4.1- Profile effect

In comparison, the square bio sandwich pipe profile performs better under quasi-static crush loadings than the circular tube. The findings revealed that the empty jute/polyester composite tube offers less improvement compared with the foam-filled tube [175] Ismail and Othman.

I.5.4.2- Winding angle effect

Kari et al. determined that the fiber orientation angle has a direct impact on the mechanical properties of composite tubes, with tubes at an angle of 65° having the highest specific stiffness and 90° having the greatest circumferential compressive The elastic modulus in circumferential compression, the circumferential tensile strength, the maximum value of the apparent circumferential tensile strength sigma tc, and the mechanical features of composite tubes formed by filament winding are highly impacted by the winding angle [83].

The potential of jute/glass hybrid composite tube to be employed as energy absorbers during an impact is influenced by the number of layers, the ratio of jute to glass layers, and finally the crush force efficiency [196].

The performance of crashworthiness loading of kenaf/glass hybrid composite tubes is related to the increase of winding fibers orientation parameters, under dynamic impact load conditions, the effect of the higher winding orientation parameter provides the maximum specific energy absorption of filament-wound kenaf/glass hybrid composite tube over glass composite tube [148].

I.5.4.3- Hybrid materials effect

The hybrid composite tube specimens (kenaf/glass) outperformed the single-fiber composite tube specimens made of synthetic glass in terms of crashworthiness. [148].

I.6- MULTILEVEL APPROACH

It is important to note that composites are known by their multiscale architecture, namely: microscopic (components: fiber and matrix), mesoscopic (composite layer or plie), macroscopic (stratified or stack of layers), and finally structural (structure tubular). Any development of a deterministic or reliable sizing model for multilayer or sandwich-type composites must take this particular configuration into account. A literature review is conducted in this section for the scales mentioned below.

I.6.1- Micromechanical approach

In order to accurately predict the material properties of the natural fiber composite materials, many analytical and FEA models using different micromechanics approaches have been formulated.

A large number of Finite Element Model (FEM) and analytical micromechanical models have been proposed in the literature for predicting various mechanical properties of composite materials [29–32] For the FEM model, the representative volume elements RVE of bio-composites were established in different software such as ANSYS, ABAQUS, and DIGIMAT [30–32] to determine the micromechanical properties and failure mechanism of bio-composites. Currently, many researchers are attempting to anticipate the natural fiber polymer composite's mechanical performance using various mathematical and numerical methods. The rule of mixtures (ROM), inverted ROM (IROM), Halpin–Tsai model, The Kelly–Tyson model, The Cox model [211] and Mori-Tanaka model [8], [212]–[214] are the most widely used and well-known theories for defining mechanical characteristics. In addition, several additional models, such as Hashin and Rosen, the bridging model, Double-Inclusion model [215], Christensen

equation, and Chamis model, have been used to determine the mechanical properties of composite materials.

The estimation of the mechanical properties is a great challenge for the researchers, where some analytical and FEA results are developed and compared to experimental results for different biocomposite materials using analytical theories such as ROM, MROM, Chamis, Halpin-Tsai, Hashin and Rosen, and bridging models. Rakesh et al. evaluate the material properties of the PALF/Epoxy uni-directional composite in function of the natural fiber volume fraction. The figures present the longitudinal and transversal Young's modulus variations [1]. Such cases are depicted in Figure 13.

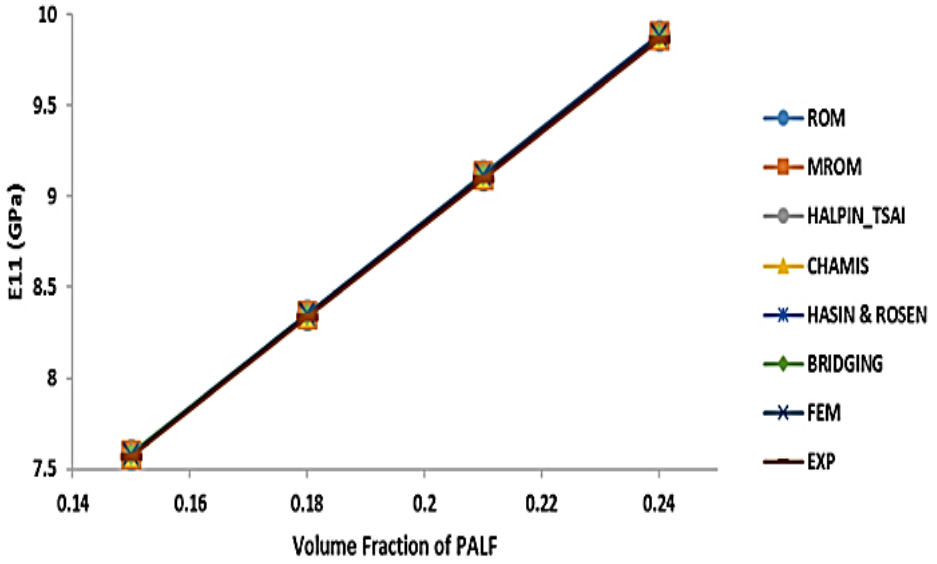

(a)

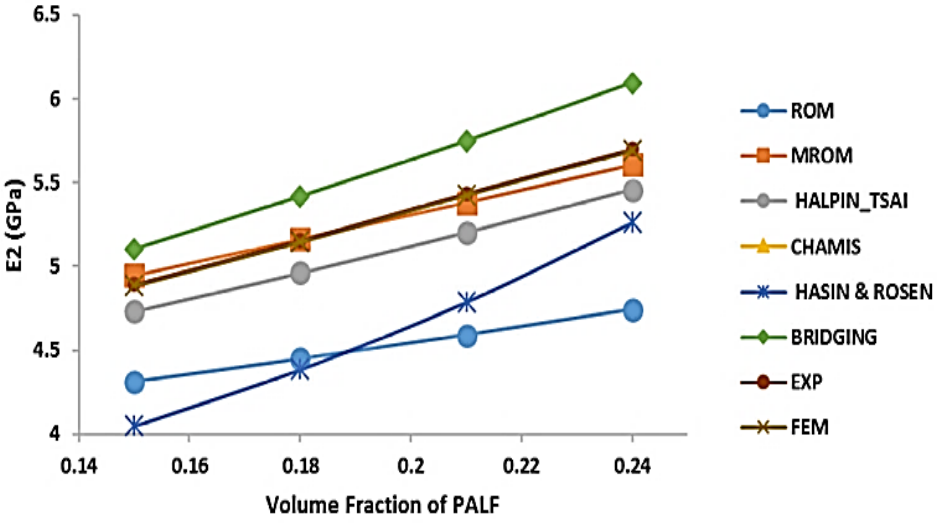

(b)

Figure 13. The predicted analytical, numerical, and experimental findings for (a) E_{11} and (b) E_{22} in terms of volume fraction [1].

I.6.2- Macromechanical approach

Following the micromechanical analysis, which involves predicting the thermomechanical properties of composites, a number of studies have focused on the macroscopic analysis of the elements of composite structures, represented by laminates. The literature indicates that the sandwich laminated plate theory (SLPT) and the elastic solution are the most commonly used theories for predicting the mechanical behavior of sandwich structures at the macroscopic level.

Avinash et al. [216] used elasticity theory to determine the stress distribution across each layer of the laminate element to conduct failure analysis via the Tsai-Wu criterion.

While the composite tubular structures are being used, damage like matrix cracking, fiber/matrix deboning, delamination between plies and fiber rupture will happen before the material finally breaks. Hence the interest in analyzing damage on a macroscopic scale.

Laminate damage analysis has been the subject of numerical model development based on rupture limit thresholds. Ludovic [217] has developed a fatigue damage model for laminates based on Degriek and Van Paepegem's (damage/failure limit) relationship, using Tsai Wu's failure criterion.

For delamination-type damage, several works have been devoted to the experimental investigation of delamination propagation criteria using tests on specimens with different types of loading (Benzeggagh et al. [218], Lachaud [219]).The work of Yong [220] and Xiaolin [221] showed a significant influence of fiber orientation on the propagation of delamination in laminates.

Macroscopically, the effect of temperature and humidity variation on laminated elements has been reported in several research works and has shown their great influence on the diffusion of water within composite materials at the macroscopic scale [222]. Padmavathi et al. [223] showed the dependence between the mass of water absorbed and the temperature variation; their results are represented in the following Figure 14 for a laminated plate immersed at several temperatures.

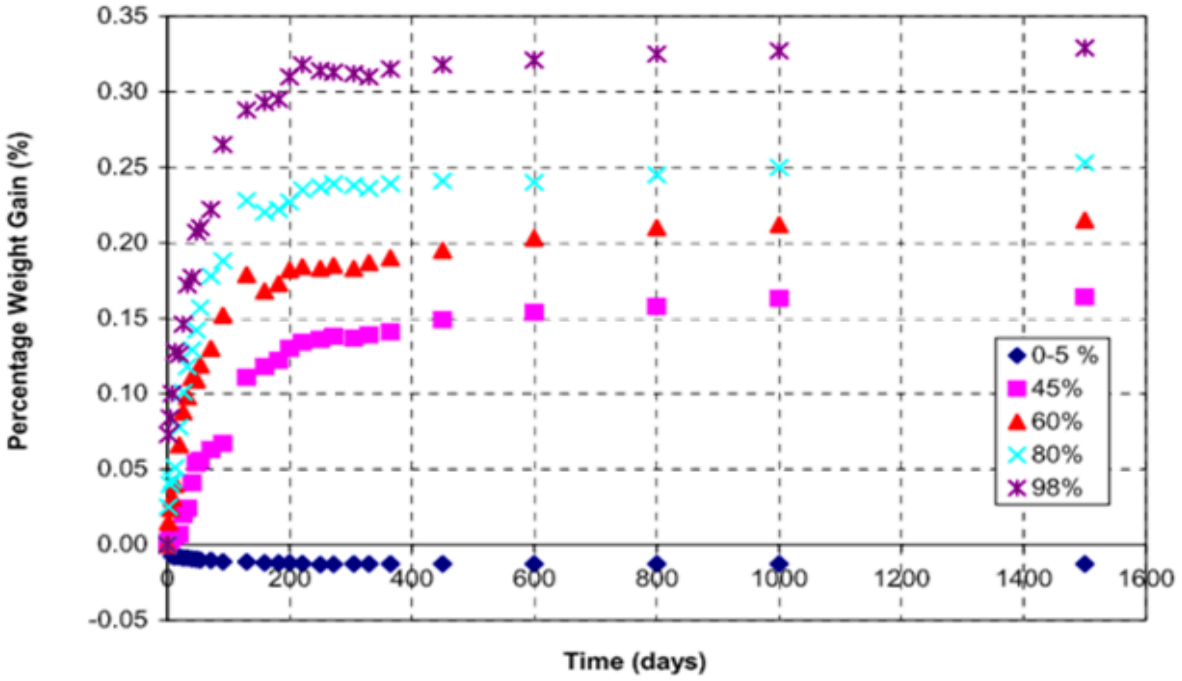

Figure 14. Water absorption of an E-glass/Vinylester laminated plate immersed in deionized water at several temperatures [223].

The presence of humidity can have a detrimental effect on the behavior of composite materials. For this, the work of Castaing [224], Shen and Springer [225] , and Weitsman [226] focused on the hygroscopic aging of laminates, which induces a decrease in stiffness and stress at rupture on a macroscopic scale, as represented by the following figures: (Figure 15, Figure 16, and Figure 17).

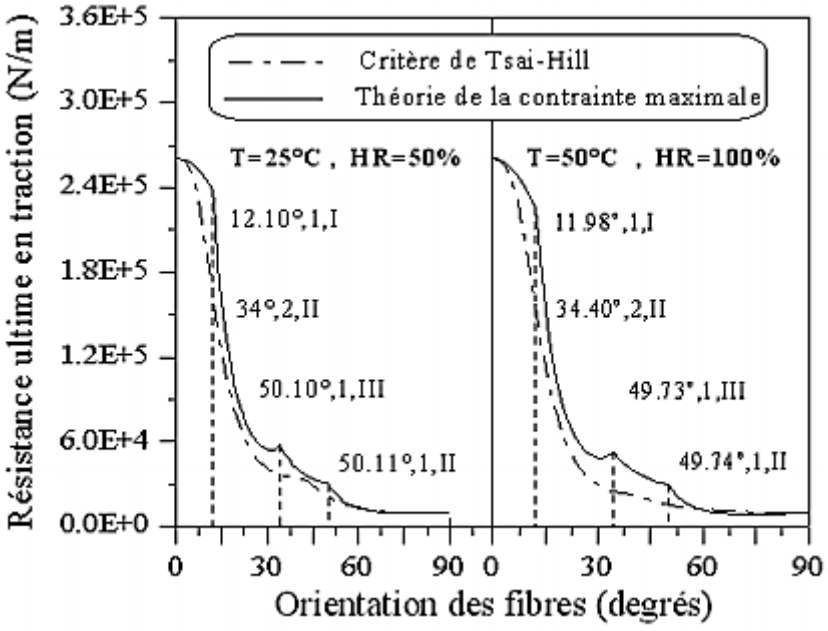

Figure 15. Evolution of the ultimate tensile strength of a laminate [227].

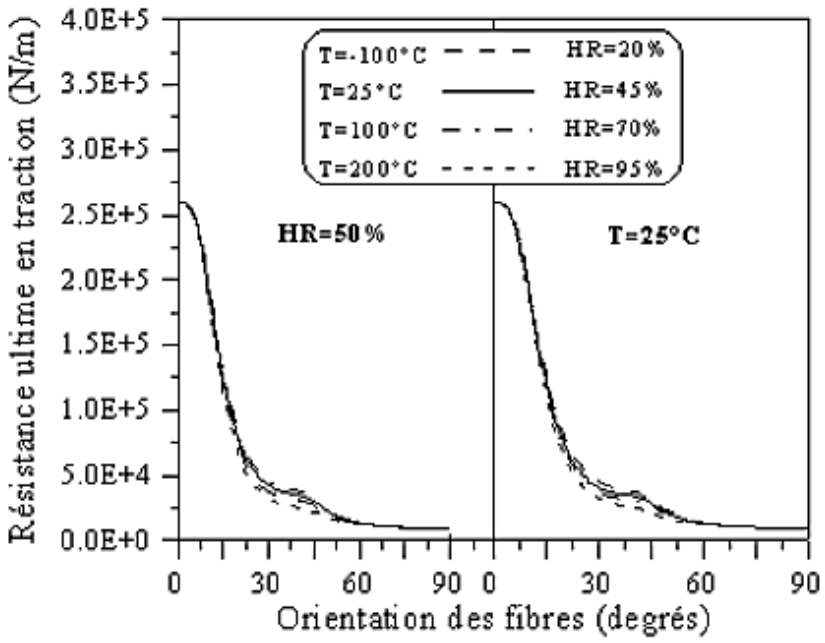

Figure 16. Evolution of the ultimate tensile strength of a balanced symmetrical laminate $[+\theta/-\theta]_{4S}$ according to different hygrothermal loadings [227].

Temperature variation can modify the multiscale properties of a composite material.

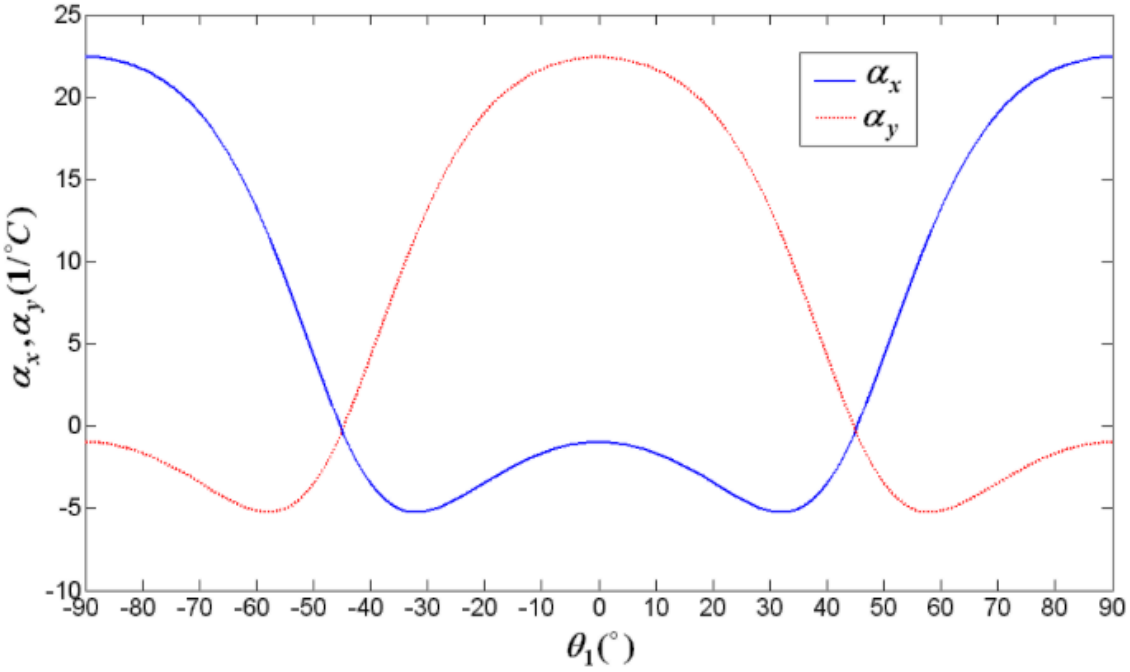

Figure 17. Variation of thermal expansion coefficients (αx, αy) as a function of the winding angle θ1 for balanced symmetrical laminates (E glass/epoxy), $[\pm\theta_1]s$, [228].

I.6.3- Tube structure approach

The last step of multiscale analysis is to focus on the response of cylindrical composite structure under different types of loading. Most previous studies have focused on thin-walled

cylindrical shells. However, only limited studies have been published dealing with thick-walled cylindrical pipe behaviors.

Boria et al. [90] examined the response to the low-velocity impact of sandwich constructions with thin flax/epoxy face sheets and an agglomerated cork core by utilizing a non-linear dynamic FE model solved using LS-DYNA. More research can be found in Table 4 of Chapter I.

For all these reasons, based on the multiscale configuration of the sandwich cylindrical structure, the distribution of the thesis manuscript is based on the particular configuration of the composites, where each analysis level provides a large data set at the following scale.

I.7- CONCLUSION

This state of art provides the tool design of synthetic multilayered and sandwich pipe and examines its performance under different practical loading conditions. The predominant effect of the parameter design of multilayered and sandwich-typical composite materials on pipe structures is indicated.

Throughout this literature review, various computer models have been developed to analyze the stresses and strains of filament-wound pipes in two configurations: multilayered and few are thick-walled sandwiches. This state of art is focused on understanding the behavior of filament winding pipes under both quasi-static and dynamic loads using one of the two theories: the conventional laminated plate theory or elasticity theory. A detailed review includes linear and nonlinear behavior applying analytical and finite element modeling approaches, and some are validated with experimental study.

The most sandwich-treated pipe has a non-reinforced core layer and a synthetic alternate-ply material for the skin layers. Knowing the complexity of the material properties of the skin layers reinforced by alternating ply composites, some study is centered on dealing with typical three-dimensional, cylindrical, and orthotropic sandwich pipes.

For a progressive, reliable, and correct replacement of synthetic composites, the use of single natural fibers or hybridization as a replacement has attracted attention in different areas of research where the aim is to protect the environment and minimize reliance on synthetic materials. A state-of-the-art assessment of the research work carried out on using natural fibers in the design of multilayered pipes is provided in this thesis.

CHAPTER I: LITERATURE REVIEW

The idea of substituting conventional composite materials with bio-composite in the design of hydrogen transportation sandwich pipes is a new concept that hasn't been treated before, and it depends on several factors, such as material property prediction, the optimization of thickness, stacking sequences, winding angle, and predicting the failure depending on the type of loading.

In addition, this literature review reveals that there has been no literature experimentation, analytical, or FEM investigations on the stress and failure analysis of biosandwich composite pipes under thermo-mechanical static or cyclic loading, as well as pressure and temperature.

On this bibliographic basis, this contribution was constructed in order to develop a multiscale model for the analysis of cylindrical FW eco-sandwich structures for hydrogen transport and a failure prediction tool.

Before achieving the sizing of the tubular eco-sandwich cylinder under static and dynamic loading (Chapter V), a multiscale characterization is performed, beginning with the micro and macromechanical scales. The micromechanical approach (Chapter III) is used to predict the mechanical properties of bio skins based on natural fibers and epoxy matrix. The second scale characterization focuses on understanding the behavior of a sandwich element of the tubular structure through a macro-mechanical model (Chapter IV).

The second chapter of this thesis focused on the presentation of the mathematical formulation of different scale approaches treated on this thesis.

CHAPTER II:

MATHEMATICAL FORMULATIONS

CHAPTER II: MATHEMATICAL FORMULATIONS

II.1- INTRODUCTION

This chapter presents the mathematical formulations of the multiscale of eco-sandwich pipes, namely: micromechanical level, macromechanical level, and finally the law behavior of tubular structure, as illustrated in Figure 18.

This chapter is based on elasticity theory, with small deformation and without taking into account the visco-behavior of the matrix component. The distribution of the fibers through the skin is assumed to be perfect, and no damage occurs during loading.

The elasticity theory of sandwich plates and tubular sandwiches provides the theoretical foundation for the macro-mechanical and structural models developed in this investigation.

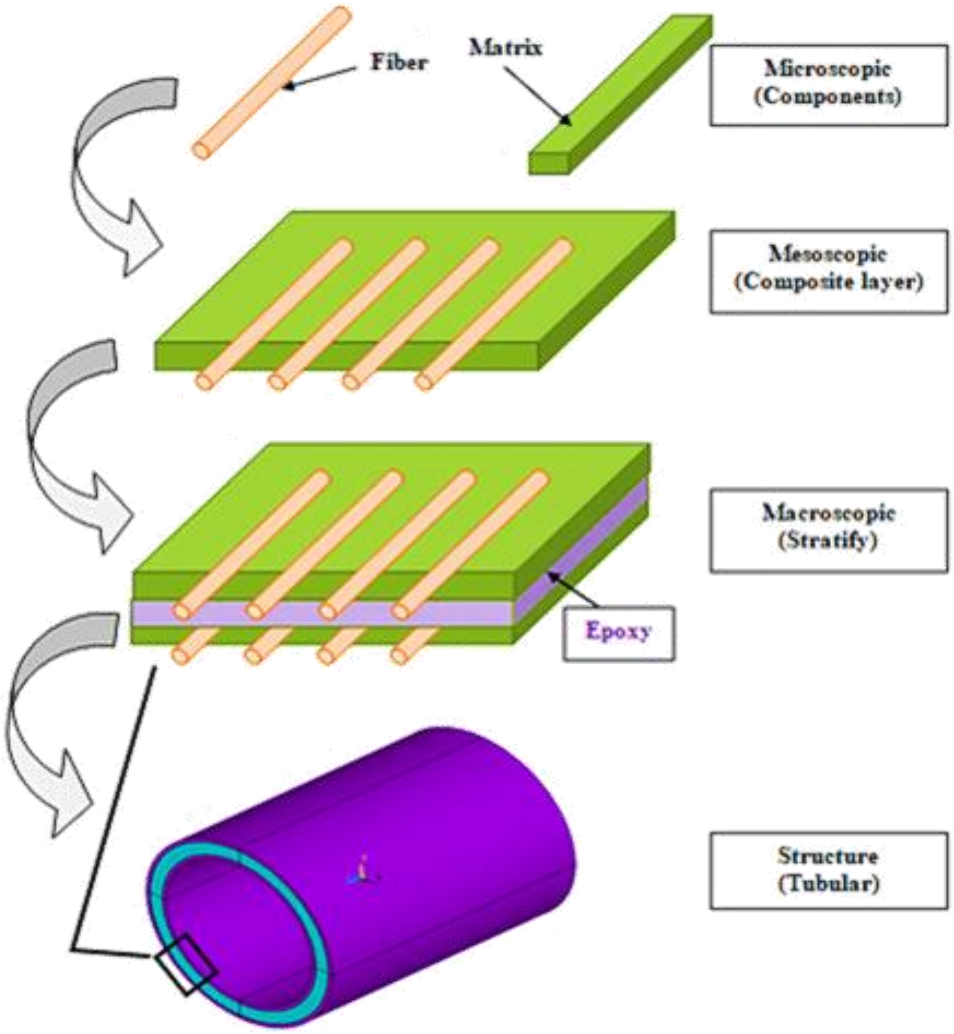

Figure 18. Multiscale composite material analysis, from the micro level to the tubular structure level.

II.2- MICRO SCALE ANALYSIS

II.2.1- Analytical

Many studies have been performed to predict the mechanical properties of composites. To evaluate the elastic properties of composites, various micromechanical models have been proposed, such as the Halpin-Tsai model, the Chamis model, the rule of mixtures (ROM), and the Hashin and Rosen model. The analytical models were developed using [229]. The specific equations for each of these four models are depicted as:

II.2.1.1- ROM model

The Rule of Mixture (ROM) is a method used to estimate the stiffness of the composite material and its components. It is a balanced median approach to measuring different composite properties, especially those of continuous long-fiber reinforced composites. Based on the analyzed responses from the fiber and matrix, ROM is commonly used for predicting the modulus and strength of fiber-reinforced composites.

$$E_{11} = \mathrm{V_F E_F} + \mathrm{V_M E_M} \tag{1}$$

$$E_{22} = \frac{\mathrm{E_F E_M}}{\mathrm{E_M . V_F + E_F . V_M}} \tag{2}$$

$$v_{12} = V_F v_F + V_M v_M \tag{3}$$

$$G_{12} = \frac{G_F . G_M}{G_F . V_M + G_M . V_F} \tag{4}$$

II.2.1.2- Halpin-Tsai model

In 1969, Halpin and Tsai created a semi-empirical model for predicting composite attributes. Fiber-reinforced composites with ideal fiber orientation are commonly predicted using the Halpin-Tsai model. Tsai altered the rule of mixtures to incorporate the irregularities in the fiber orientation. The modulus of composites may be predicted using this model.

$$\mathrm{E_{11} = E_F V_F + E_M V_M} \tag{5}$$

$$\mathrm{E_{22} = E_M . \left(\frac{1+\zeta_\eta . V_F}{1-\eta V_F}\right)} \quad \text{with:} \quad \eta = \left(\frac{\left[\frac{E_F}{E_M}\right]-1}{\left[\frac{E_F}{E_M}\right]+\zeta}\right) \tag{6}$$

$$v_{12} = v_F V_F + v_M V_M \tag{7}$$

$$\mathrm{G_{12}} = \mathrm{G_M}\left(\frac{1+\zeta_\eta.\mathrm{V_F}}{1-\eta\mathrm{V_F}}\right) \tag{8}$$

II.2.1.3- Chamis model

The Chamis model is a commonly used analytical method by researchers to confirm the accuracy of finite element analysis results, ensuring their suitability for predicting the properties of composite materials.

$$\mathrm{E_{11}} = \mathrm{V_F E_F} + \mathrm{V_M E_M} \tag{9}$$

$$\mathrm{E_{22}} = \frac{\mathrm{E_M}}{1-\sqrt{\mathrm{V_F}}(1-\mathrm{E_M}/\mathrm{E_F})} \tag{10}$$

$$v_{12} = V_F v_F + V_M v_M \tag{11}$$

$$\mathrm{G_{12}} = \frac{\mathrm{G_M}}{1-\sqrt{\mathrm{V_F}}\,(1-\mathrm{G_M}/\mathrm{G_F})} \tag{12}$$

II.2.1.4- Hashin and Rosen model

To analyze the failure behavior of fiber reinforced composites, which consist of fibers immersed in a matrix, the Hashin and Rosen model is usually used.

$$E_{11} = V_F E_F + V_M E_M + \frac{4 \times V_F V_M (v_F - v_M)^2}{\frac{V_F}{K_M} + \frac{1}{G_M} + \frac{V_M}{K_F}} \tag{13}$$

$$E_{22} = 2 \times (1 + v_{23}).G_{23} \tag{14}$$

$$v_{12} = V_F.v_F + V_M.v_M + \frac{V_F V_M (v_F - v_M)\left(\frac{1}{K_M} - \frac{1}{K_F}\right)}{\frac{V_F}{K_M} + \frac{1}{G_M} + \frac{V_M}{K_F}} \tag{15}$$

$$G_{12} = G_M.\frac{G_F(1+V_F) + G_M.V_M}{G_F.V_M + G_M(1+V_F)} \tag{16}$$

II.3- MACRO SCALE ANALYTICAL MODEL

II.3.1- Analytical analysis

The theory of sandwich plates, concentrating on the elasticity of micro deformations, provides the theoretical foundation for the model created in this investigation. It supports the fundamental, essential theories listed below:

1. The core's thickness is substantially greater than the skins: $h \gg h_1, h_2$ and it solely transmits transverse shear stresses σ_{xz} and σ_{yz}. And σ_{xz} and σ_{yz}
2. Skins ignore transverse shear stresses σ_{xx}, σ_{yy}, σ_{xy} and σ_{zz}.
3. The displacements of the core, u_a and v_a, along the x and y directions respectively, are linear functions of the coordinate z.
4. The displacements u and v along the x and y directions respectively are uniform throughout the thickness of the skins.
5. The transverse displacement w is independent of the variable z the strain ε_{zz} is neglected.

Finally, the theory deals with problems of elasticity under small deformations.

Figure 19 gives an example of a Sandwich sample evaluations used in this thesis.

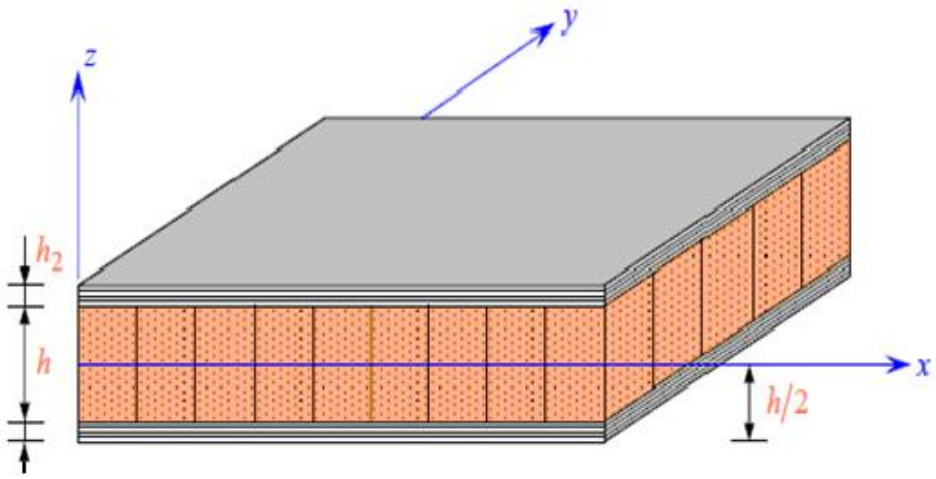

Figure 19. Sandwich sample evaluations [230].

In the classical theory of linear elasticity, the tensor representation of the generalized Hooke's law is given by the equation.

$$\sigma_{ij} = C_{ijkl} \cdot \varepsilon_{kl} \qquad i, j, k, l = 1, 2, 3 \tag{17}$$

This law can be expressed in the following inverse form:

$$\varepsilon_{ij} = S_{ijkl} \cdot \sigma_{kl} \qquad i,j,k,l = 1,2,3 \tag{18}$$

II.3.1.1-Expression of the strain field

The field of deformation in the upper and lower skins is written as:

$$\begin{bmatrix} \varepsilon_{xx}^{1} \\ \varepsilon_{yy}^{1} \\ \gamma_{xy}^{1} \end{bmatrix} = \begin{bmatrix} \varepsilon_{xx}^{0} \\ \varepsilon_{yy}^{0} \\ \gamma_{xy}^{0} \end{bmatrix} - \frac{h}{2} \begin{bmatrix} K_x \\ K_y \\ K_{xy} \end{bmatrix} \tag{19}$$

$$\begin{bmatrix} \varepsilon_{xx}^{2} \\ \varepsilon_{yy}^{2} \\ \gamma_{xy}^{2} \end{bmatrix} = \begin{bmatrix} \varepsilon_{xx}^{0} \\ \varepsilon_{yy}^{0} \\ \gamma_{xy}^{0} \end{bmatrix} + \frac{h}{2} \begin{bmatrix} K_x \\ K_y \\ K_{xy} \end{bmatrix} \tag{20}$$

The strain field has the same writing as the strain field of the laminate theory with transverse shear. It is the superposition of two strain fields:

The field of strains in membrane-bending:

$$\begin{bmatrix} \varepsilon_{xx}^{a} \\ \varepsilon_{yy}^{a} \\ \varepsilon_{xy}^{a} \end{bmatrix} = \begin{bmatrix} \varepsilon_{xx}^{0} \\ \varepsilon_{yy}^{0} \\ \varepsilon_{xy}^{0} \end{bmatrix} + Z \begin{bmatrix} k_x \\ k_y \\ k_{xy} \end{bmatrix} \tag{21}$$

- The transverse shear deformation field :

$$\begin{bmatrix} \gamma_{yz}^{a} \\ \gamma_{xz}^{a} \end{bmatrix} = \begin{bmatrix} \dfrac{\partial \omega_0}{\partial y} + \varphi_y \\ \dfrac{\partial \omega_0}{\partial x} + \varphi_x \end{bmatrix} \tag{22}$$

II.3.1.2-Expression of the constraint field

The field of constraints in the core is deduced from the hypothesis [230] :

$$\sigma_{xx}^{a} = \sigma_{yy}^{a} = \sigma_{xy}^{a} = \sigma_{zz}^{a} = 0 \tag{23}$$

Only shear stresses are transmitted via the core:

$$\begin{bmatrix} \sigma_{yz}^{a} \\ \sigma_{xz}^{a} \end{bmatrix} = \begin{bmatrix} C_{44}^{\prime a} & C_{45}^{\prime a} \\ C_{45}^{\prime a} & C_{55}^{\prime a} \end{bmatrix} \begin{bmatrix} \gamma_{yz}^{a} \\ \gamma_{xz}^{a} \end{bmatrix} \tag{24}$$

The following relationships are utilized to deduce the remaining stresses from the skin's deformations:

$$\begin{bmatrix}\sigma_{xx}^{k}\\ \sigma_{yy}^{k}\\ \sigma_{xy}^{k}\end{bmatrix}=\begin{bmatrix}Q'_{11} & Q'_{12} & Q'_{16}\\ Q'_{21} & Q'_{22} & Q'_{26}\\ Q'_{16} & Q'_{26} & Q'_{66}\end{bmatrix}_{k}\begin{bmatrix}\varepsilon_{xx}^{i}\\ \varepsilon_{yy}^{i}\\ \varepsilon_{xy}^{i}\end{bmatrix}, \text{i=1,2} \quad (25)$$

For the k-layer of the lower skin (i=1) or the upper skin (i=2).

II.3.1.3-Constitutive equation:

The constituent equation of sandwich plates involves the results and moments already introduced in the stratified theory:

- **membrane results:**

$$\begin{bmatrix}N_x\\ N_y\\ N_{xy}\end{bmatrix}=\int_{-(h/2+h_1)}^{-h/2}\begin{bmatrix}\sigma_{xx}\\ \sigma_{yy}\\ \sigma_{xy}\end{bmatrix}dz+\int_{h/2}^{h/2+h_2}\begin{bmatrix}\sigma_{xx}\\ \sigma_{yy}\\ \sigma_{xy}\end{bmatrix}dz \quad (26)$$

N_x,N_y ,N_{xy} are the results per unit length, respectively, of the normal stresses according to x, y and of the shear stresses in the plane (x, y).

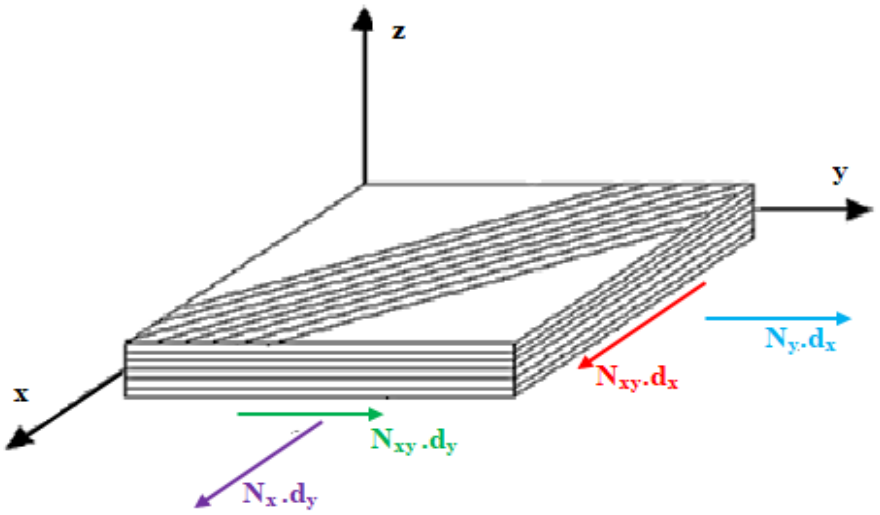

Figure 20. Membrane loading mode [231].

- **Bending-torsional moments:**

$$\begin{bmatrix}M_x\\ M_y\\ M_{xy}\end{bmatrix}=\int_{-(h/2+h_1)}^{-h/2}\begin{bmatrix}\sigma_{xx}\\ \sigma_{yy}\\ \sigma_{xy}\end{bmatrix}z\,dz+\int_{h/2}^{h/2+h_2}\begin{bmatrix}\sigma_{xx}\\ \sigma_{yy}\\ \sigma_{xy}\end{bmatrix}z\,dz \quad (27)$$

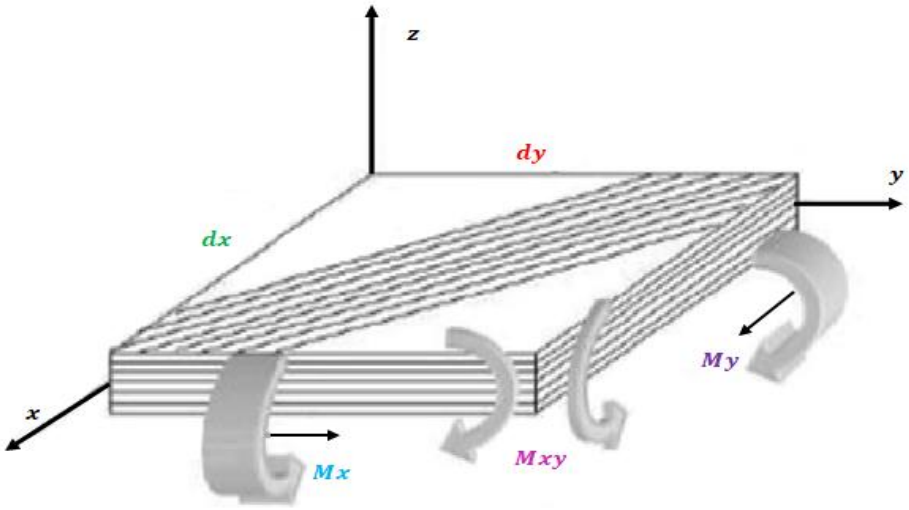

Figure 21. Torsional bending loading mode [231].

- **The shear results:**

$$\begin{bmatrix} Q_y \\ Q_x \end{bmatrix} = \int_{-h/2}^{h/2} \begin{bmatrix} \sigma_{yz} \\ \sigma_{xz} \end{bmatrix} dz \tag{28}$$

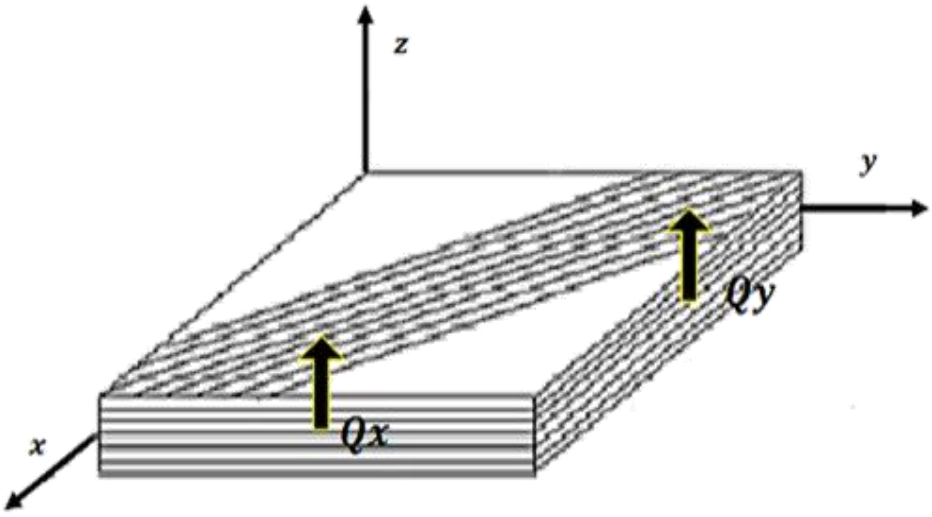

Figure 22. Shear loading mode [231].

By substituting the expressions of the constraints (24) for (25) in the previous expressions of the resultants and moments, we obtain the constitutive equation:

$$\begin{bmatrix} N_x \\ N_y \\ N_{xy} \\ M_x \\ M_y \\ M_{xy} \\ Q_y \\ Q_x \end{bmatrix} = \begin{bmatrix} A_{11} & A_{12} & A_{16} & B_{11} & B_{12} & B_{16} & 0 & 0 \\ A_{21} & A_{22} & A_{26} & B_{21} & B_{22} & B_{26} & 0 & 0 \\ A_{61} & A_{62} & A_{66} & B_{61} & B_{62} & B_{66} & 0 & 0 \\ G_{11} & G_{12} & G_{16} & D_{11} & D_{12} & D_{16} & 0 & 0 \\ G_{21} & G_{22} & G_{26} & D_{21} & D_{22} & D_{26} & 0 & 0 \\ G_{61} & G_{62} & G_{66} & D_{61} & D_{62} & D_{66} & 0 & 0 \\ 0 & 0 & 0 & 0 & 0 & 0 & F_{44} & F_{45} \\ 0 & 0 & 0 & 0 & 0 & 0 & F_{45} & F_{55} \end{bmatrix} \begin{bmatrix} \varepsilon_{xx}^0 \\ \varepsilon_{yy}^0 \\ \gamma_{xy}^0 \\ K_x \\ K_y \\ K_{xy} \\ \gamma_{yz}^0 \\ \gamma_{xz}^0 \end{bmatrix} \tag{29}$$

$$\begin{aligned} A_{ij} &= A_{ij}^1 + A_{ij}^2 \\ B_{ij} &= \frac{h}{2}(A_{ij}^2 + A_{ij}^1) \\ G_{ij} &= G_{ij}^1 + G_{ij}^2 \\ D_{ij} &= \frac{h}{2}(G_{ij}^2 - G_{ij}^1) \end{aligned} \tag{30}$$

And:

$$\begin{aligned} A_{ij}^1 &= \int_{-(h/2+h_1)}^{-h/2} \left(Q'_{ij}\right)_k dz = \sum_{K=1}^{n_1} \int_{h_{k-1}}^{h_1} \left(Q'_{ij}\right)_k dz = \sum_{k=1}^{n_1} \left(Q'_{ij}\right)_k e_k \\ G_{ij}^1 &= \int_{-(h/2+h_1)}^{-h/2} Z\left(Q'_{ij}\right)_k dz = \sum_{k=1}^{n_1} \int_{h_{k-1}}^{h_1} Z\left(Q'_{ij}\right)_k dz = \sum_{k=1}^{n_1} \left(Q'_{ij}\right)_k e_k z_k \\ A_{ij}^2 &= \int_{h/2}^{h/2+h_2} \left(Q'_{ij}\right)_k dz = \sum_{k=1}^{n_2} \int_{h_{k-1}}^{h_1} \left(Q'_{ij}\right)_k dz = \sum_{k=1}^{n_2} \left(Q'_{ij}\right)_k e_k \\ G_{ij}^2 &= \int_{h/2}^{h/2+h_2} Z\left(Q'_{ij}\right)_k dz = \sum_{k=1}^{n_2} \int_{h_{k-1}}^{h_1} Z\left(Q'_{ij}\right)_k dz = \sum_{k=1}^{n_2} \left(Q'_{ij}\right)_k e_k z_k \\ F_{ij}^2 &= h.C_{ij}'^a \end{aligned} \tag{31}$$

In the preceding expressions of the stiffness coefficients: n_1 and n_2 represent the numbers of layers in the lower skin and the upper skin respectively, while $C_{ij}'^a$ are the coefficients related to the transverse shear of the core.

The constitutive equation has a similar form to the equation obtained in the case of laminated theory with transverse shear. However, it differs by the inclusion of the terms G_{ij}, which introduce an asymmetry in the stiffness matrix.

II.3.2-Failure criteria

In this part, we investigate skin failure using the Tsai-Wu failure criterion and isotropic core failure using the von Mises yield criterion. They are linked to Cartesian coordinates through the transformation matrix:

$$\begin{Bmatrix} \sigma_1 \\ \sigma_2 \\ \sigma_3 \\ \tau_{23} \\ \tau_{13} \\ \tau_{12} \end{Bmatrix} = \begin{bmatrix} m^2 & n^2 & 0 & 0 & 0 & 2mn \\ n^2 & m^2 & 0 & 0 & 0 & -2mn \\ 0 & 0 & 1 & 0 & 0 & 0 \\ 0 & 0 & 0 & m & -n & 0 \\ 0 & 0 & 0 & n & m & 0 \\ -mn & mn & 0 & 0 & 0 & m^2 - n^2 \end{bmatrix} \begin{Bmatrix} \sigma_x \\ \sigma_y \\ \sigma_z \\ \tau_{yz} \\ \tau_{xz} \\ \tau_{xy} \end{Bmatrix} \tag{32}$$

Where: $m = \cos \emptyset$ and $n = \sin \emptyset$; $\emptyset$ is the fiber angle with respect to the cylindrical axial direction.

The criterion of Tsai-Wu [232] in plane stresses is written as:

$$\left(\frac{1}{X_t} - \frac{1}{X_c}\right)\sigma_L + \left(\frac{1}{Y_t} - \frac{1}{Y_c}\right)\sigma_T + \frac{\sigma_L^2}{X_t X_c} + \frac{\sigma_T^2}{Y_t Y_c} + \frac{\sigma_{LT}^2}{S_{LT}^2} - \frac{\sigma_L}{X_t}\frac{\sigma_T}{X_c} = 1 \tag{33}$$

Circumferential stress:

$$\sigma_\theta = {}^{pr}/_{t} \tag{34}$$

Axial stress:

$$\sigma_x = {}^{pr}/_{2t} \tag{35}$$

With:

$$\sigma_\theta = 2\sigma_x \tag{36}$$

II.4- PIPING ANALYSIS

The analytical modeling of static and dynamic loading of the sandwich transport solution is established in this section. Firstly, the hypotheses that define the limits of application of the

model and the resulting equations are established within the framework of the theory of elasticity, taking into account the small deformation formalism.

This analytical model allows consideration of several loading modes: pure internal pressure, axial loading, internal pressure with background, and torsion.

II.4.1- Quasi static loading

II.4.1.1- Analytical analysis

For the analytical model, all displacements, strains, and stresses are independent of Θ for the axisymmetric sandwich pipe. The radial displacements r are independent of axial displacements. Z as well as axial coordinates is not dependent on the radial ones. Therefore, the displacements are:

$$U_r = U_r(r)\ ,\ U_\theta = U_\theta(r,z)\ ,\ U_z = U_z(z) \tag{37}$$

The strain-displacement relations can be expressed as:

$$\begin{cases} \varepsilon_r^{(k)} = \dfrac{dU_r^{(k)}}{d_r}, \varepsilon_\theta^{(k)} = \dfrac{U_r^{(k)}}{r}, \varepsilon_z^{(k)} = \dfrac{dU_z^{(k)}}{d_z} = \varepsilon_0 \\ \gamma_{zr}^{(k)} = 0\ , \gamma_{\theta r}^{(k)} = \dfrac{dU_\theta^{(k)}}{d_r} - \dfrac{U_\theta^{(k)}}{r}, \gamma_{z\theta}^{(k)} = \dfrac{dU_\theta^{(k)}}{d_z} = \gamma_0 r \end{cases} \tag{38}$$

The general stress-strain relationship for each k-component exposed to axisymmetric thermo-mechanical loading [12] is shown below :

$$\begin{Bmatrix} \sigma_z \\ \sigma_\theta \\ \sigma_r \\ \tau_{\theta r} \\ \tau_{zr} \\ \tau_{z\theta} \end{Bmatrix} = \begin{bmatrix} C_{11} & C_{12} & C_{13} & 0 & 0 & C_{16} \\ C_{12} & C_{22} & C_{23} & 0 & 0 & C_{26} \\ C_{13} & C_{23} & C_{33} & 0 & 0 & C_{36} \\ 0 & 0 & 0 & C_{44} & C_{45} & 0 \\ 0 & 0 & 0 & C_{45} & C_{55} & 0 \\ C_{16} & C_{26} & C_{36} & 0 & 0 & C_{66} \end{bmatrix}^{(k)} \begin{Bmatrix} \varepsilon_z - \alpha_z \Delta T \\ \varepsilon_\theta - \alpha_\theta \Delta T \\ \varepsilon_r - \alpha_r \Delta T \\ \gamma_{\theta r} \\ \gamma_{zr} \\ \gamma_{z\theta} \end{Bmatrix}^{(k)} \tag{39}$$

The local balancing equations are as below in each k-component:

$$\frac{d\,\sigma_r^{(k)}}{dr} + \frac{\sigma_r^{(k)} - \sigma_\theta^{(k)}}{r} = 0 \tag{40}$$

The following differential equation is constructed by substituting the expression of radial and hoop stresses from equation (39) into equation (40) and applying equation (38):

$$\frac{d^2U_r^{(k)}}{dr^2}+\frac{1}{r}\frac{dU_r^{(k)}}{dr}-\frac{N_1^{(k)}}{r^2}U_r^{(k)}=\left[N_2^{(k)}\varepsilon_0+N_3^{(k)}\Delta T\right]\frac{1}{r}+N_4^{(k)}\gamma_0 \tag{41}$$

Where:

$$N_1^{(k)}=\frac{C_{22}^{(k)}}{C_{33}^{(k)}};\ N_2^{(k)}=\frac{C_{12}^{(k)}-C_{13}^{(k)}}{C_{33}^{(k)}};$$

$$N_3^{(k)}=\frac{K_3^{(k)}-K_2^{(k)}}{C_{33}^{(k)}}\ ;N_4^{(k)}=\frac{C_{26}^{(k)}-2C_{36}^{(k)}}{C_{33}^{(k)}}\ ; \tag{42}$$

$$\alpha_2^{(k)}=\frac{N_2^{(k)}}{1-N_1^{(k)}}\ ;\alpha_3^{(k)}=\frac{N_3^{(k)}}{1-N_1^{(k)}}\ ;\alpha_4^{(k)}=\frac{N_4^{(k)}}{4-N_1^{(k)}}$$

And:

$$\begin{aligned}K_1^{(k)}&=\alpha_z^{(k)}C_{11}^{(k)}+\alpha_\theta^{(k)}C_{12}^{(k)}+\alpha_r^{(k)}C_{13}^{(k)}\\K_2^{(k)}&=\alpha_z^{(k)}C_{12}^{(k)}+\alpha_\theta^{(k)}C_{22}^{(k)}+\alpha_r^{(k)}C_{23}^{(k)}\\K_3^{(k)}&=\alpha_z^{(k)}C_{13}^{(k)}+\alpha_\theta^{(k)}C_{23}^{(k)}+\alpha_r^{(k)}C_{33}^{(k)}\\K_4^{(k)}&=\alpha_z^{(k)}C_{16}^{(k)}+\alpha_\theta^{(k)}C_{26}^{(k)}+\alpha_r^{(k)}C_{36}^{(k)}\end{aligned} \tag{43}$$

The value of $\beta^{(k)}=\sqrt{N_1^{(k)}}$ determines the solution of equation (41), and can be expressed as:

For $\beta^{(k)}=1$:

$$U_r^{(k)}=D^{(k)}r+\frac{E^{(k)}}{r+r\,ln(r)\,(N_2^{(k)}\,\varepsilon_0+N_3^{(k)}\,\Delta T)}+\alpha_4^{(k)}\gamma_0 r^2 \tag{44}$$

For $\beta^{(k)}=2$:

$$U_r^{(k)}=D^{(k)}r^{\beta^{(k)}}+E^{(k)}r^{-\beta^{(k)}}+(\alpha_2^{(k)}\varepsilon_0+\alpha_3^{(k)}\Delta T)r+\frac{N_4^{(k)}}{2}\gamma_0 r^2\,ln\,(r) \tag{45}$$

For $\beta^{(k)}\neq 1\ or\ (2)$:

$$U_r^{(k)}=D^{(k)}r^{\beta^{(k)}}+E^{(k)}r^{-\beta^{(k)}}+(\alpha_2^{(k)}\varepsilon_0+\alpha_3^{(k)}\Delta T+\alpha_4^{(k)}\gamma_0 r^2 \tag{46}$$

The superscript k is such as: $k\in[1,w]$ where:

$$w = n_s + n_c + n_s \tag{47}$$

The continuity conditions for the displacements and stresses in the interfaces lead to:

The radial displacements' continuity is determined by:

$$\forall\, k\ [1, w-1],\ U^{(k)}\left(r_{ext}^{(k)}\right) = U^{(k+1)}\left(r_{ext}^{(k)}\right) \tag{48}$$

- The continuity of the radial stress gives:

$$\begin{cases} \forall\, k\ [1, w-1], \sigma_r^{(k)}\left(r_{ext}^{(k)}\right) = \sigma_{ext}^{(k+1)}\left(r_{ext}^{(k)}\right) \\ \sigma_r^{(1)}(r_i) = -p_0 \\ \sigma_r^{(w)}(r_o) = 0 \end{cases} \tag{49}$$

- The axial equilibrium of a cylinder with closed ends is satisfied by the following relation:

$$2\pi \sum_{k=1}^{w} \int_{r^{(k-1)}}^{r^{(k)}} \sigma_z^{(k)}(r) r dr = \pi\, r_i^2\, p_0 \tag{50}$$

- Because the torque is zero, the expression takes the form:

$$2\pi \sum_{k=1}^{w} \int_{r^{(k-1)}}^{r^{(k)}} \tau_{z\theta}(r) r^2 dr = 0 \tag{51}$$

- The equations that follow make it possible to express the vectors' deformations and stresses in the reference fiber.

$$\begin{cases} \varepsilon' = T_\varepsilon\, \varepsilon \\ \sigma' = T_\sigma\, \sigma \end{cases} \tag{52}$$

Where:

$$T_\sigma = \begin{bmatrix} cos^2\varphi & sin^2\varphi & 0 & 0 & 0 & 2sin\varphi\, cos\varphi \\ sin^2\varphi & cos^2\varphi & 0 & 0 & 0 & -2sin\varphi\, cos\varphi \\ 0 & 0 & 1 & 0 & 0 & 0 \\ 0 & 0 & 0 & cos\varphi & -sin\varphi & 0 \\ 0 & 0 & 0 & sin\varphi & cos\varphi & 0 \\ -sin\varphi\, cos\varphi & sin\varphi\, cos\varphi & 0 & 0 & 0 & cos^2\varphi - sin^2\varphi \end{bmatrix} \tag{53}$$

And:

$$T_\varepsilon = \begin{bmatrix} cos^2\varphi & sin^2\varphi & 0 & 0 & 0 & sin\varphi\, cos\varphi \\ sin^2\varphi & cos^2\varphi & 0 & 0 & 0 & -sin\varphi\, cos\varphi \\ 0 & 0 & 1 & 0 & 0 & 0 \\ 0 & 0 & 0 & cos\varphi & -sin\varphi & 0 \\ 0 & 0 & 0 & sin\varphi & cos\varphi & 0 \\ -2\, sin\varphi\, cos\varphi & 2sin\varphi\, cos\varphi & 0 & 0 & 0 & cos^2\varphi - sin^2\varphi \end{bmatrix} \quad (54)$$

The Tsai-Wu criterion is introduced in the analytical model in order to evaluate the sandwich pipe strength:

$$F_{11}(\sigma_x^{(k)})^2 + F_{22}(\sigma_y^{(k)})^2 + F_{66}(\sigma_{yx}^{(k)})^2 + 2F_{12}\sigma_y^{(k)}\sigma_x^{(k)} + F_1\sigma_x^{(k)} + F_2\sigma_y^{(k)} \leq 1 \quad (55)$$

With:

$$F_{11} = \frac{1}{\sigma_{xU}\ \sigma'_{xU}}\ ; F_{22} = \frac{1}{\sigma_{yU}\ \sigma'_{yU}}\ ; F_{12} = -\frac{1}{2}\frac{1}{\sqrt{\sigma_{yU}\ \sigma'_{yU}\ \sigma_{xU}\ \sigma'_{xU}}}$$
$$F_{66} = \frac{1}{\sigma_{yxU}^2}\ ;\ F_1 = \frac{1}{\sigma_{xU}} - \frac{1}{\sigma'_{xU}}\ ; F_2 = \frac{1}{\sigma_{yU}} - \frac{1}{\sigma'_{yU}} \quad (56)$$

The solutions are obtained by using the MATLAB numerical code. The results are represented as functions of the non-dimensional ratio R:

$$R = \frac{r - r_i}{r_o - r_i} \quad (57)$$

II.4.2- Cyclic loading

II.4.2.1- Thermomechanical analysis

In a thermomechanical condition, a sandwich pipe with inner and outer radius R_{in} and R_{out} respectively, is subjected to cyclic internal pressure and thermal cycling. After a heating period, the cyclic internal pressure and temperature are provided with the same frequency f. The inner surface of the cylinder is gradually heated to the typical operating temperature T_m over a time period t_h to reduce thermal stress. The internal pressure and temperature of the cylinder are assumed to fluctuate according to the following relations:

$$\begin{cases} T_{(r_i,t)} = T_i + \frac{t}{t_h}(T_m - T_i) & 0 \le t \le t_h \\ T_{(r_i,t)} = T_m + T_a\, sin(2\pi f t) & t \ge t_h \end{cases} \quad (58)$$

$$\begin{cases} P_{(t)} = 0 & 0 \le t \le t_h \\ P_{(t)} = P_m + P_a\, sin(2\pi f t) & t \ge t_h \end{cases} \quad (59)$$

Additionally, it is presumed that:

$$\begin{cases} 0 \le T_a \le T_m \\ 0 \le P_a \le P_m \end{cases} \quad (60)$$

We assess the yielding of the isotropic core using the well-known Von Mises criteria, which states that core failure occurs when the Von Mises stress (σ_{vm}) approaches the material's yield strength:

$$\sigma_{vm} = \sqrt{\frac{(\sigma_{11} - \sigma_{22})^2 + (\sigma_{22} - \sigma_{33})^2 + (\sigma_{33} - \sigma_{11})^2 + 6 \times (\sigma_{23}^2 + \sigma_{31}^2 + \sigma_{12}^2)}{2}} \quad (61)$$

II.5- CONCLUSION

Mathematical models formulating the behavior of composites at all levels are presented in this second chapter. These formulations are based on elasticity theory, with small deformations, without taking into account the visco-behavior of the matrix component. Additionally, no damage occurs during loading.

For the prediction of the material properties of a biocomposite based on natural fibers, the third chapter presents a micro-analysis using analytical and numerical models.

CHAPTER III:

MICROMECHANICAL ANALYSIS

CHAPTER III: MICROMECHANICAL ANALYSIS

III.1- INTRODUCTION

The third chapter of this contribution thesis attempts to predict the mechanical properties of skin layers using PALF (pineapple leaf fiber), date palm, and Alfa fibers at various volume fractions, which are some of the most plentiful plant resources in Algeria. Micromechanical analytical and FE models were developed in this order using MATLAB 8.3 and ANSYS 18.1 software. The impact of the volume fraction of reinforcement on Young's and shear modulus and Poisson's ratios is examined.

Some analytical results based on Halpin-Tsai, Chamis, Hashin Vs. Rosen and ROM models are compared to experimental data [1].

III.2- MATERIALS

The different material properties of both the matrix and fiber are shown in Table 6 By altering the volume fraction of the long fiber, material properties are utilized to establish the mechanical properties of the composites, which are longitudinal young's modulus (E_{11}), transverse young's modulus (E_{22}), longitudinal shear modulus (G_{12}), and major Poisson's ratio (v_{12}).

Table 6. Properties of the constituents.

Material	Young's modulus [GPa]	Poisson's Ratio	References
Epoxy	3.75	0.35	[1]
PALF	29.3	0.30	
DB date palm tree fiber	6.63	0.152	[52]
Alfa fiber	19.77	0.34	[233]

Figure 23 shows the different natural fiber plants used in this thesis.

(a) **(b)** **(c)**

Figure 23**.** Natural fiber plants: (a) Pineapple [44], (b) Palm and (c) Alfa [69].

III. 3- FEM ANALYSIS

II.3.1- Fiber-reinforced composite numerical homogenization

Epoxy and one of the fibers (PALF, Palm fiber, or Alfa fiber) are the main components of the Particle Reinforced Composite. To accomplish the analysis, the homogenization approach is used to a fiber-reinforced composite by selecting continuous fibers as reinforcement. Figure 24 illustrates a uniform distribution of long fiber in the epoxy, by using the finite element software ANSYS 18.1 for solving the problem.

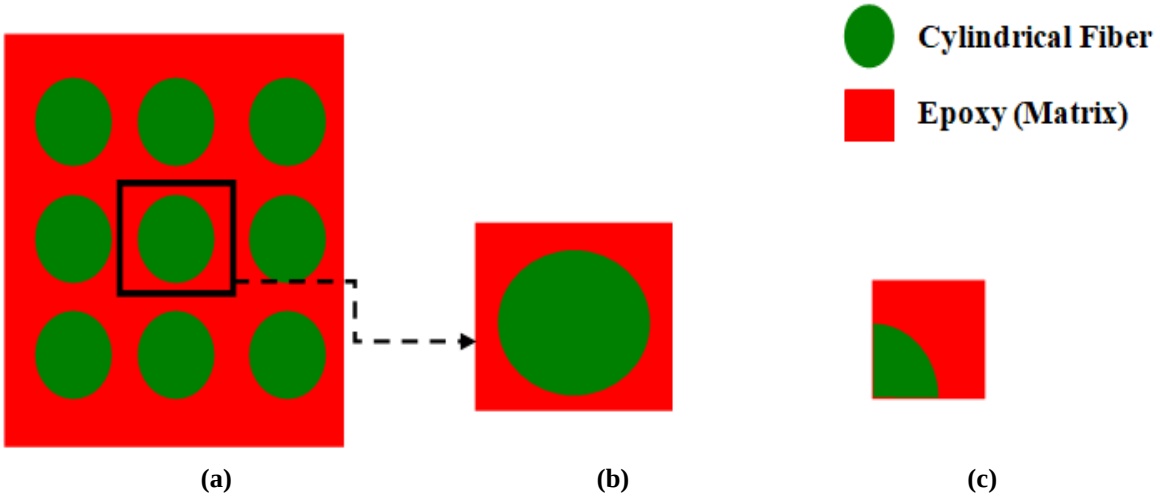

(a) **(b)** **(c)**

Figure 24. (a) Uniform distribution of fibers in the matrix; (b) Isolated Unit cell; (c) One-eighth Model.

II.3.2- Element type

The ANSYS SOLID 186 element shown in Figure 25, which is a higher-order 3D 20-node solid element with quadratic displacement behavior, was used in this study. There are 20 nodes in the element, each with three degrees of freedom (DOF) (translations in the three nodal directions).

The SOLID 186 is a 20-node higher-order 3D solid element with quadratic displacement behavior. The element has 3 degrees of freedom per node: translations in the x, y, and z directions. It can support plasticity, hyper-elasticity, stress stiffening, creep, large deflection, and large strain capabilities. Deformation of almost incompressible elastoplastic and completely incompressible hyper-elastic materials can be simulated.

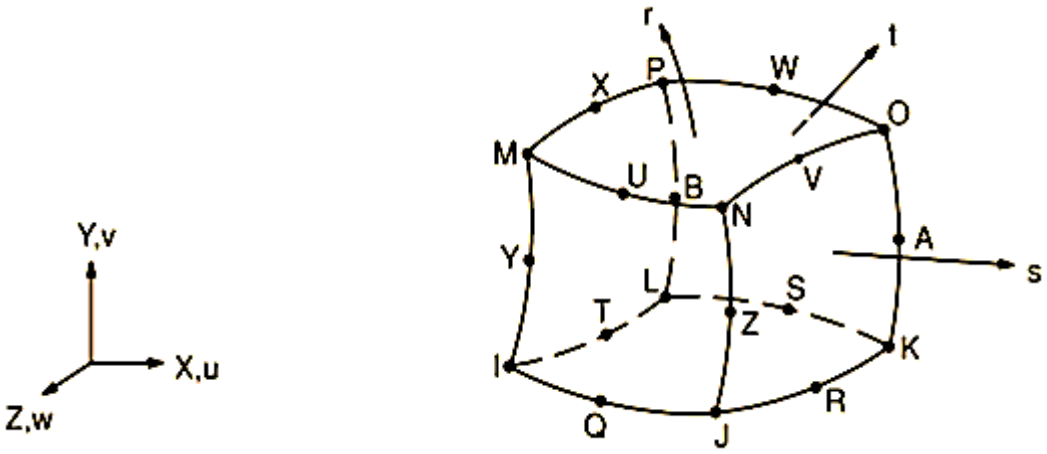

Figure 25. The element used for meshing the finite element models, adapted from [234].

II.3.3- Geometry and Finite element modelling

The representative volume element (RVE) used for the hybrid analysis has the form of a square cube. Due to the symmetry in geometry, loading, and boundary conditions, only one-fourth of the RVE's cross-section is modeled and studied. As one-fourth of the unit cell is used for FE modeling, the FE model consists of a cube with dimensions x=100 mm, y=100 mm, and z=10 mm, with an embedded one-fourth portion of continuous fiber (PALF, Palm, or Alfa fiber) of radius rf at one of the square cube's corners, which is the center of the tubular fiber, where the length of the fiber is taken as 10 mm. As a result, the analysis will be faster and computational time will be lowered.

The radius of the fiber is calculated for various weight percentages of the fibers. The weight percentages are converted into volume fractions. Four different volume fractions of fiber have

been studied for the analysis, ranging from 15% to 24% with an increment of 3% of the volume fraction of the fiber. Thus, the following (62) is obtained:

$$rf = \sqrt{\frac{Vf \times 100^2 \times 4}{\pi}} \tag{62}$$

Figure 26 gives an example of the converged mesh models of a composite at different volume fractions of natural fibers.

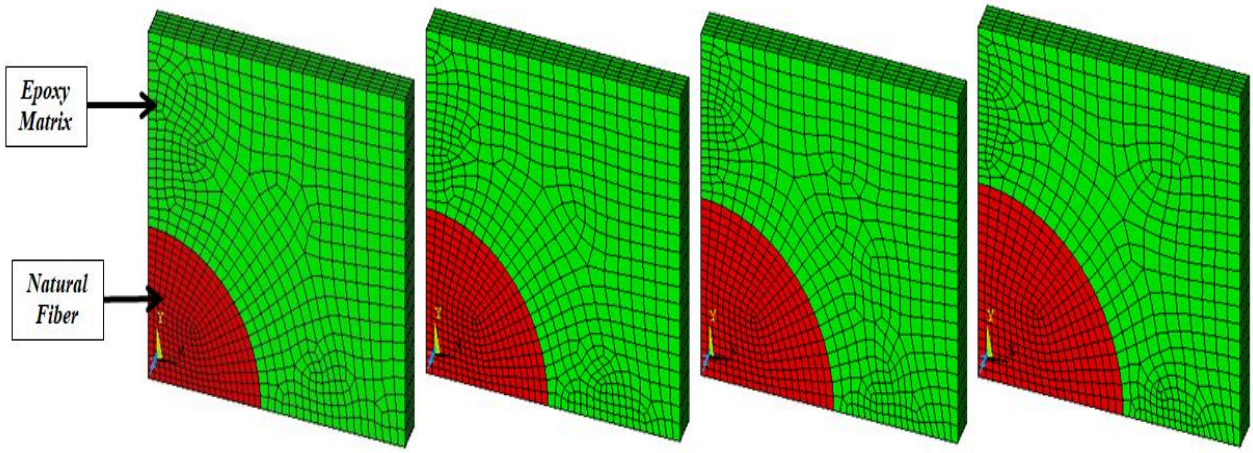

Figure 26. Converged mesh models of composite (RVE dimension) at: (a) 15 %; (b) 18 %; (c) 21 % and (d) 24 % of volume fraction of natural fibers.

II.3.4- Loading and Boundary conditions

The finite element model is subjected to boundary conditions that force it to behave as if it were a component of the entire array of composite materials. One-eighth of the unit cell is modeled in the analysis due to symmetry in loads, geometry, and boundary conditions. The mentioned symmetrical boundary conditions were applied due to the symmetry of the problem. An overlapped volume connection is used between the fiber and the matrix.

A uniform displacement load of 1 mm is applied to the face to establish a uniaxial state of stress in that direction, allowing the Young's modulus and Poisson's ratio of the resultant composite to be predicted using simple Hook's law. The uniaxial state of displacement on the surface z=10 mm is used to estimate longitudinal Young's modulus E_{11} and Poisson's Ratio v_{12}.

The area at x=100 mm is exposed to a uniaxial displacement condition to predict transverse Young's modulus E_{22}. A uniaxial stress condition is given to the area at y=100 mm to predict shear modulus G_{12}. In Figure 27 is possible to see the boundary conditions.

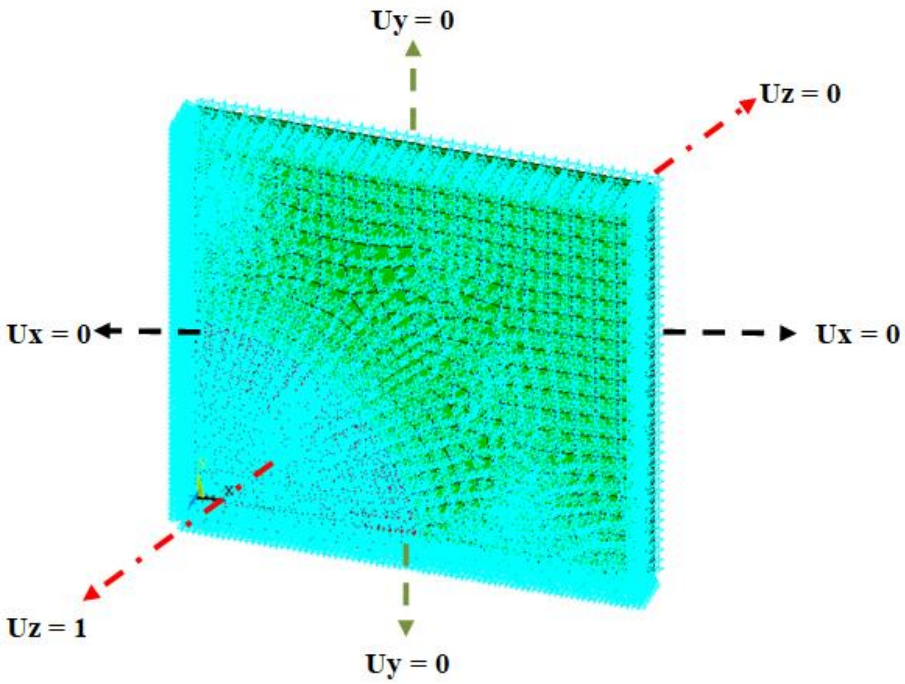

Figure 27. Loading and boundary conditions of the numerical model for predicting E_{11}.

A mesh convergence is performed on the longitudinal young's modulus of PALF at a 15% volume fraction to verify the accuracy of our findings. It's clear that we've arrived at a converged solution. The results of the FEA model are independent of mesh size.

The results of the convergence analyses based on changing the number of elements in the mesh are summarized in Figure 28.

For varied mesh sizes, Figure 28 illustrates a fairly similar study for: longitudinal Young's modulus E_{11}, Transverse Young's modulus E_{22} and shear modulus G_{12}. It demonstrates that the FEA model's results are unaffected by the number of elements in the mesh.

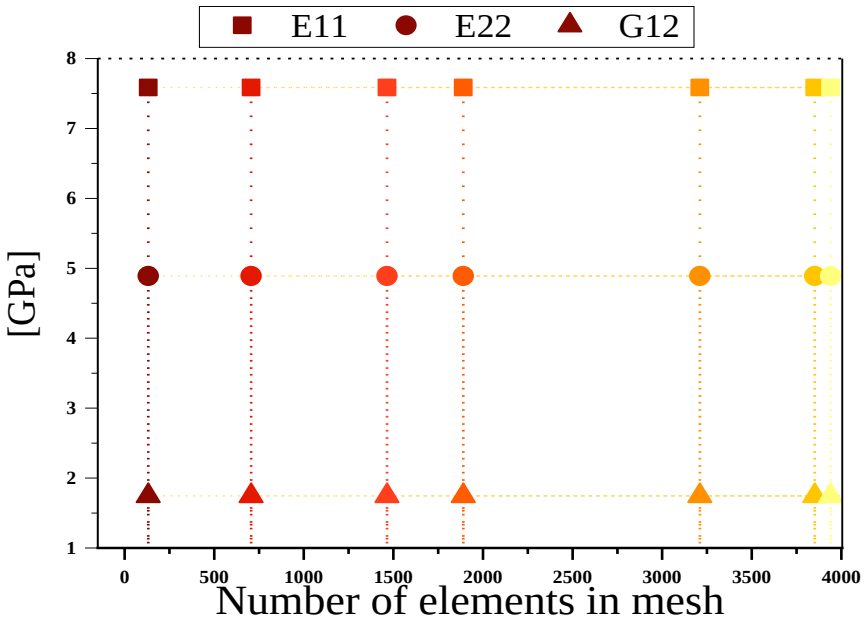

Figure 28. Mesh convergence analysis for finite elements of: E_{11}, E_{22} and G_{12} at 15 % of volume fraction of natural fiber.

By choosing a unit value of applied strain, and once the problem defined by the boundary conditions is solved, it is possible to compute the stress field σ_α, whose average gives the required components of the elastic matrix, one column at a time, as:

$$C_{\alpha\beta} = \bar{\sigma}_\alpha = \frac{1}{V}\int_V \sigma_{\alpha(x_1,x_2,x_3)dV} \quad \text{with} \quad \epsilon^0_\beta = 1 \tag{63}$$

Where: $\alpha, \beta = 1$. The integral sin (63) is evaluated within each finite element using the Gauss-Legendre quadrature. Commercial programs, such as ANSYS®, have the capability to compute the average stress and volume ,element by element [235].

For the elastic domain:

$$W = \int_0^\varepsilon \sigma d\varepsilon = \frac{1}{2}\sigma\varepsilon = \frac{\sigma^2}{2E} \tag{64}$$

III.4- RESOLUTION PROCEDURE

Flowchart 1 illustrates an elaborate depiction of the analytical (mathematical formulation-Chapter II) and numerical (Finite Element Method) methodologies employed to assess the mechanical properties of the fiber-based biocomposite treated in this work. These two

methodologies were carried out using MATLAB and ANSYS 18.1 software platforms, respectively.

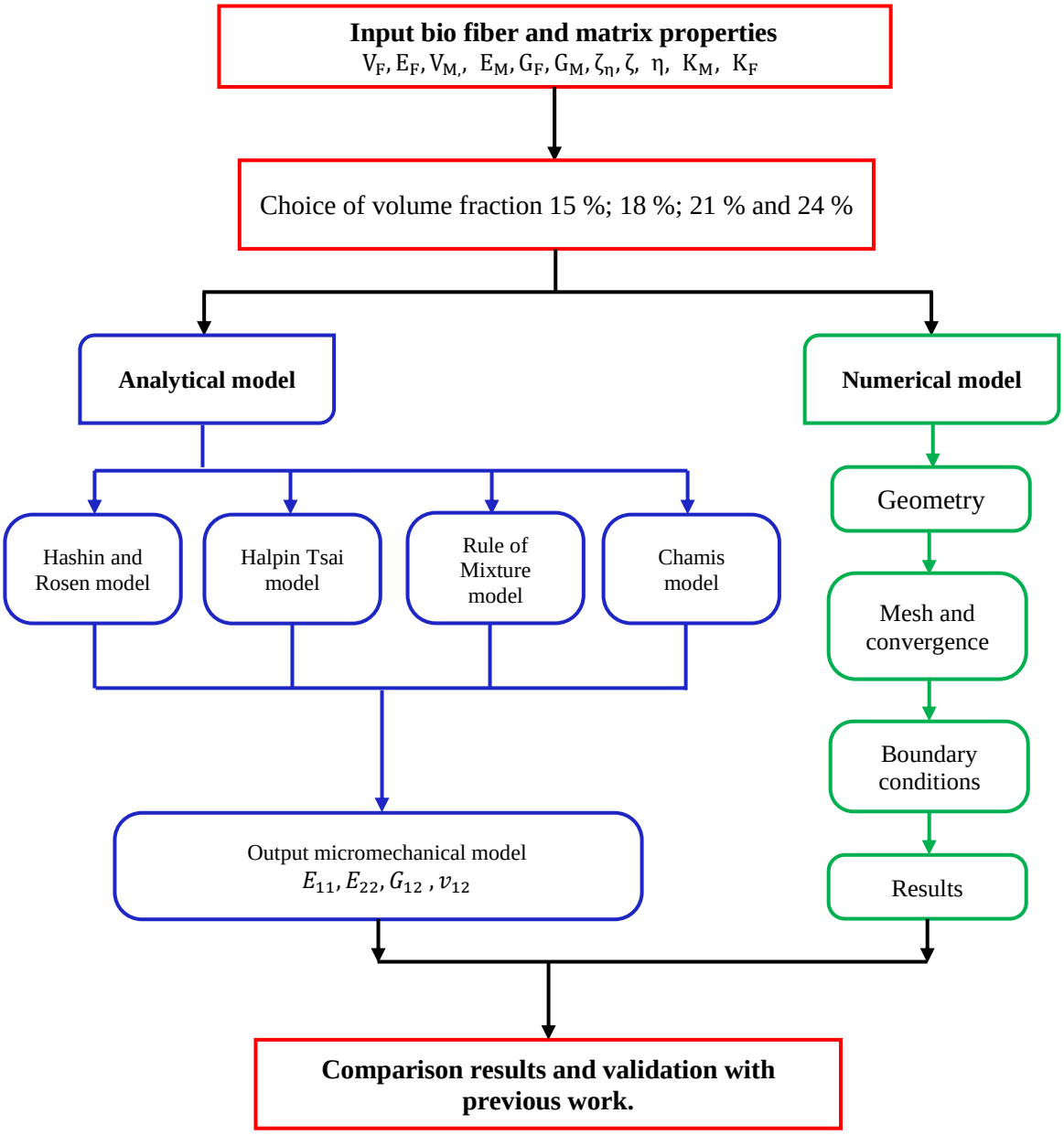

Flowchart 1. Micromechanical properties estimation steps.

III.5- RESULTS AND DISCUSSION

The results of the analytical models developed for the fiber reinforced composite are compared to the experimental results for the PALF/epoxy unidirectional composite from Rakesh's study [1], as shown in figures below.

The predicted results for all the analyzed models agree with the experimental data for composites (PALF/epoxy) with varying volume fractions. To characterize the tensile properties,

unidirectional composite specimens were manufactured according to the necessary standard. The specimens were 160, 12.5, and 3 mm in size, respectively. For each volume fraction of the fiber, five identical samples were manufactured, and all specimens were examined using an electronic tensometer at a strain rate of 0.5 mm/min. Single fiber testing was used to characterize the PALF fiber's tensile modulus according to the ASTM D3379 standard. A total of 23 specimens were evaluated in order to obtain an exact figure for the PALF fiber's property [1].The composites' longitudinal Young's modulus increases as the volume fraction of fiber rises, As can be shown in Figure 29.

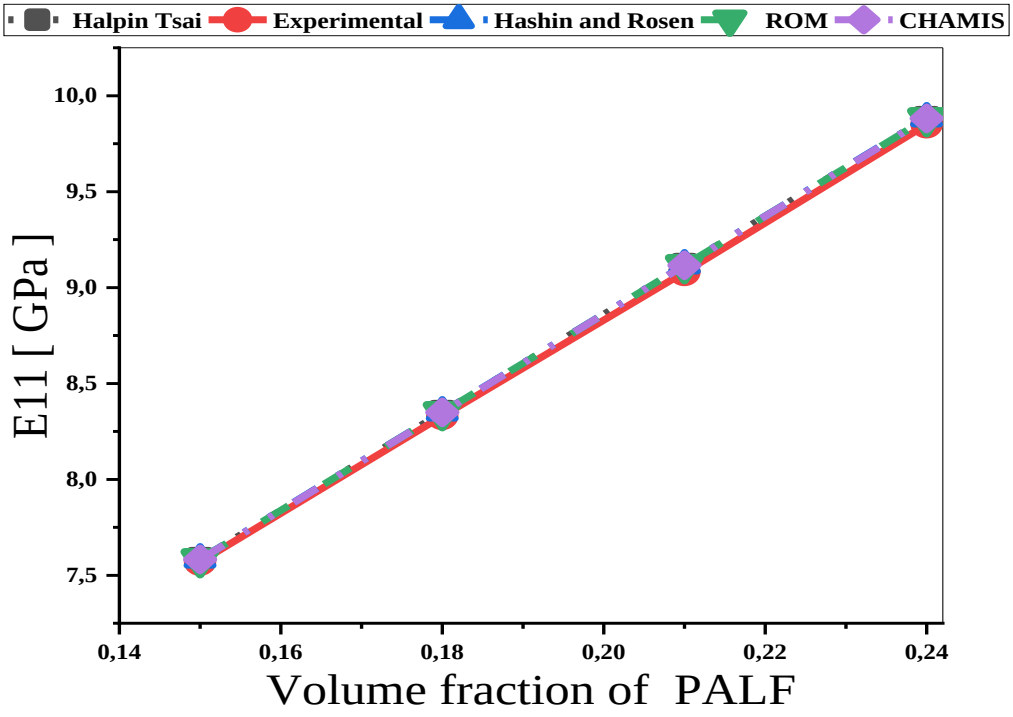

Figure 29. Comparison (analytical vs. experimental) of Longitudinal Young's modulus E_{11} of PALF/epoxy in terms of volume fractions.

Figure 30 shows that the transverse young's modulus E_{22} of composites increases along with the volume fraction of fiber, but the increment is lower when compared with the magnitude of E_{11}. The closest agreement with the experimental results belongs to Halpin Tsai model.

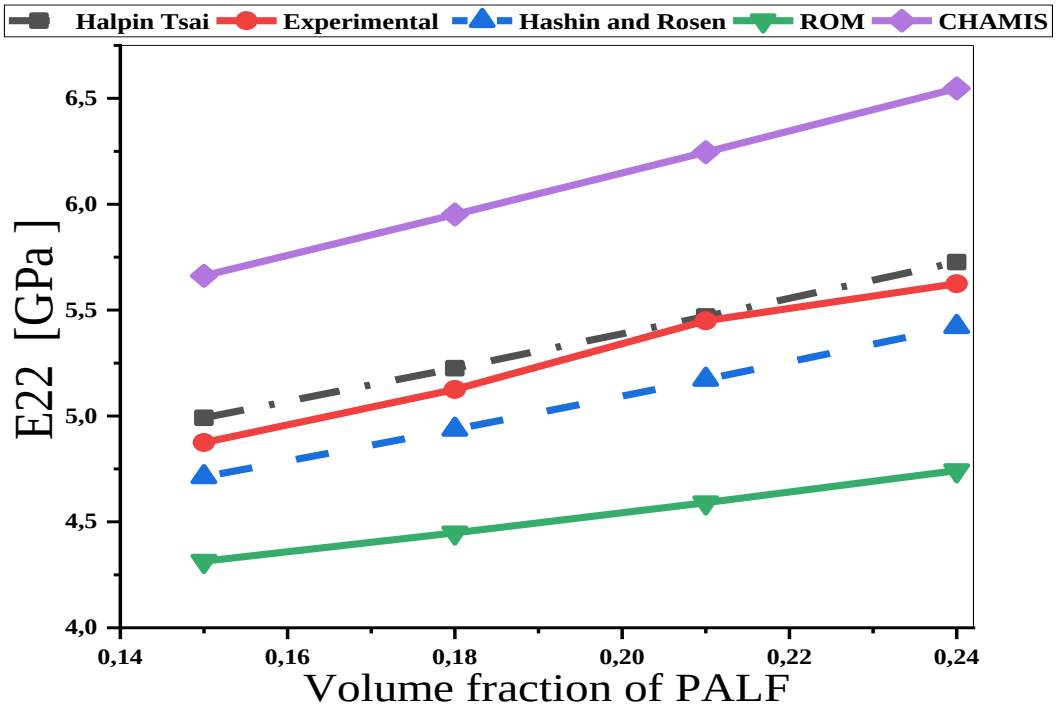

Figure 30. Transverse Young's modulus E_{22} of PALF /epoxy in terms of different volume fractions of fiber.

The analytical analysis results are compared to the experimental data in Figure 31. When compared to experimental data, the results generated by the analytical model of Chamis offer remarkably similar results.

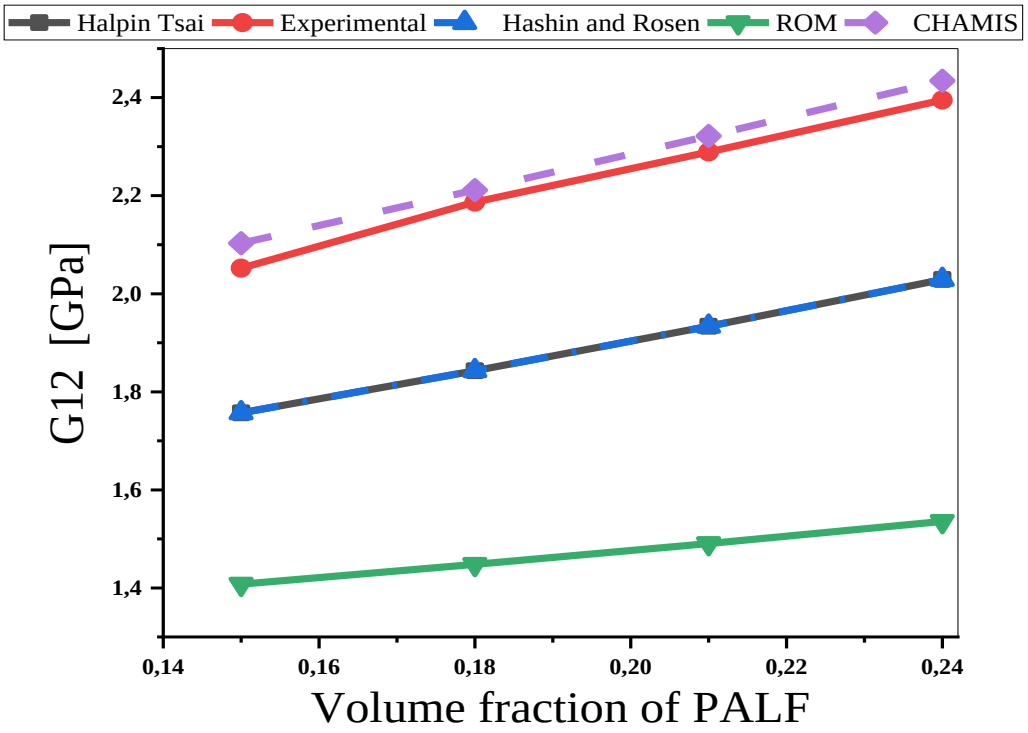

Figure 31. The comparison of shear modulus G_{12} of PALF/epoxy in terms of volume fractions.

It's well noticed that the predicted values of the Poisson's ratio υ_{12} for all tested models are in good agreement; this is illustrated in Figure 32.

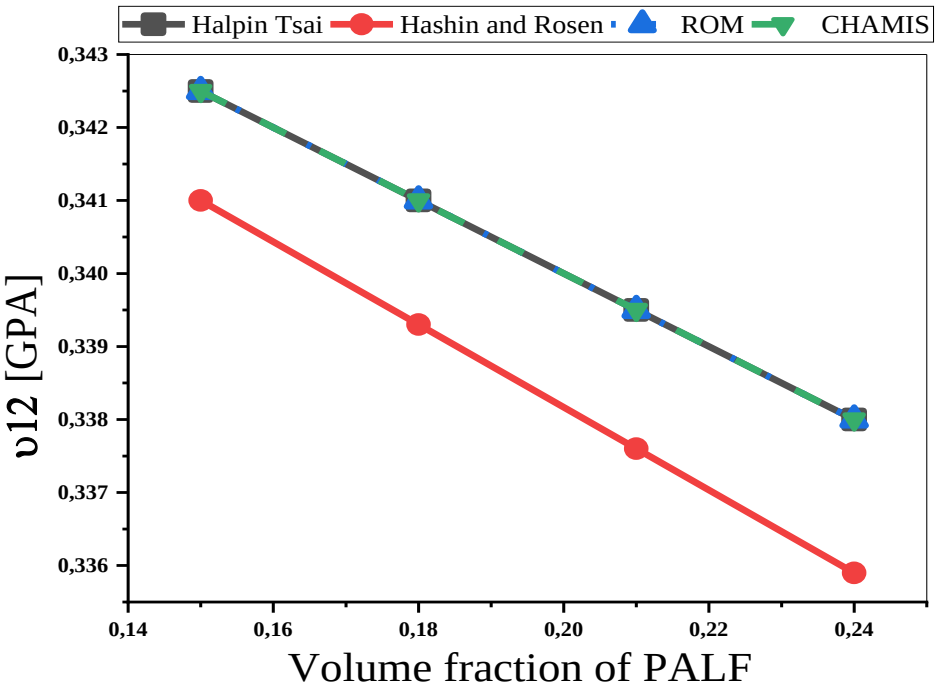

Figure 32. The Poisson's ratio of PALF/epoxy in terms of V_F.

The first analytical part permitted to select the analytical method that allows us to have mechanical properties that best converge with the experimental results. To forecast E_{11} and E_{22}, the Halpin-Tsai approach was chosen. For G_{12}, it is Chamis, and for υ_{12}, it is ROM. A FEM approach is established and compared with the results of the analytical analysis in order to strengthen our prediction.

The variation of E_{11} and E_{22} as a function of the volume fraction of natural fibers, obtained by Halpin-Tsai and numerical analysis.

For all composites with varied V_F, the predicted results of FEM for E_{11} are in agreement with the analytical results. These examples are depicted in Figure 33. The prediction of the longitudinal modulus show that the composite based on PALF fibers presents the best behavior in tension.

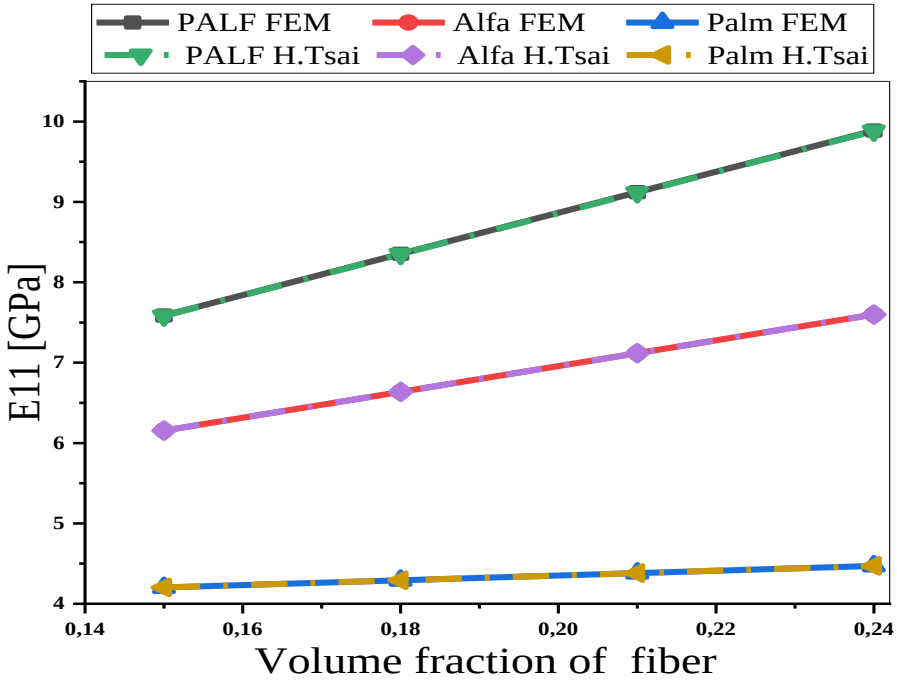

Figure 33. Predicted analytical (Halpin-Tsai model) and numerical results for E_{11} in terms of V_F.

The FEM anticipated results are in good correlation with the analytical results. Figure 34 shows a comparison of the results obtained for E_{22} using the FEM and the analytical analysis. The prediction of the transverse modulus show that the composite based on PALF fibers presents the best behavior in compression.

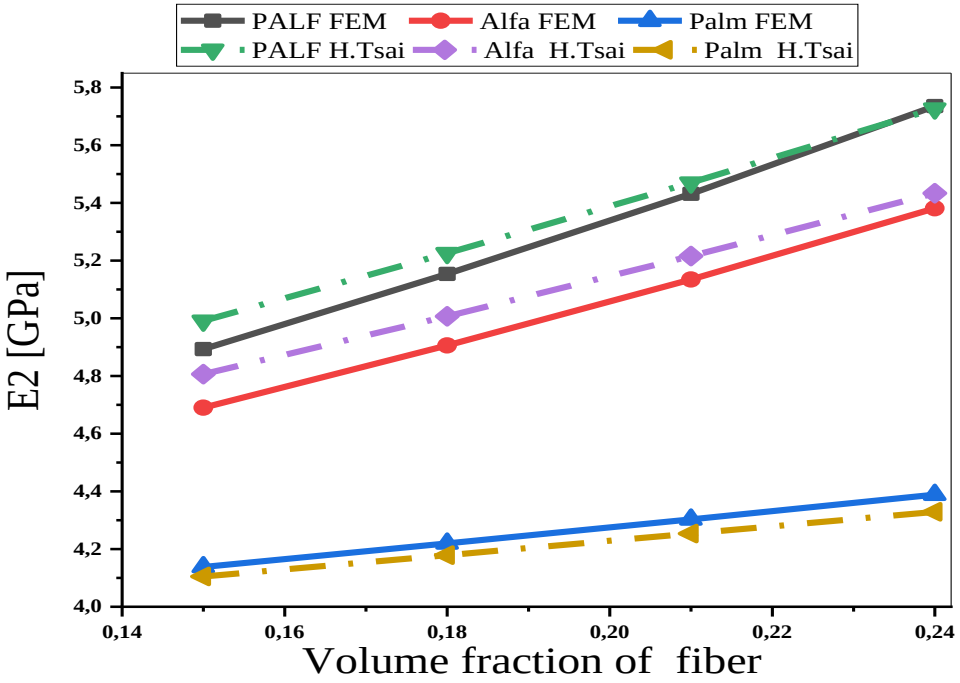

Figure 34. Predicted analytical (Halpin-Tsai model) and numerical results for E_{22} in terms of V_F.

Chamis and numerical analysis were used to determine the variation of G_{12} as a function of the volume fraction of natural fiber. When compared to analytical results, the numerical approach of finite element analysis yields good results this can be found in Figure 35. The prediction of the shear modulus show that the composite based on PALF fibers presents the best behavior in shear.

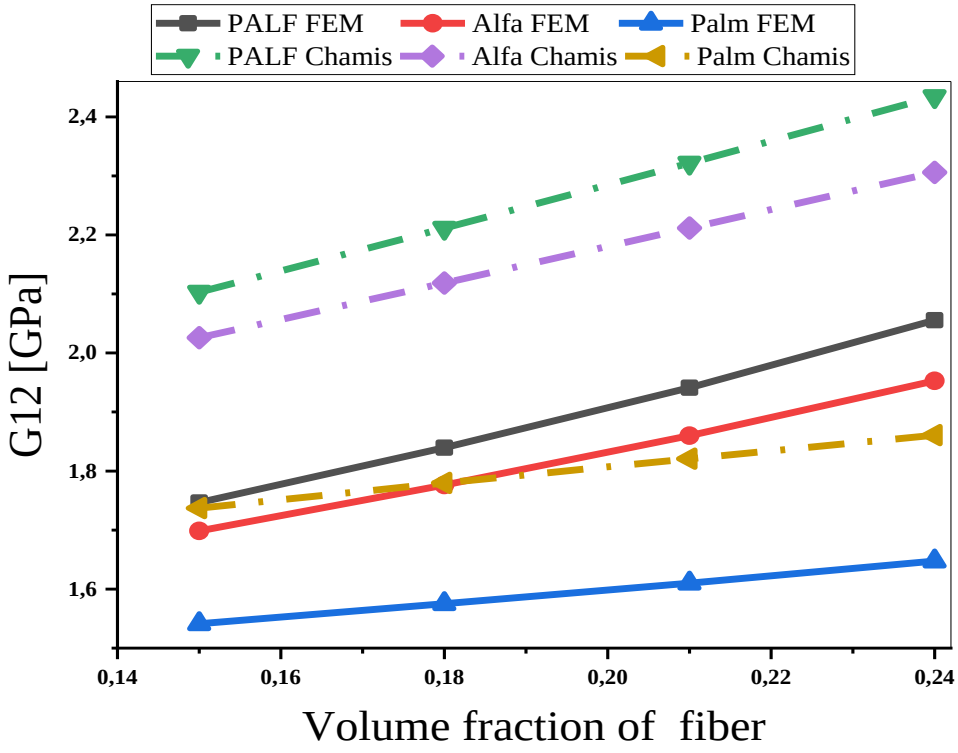

Figure 35. Predicted analytical (Chamis model) and numerical results for Shear Modulus G_{12} in terms of V_F.

Concerning the major Poisson's ratio, the results were obtained only from the ROM model and the FEM. Concerning the Poisson's ratios, the obtained results of the analytical models shows that the Alfa/epoxy has the highest Poisson's ratio compared to PALF/epoxy and palm/epoxy.

Figure 36 shows that for the major Poisson's ratio ν_{12}, all analytical and numerical models correlate well with each other.

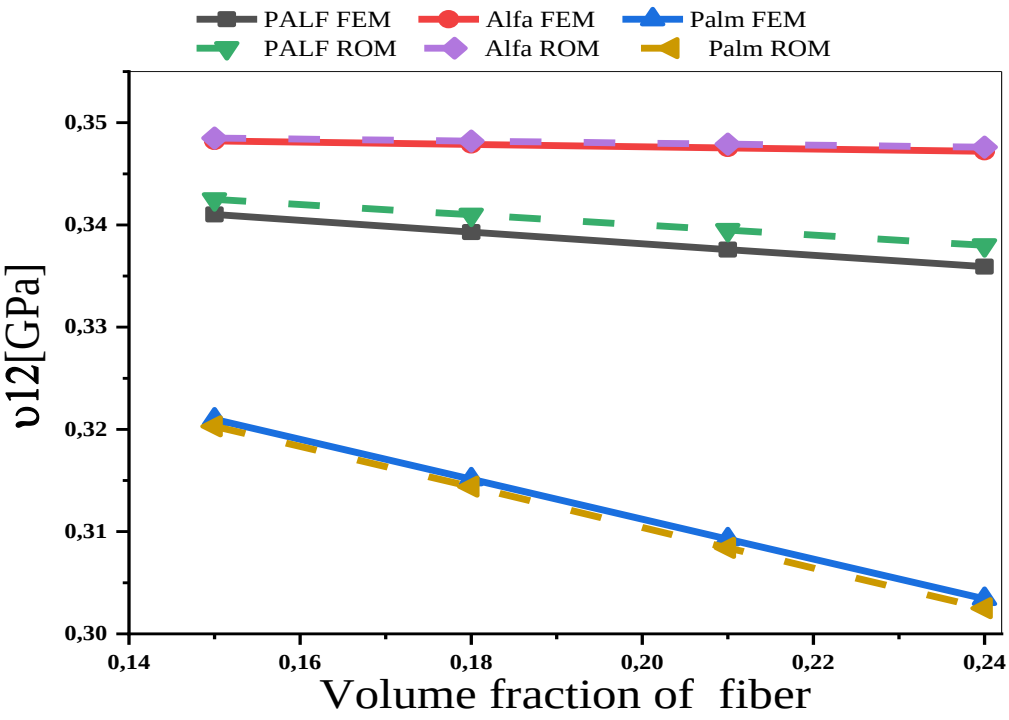

Figure 36.Predicted analytical (ROM model) and numerical results of Poisson's ratios v_{12} in terms of V_F.

III.6- CONCLUSION

In this study, the analyzed results for the elastic properties of the analytical micromechanical models, as well as FE modeling methods, are compared to available experimental data for PALF/epoxy composite. It should be noted that the cases studied include three different kinds of natural fiber-reinforced composites: PALF, date palm fiber, and Alfa fiber. The analytical micromechanical models are based on four theories which are Halpin-Tsai, Chamis, Hashin vs. Rosen and ROM.

It is observed that the change in volume fraction of fiber has a significant effect on elastic properties.

In this study, the micromechanical approaches are used to predict the mechanical properties of bio skins layers based on PALF (Pineapple leaf fiber), date palm and Alfa fibers at different volume fractions. The influence of volume fraction of reinforcement on Young's and shear Modulus and Poisson's ratios is studied.

In this order, a micromechanical analytical and FEM models are developed with MATLAB 8.3 and ANSYS 18.1 software. The analytical micromechanical models are based on four theories

which are: Halpin-Tsai, Chamis, Hashin vs. Rosen and ROM. The FEM used four RVE depending on volume fraction of natural fibers.

The analyzed results of the models developed for the elastic properties are compared to available experimental data for PALF/epoxy composite.

Summing up the results, it can be concluded that:

- It is observed that the change in volume fraction of fiber has a significant effect on elastic properties.
- The Young's modulus rises in tandem with the reinforcement weight percentage.
- The Poisson's ratio decreases as the weight fraction of reinforcement increases.
- The Shear modulus is calculated using the analytical expression and it is also increasing along with the reinforcement.
- The analytical results of mechanical properties $E_{11}, E_{22}, G_{12}, \nu_{12}$ compared with the experimental results and it is found that the analytical results are in good agreement.
- The analytical micromechanical models permitted us to select the suitable theory that allows us to have mechanical properties of PALF fibers that best converge with the experimental results. To forecast E_{11} and E_{22}, the Halpin-Tsai approach was chosen. For G_{12}, it is Chamis, and for ν_{12}, it is ROM.
- The suitable theory was used with the FEM model, to predict the mechanical properties of skins layers based on: PALF, date palm and Alfa fibers, where the results are in efficient accord.
- The present work shows the successful prediction of elastic properties of composites by Finite Element Analysis.
- The prediction of the elastic properties of the three fiber-based eco-composites showed a dispersion in terms of stiffness, where the composite based on PALF presents the best behavior in tension, compression, and shear because of its mechanical properties, followed by the composite based on Alfa fibers, and finally that based on Palm fibers.

CHAPTER IV:

MACROMECHANICAL ANALYSIS

CHAPTER IV: MACROMECHANICAL ANALYSIS

IV.1- INTRODUCTION

This part of our contribution focuses on the analysis of the response of eco-sandwich element with natural skins, compared to traditional sandwich. The item in question has a stacking sequence $[-\emptyset/+\emptyset/$ core $/+\emptyset/-\emptyset]$. The analytical model is based on the sandwich laminated plate theory (SLPT).

IV.2- MATERIALS AND PROPERTIES

IV.2.1- Skin materials

Through this macromechanical analysis, different biomaterials were used for the skin part, based on PALF, Alfa, Jute and Palm natural fibers. Glass/epoxy is chosen for the traditional sandwich. All the material properties cited before are presented in Table 7.

IV.2.2- Core material

The APC-2 PEEK was selected as the core for the eco-sandwich composite based on the literature. The APC-2 composites of Cytec Engineered Materials have a thermoplastic polymer matrix known as PEEK. With a glass transition temperature of 143°C, the polymer is semi-crystalline. Due to the semi-crystalline form of the polymer, composites can be employed in lightly loaded applications at temperatures up to 260°C [236]. Table 7 presents the material properties of the APC-2 PEEK.

We note that: E, G and ν are the usual elastic modulus, shear modulus, Poisson's ratio; X, Y are tensile or compressive strengths (subscripts 't' and 'c').

Table 7. Mechanical properties of the constituents [36].

Properties	E_x ***[MPa]***	E_y ***[MPa]***	ν_{xy}	G_{xy} ***[MPa]***	X_t ***[MPa]***	X_c ***[MPa]***	Y_t ***[MPa]***	Y_c ***[MPa]***	SI ***[MPa]***
Glass/epoxy	40000	10000	0.32	4950	2000	750	60	160	200
Jute/epoxy [237]	1250	5633	0.3395	7240	55	55	62	62	27.5
Palm/epoxy	4153.6	4080.7	0.322	1351.6	-				
Alfa/epoxy	5993	4721.4	0.348	1682.7					
PALF/epoxy	7327	4888.7	0.343	1729.7					
Core APC-2 PEEK [236]	4100		0.41	2252.7					

The geometric model used under Matlab software contained three main elements: the two skins (upper and lower skins) and the core as shown in schematic view (Figure 37).

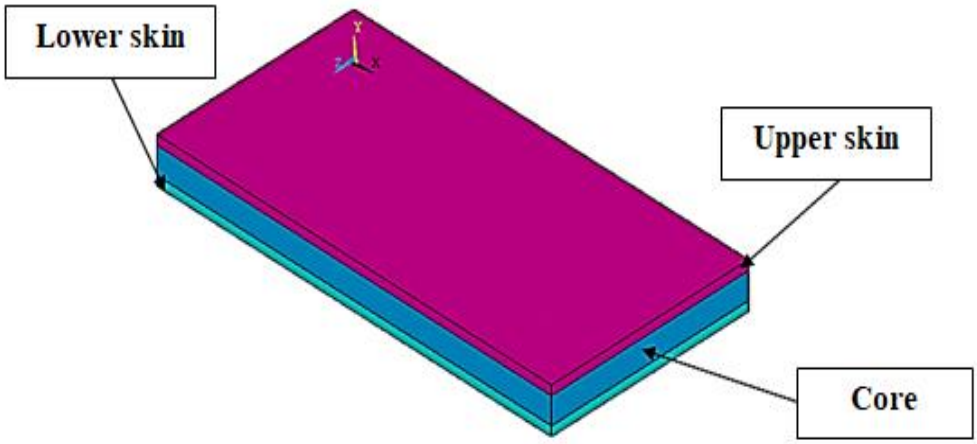

Figure 37. Geometrical model.

IV.3- RESOLUTION PROCEDURE

The approach for macromechanical analysis regarding the behavior of an element of the tubular sandwich structure under biaxial loading, simulating the internal pressure exerted is presented by Figure 38.

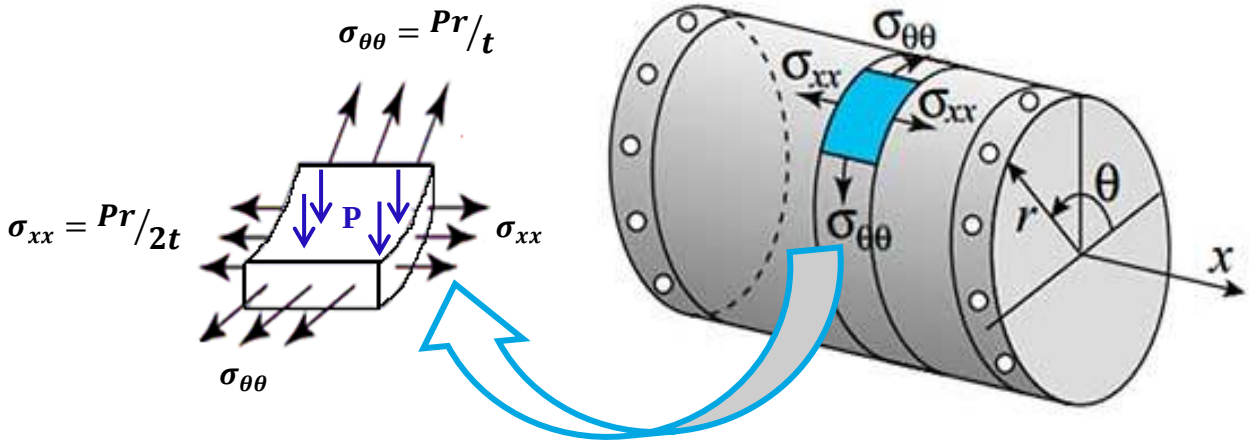

(a) Stratified element under axial and transverse loading.

(b) Representation of axial and hoop stress of multilayered pipe.

Figure 38. Macromechanical approach of multilayered tubular structure under pressure.

The developed macromechanical model adheres to the law of laminates with transverse shear effects, excluding bending. This model, seen in Flowchart 2, was constructed using MATLAB. Furthermore, failure analysis was conducted for the skin parts, employing the Tsai-Wu criterion.

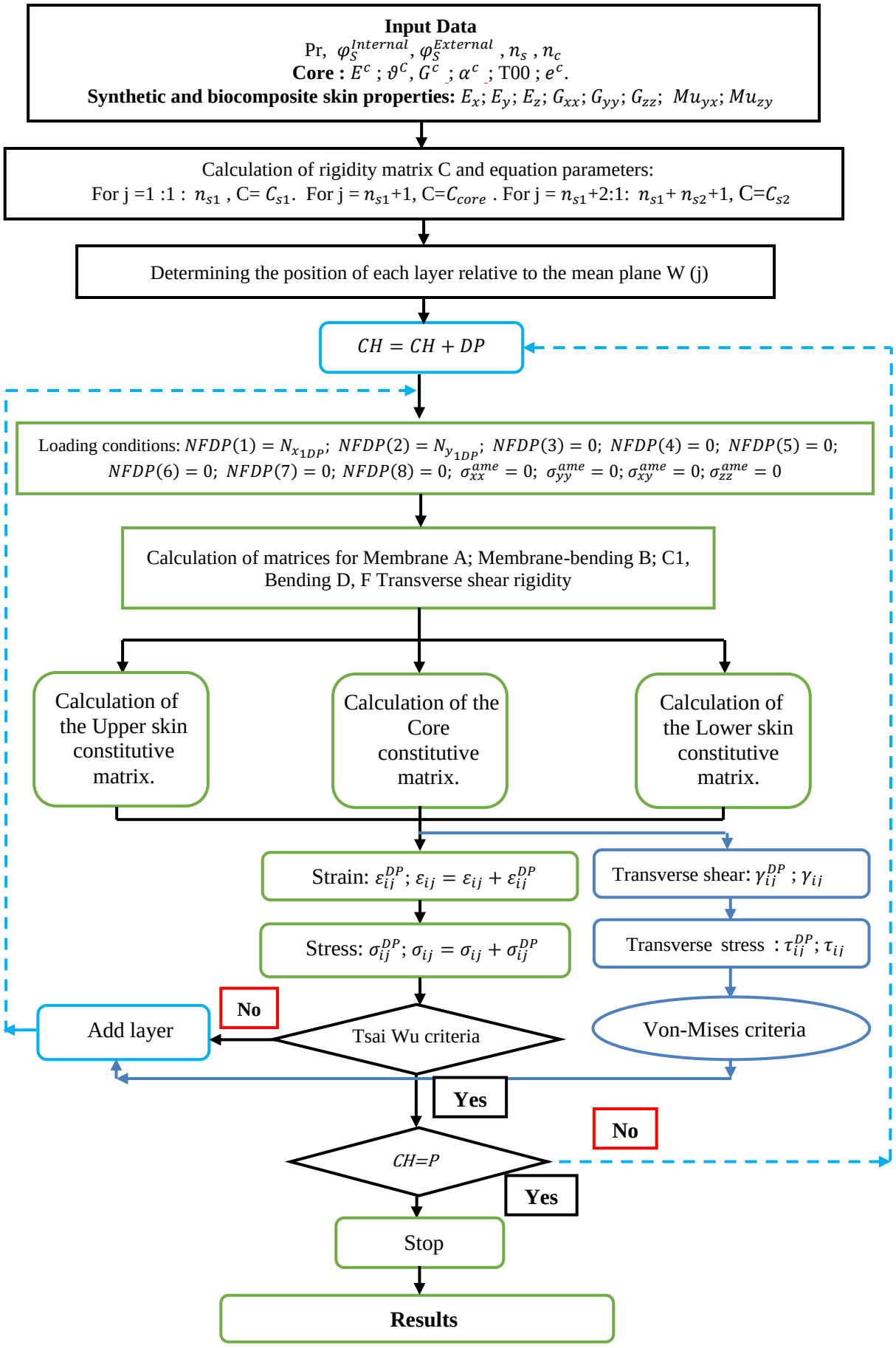

Flowchart 2. Macromechanical steps calculation.

IV.4- RESULTS AND DISCUSSIONS

The results of the analytical models developed are presented and discussed in this section.

The symmetrical configuration of the sandwich influenced the magnitude of the stresses and strains, which is similar to that of laminate behavior due to the similarity of the constitutive equations between the two theories for this type of stacking.

IV.4.1- Stress analysis in Plate plan X-Y

The distributions of longitudinal σ_{xx} and transversal σ_{yy} stresses across the thickness of the sandwich element for a composite made of Glass/epoxy synthetic fibers and biocomposites are illustrated in Figure 39 and Figure 40. Figure 41 illustrates the symmetrical shear stress σ_{xy} distribution across the thickness of the sandwich elements, with the core part neglected.

As a general remark, the stress distribution reflects the conditions imposed by the theory of sandwich plates, where the longitudinal, transverse, and shear stresses are zero in the core part. The magnitude of the transverse stresses is twice the magnitude of the longitudinal stresses, aligning perfectly with the distribution of axial and circumferential stresses observed in a pressurized tube.

The material properties play a crucial role in the response of sandwich plates to bi-axial loading.

The results of the longitudinal σ_{xx} , transversal σ_{yy} and shear σ_{xy} stresses of the stratified sandwich reveal a discontinuity of stress between the skins and the core component.

The primary observations drawn from the stress distributions across the thickness of the sandwich plate can be summarized as follows:

- The stress distribution is nearly symmetrical with respect to the mid-plane.
- The effect of stacking sequence is almost negligible for palm and Alfa fiber-based materials.
- Access to data regarding tensile, compressive, and shear rupture limits is essential for determining the rigidity of each material analyzed during this macromechanical approach.
- Due to the significant magnitude of the shear modulus, the jute/epoxy material exhibits a different behavior compared to the materials treated during the distribution of longitudinal and shear stresses.

- It is observed that the second layer of the lower skin and the first layer of the upper skin record higher stresses compared to the other layers.
- The increase in pressure within the composite tube can lead to the initiation of micro cracks at the levels of the most stressed layers.

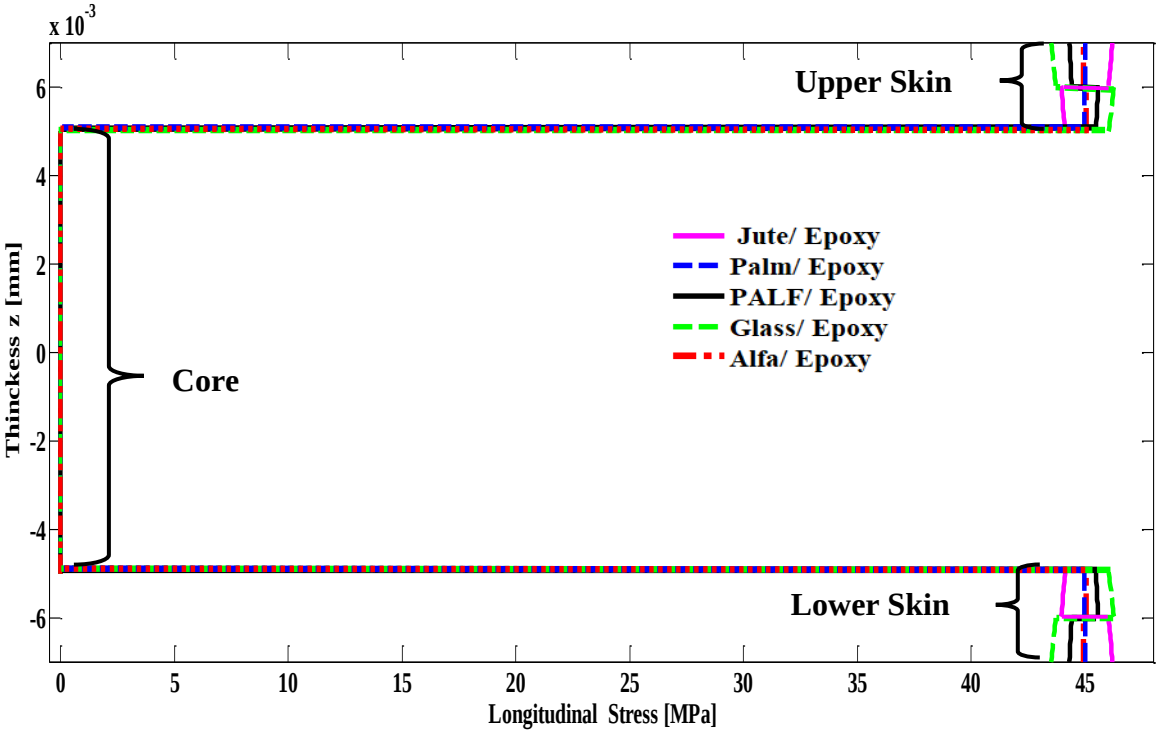

Figure 39. Variation of longitudinal stress across the thickness of the sandwich for five bi-directional types of layering materials.

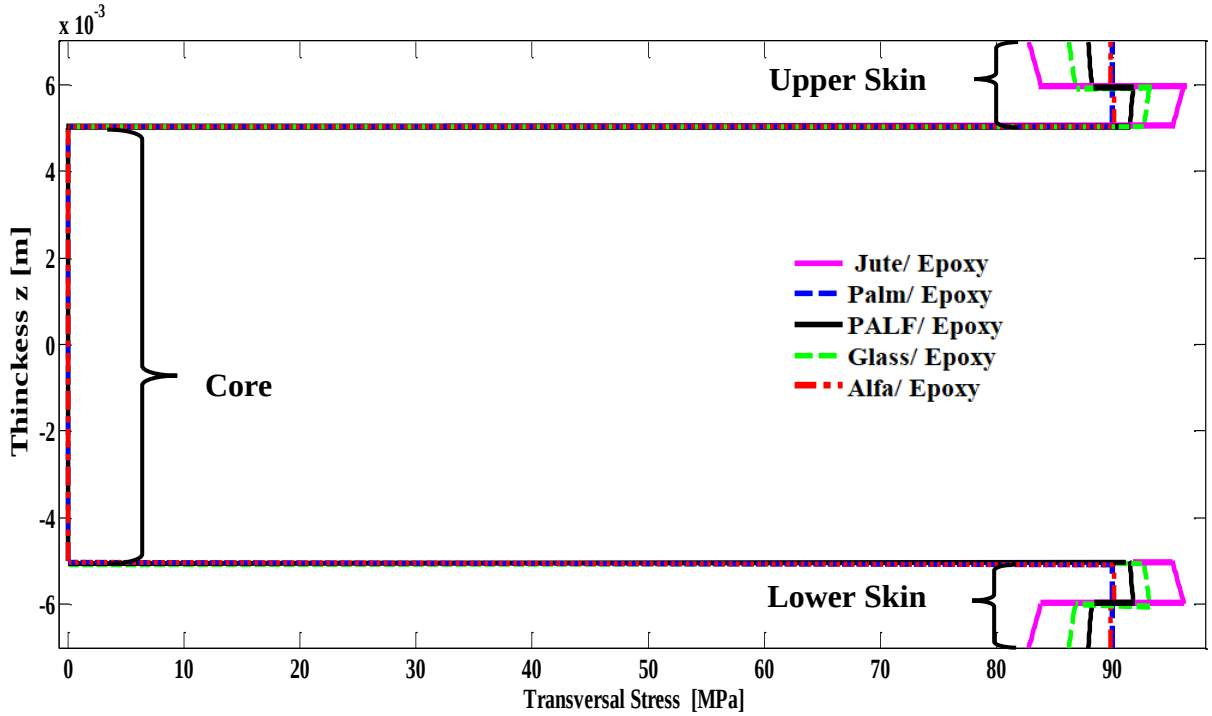

Figure 40. Variation of transversal stress across the thickness of the sandwich for five bi-directional types of layering materials.

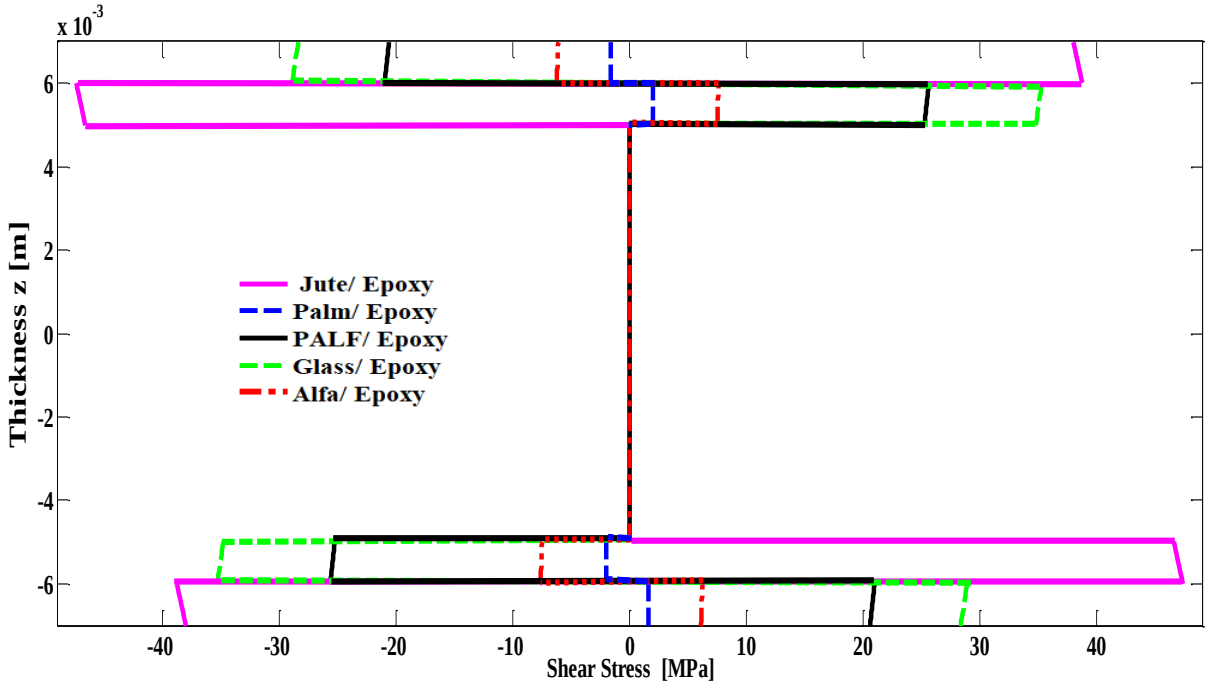

Figure 41. Variation of shear stress across sandwich thickness for five bi-directional laminated materials.

IV.4.2- Stress analysis in the fibers plane L-T

The distribution of stresses in the fiber plane through the thickness of the sandwich panel is depicted in Figure 42, Figure 43, and Figure 44 for two materials: synthetic Glass/epoxy and

biocomposite Jute/epoxy. The mechanical properties directly influence the magnitude of the longitudinal σ_L, transverse σ_T and shear τ_{LT} stresses.

In the longitudinal direction within the fiber plane, Glass/epoxy is more sensitive to bidirectional loading applied to the sandwich panel compared to Jute/epoxy. It is observed that the ultimate tensile strength in the longitudinal direction is approximately 2000 MPa for Glass/epoxy and 55 MPa for Jute/epoxy (refer to Table 7). The stress magnitudes obtained and depicted in Figure 42 show that any increase in pressure can be detrimental to Jute/epoxy, based on the maximum stress criterion.

For the distribution of transverse stresses, shown in Figure 43, Jute/epoxy is characterized by a stress magnitude of around 98 MPa within the surface layers, potentially leading to damage initiation, given that the ultimate tensile strength in the transverse direction Y_t is approximately 62 MPa. On the other hand, Glass/epoxy is found in a safety zone in the transverse direction.

For the distribution of shear stresses, Jute/epoxy records a stress magnitude of around 45 MPa, which exceeds its S_I shear limit estimated at 27.5 MPa, thereby leading to damage. Conversely, the Glass/Epoxy composite provides more security for the plate under such biaxial loading conditions, with a shear rupture limit of 200 MPa.

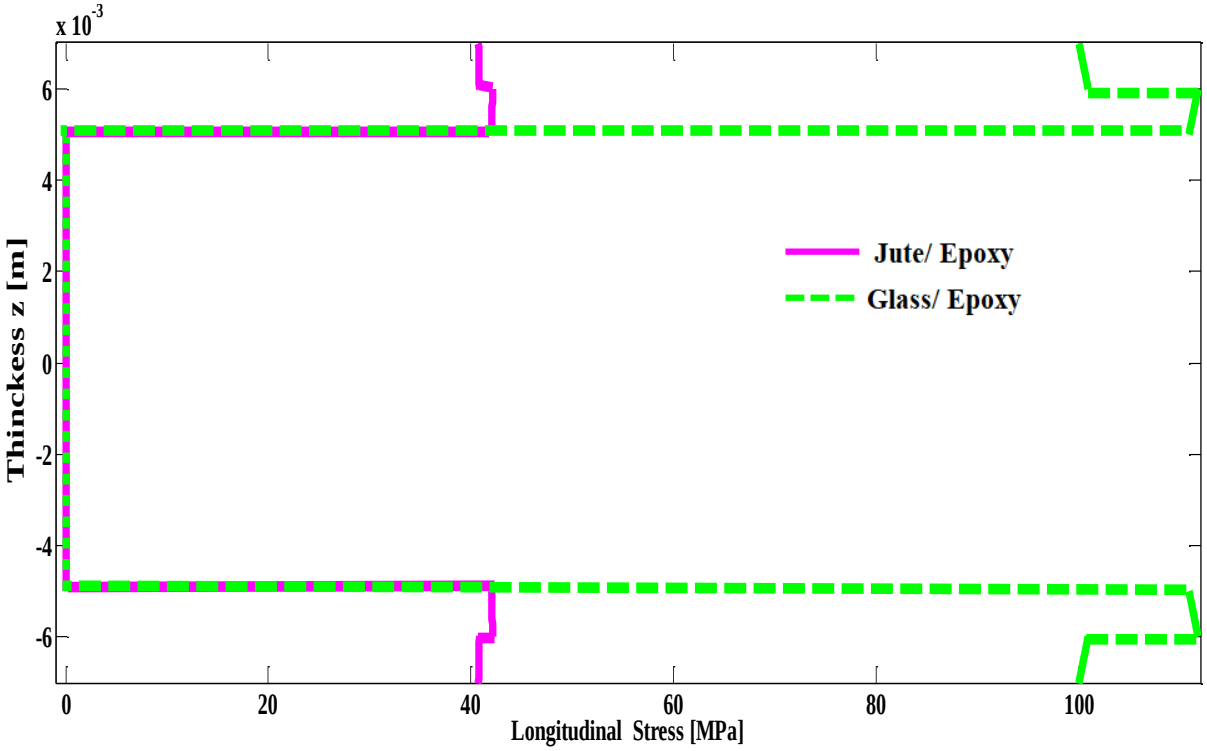

Figure 42. Variation of longitudinal stress σ_L within the fiber plane across the thickness of the sandwich.

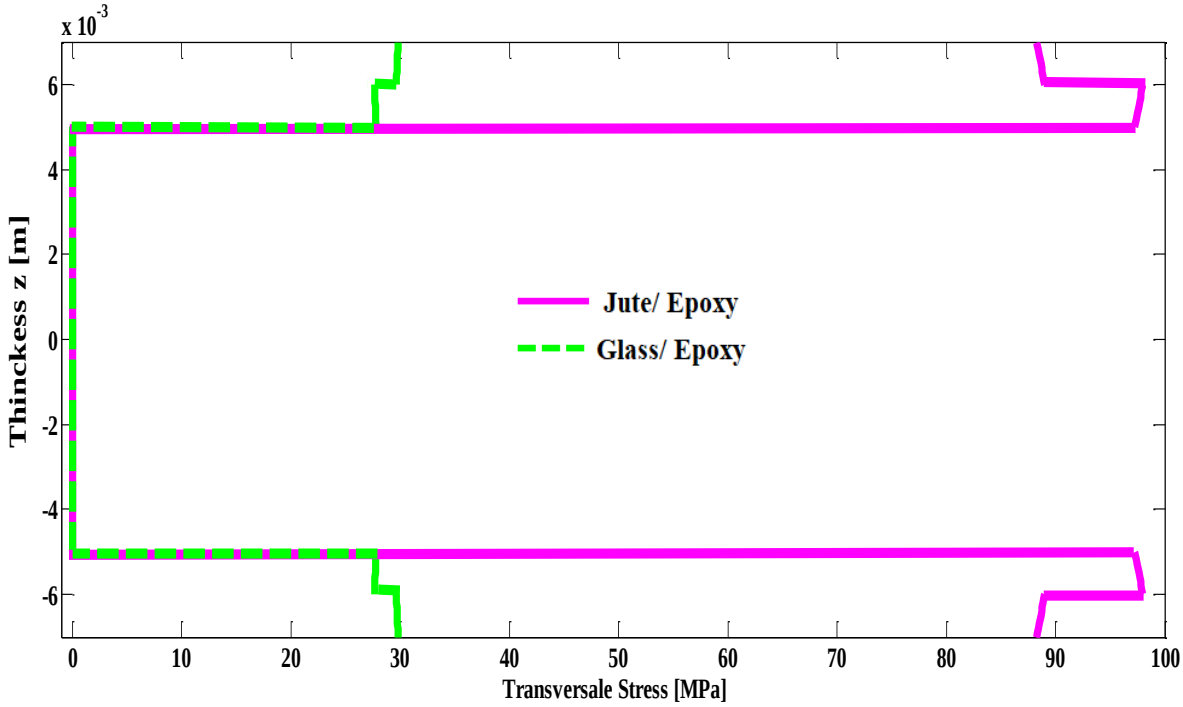

Figure 43. Variation of transverse stress σ_T within the fiber plane across the thickness of the sandwich.

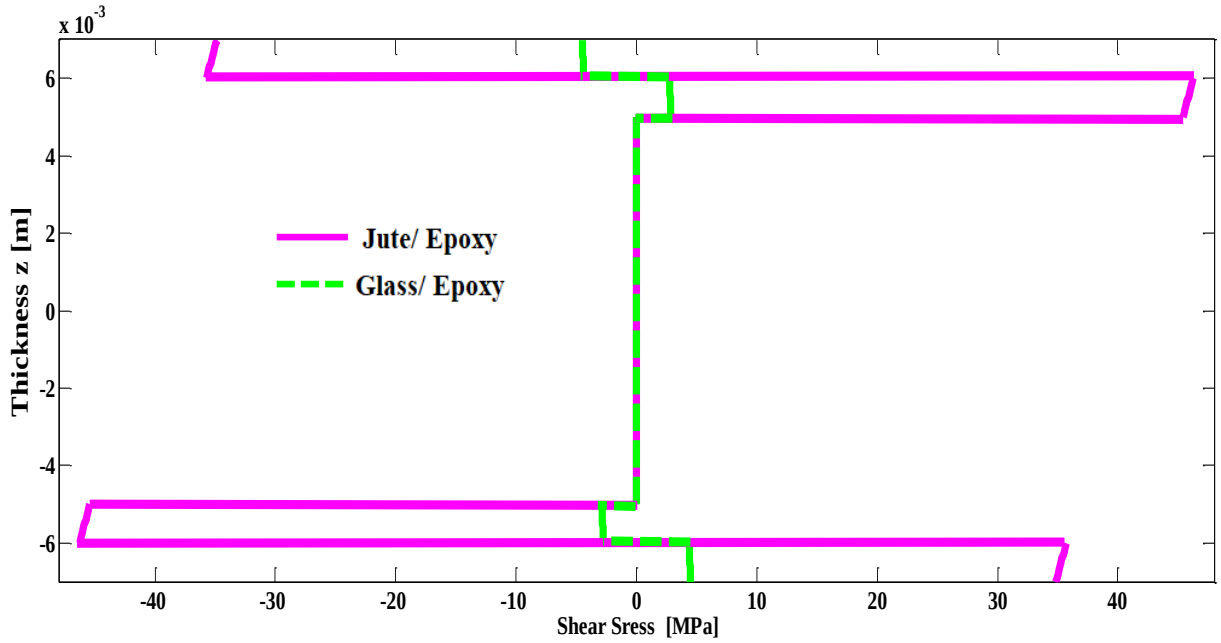

Figure 44. Variation of shear stress τ_{LT} within the fiber plane across the thickness of the sandwich.

IV.4.3- Failure Analysis

Due to a lack of data, the failure analysis was limited to only two materials: the synthetic Glass/Epoxy and the biocomposite Jute/Epoxy. Figure 45 presents the variation of the Tsai-Wu criterion as a function of the increment of the internal pressure. The latter is represented by the axial and transverse stresses applied to the sandwich plate sample.

Both trends accurately represent the rigidity of each material. To reduce the gap, which is evaluated at 78.87%, and enhance the stiffness of the biocomposite, it is essential to simultaneously increase the number of layers in both the lower and upper skins.

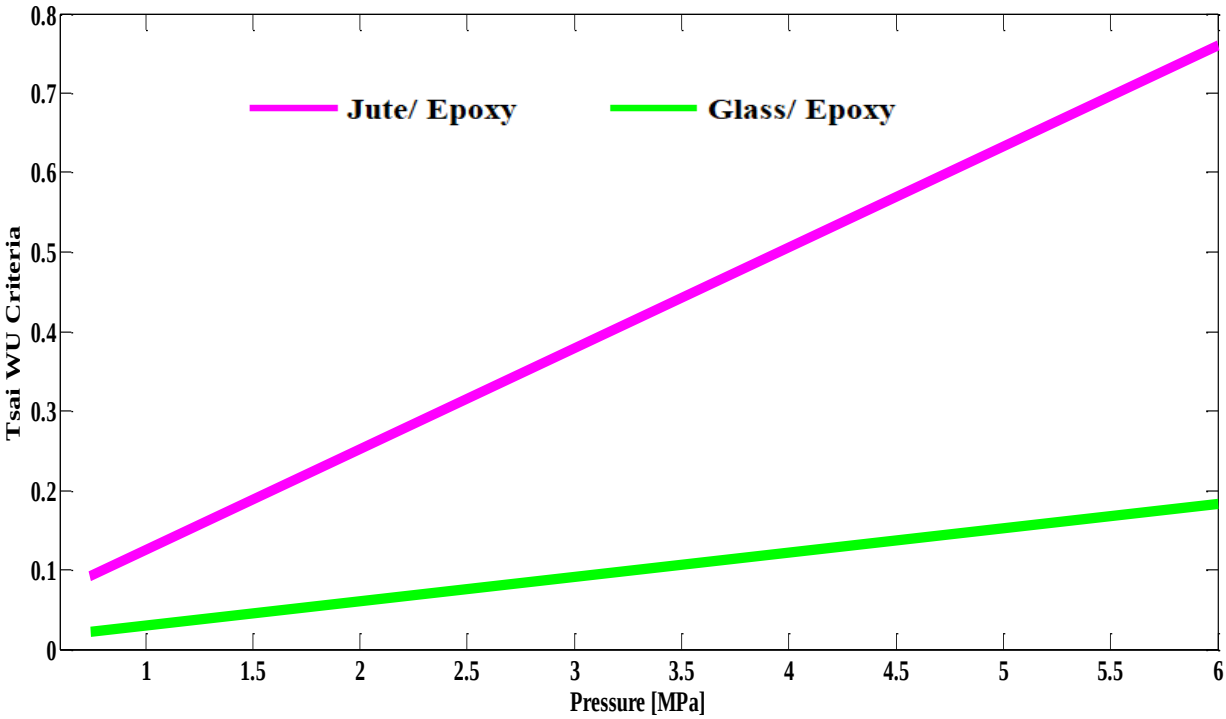

Figure 45. Variation of Tsai Wu criteria regarding pressure for skin components.

IV.5- CONCLUSION

- The aim of the macromechanical chapter is to understand the response of a tubular structure's sandwich element under pressure by developing an analytical model for evaluating the distribution of stress through the thickness of the sandwich plate, considering a stacking sequence configuration of : $[-\emptyset/+\emptyset/\text{core}/+\emptyset/-\emptyset]$.
- This analysis includes a comparison between natural and synthetic fiber composite layers for both inner and outer skins.
- The magnitudes of the forces applied to the sandwich plate reflect the internal pressure loading of the sandwich tubular structure.
- The macromechanical analysis helps locate the layer of the lower or upper skin that is most stressed, enabling a failure analysis and suggesting reinforcement solutions.
- The obtained results have demonstrated the influence of mechanical properties on the behavior of composite sandwiches based on synthetic or natural fibers.

- Limiting the loading pressure is essential in order to avoid any scenario of creating micro cracks, which can lead to the ruin of the sandwich skins.
- The results achieved during this chapter will be a good indicator for the third and last analysis scale and it will be covered by the next chapter.
- Based on failure analysis, it is essential to simultaneously increase the number of layers in both the lower and upper skins to reduce the gap between the synthetic and biocomposite materials, which is evaluated at 78.87%, in order to enhance the stiffness of the biocomposite.

CHAPTER V:

BEHAVIOR OF TUBULAR SANDWICH UNDER STATIC AND DYNAMIC LOADING

CHAPTER V: BEHAVIOR OF TUBULAR SANDWICH UNDER STATIC AND DYNAMIC LOADING

V .1- INTRODUCTION

The current chapter concentrates on the stress and strain of sandwich pipes subjected to static and cyclic internal pressure using the three-dimensional anisotropic elasticity model developed in Chapter II. The pressure loading is assumed to be symmetrical about the cylinder's axis and independent of the axial coordinate. An isotropic material with linearly elastic behavior makes up the core layer of sandwich pipes, whereas each layer of the skins—internal or external—is composed of a homogenous, anisotropic material characterized by long fibers. The sandwich's anisotropic skin and isotropic core are each subjected to an analytical failure using Tsai-Wu and Von-Mises, respectively. The major purpose of this chapter is to assess the possible uses of bio-fibers to replace glass synthetic fibers that are commonly used in sandwich pipes under static and cyclic loads.

V .2- STATIC ANALYSIS OF SANDWICH COMPOSITE PIPE UNDER PRESSURE

In this section, the results of the stress, strain, and displacement distribution of the analytical model were compared to the FEM results. Gradual reinforcing tests were performed to enhance the rigidity of the biocomposite sandwich and minimize the gap when compared to a synthetic sandwich. The model design developed for this thesis was used to estimate the number of biocomposite layers, calculate the ultimate pressure, and determine safety factors.

V .2.1- FE analysis

In order to validate our analytical approach, finite element simulations with ANSYS 18.1 and 3D elements are used in our study, which is shown in Figure 46. The numerical model presents a uniform mesh of the global geometry, characterized by: 43911 nodes and 8640 quadratic elements. Figure 47 illustrates the entire FE model as well as its characteristics.

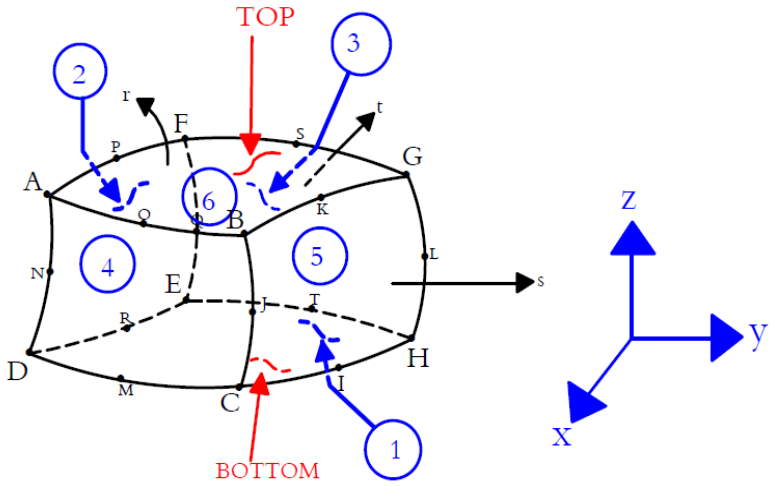

Figure 46. The meshing element used for finite element models.

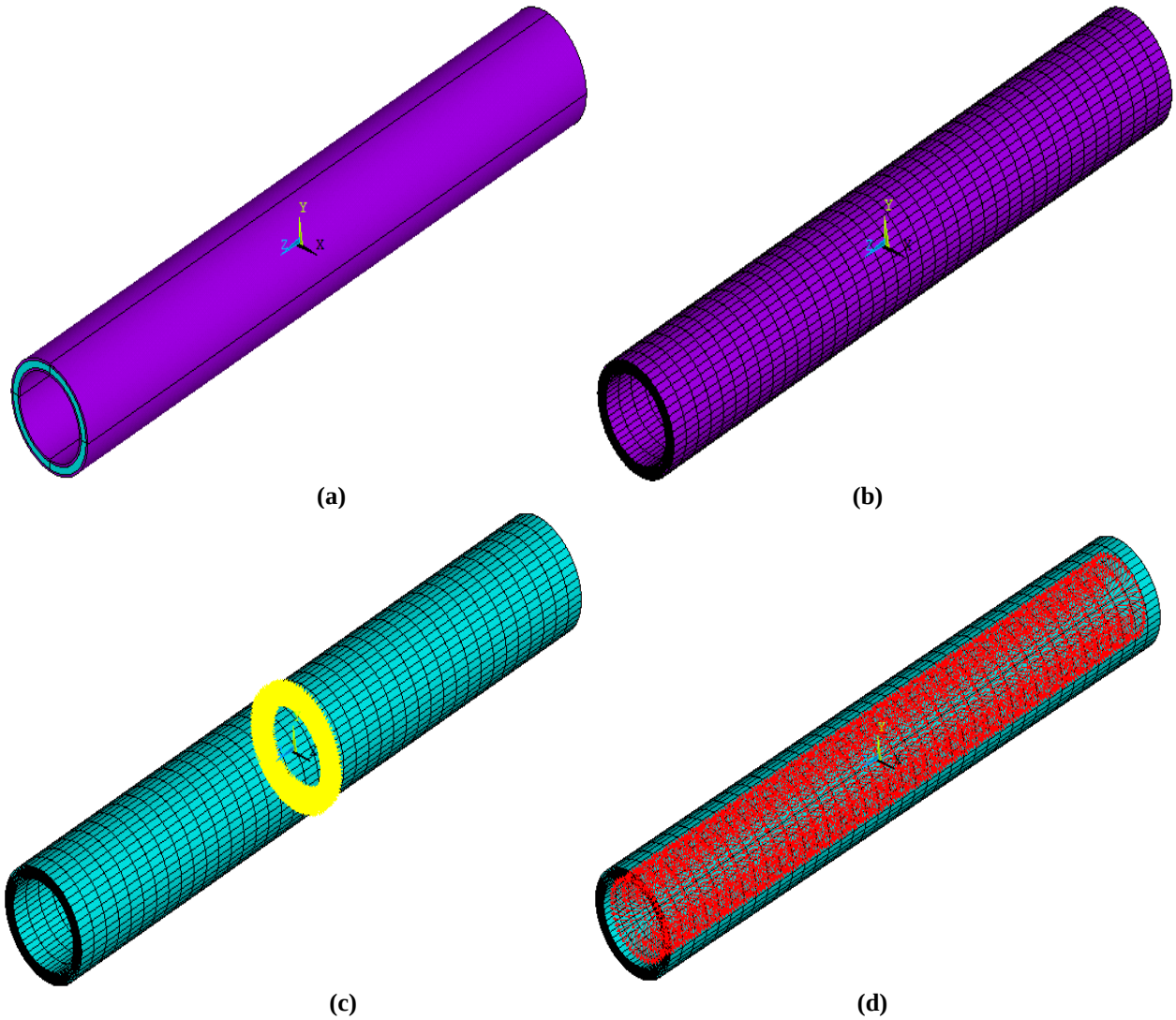

(a) **(b)**

(c) **(d)**

Figure 47. The sandwich pipe structure. (a) The geometry, (b) the mesh, (c) boundary conditions, and (d) loading of the numerical model.

V .2.1.1- Geometry, materials and loading

The sandwich pipe configuration has an inner radius of 60 mm, a core-layer thickness of 10 mm, a skin-layer thickness of 0.27 mm and a length of 500 mm.

In the current study, two types of bio-skin material based on long jute and pineapple leaf fibers compared to glass fibers were carried out. The skin materials characteristics are shown in Table 8. The core epoxy is shown in

Table 9. The used layered skin stacking sequences are listed in Table 10.

The internal pressure applied to the sandwich pipe is 6 MPa and it is equal to the double pressure service of hydrogen transportation. This pressure threshold was chosen in order to remain within the elastic range.

Table 8. Material properties of Jute/epoxy, Glass/epoxy and, PALF/epoxy in the UD orthotropic frame.

Materials / ***Properties***	***Jute/epoxy*** [237]	***Glass/epoxy [36]***	***PALF/epoxy [36]***
$\mathbf{E_1}$ [GPa]	12.5	40	7.327
$\mathbf{E_2 = E_3}$ [GPa]	5.633	10	4.888
$\mathbf{G_{12} = G_{13}}$ [GPa]	7.24	4.95	1.729
$\mathbf{G_{23}}$ [GPa]	2.10	3.34	1.679
$\boldsymbol{\nu_{12}} = \boldsymbol{\nu_{13}}$	0.3395	0.32	0.343
$\boldsymbol{\nu_{23}}$	0.3395	0.495	0.455
α_L [°C^{-1}]	40×10^{-6}	0.006×10^{-6}	-
$\mathbf{X_t}$	55	2000	
$\mathbf{X_c}$	55	750	

Y_t	62	60	
Y_c	62	160	
SI	27.5	200	

Table 9. Material properties of Epoxy core in the UD isotropic frame [1].

Material \ Properties	Young's modulus [GPa]	Poisson's Ratio	Shear modulus [GPa]	Elastic limit [MPa][162]
Epoxy core	4.1	0.41	1.453	102.49

Table 10. Stacking sequences of sandwich pipe parts with Epoxy core.

Stacking sequence of sandwich pipe parts	
Seq 1	$[\ [\pm 60]_1$ / core / $[\pm 60]_1\ ]$
Seq 2	$[\ [\pm 60]_3$ / core / $[\pm 60]_3\ ]$
Seq 3	$[\ [\pm 60]_4$,[+60] / core / $[\pm 60]_4$,[+60]]
Seq 4	$[\ [\pm 60]_5$ / core / $[\pm 60]_5\ ]$
Seq 5	$[\ [\pm 60]_7$ / core / $[\pm 60]_7\ ]$

To validate the accuracy of our results, we performed a mesh convergence on the hoop stress of jute/epoxy along a non-dimensional radial distance. We've clearly arrived at a convergent solution.

V .3- RESOLUTION PROCEDURE

V .3.1- Static

Flowchart 3 shows the development stages of the two programs for calculating the behavior of the tubular sandwich structure under quasi-static loading with pure internal pressure. The first analytical program was carried out in MATLAB with an incremental pressure loading and an accumulation of responses in terms of displacement, deformation, and stresses. This methodology enabled the verification of pre-failure conditions for the skins and core through the Tsai-Wu and Von-Mises criteria, respectively. Additionally, this approach will facilitate the incorporation of progressive damage into the behavioral laws of composite skins and the plasticization of the core section in the near future. The second numerical program was conducted using ANSYS for the identical structure and loading conditions.

V .3.2- Dynamic

The consideration of dynamic loading for the sandwich tubular structure was accomplished through the adaptation of the program originally established for static loading. The analytical program was carried out using MATLAB. Flowchart 4 outlines the various steps involved in achieving the behavior of the structure under such conditions.

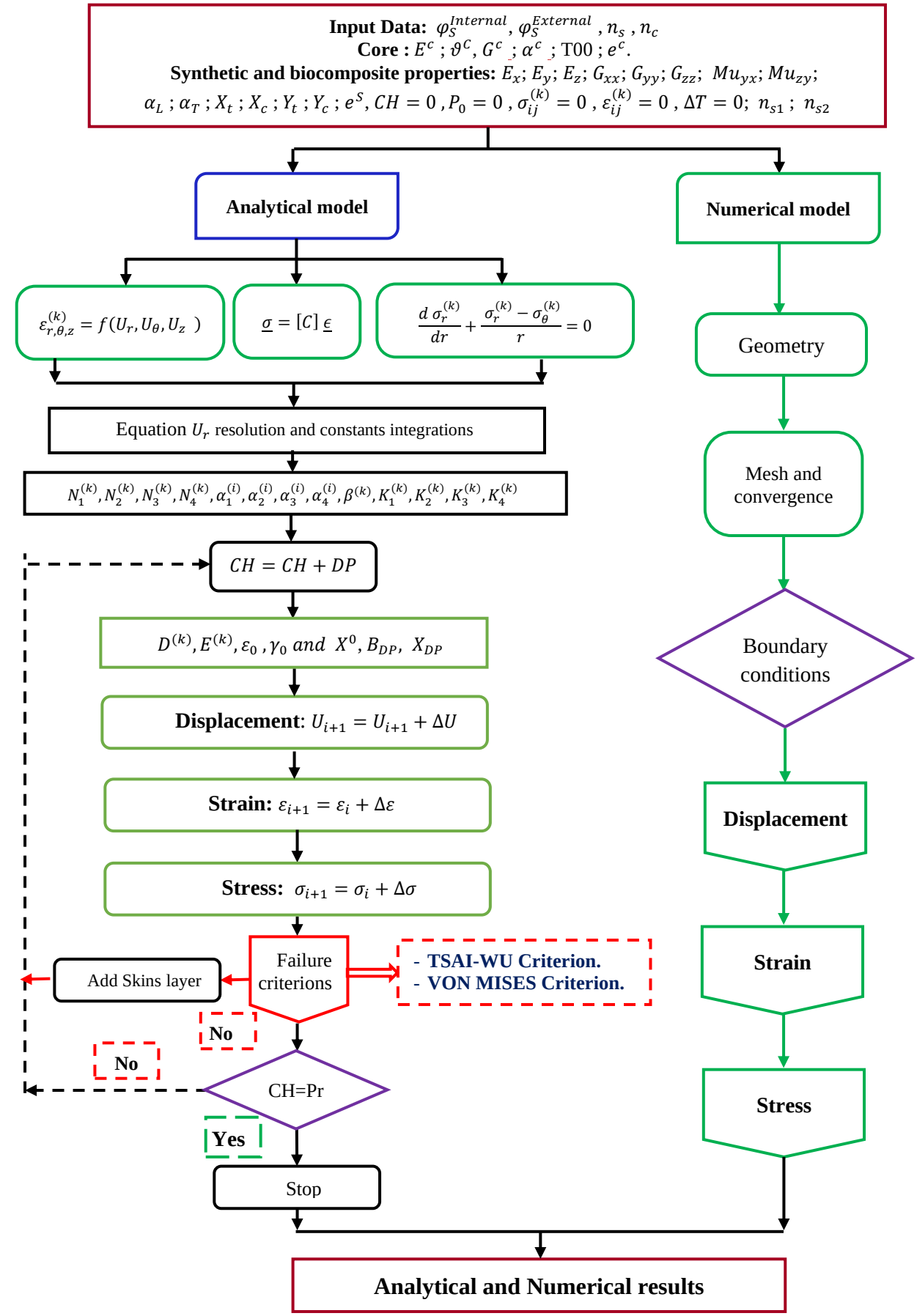

Flowchart 3. Flowchart of analytical and numerical steps resolution of sandwich pipe under Quasi-static internal pressure.

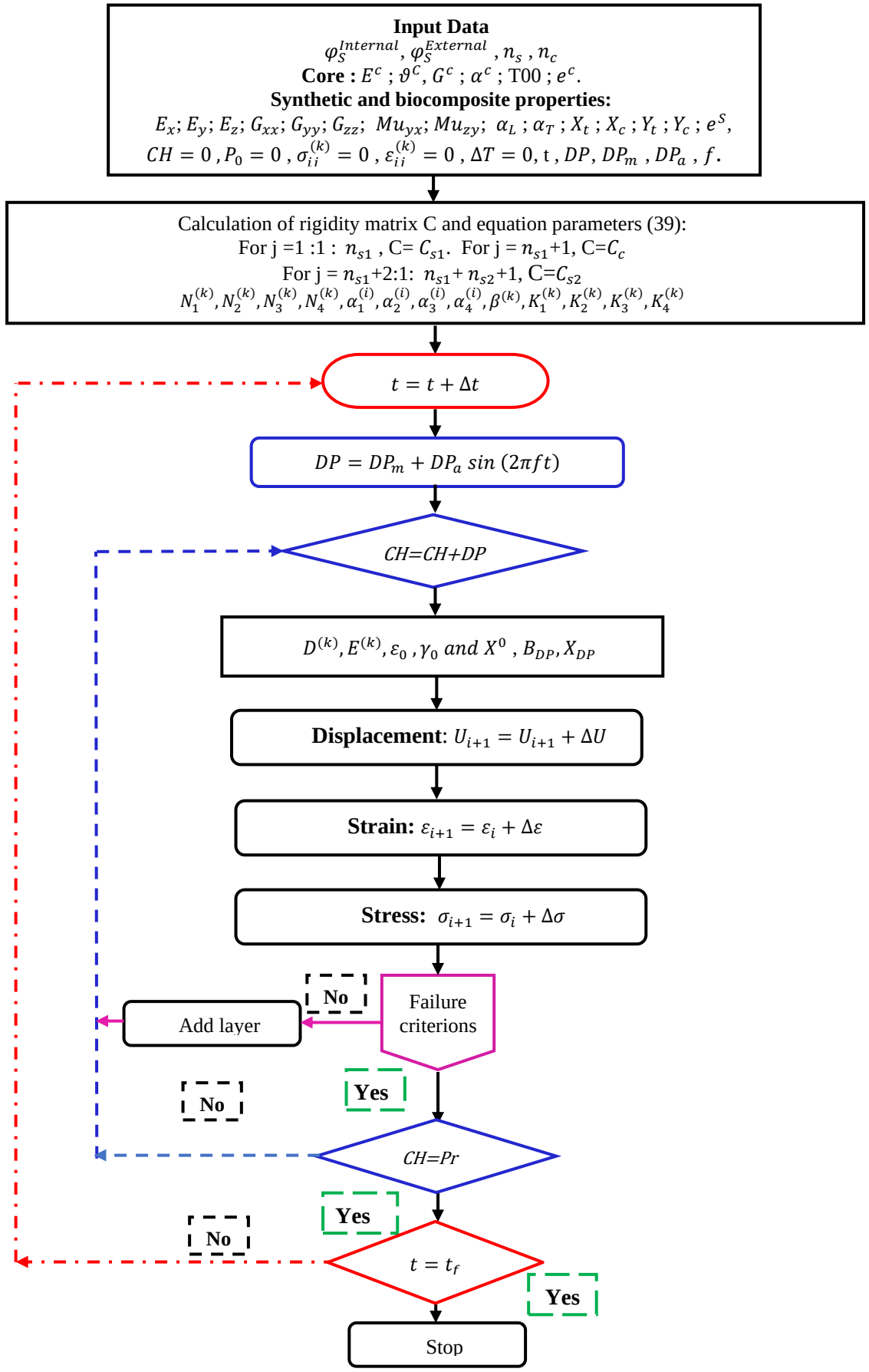

Flowchart 4. Flowchart of analytical and numerical steps resolution of sandwich pipe under dynamic loading of internal pressure.

V .4- ANALYSIS OF A COMPOSITE SANDWICH PIPE UNDER QUASI-STATIC LOADING

This section is dedicated to present the results of sandwich pipe behavior under static loading.

V .4.1- Mesh convergence for F.E.M

A convergence exercise was undertaken through this section to establish an appropriate mesh. Refining element density in three directions concurrently is straightforward. To achieve this, increasing numbers of elements (3600, 8640, 18000, and 48000) through the thickness of incremental meshes are chosen to make a sensitivity study.

Figure 48 summarizes the results of the convergence analyses based on adjusting the number of elements in the mesh, where good convergence was achieved, and we limit our mesh to 8640 elements through the sandwich wall.

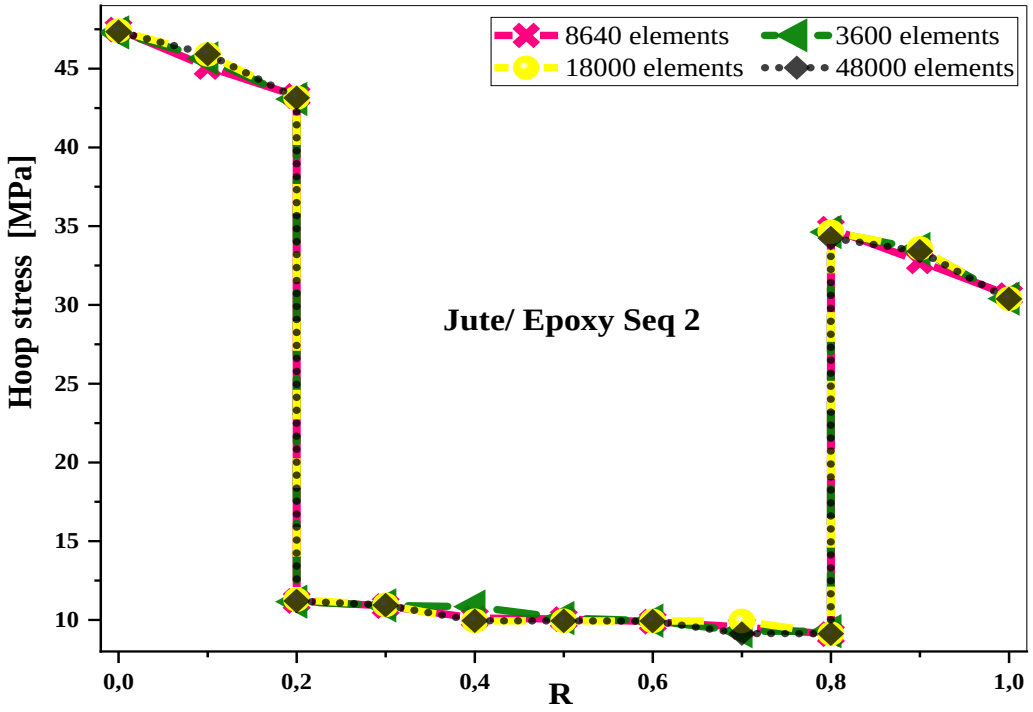

Figure 48. Analysis of mesh convergence for finite elements of hoop stress distributions versus R.

V .4.2- Analytical and Numerical results comparison

Before developing the analytical results, a comparison is made between the analytical and FEM results.

Figure 49 represents the comparison between both analytical (developed using Matlab) and numerical results obtained by means of commercial software (ANSYS 18.1) for the radial displacement, hoop, and axial stress. This comparison shows a very good agreement and demonstrates that the responses of the structures are relatively well anticipated.

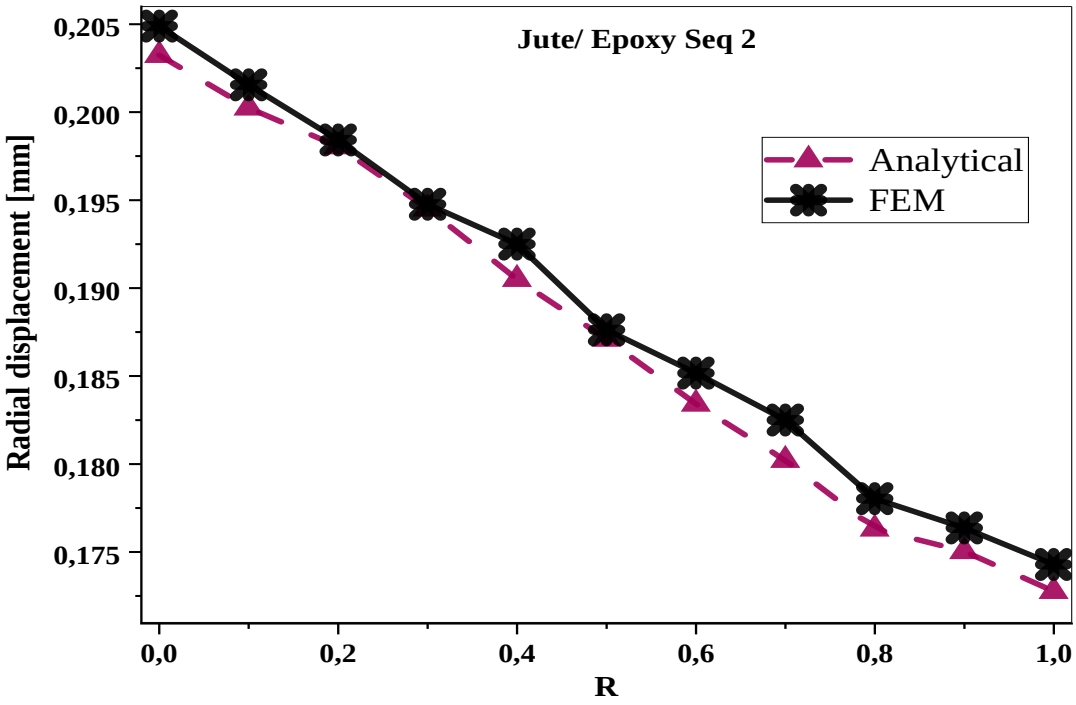

(a)

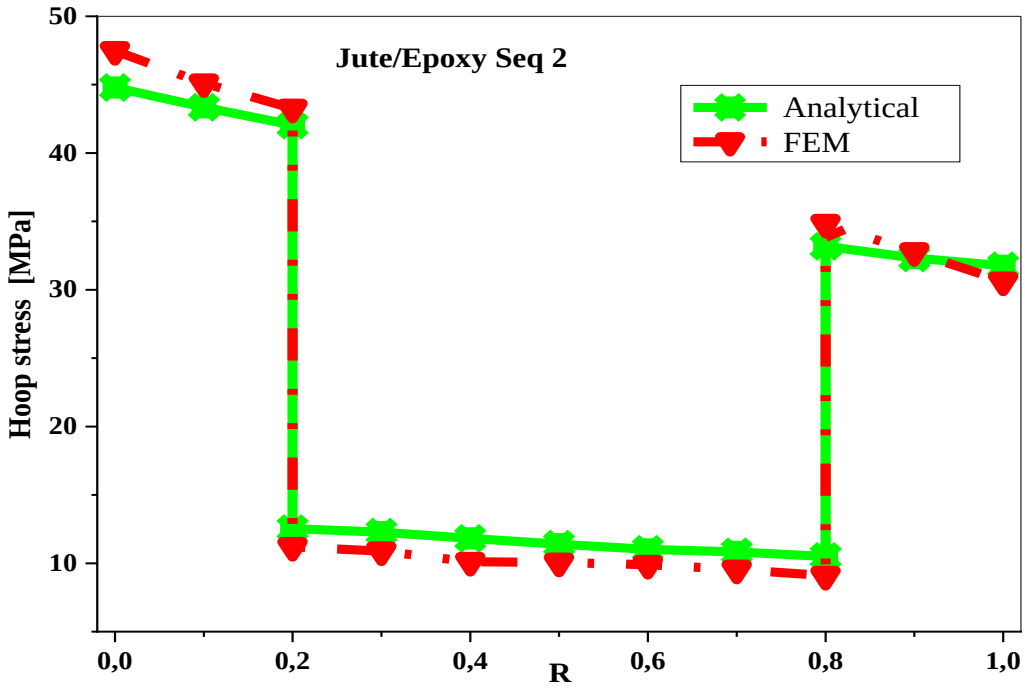

(b)

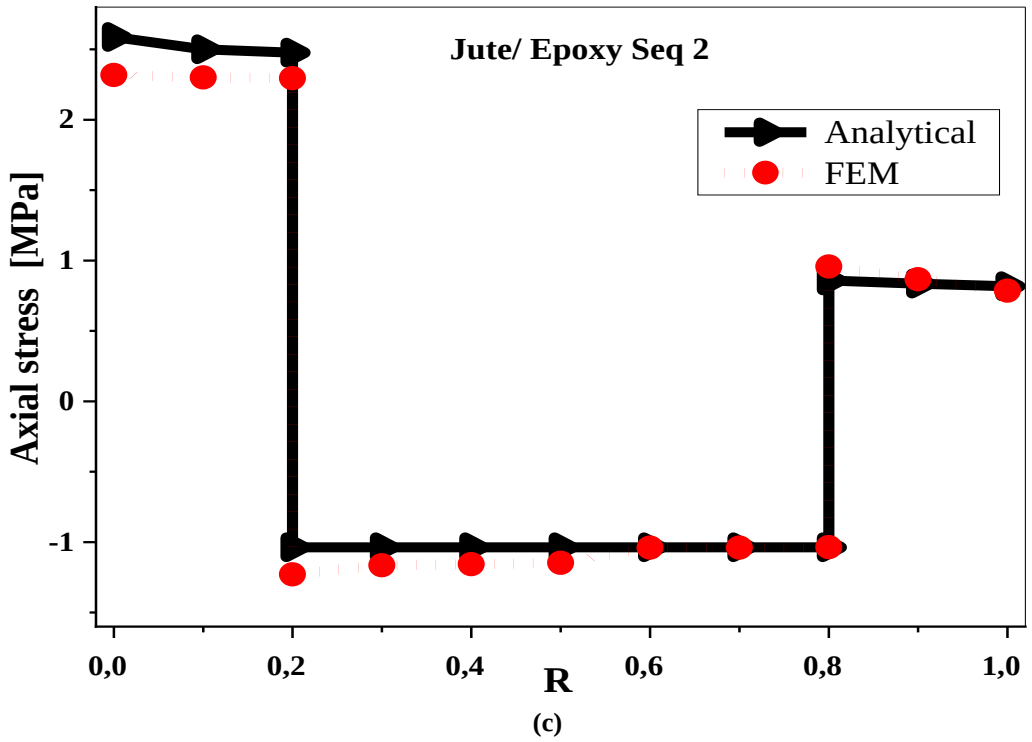

Figure 49. Comparison of analytical and numerical results of Jute/epoxy. (a) Radial displacement, (b) Hoop stress and (c) Axial stress distributions versus R.

V .4.3- Finite element analysis of sandwich components

The hoop stress distributions over the wall thickness of the sandwich pipe components (the inner and outer skins, as well as the core) using the color FE contour presented in Figure 50.

The inner skin has the maximum stress distribution values compared to the outer skin and core and reflect the boundary conditions applied.

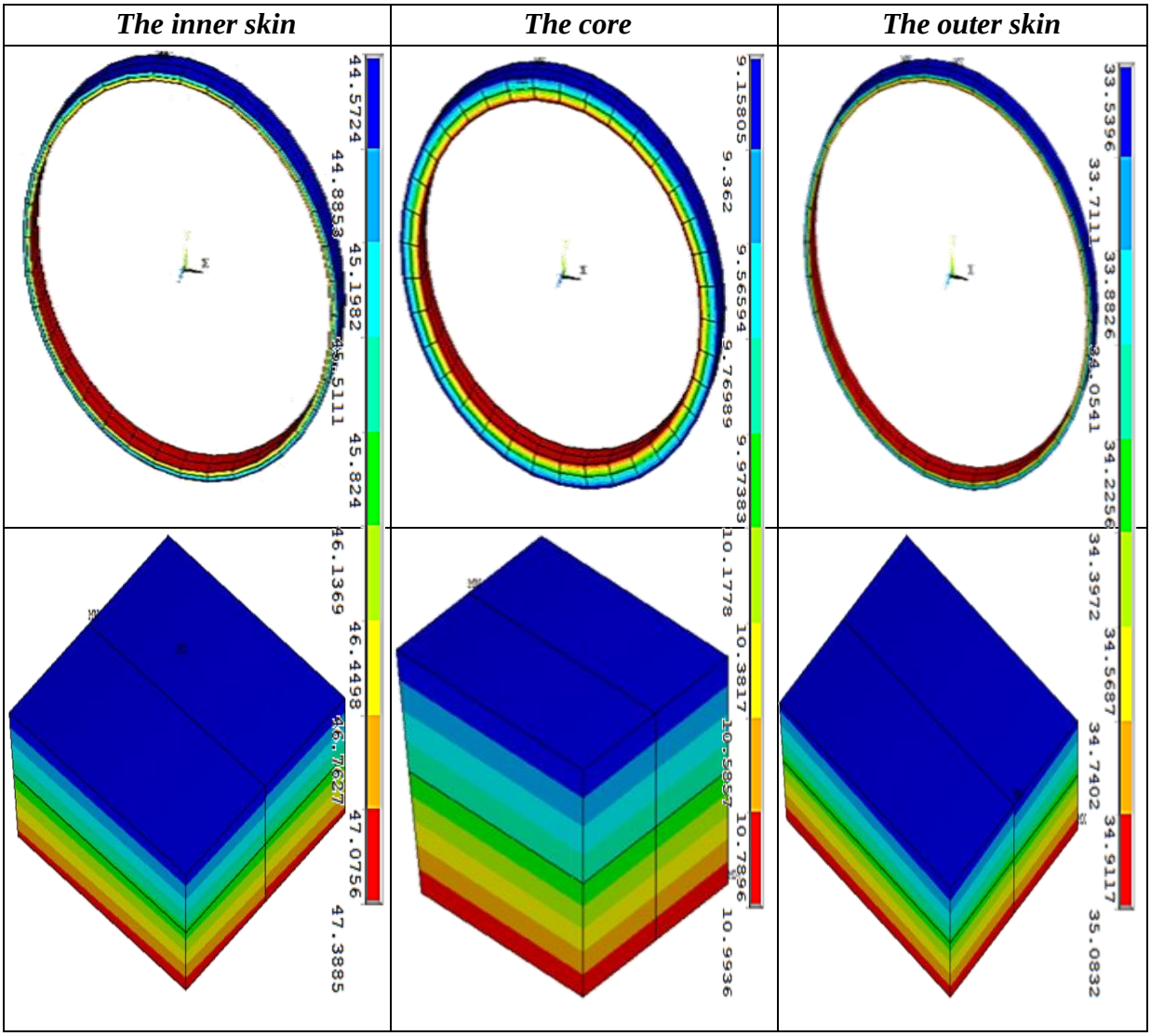

Figure 50. The evolution of Hoop stress distribution for the sandwich pipe parts (inner, outer skins and the core) through thickness.

V .4.4- Analysis of eco-sandwich pipe compared to synthetic sandwich

A comparison of stress, strain and radial displacement distributions through the wall thickness in the sandwich pipes is established, between synthetic and natural composite materials design as Glass/epoxy, PALF/epoxy and Jute/epoxy for the same stacking sequence as shown in Table 10.

V .4.4.1- Radial displacement analysis

Figure 51 shows a quasi-linear behavior of the variation of radial displacement through the radius. The structure's stiffness allows for a progressive decrease in radial displacement from one layer to another, which is determined by the material properties of the composite used as well as the stacking sequence of the lower and upper skins. The passage from one layer to another for

skins or from skin to core translates the continuity of displacement imposed by the model. The magnitudes of radial displacement show that synthetic structures based on glass/epoxy undergo lower radial swelling compared to that of biocomposite.

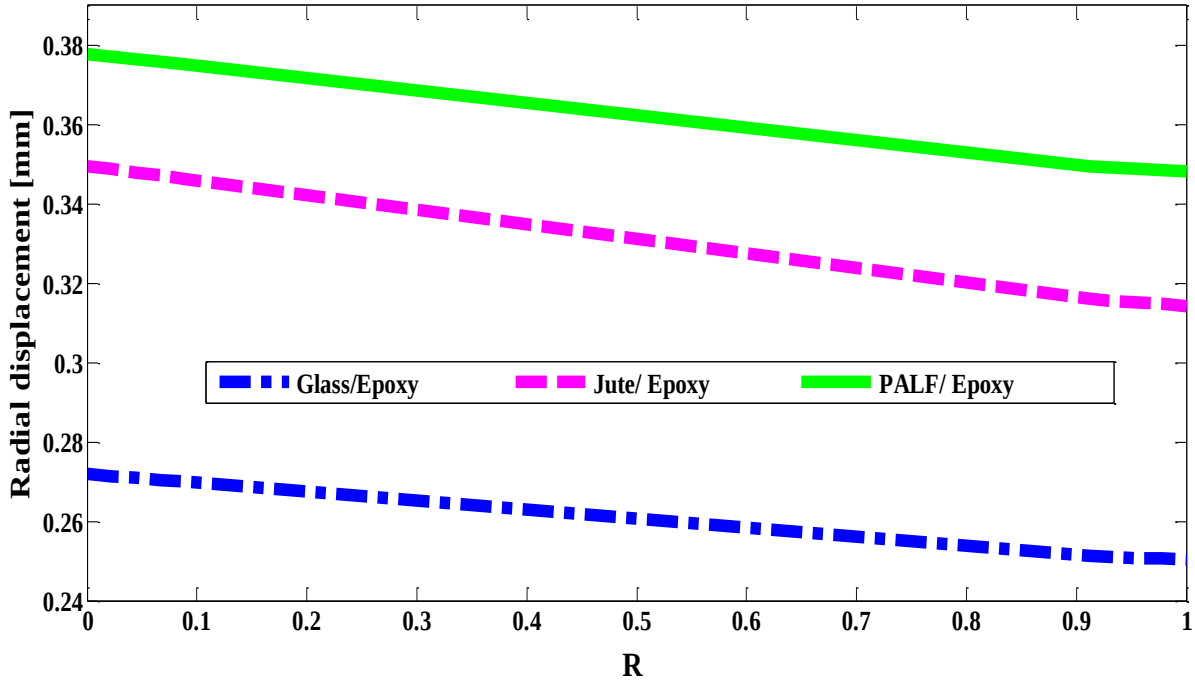

Figure 51. The evolution of radial displacement distributions versus R of Seq 1.

V .4.4.2- Stress analysis

The Figure 52 (a) shows the distribution of radial stress through the thickness of the sandwich pipe. For the three materials, a compressive radial stress increases from the inner skin to the outer through the core of the sandwich pipe. The maximum radial stress of -6 MPa is found at the inner skin which decries to zero at the outer skin, which reflects the boundary conditions applied.

The findings of the hoop and axial stress distributions between the core and the skins demonstrate a large variation for the multilayered composite based on glass compared to natural fibers PALF and jute because these observations reveal the large anisotropic properties of glass.

The hoop stress presented in Figure 52 (b) is a tensile state. The skin layers are subjected to significantly greater stresses which are about ten times compared to the core layer one. Moreover, the stress of inner skin is more than double compared to the outer skin. The Jute/epoxy and PALF/epoxy sandwiches are less sensitive compared to Glass/epoxy, where the stress magnitude is lower. The same remarks characterize the axial stress distribution, with a compression state being recorded in the core for all materials compared. The ratio between hoop stress and axial

stress which is about ten reflects the internal pressure applied to the structure, and it can lead to a discontinuity between the core and the upper layer of the lower skin and the inner layer of the upper skin, (Figure 52 (c)).

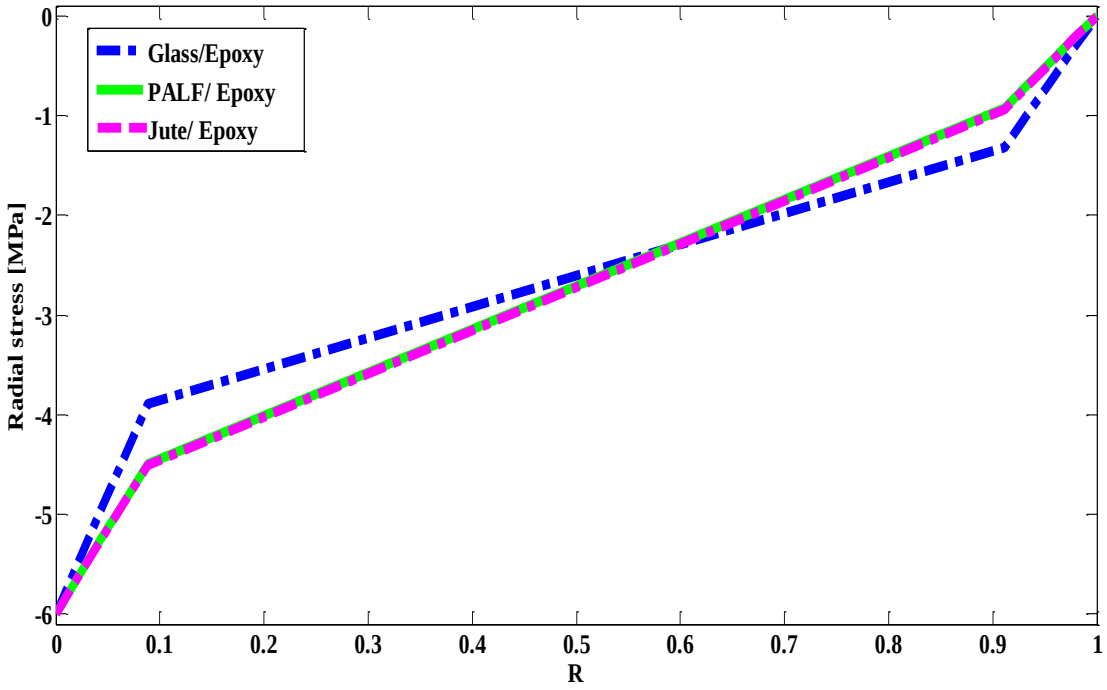

(a)

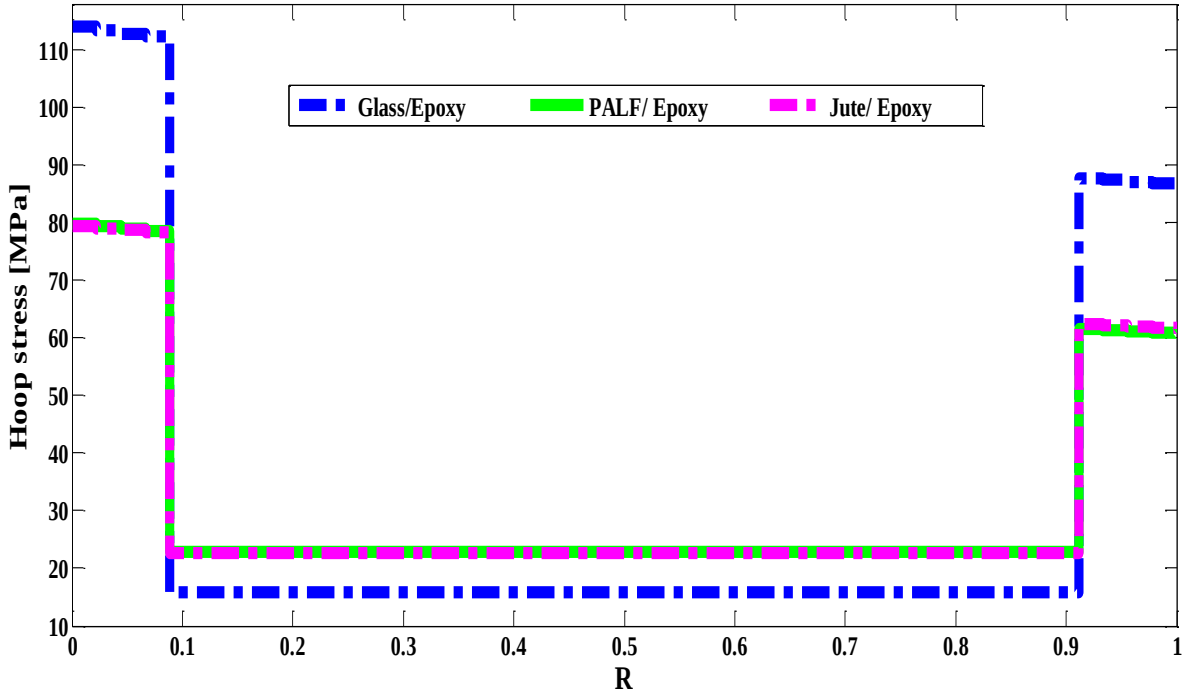

(b)

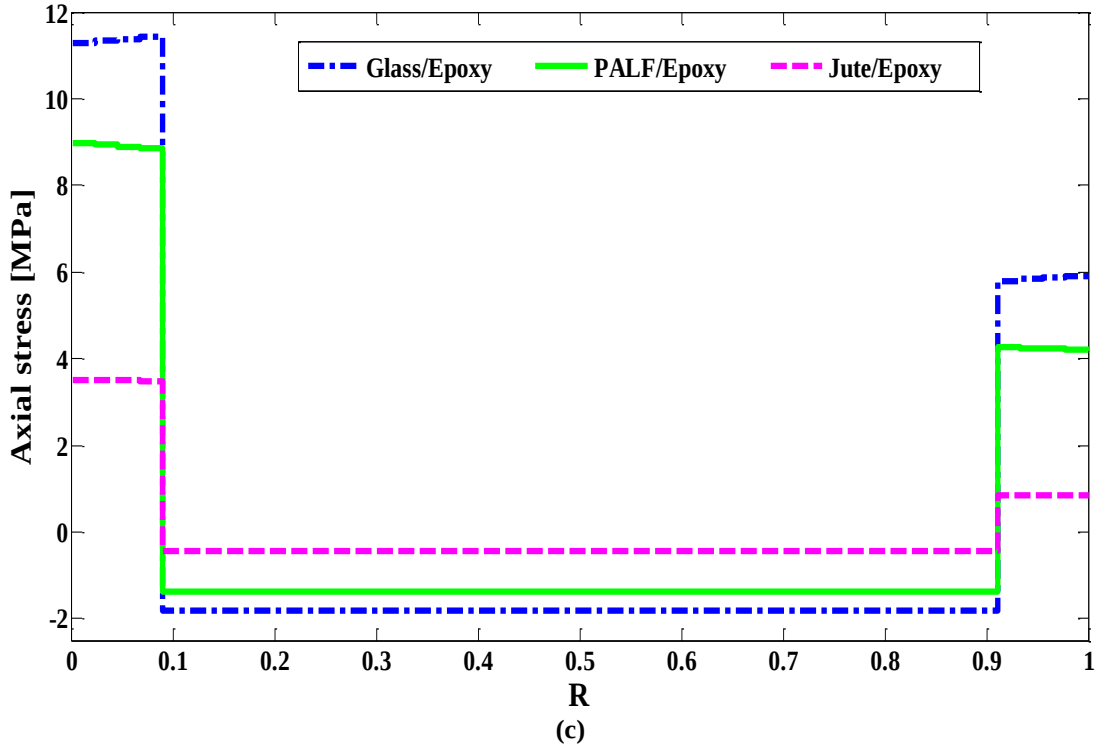

Figure 52. The evolution of: (a) Radial stress, (b) Hoop stress and (c) Axial stress distributions versus R of Seq 1.

Figure 53 shows the shear stress distribution through the radius, which is predominantly carried by the skins, with the sign of shear stress alternating through plies. The shear stress jump occurs depending on the layer fibers orientations between 60 and -60 degrees, while, it is around zero in the core layer. The essential function of the sandwich core is to transmit, through shearing, the mechanical actions from one skin to the other. In terms of shear behavior, the stress magnitudes obtained for the biocomposite are better than those of the synthetic.

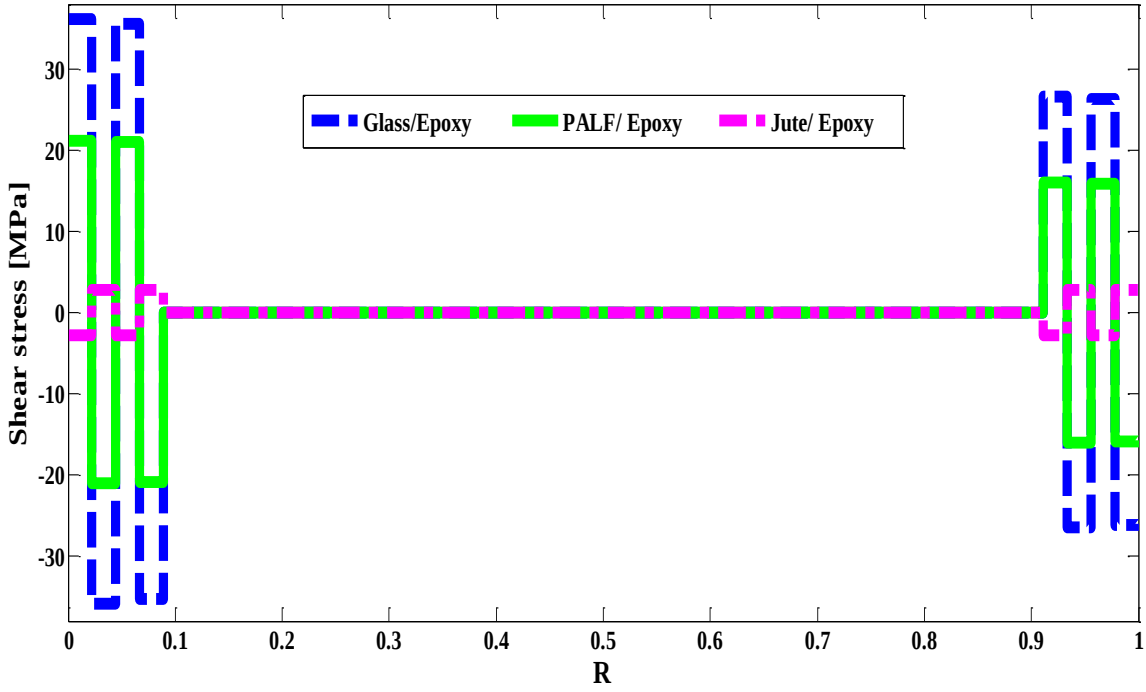

Figure 53. The evolution of shear stress distributions of the three composites versus R of Seq 1.

V .4.4.3- Strain analysis

The axial strain versus R is constant which reflect the impose boundary conditions and negligible compared to hoop strain due to loading mode (pure internal pressure). While, it depends on the material of the skin and the largest values is obtained for PALF/epoxy, followed by Glass/epoxy and the lowest is attributed to Jute/epoxy (Figure 54 (a)).

The hoop strain versus R is quasi-linear regressive and the maximal values are located at the internal wall of the pipes for the three materials investigated where the damage can be initiated (Figure 54 (b)).

The pressure tested about 6 MPa represents a ratio of 2 to 3 of the service pressure, estimated 3 MPa which gives a very good safety margin for using biocomposites for manufacturing sandwich pipes.

Figure 54 (c) shows the distribution of radial strain through the wall thickness, for the three different types of materials, where discontinuous variation is registered at the interface between the skin and the core and show compression state. The Jute/epoxy has the largest radial strain in the internal part of the skin, followed by the PALF/epoxy, and the lowest for the Glass/epoxy.

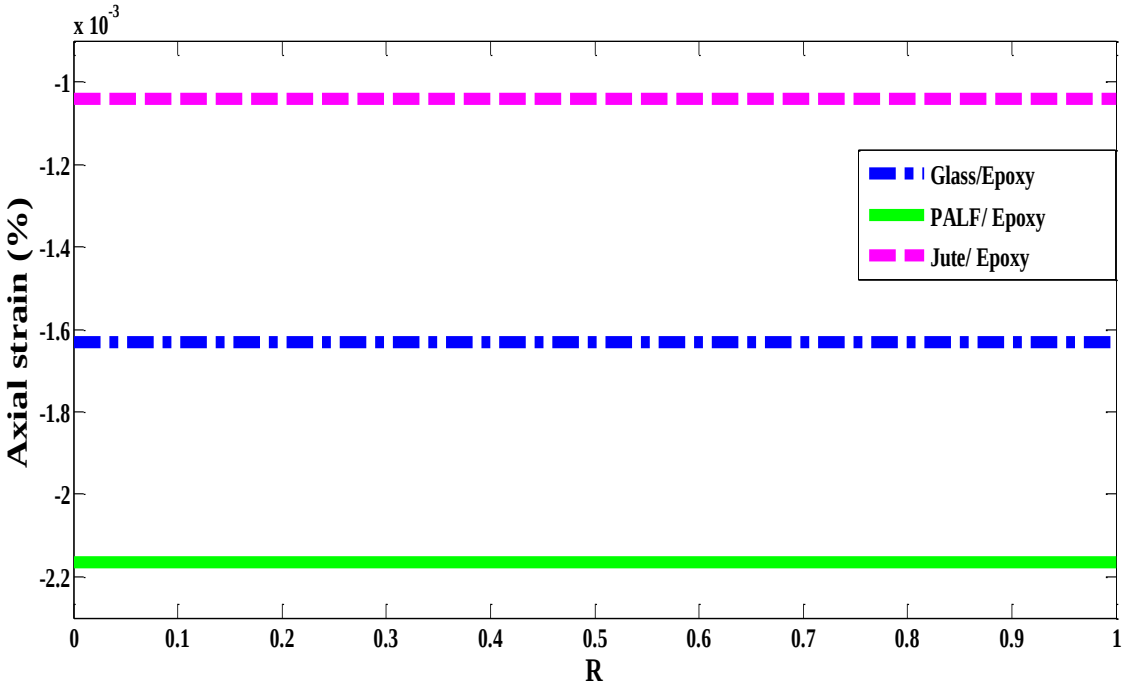
x 10^-3
-1
-1.2
-1.4
-1.6
-1.8
-2
-2.2
Axial strain (%)
Glass/Epoxy
PALF/ Epoxy
Jute/ Epoxy
0
0.1
0.2
0.3
0.4
0.5
0.6
0.7
0.8
0.9
1
R

(a)

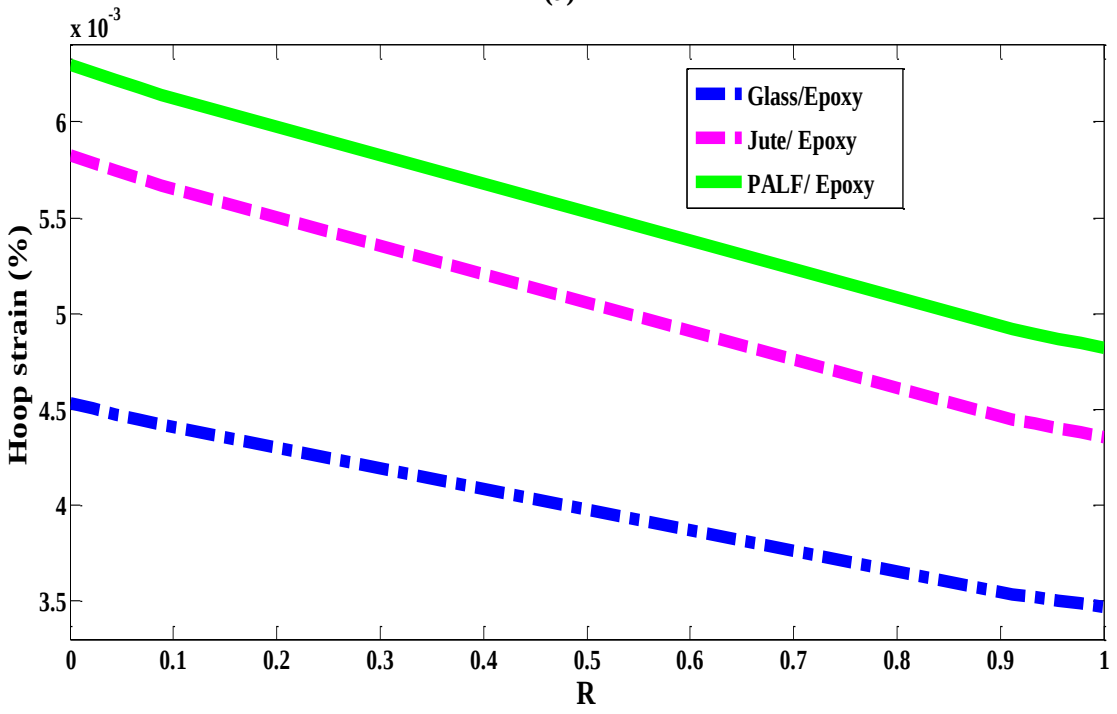
x 10^-3
6
5.5
5
4.5
4
3.5
Hoop strain (%)
Glass/Epoxy
Jute/ Epoxy
PALF/ Epoxy
0
0.1
0.2
0.3
0.4
0.5
0.6
0.7
0.8
0.9
1
R

(b)

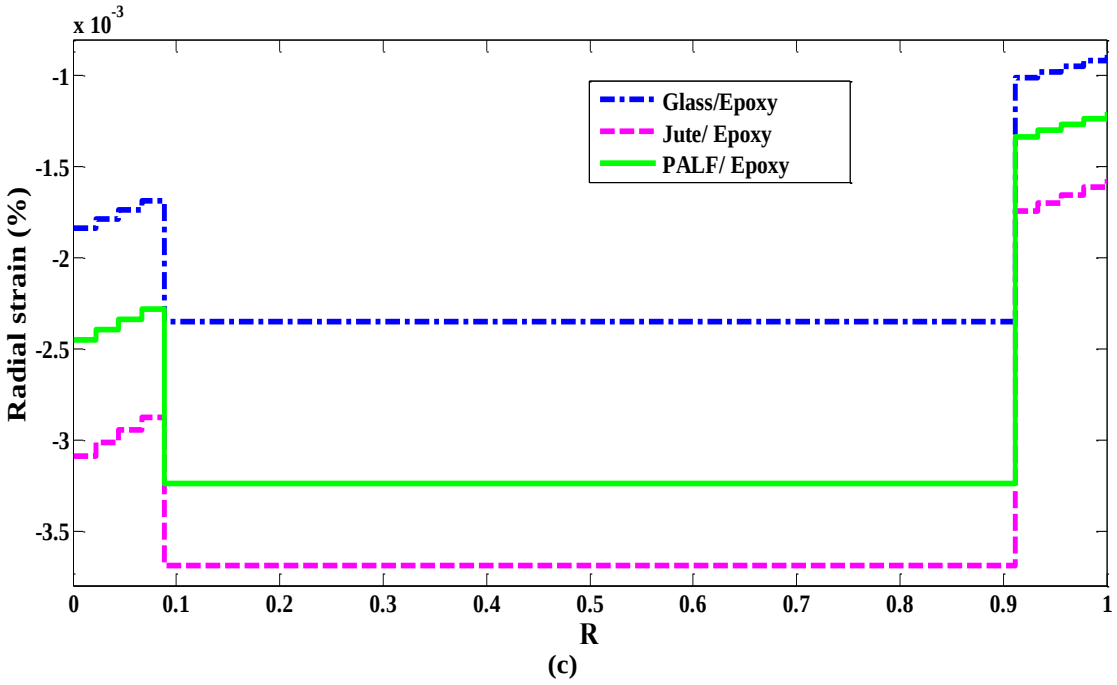

Figure 54. The evolution of (a) Axial strain, (b) Hoop strain and (c) Radial strain distributions versus R of Seq 1.

V .4.4.4- Analytical response of sandwich pipe under pure internal pressure

Figure 55 shows the analytic response of sandwich pipe under pure internal pressure which is in good agreement with the evolution of hoop stress versus axial and hoop strains.

The Jute/epoxy has the best results (i.e., having the smallest values of hoop stress, axial and hoop strains) followed by the PALF/epoxy and the Glass/epoxy.

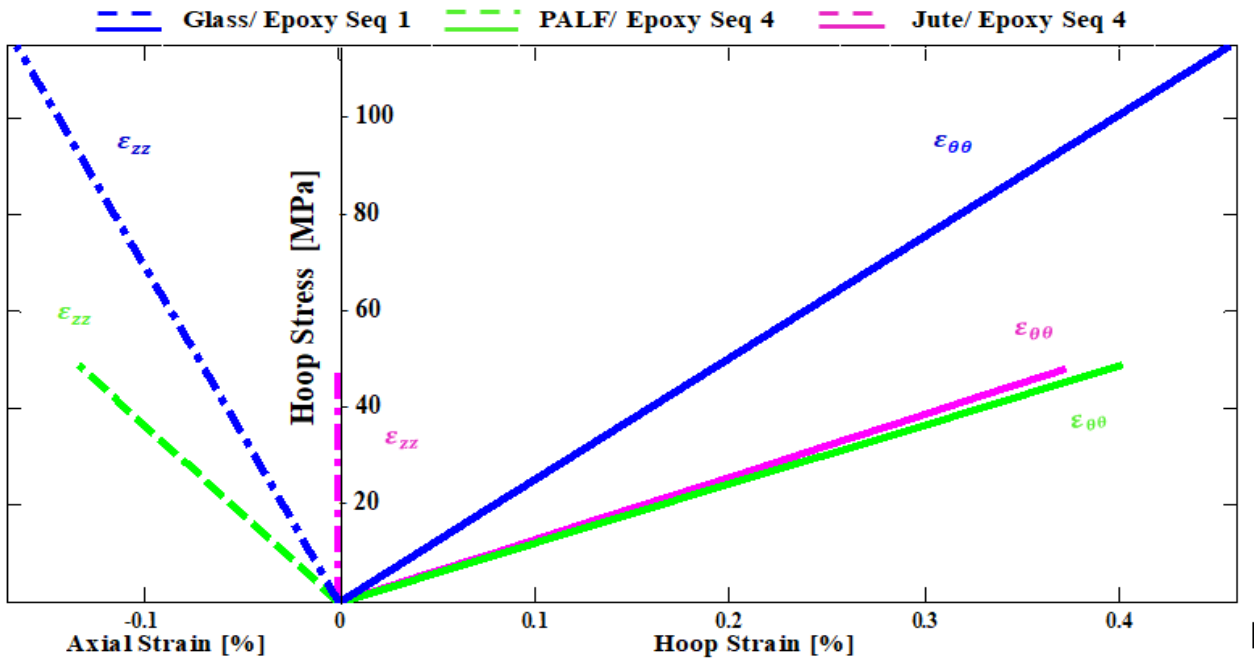

Figure 55. The evolution of hoop stress versus hoop and axial strains.

V .4.5- Failure analysis

The Tsai-Wu criterion allows us to determine the rupture limit of the most stressed internal layers according to the increment of the loading pressure for the material configurations chosen in this work. Sandwich pipes composed of Glass/epoxy and biocomposite: Jute/epoxy, are compared, (See Figure 56).

In this part, since there isn't any experimental data available regarding the fracture limits of PALF/epoxy, Palm/epoxy, and Alfa/epoxy biocomposites, we limit ourselves to comparing the failure behavior of the synthetic Glass/Epoxy with the Jute/Epoxy biocomposite.

It is noticed that gradually reinforcing biocomposite sandwich by increasing the number of layers from Seq 1 to Seq 4 (see Table 10) increases their rigidity. The results show that for biocomposite sandwich pipe Jute/epoxy, the ultimate pressure is around 33 bars for Seq 1, 60 bars for Seq 2, 80 bars for Seq 3, and finally 85 bars for Seq 4.

The limit pressure for a sandwich tube based on biocomposite reaches 85 bars for Seq4, allowing for a safety factor of 2.66 for Jute/epoxy. It is noticed that the overall process is operated at 30 bar of high pressure for hydrogen transportation pipelines [238]. The safety factors obtained for biocomposites are larger than 2.25 reported by Nghiep et al. for storage composite pressure vessels [183].

In other words, these results obtained allow us to have confidence in the substitution of synthetic fibers by natural ones while optimizing the number of layers.

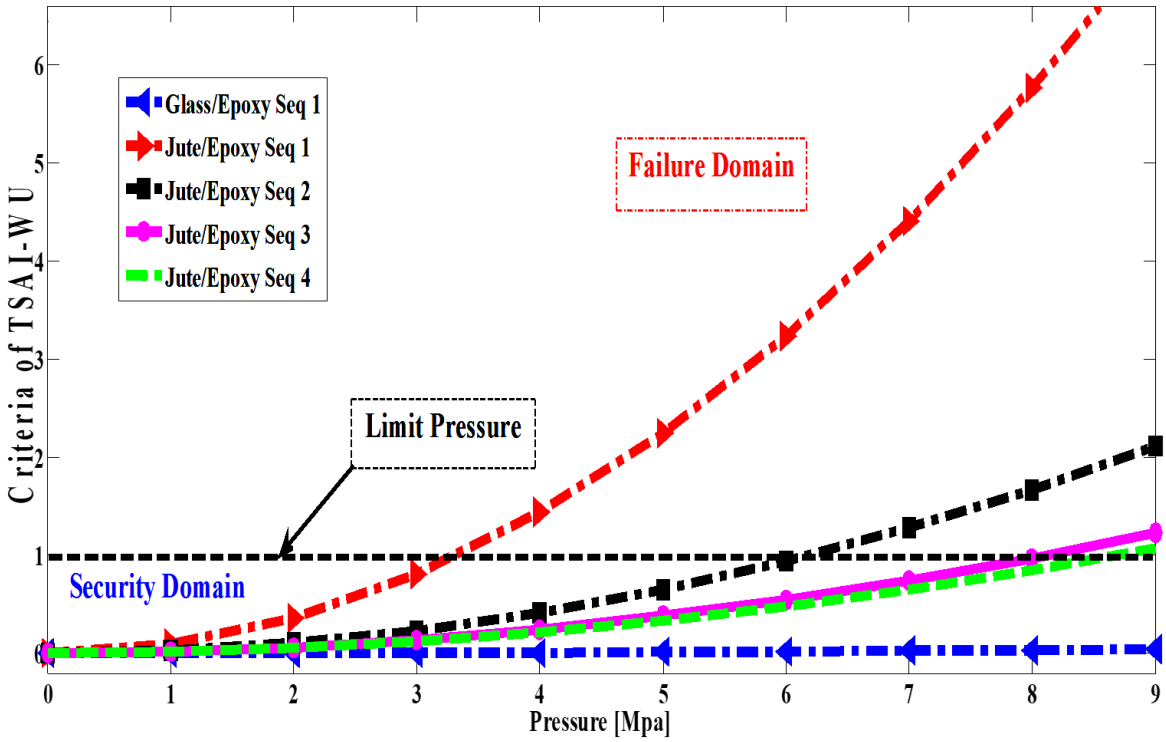

Figure 56. Variations of Tsai-Wu criterion versus internal pressure for various layer counts.

Figure 57 shows that the rupture threshold is not reached for the three materials, and it remains low compared to the elastic limit of the epoxy core of size 102.49 MPa [162]. The contribution of Jute/Epoxy with layered reinforcement guarantees the safety and reliability of the hydrogen transport structure.

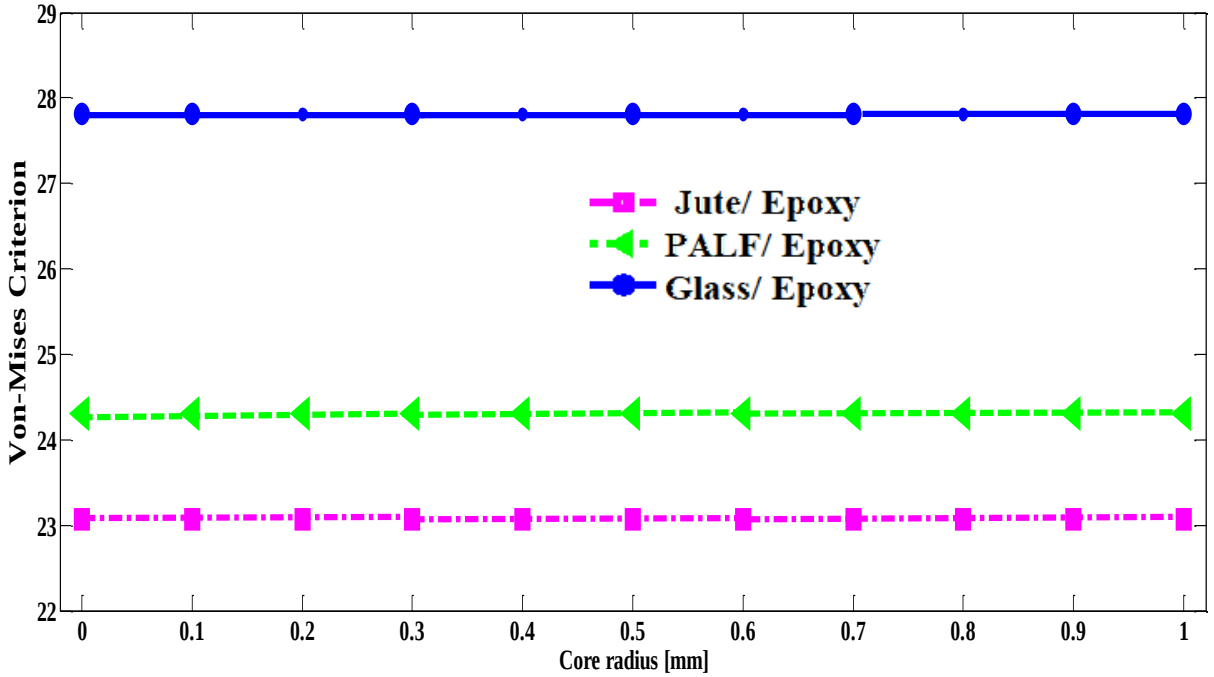

Figure 57. Variations of Von-Mises criterion of the three composites versus core radius.

V .5- ANALYSIS OF SANDWICH COMPOSITE PIPE UNDER CYCLIC LOADING

The current section illustrates the stress and strain of a sandwich pipe subjected to only cyclic pure internal pressure. Analytically, the time-dependent displacement, stress, strain, and deformation distributions are determined.

V .5.1-Analysis of Jute/Epoxy pipe behavior

In the present section, an examination is conducted on the behavior of a sandwich pipe composed of Glass/Epoxy material. This analysis involves the presentation of radial displacement, stress, and strain distribution across the thickness of the structure, specifically focusing on the stacking sequence Seq1: [[±60] / core / [±60]].

V .5.1.1- Radial displacement analysis

Radial displacement and radial coordinates are demonstrated to be inversely related. Through the thickness direction, the solution provides a continuous displacement field along interfaces. The rigidity of the structure allows for a gradual reduction in radial displacement from one layer to the next, which is governed by the material properties of the composite employed in addition to the stacking sequence of the bottom and top skins. The transition between layers for skins or between skins and cores translates into the displacement continuity that the model requires, (See Figure 58).

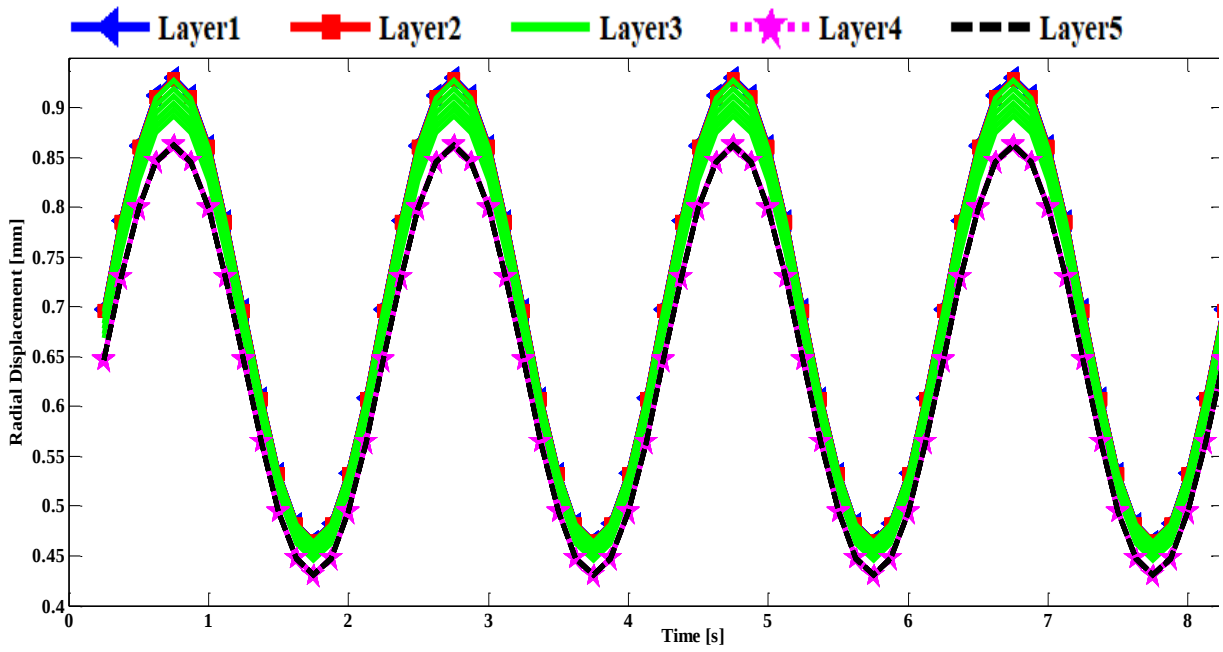

Figure 58. Radial Displacement distribution under cyclic internal pressure.

V .5.1.2- Stress analysis

The time history of radial stress over the thickness of the cylinder under cyclic internal pressure is shown in Figure 59 (a). When the cyclic internal pressure is present, a temporal discontinuity arises, and the radial stress exhibits harmonic oscillations, which may be attributed to the harmonic characteristics of mechanical loads. The continuity of the radial stress concerning the radius can also be observed. This is consistent with the continuity conditions initially imposed on the problem. The compressive radial stress progressively -increases from the inner skin to the outer skin through the core of the sandwich pipe. The inner skin has the highest radial stress of -12 MPa, which drops to zero at the outer skin due to the boundary conditions applied.

The hoop stress distribution appears in Figure 59 (b). The amount of hoop stress increases when fiber orientation tends to be in a circumferential direction.

Figure 59 (c) below shows the inverse correlation between axial stress and the absolute value of the ply angle. The amount of axial stress reduces when fiber orientation tends in a circumferential direction. Also, there are discontinuities at the interfaces of layers with various absolute values of orientation angle (there is continuity between layers with +60 and -60). The stress on the inner skin is greater than on the outer skin, with a compression state being recorded in the core.

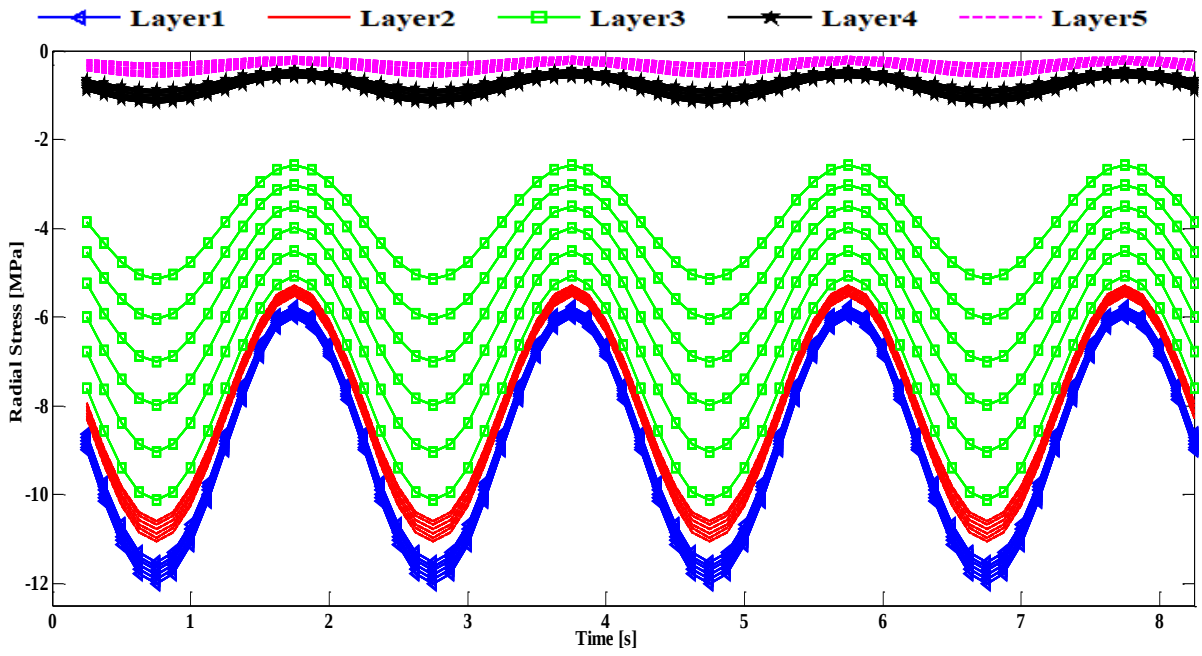

(a)

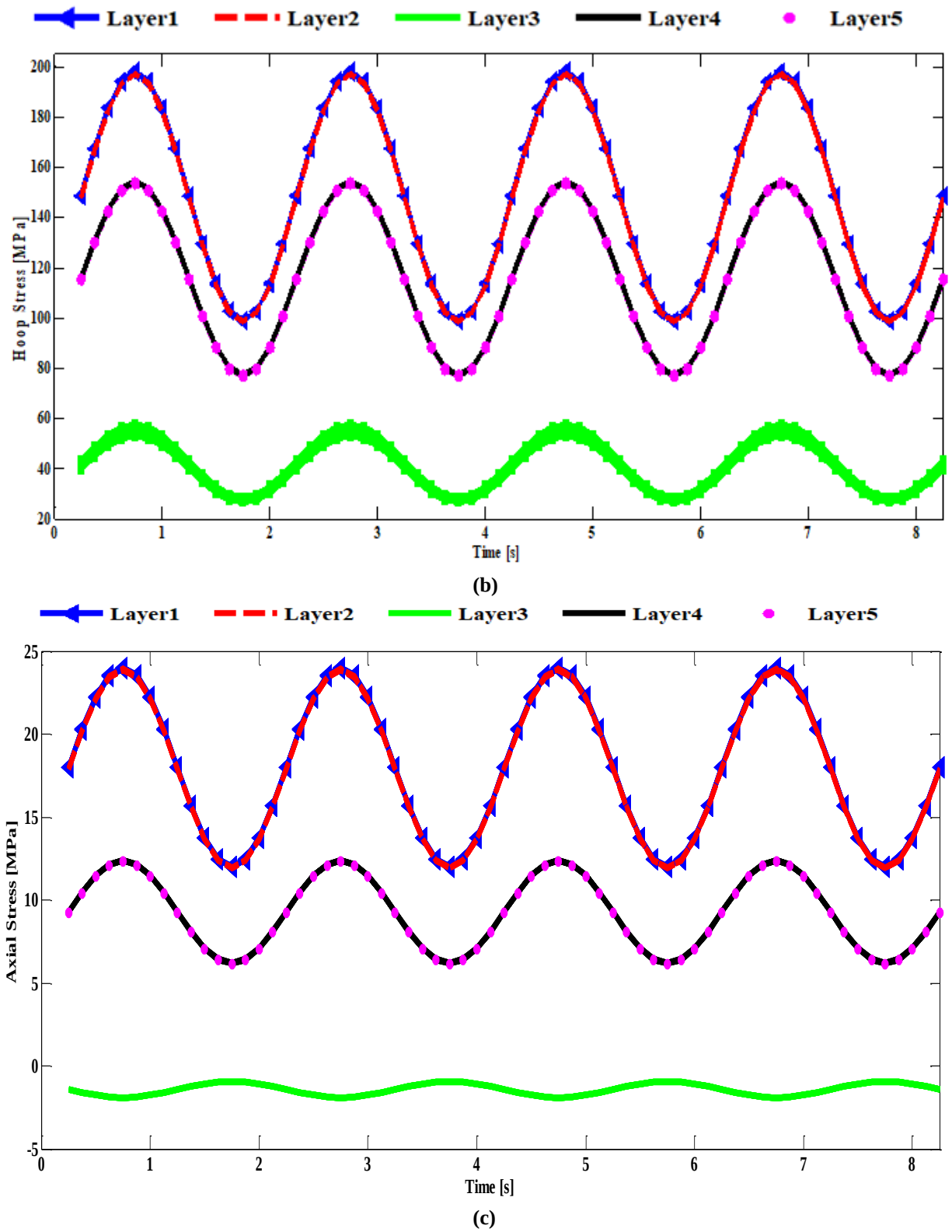

Figure 59. Time history of: (a) Radial stress, (b) Hoop stress and (c) Axial stress distribution through the thickness of the pipe under cyclic internal pressure.

Figure 60 depicts the distribution of shear stress via various layers. The shear stress drops to zero as the winding angle approaches the axial direction (0°), as seen in the figure. It reveals that for the cross-ply laminates, no shear stress is generated as a result of the internal pressure. Also,

it is worth mentioning that there is discontinuity at the interfaces of different layers for shear stress. The shear stress jump occurs between layer fibers orientations of 60 and -60, where in the core layer it is nearly zero. The sandwich core's primary role is to transfer mechanical activities from one skin to the other by shearing.

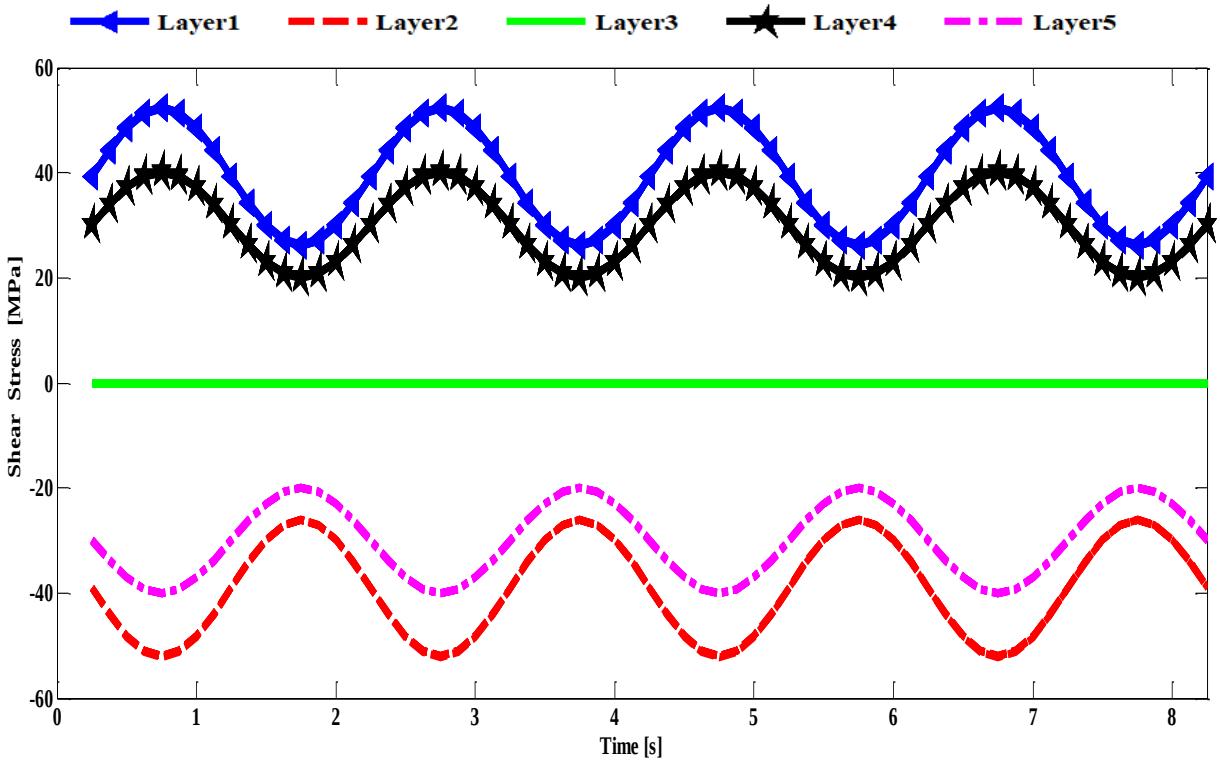

Figure 60. Distribution of the shear stresses under cyclic internal pressure.

V .5.1.3- Strain analysis

Figure 61 (a) depicted above illustrates the axial strain experienced by the biosandwich pipe When subjected to cyclic internal pressure. In this instance, the axial strain undergoes oscillations, fluctuating between negative values due to the influence of anisotropy.

Figure 61 (b) illustrates the history of hoop strains under cyclic internal pressure through the biosandwich pipe's thickness. The hoop strains are continuous, and the inner layer has the greatest amplitude. At the skin-core contact, discontinuous variation is detected, indicating a compression condition.

Figure 61 (c) displays the temporal evolution of radial strain across the thickness of the biosandwich pipe subjected to cyclic internal pressure. The consistent continuity of hoop strains is evident from the data presented. It is important to highlight that in the case of a biosandwich pipe subjected to cyclic internal pressure, the radial strain consistently maintains a negative value.

Consequently, the radial strain of a biosandwich pipe experiencing simultaneous cyclic internal pressure is significantly influenced by the primary amplitudes of internal pressure.

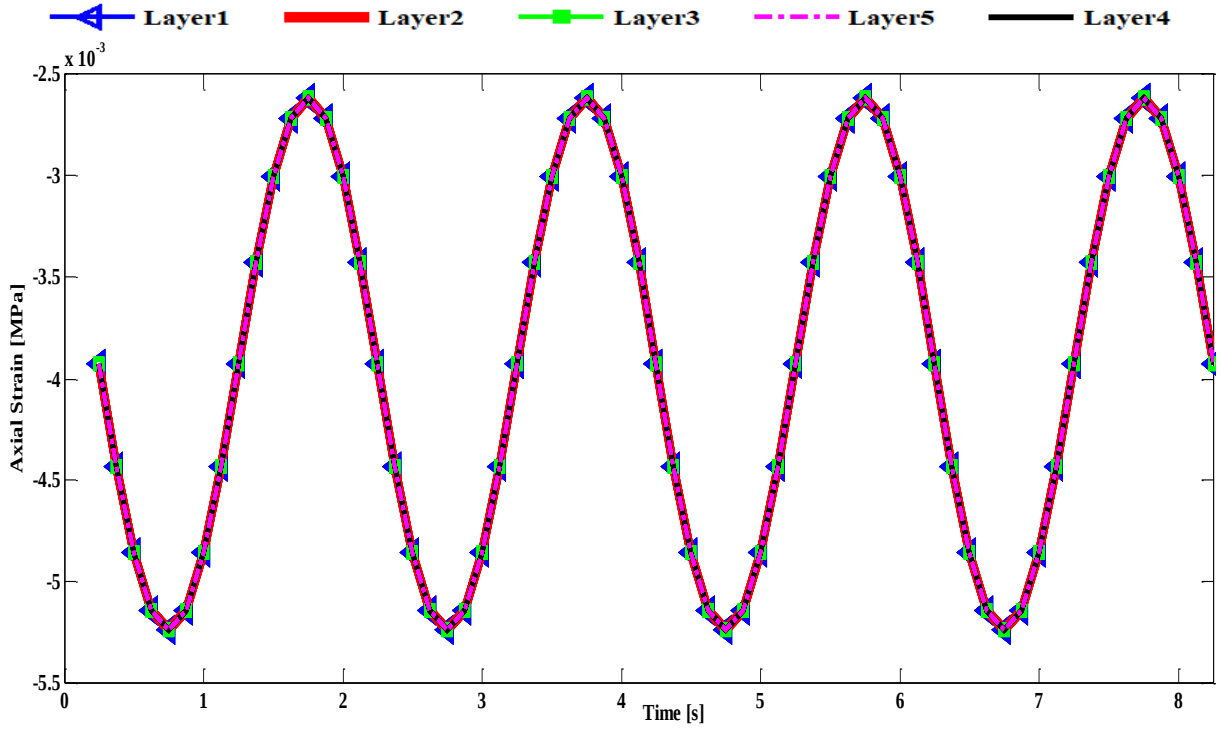

(a)

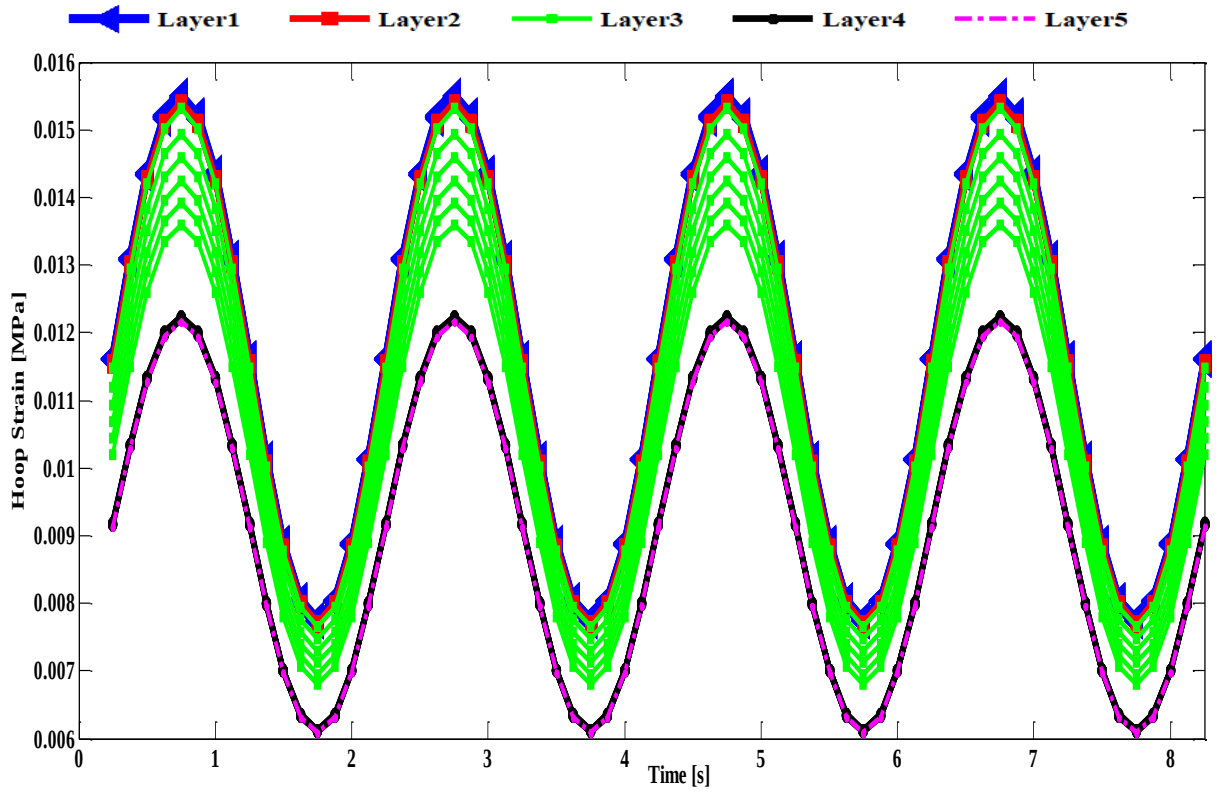

(b)

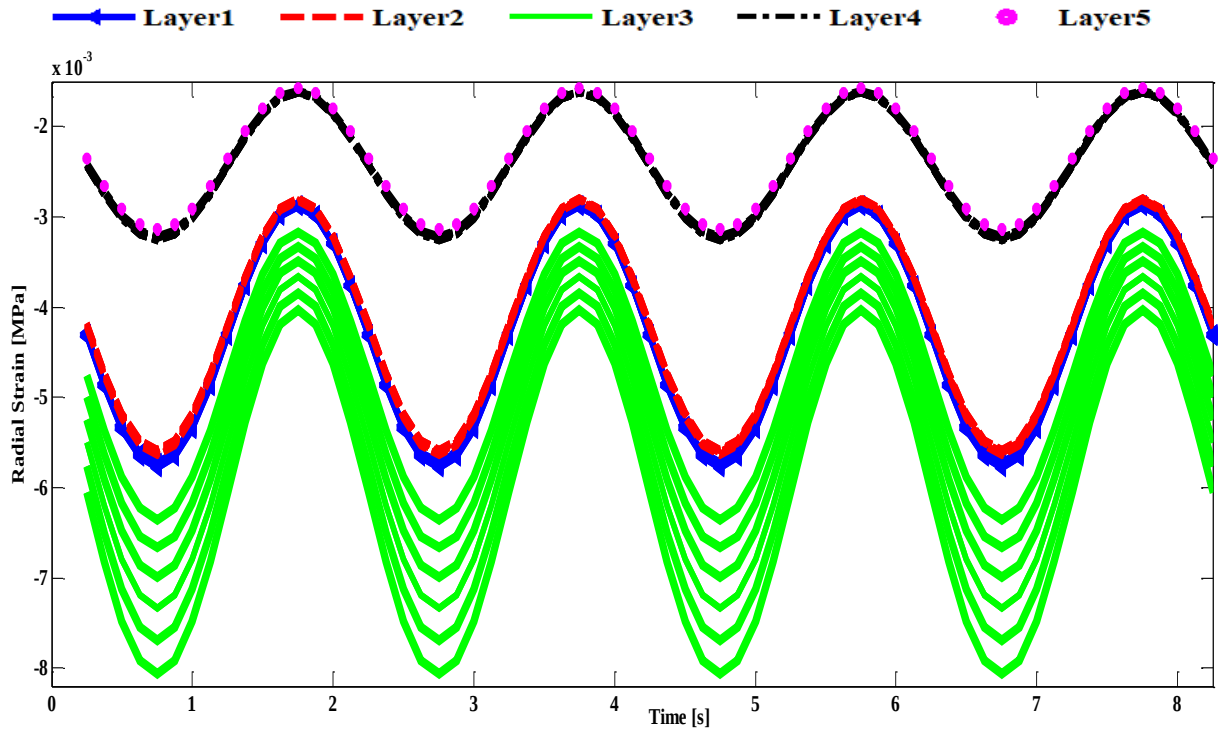

(c)

Figure 61. Time history of: (a) Axial strain, (b) Hoop strain and (c) Radial strain distribution through the thickness of the pipe under cyclic internal pressure.

V .5.2- Dynamic analysis of sandwich pipe based on natural fibers compared to synthetic

A comparative analysis was performed on three different material combinations, including two bio-composites (Jute/epoxy and PALF/epoxy) and synthetic composite Glass/epoxy, within the initially stressed layer of the inner skin. To improve the response of the eco-sandwich pipe, it is indispensable to increase the number of skin layers to converge to the results of the glass/epoxy sandwich. In this final section, sequence 5 (Seq 5 in Table 10) of biosandwich is selected.

- ***Radial displacement comparison***

The biocomposite structures exhibit less radial swelling than the synthetic Glass/epoxy structures, as indicated by the magnitudes of radial displacement in Figure 62.

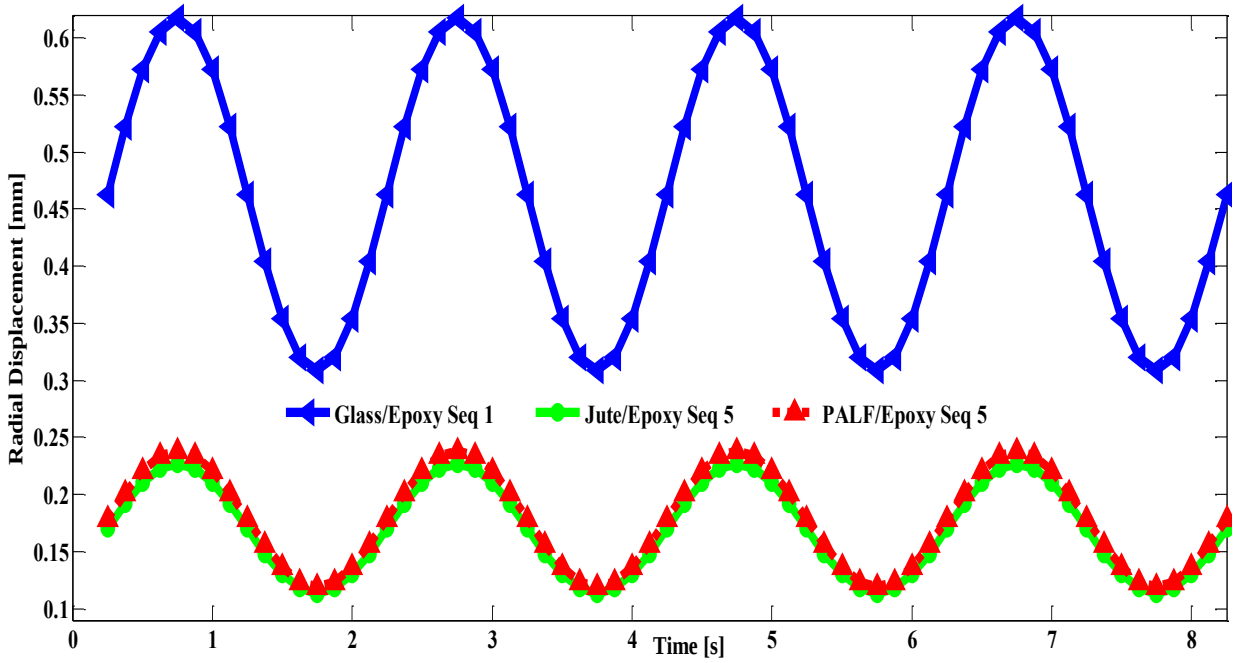

Figure 62. The effect of different materials on radial displacement distribution under cyclic internal pressure.

- ***Stress comparison***

Figure 63 (a) shows that the distribution of radial stress through the thickness of a composite sandwich pipe is not influenced by the type of material but rather by the boundary conditions applied.

The Jute/epoxy and PALF/epoxy sandwich configurations exhibit lower sensitivity compared to glass/epoxy, with lower magnitudes of stress. This observation holds for both radial and axial stress distributions (Figure 63 (b) and (c)).

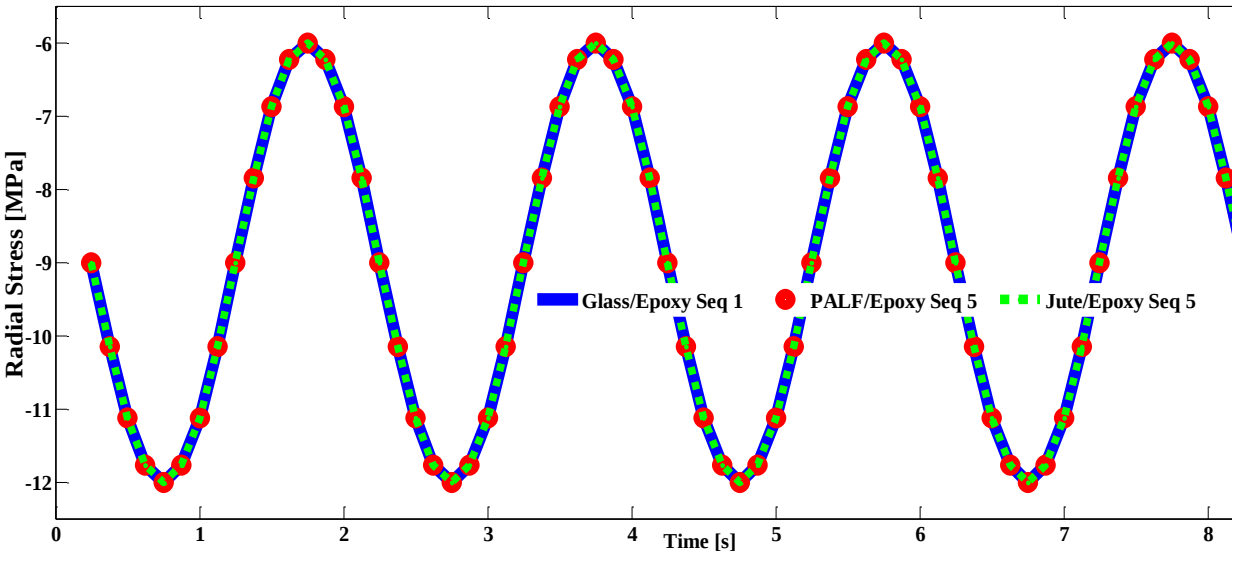

(a)

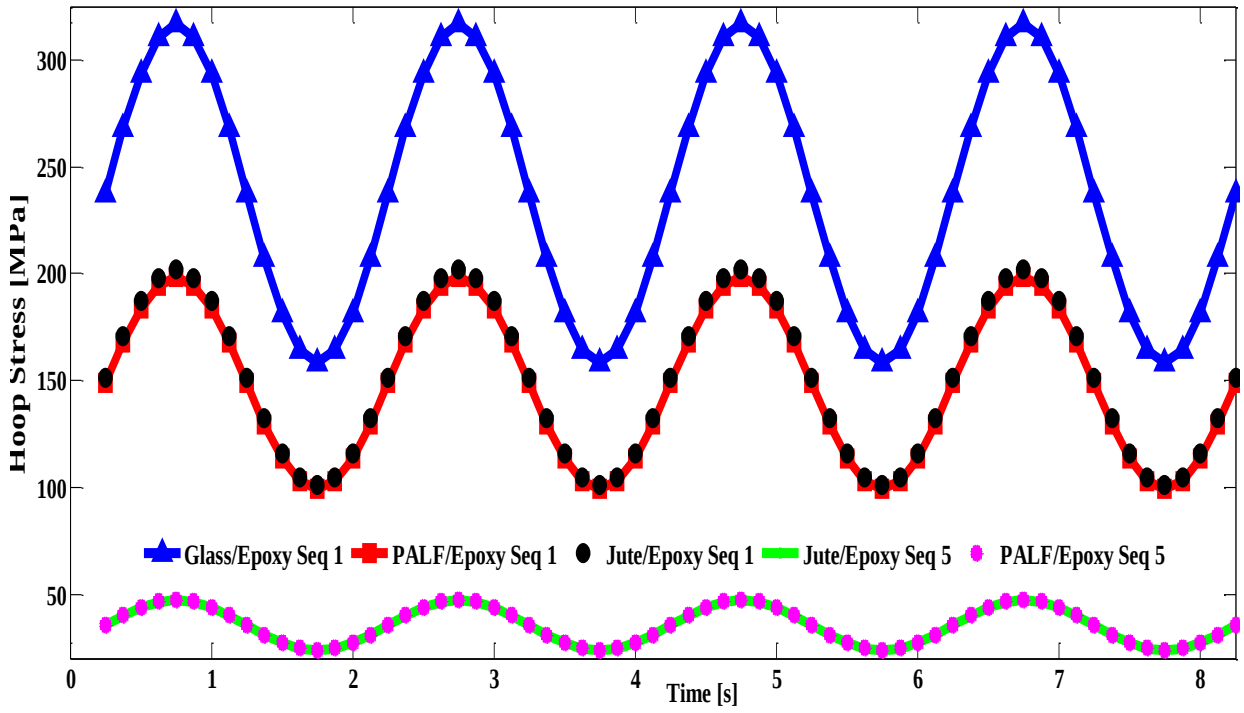

(b)

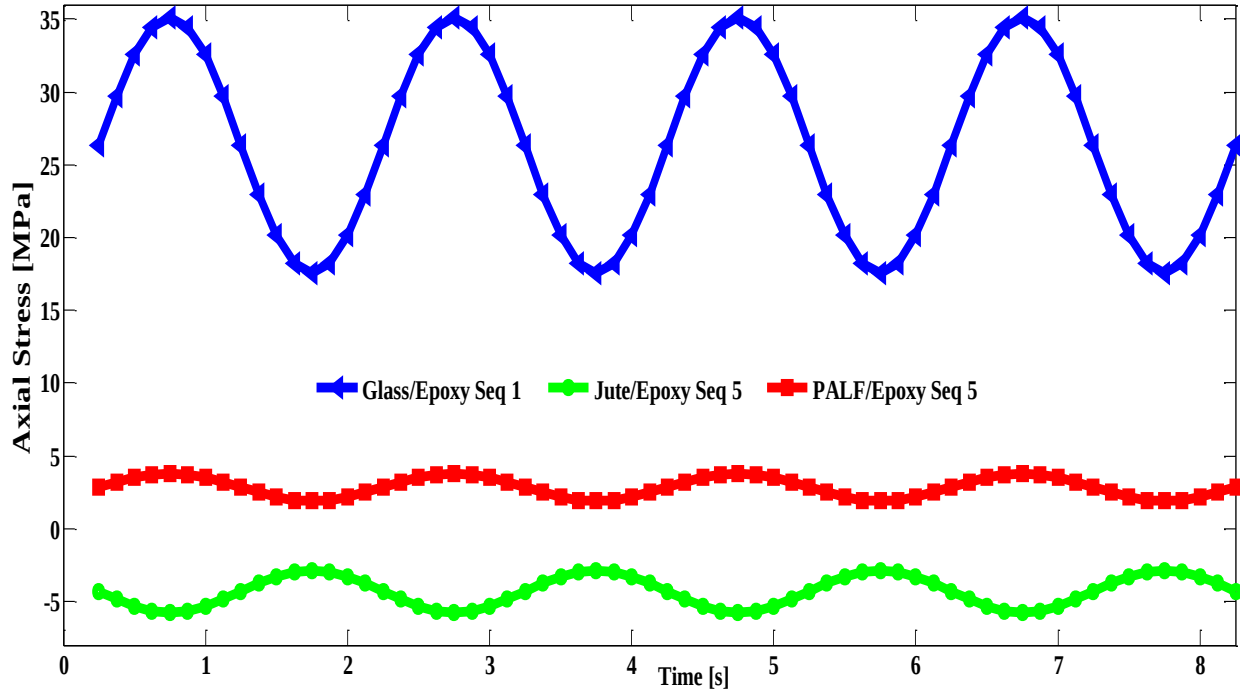

(c)

Figure 63. Effect of different materials on: (a) Radial stress, (b) Hoop stress and (c) Axial stress distribution.

Concerning the shear behavior, the stress magnitudes obtained for the biocomposite are better than those for the synthetic materials (See Figure 64).

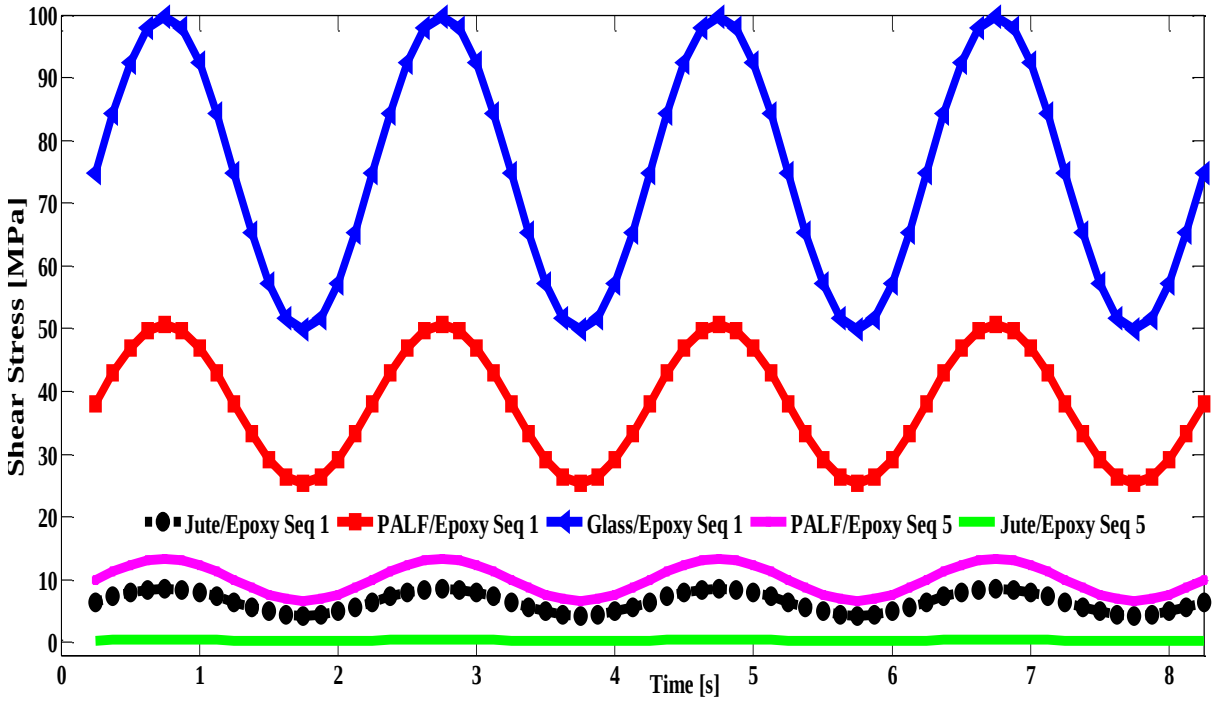

Figure 64. Distribution of the shear stresses under cyclic internal pressure for the 3 materials.

- ***Strain comparison***

The skin's material determines the axial strain; Glass/epoxy provides the highest values, followed by PALF/epoxy, and Jute/epoxy provides the lowest values (See Figure 65 (a)).

The results of this comparison can influence material selection for this application, allowing engineers to choose materials that demonstrate better durability and performance under cyclic internal pressure loading. Analyzing variations in hoop strains provides a full understanding of the materials' behavior and aids in designing structures with increased fatigue resistance. As illustrated in Figure 65 (b), biocomposites have the greatest hoop strain amplitude when compared with synthetic ones.

Figure 65 (c) depicts the distribution of radial strain via the thickness of the sandwich pipe under cyclic internal pressure for the three materials, with the Glass/epoxy having the largest amount of radial strain, followed by the Jute/epoxy, and the PALF/epoxy having the least.

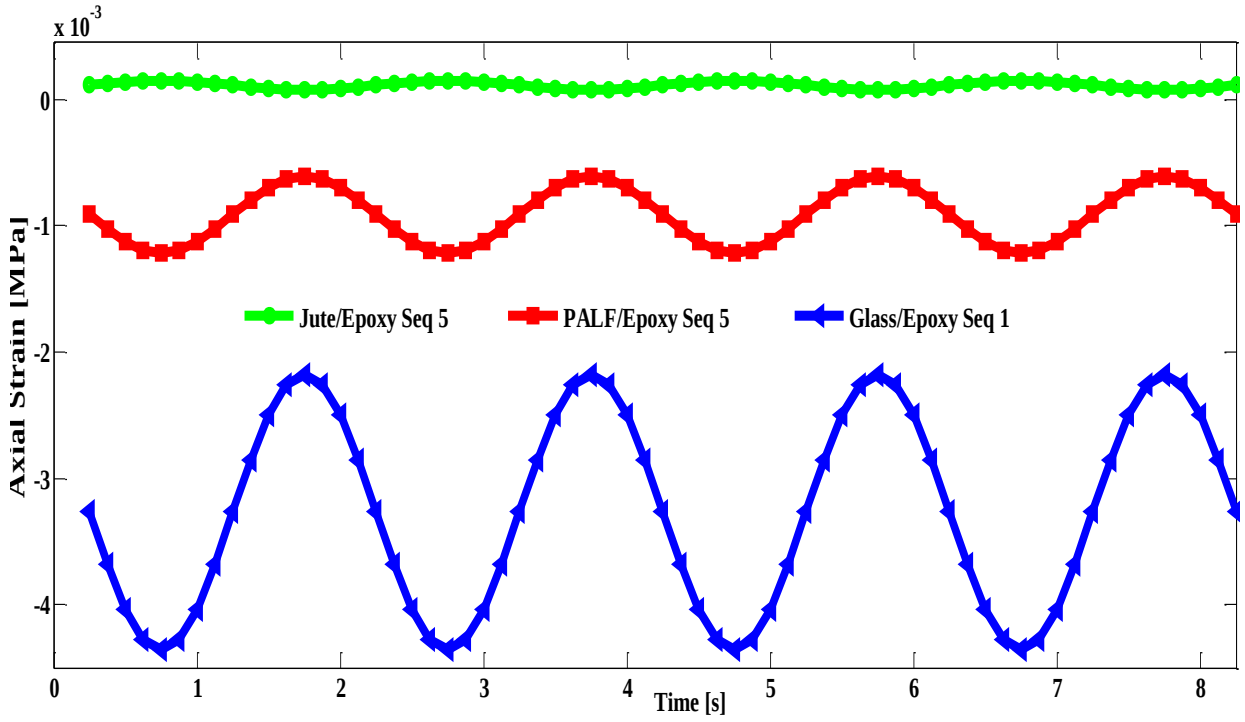
x 10^-3
Axial Strain [MPa]
Jute/Epoxy Seq 5
PALF/Epoxy Seq 5
Glass/Epoxy Seq 1
Time [s]

(a)

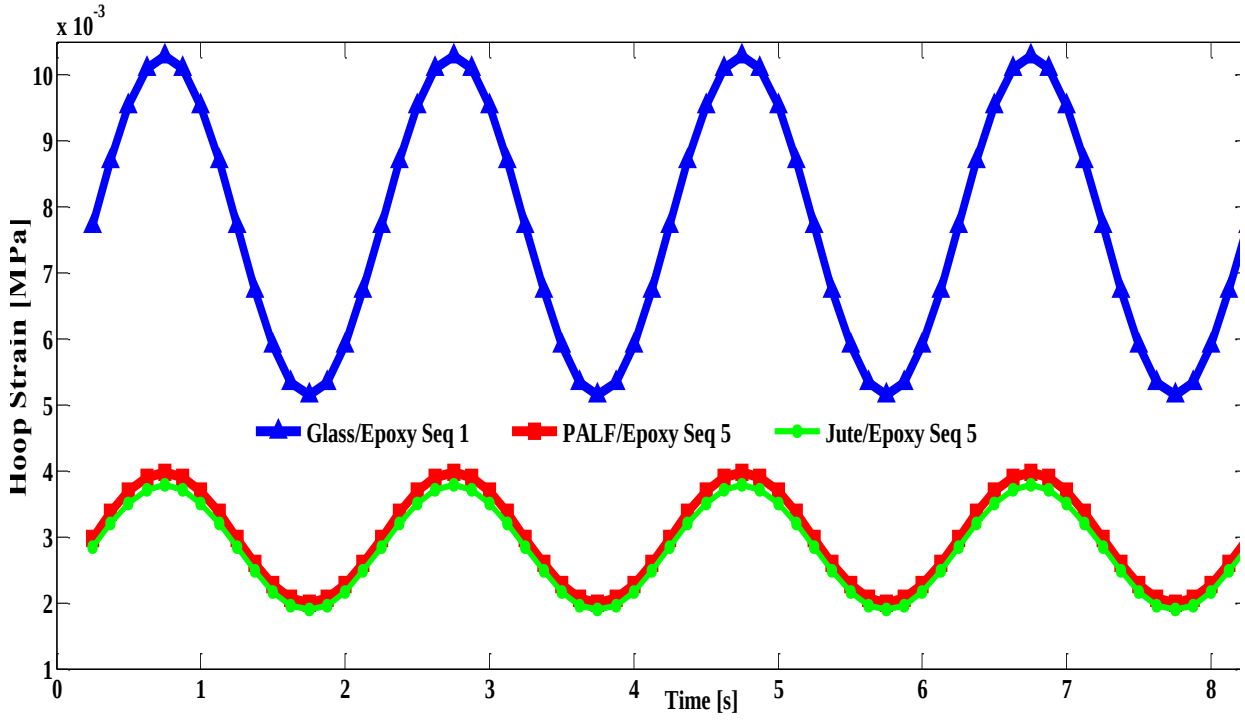
x 10^-3
Hoop Strain [MPa]
Glass/Epoxy Seq 1
PALF/Epoxy Seq 5
Jute/Epoxy Seq 5
Time [s]

(b)

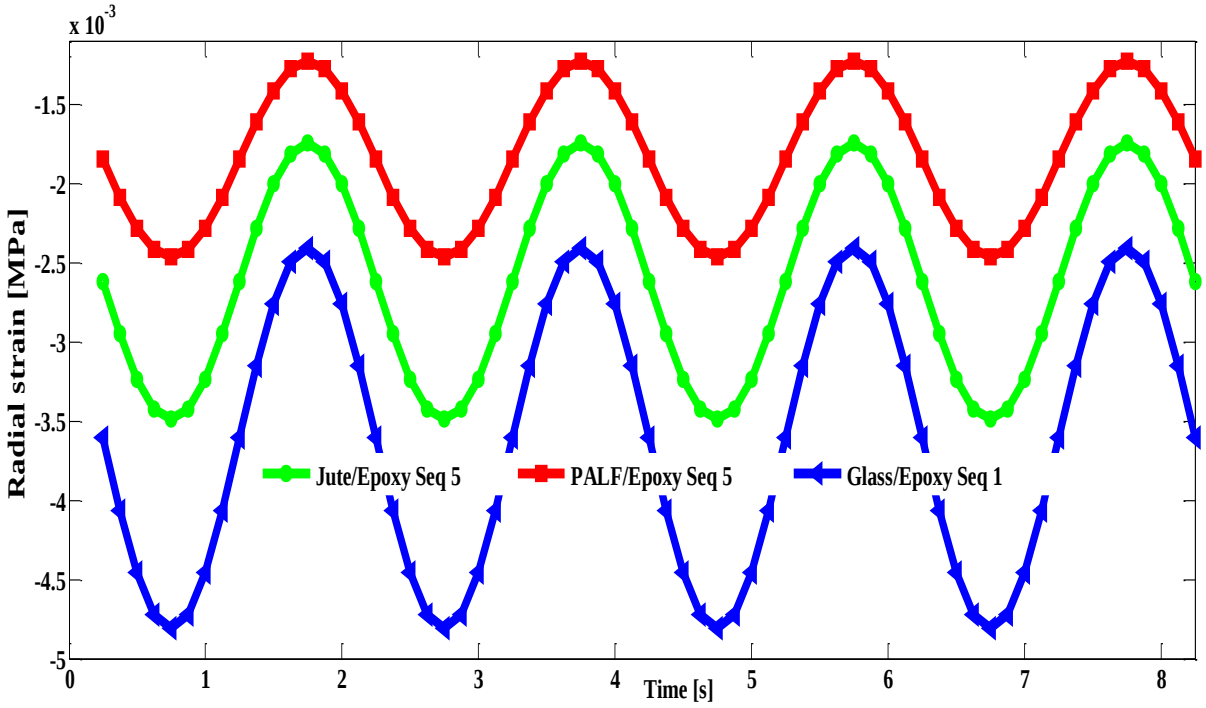

(c)

Figure 65. Effect of different materials on: (a) Axial strain, (b) Hoop strain and (c) Radial strain distribution.

- ***Failure comparison***

The highly stressed material configurations selected for this study can have their rupture limit determined using the Tsai-Wu criteria, where the stress used in this criterion are obtained in plane fiber, such as (longitudinal σ_L, transverse σ_T and shear τ_{LT} stresses). Under cyclic internal pressure, sandwich pipes made of glass/epoxy and biocomposite (Jute/epoxy) are examined (see Figure 66). Reinforcing biocomposite sandwich up to Seq 5 (7 layers of biocomposite layers) increases their rigidity. Compared to the static loading (see Figure 56), the Seq 4 with 5 layers in each skin provides security for sandwich pipelines under 85 bars. These results show the effect of dynamic loading on the security of structures compared to static loading.

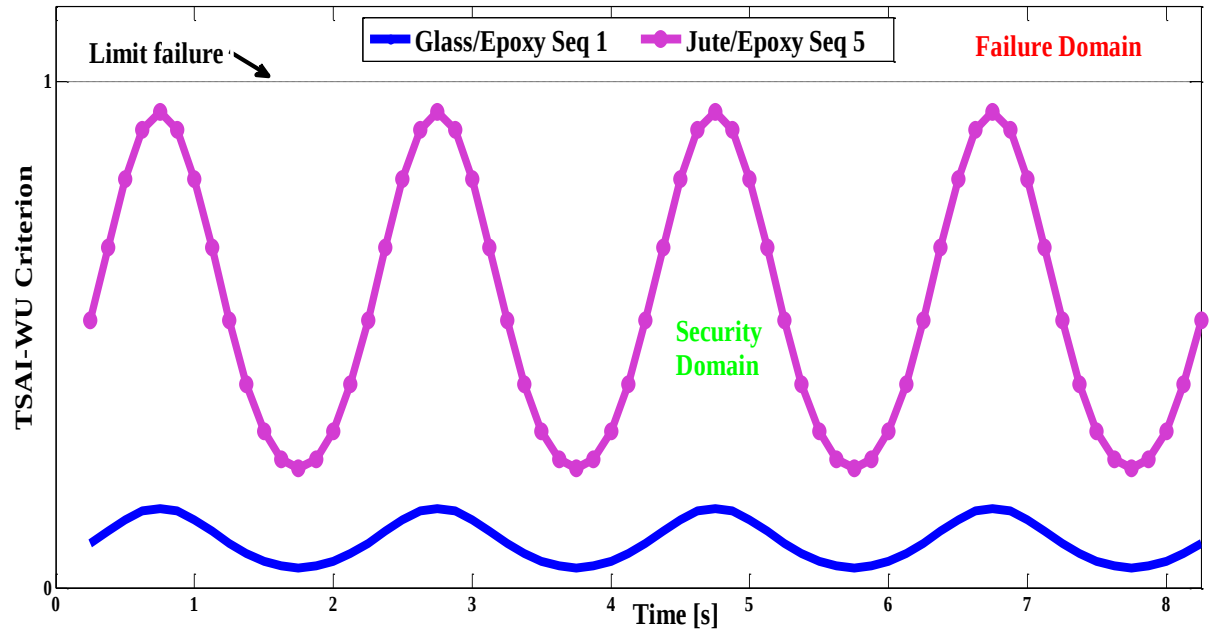

Figure 66. Variations of Tsai-Wu criterion versus time for various skin materials.

Figure 67 depicts the distribution of the Von Mises criteria as a function of the time loading of the epoxy core component in synthetic and biocomposite materials, where the core is considered an isotropic material and the stress equivalent is obtained in a cylindrical plane structure. The addition of biocomposite layer skins enhances the rigidity of the epoxy core and enables it to stay better than the core of a synthetic composite sandwich. The Von Mises criteria findings are below the elastic limit, estimated 102.49 MPa [162], providing credibility to the model created using the linear elastic approach.

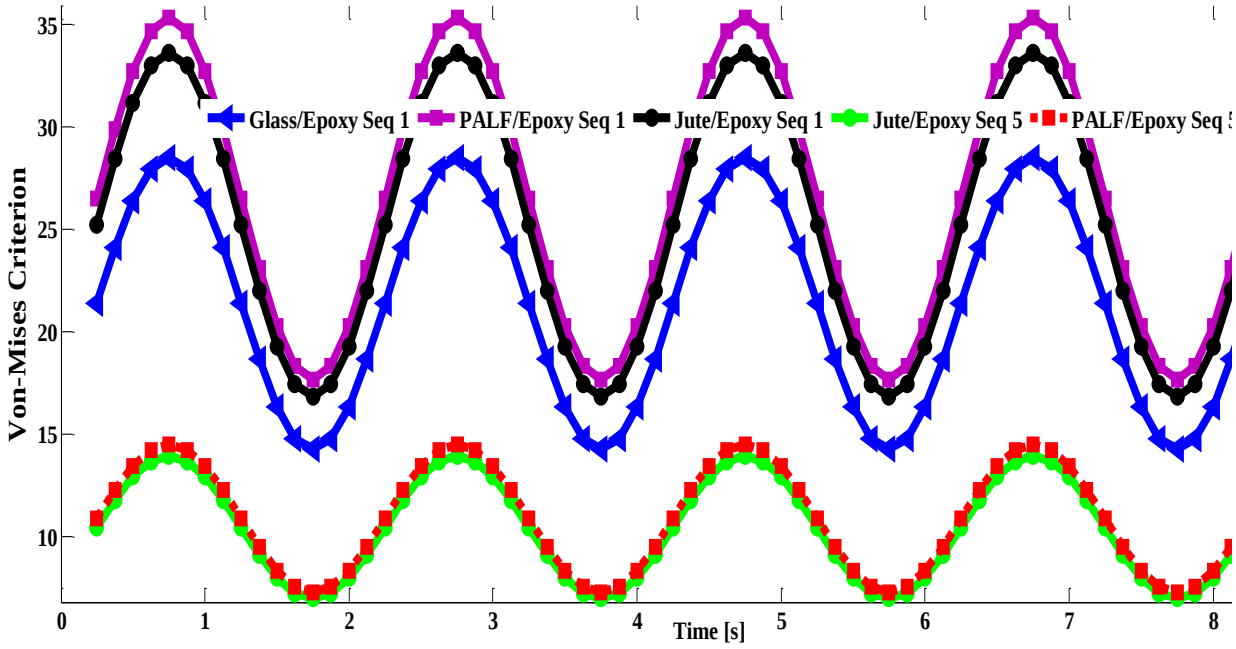

Figure 67. Variations of Von-Mises criterion versus time.

V .6- ECONOMIC APPROACH

This section, which concludes the last chapter, aims to develop a comparative approach to estimating the cost of tubes made from synthetic fibers (Glass) compared with those made from natural fibers (PALF and Jute).

A synoptic economic analysis for all types of Glass/epoxy, PALF/epoxy, and finally Jute/epoxy materials is given in the table below. The price of each of the components is expressed together with its percentage by volume. The results obtained show that, for the same thickness of the layer, the price of a biocomposite pipe is four times lower than that of a pipe based on Glass/epoxy.

The specificity of biocomposite recycling and the environmental specificity reinforce this advantage of using biocomposite in manufacturing hydrogen pipeline transport in this a range of internal pressure.

Table 11. Economic comparative approach between synthetic and biocomposites pipe solutions.

	Glass fiber	***Natural fibers***		***Epoxy***	***Glass/epoxy***	***Biocomposite***	
		PALF	***Jute***			***PALF/epoxy***	***Jute/epoxy***
Volumetric mass [Kg/m^3]	2400	953	1300	1200	1620	1162	1215
Volume fraction	0.35	0.15	0.15	0.65 – 0.85	-		
Pipe Volume: Thickens = 0.27×10^{-3}m, Diameter = 66×10^{-3} m, Length =1 m.					35.64×10^{-3} L		
Mass [Kg]					577×10^{-4}	414×10^{-4}	433×10^{-4}
Material Price [$ /Kg] [239] *'12-02-2024'*	2.90	0.75	0.90	0.50	(2.9×0.35×2400)+(0.5×0.65×1200) = 2826	617.21	685.5
A layer pipe price (Liter)					100.71	23.93	24.43
Price Synthetic/Biocomposite pipe comparison					201.42 = 2 Layers	8.41 Layers	8.24 Layers

V .7- CONCLUSION

Chapter V is based on analytical and numerical methods established to evaluate the potential applications of eco-composites sandwich pipes under pure internal pressure in order to replace synthetic composites (Glass/epoxy). The present chapter focuses on two types of analysis: static and dynamic behavior.

For the section of static analysis:

- A substantial level of concurrence is observed between the analytical and Finite Element Method (FEM) results, notably for radial displacement, stress, and strain.
- As the internal pressure loading on the sandwich pipe increases, the Tsai-Wu criterion is applied to prevent its failure. The progressive reinforcement of bio-composite sandwiches through the augmentation of layer count enhances their overall rigidity.

For the section of dynamic analysis:

- When it comes to the radial displacement and radial stress of composite sandwich pipelines, the analytical method developed can handle complicated time-dependent and integral boundary conditions related to internal pressure and continuity.
- The analytical solution developed can be effectively employed for the dynamic analysis of functionally graded pipes and pressure vessels subjected to cyclic loads.
- The distributions of time-dependent stress, strain, and deformation were obtained.
- In the case of a sandwich pipe subjected to simultaneous cyclic internal pressure, the sign of axial strain is significantly influenced by the mean amplitude of the cyclic loading and reflects the imposed boundary conditions.
- The Tsai-Wu criterion is used to avoid failure of the three different sandwich pipes. The gradual reinforcement of bio-composite sandwiches by increasing the number of layers increases their rigidity.

The main results for both static and cyclic analysis lead to the following conclusions:

- The results highlight that hoop and axial stresses are highly dependent on the properties of the materials involved.
- Hoop and axial stress demonstrate that the inner skins are substantially strained compared to the outer layer. This may result in the commencement of progressive damage to the inner

wall of the sandwich tube, necessitating an augmentation in the number of layers for the internal skin as compared to the external one.

- Shear stress findings demonstrate that the core part of the sandwich pipe does not contribute to the shearing state resistance, which is only supported by the skin parts.
- When it comes to hoop strain, the biosandwich responds better in terms of stiffness compared to the synthetic sandwich since it has more layers of natural fiber-based skins.
- Optimizing the number of layers of natural fiber-based skins is crucial for achieving a favorable quality/price ratio.
- The findings of axial strain indicate that the structure is compressed in the axial direction. In this context, the jute/epoxy combination exhibits favorable behavior compared to glass/epoxy.
- The hoop strain results demonstrate swelling in the sandwich pipe, which is more noticeable for the natural fiber composite in comparison to the synthetic fiber composite.
- With a concentration in the core, the radial strain values show a condition of compression of the sandwich pipe wall through its thickness.
- The pressure examined in this study is three times the anticipated service pressure, which is expected to be 30 bars. This provides a substantial safety margin when utilizing biocomposites in the production of sandwich tubes.
- By increasing the number of layers, substituting bio-fibers for synthetic fibers produces suitable results and can play the same role at this point of analysis.
- Taking into account a dynamic loading that reflects the reality of the behavior of a gas transport tube has influenced the integrity of the tubular structure compared to a quasi-static loading (with a number of 10 layers for each skin). In order to remedy this, additional reinforcement of layers in the lower and upper skins was suggested, increasing the total number of layers to 14 for each skin.
- A comparative economic analysis was conducted, revealing that the price of the synthetic fiber-based solution is four times higher than that of the natural fiber-based solution.

CONCLUSIONS AND FUTURE DEVELOPMENTS

CONCLUSIONS AND FUTURE DEVELOPMENTS

The present thesis focuses on the dimensioning of eco-sandwich tubular structures with a comparison of results with tubes based on synthetic fibers (Glass), using natural fibers (PALF and Jute), Two models were developed to achieve this objective: the analytical model under Matlab software and the FEM model under Ansys. The developed models were used for the deterministic analysis of composite sandwiches under static internal pressure. To simulate the fatigue phenomenon, the analytical dynamic analysis is developed under cyclic loading of internal pressure.

The multilevel structure of the composite sandwich and the effect of the behavior of the components of the composite material as fibers and matrix must be developed through micro- and macro-analysis before reaching the behavior of the sandwich tubular structure under different loadings.

The initial contribution of this thesis was provided in Chapter 3, where analytical micromechanical models were developed using MATLAB and FE modeling methods using ANSYS Software, and the results were compared to existing experimental data. During this first contribution, three different natural fiber-reinforced composites were studied: Pineapple leaf fiber, Date palm fiber, and Alfa fiber. The analytical micromechanical models are based on four theories, which are: Halpin-Tsai, Chamis, Hashin vs. Rosen, and ROM.

The micromechanical models developed allow for the prediction of the elastic properties of the three fiber-based eco-composites, which showed dispersion in terms of stiffness, where the composite based on PALF fibers presents the best behavior in tension, compression, and shear, followed by the composite based on Alfa fibers, and finally that based on Palm fibers.

The second contribution of this thesis is focused on the macro-mechanical analysis of the element of the tubular composite sandwich, represented by stratification under loading, which represents the static internal pressure. The objective of this level of analysis is to develop an analytical model of sandwich element behavior with natural skins. A comparison was made between natural and synthetic fiber composites. The results obtained are significant in favor of replacing synthetic composites with natural ones, but more research is needed to decide on this solution. So, the structure-level analysis is important, and it is the objective of the last chapter.

- The forces applied to the sandwich plate simulate the internal pressure load that the tubular sandwich structure undergoes.
- Macromechanical analysis assists in pinpointing the highly stressed layer, whether it pertains to the upper or lower skin, there by aiding in failure analysis and suggesting potential reinforcement measures.
- The results obtained have illustrated that the mechanical properties play a significant role in influencing the behavior of composite sandwiches constructed from either synthetic or natural fibers.

In the third part of this present study, a three-dimensional elasticity analytical model design for eco-sandwich pipes has been employed to evaluate the performance of composite pipes under the influence of both static and cyclic internal pressure. This comprehensive dynamic solution appears to be particularly effective with cyclic mechanical loadings and may be used as an accurate model in numerous engineering applications. The principal results allow for the following conclusions:

- ❖ Improving the quality/price ratio requires optimizing the number of natural fiber-based skin layers.
- ❖ To protect the sandwich pipe against failure under static or cyclic loads, the current study reveals that gradually strengthening bio-composite sandwiches by increasing the number of layers increases their rigidity.
- ❖ The pressure analyzed for the static and cyclic analyses is a factor of three of the service pressure, which is expected to be 30 bars. This provides a very significant safety margin when integrating biocomposites for designing sandwich tubes under static or cyclic loads.
- ❖ Substituting synthetic fibers with bio-fibers produces suitable results by raising the number of biocomposite layers.
- ❖ The tubular structure's integrity is impacted by dynamic loading, similar to that of a gas transport tube, rather than quasi-static loading with 10 layers of each skin. To address this, additional layers of reinforcement were proposed for the lower and upper skins, increasing the total number of layers to 14 for each skin.
- ❖ The natural fiber-based alternative solution is four times less expensive than the synthetic fiber-based, according to a comparative economic analysis.

Future developments

Considering the work carried out in this thesis, some future developments will be presented, including the following:

- ❖ Further investigations are required for the new research axis of incorporating natural fibers into sandwich tubes using the filament winding process.
- ❖ For the development of an optimal analytical and numerical tool design, it is crucial to integrate the potential damage behavior that may occur in both the skin and the core into the macro and structure levels. This behavior will be treated in the forthcoming study.
- ❖ Propose a numerical model that integrates coupled mechanical and thermal analysis. Conducting a thermo-mechanical analysis is expected to yield different results in comparison with the findings from previous investigations,
- ❖ Carry out various experiments for both mechanical and thermal behavior to correlate the findings with the analytical and numerical analysis.
- ❖ Pipeline sandwich manufactured deals with leakages due to the porosity of the composite. To overcome this drawback, the internal skins filaments must be coated on a metal liner. This transport media conception can provide several advantages, and must be taken into account by the analytical and numerical developed.
- ❖ The development of an optimization model for the parameters of biocomposite layers based on stochastic methods is essential to guaranteeing value for money for this replacement solution for synthetic composites.
- ❖ The fatigue behavior of the composite structure requires the introduction of matrix damage and fiber laws into the developed micro model. The damage creates a plasticity behavior that leads to the loss of material properties. Using the dynamic model developed in this contribution, the fatigue behavior of the present solution can predict fatigue life and durability.
- ❖ Taking into account the energy stored following a cyclic loading.

REFERENCES

REFERENCES

[1] R. Potluri, V. Diwakar, K. Venkatesh, and B. Srinivasa Reddy, “Analytical Model Application for Prediction of Mechanical Properties of Natural Fiber Reinforced Composites,” *Mater. Today Proc.*, vol. 5, pp. 5809–5818, 2018, doi: 10.1016/j.matpr.2017.12.178.

[2] L. Hristian, M. M. Ostafe, L. R. Manea, and A. L. Leon, “The study about the use of the natural fibres in composite materials,” *IOP Conf. Ser. Mater. Sci. Eng.*, vol. 145, no. 3, 2016, doi: 10.1088/1757-899X/145/3/032004.

[3] F. Laurin, N. Carrere, and J. F. Maire, “Laminated composite structures subjected to compressive loading: A material and structural buckling analysis,” *Compos. Struct.*, vol. 80, no. 2, pp. 172–182, 2007, doi: 10.1016/j.compstruct.2006.04.074.

[4] S. Sahu *et al.*, “Characterization of natural fiber extracted from Bauhinia vahlii bast subjected to different surface treatments: A potential reinforcement in polymer composite,” *J. Nat. Fibers*, vol. 20, no. 1, 2023, doi: 10.1080/15440478.2022.2162185.

[5] S. W. Tsai and J. M. Patterson, “Simplified design of composite materials,” *Mater. Des.*, vol. 8, no. 3, pp. 135–141, 1987, doi: 10.1016/S0261-3069(87)90021-5.

[6] S. Sulaiman and S. Borazjani, “Finite element analysis of filament-wound composite pressure vessel under internal pressure,” *IOP Conf. Ser. Mater. Sci. Eng.*, vol. 50, no. November, 2013, doi: 10.1088/1757-899X/50/1/012061.

[7] Z. F. Albahash and M. N. M. Ansari, “Investigation on energy absorption of natural and hybrid fiber under axial static crushing,” *Compos. Sci. Technol.*, vol. 151, pp. 52–61, 2017, doi: 10.1016/j.compscitech.2017.07.028.

[8] K. Tserpes, V. Tzatzadakis, and J. Bachmann, “Electrical conductivity and electromagnetic shielding effectiveness of bio-composites,” *J. Compos. Sci.*, vol. 4, no. 1, 2020, doi: 10.3390/jcs4010028.

[9] F. I. Mahir, K. N. Keya, B. Sarker, K. M. Nahiun, and R. A. Khan, “A brief review on natural fiber used as a replacement of synthetic fiber in polymer composites,” *Mater. Eng. Res.*, vol. 1, no. 2, pp. 88–99, 2019, doi: 10.25082/mer.2019.02.007.

[10] A. Maizia, A. Hocine, and H. Dehmous, “Development of a Reliability-Mechanical : Numerical Model of Mechanical Behavior of a Multilayer Composite Plate,” *Appl. Mech. Behav. Mater. Eng. Syst.*, pp. 387–397, 2017, doi: 10.1007/978-3-319-41468-3.

[11] A. Maizia, A. Hocine, H. Dehmous, and D. Chapelle, “Prediction of reliability analysis of composite tubular structure under hygro-thermo-mechanical loading,” *Mech. Adv. Mater. Struct.*, vol. 26, no. 4, pp. 372–379, 2019, doi: 10.1080/15376494.2017.1387329.

[12] A. Hocine, D. Chapelle, L. M. Boubakar, A. Benamar, and A. Bezazi, “Analysis of intermetallic swelling on the behavior of a hybrid solution for compressed hydrogen storage - Part I: Analytical modeling,” *Mater. Des.*, vol. 31, no. 5, pp. 2435–2443, 2010, doi: 10.1016/j.matdes.2009.11.048.

[13] M. L. Boubakar, F. Trivaudey, D. Perreux, and L. Vang, “A meso-macro finite element modelling of laminate structures - Part I: time-independent behaviour,” *Compos. Struct.*, vol. 58, no. 2 PG-271, p. 286, 2002.

[14] V. E. Verijenko, S. Adali, and P. Y. Tabakov, “Stress distribution in continuously heterogeneous thick laminated pressure vessels,” *Compos. Struct.*, vol. 54, no. 2–3, pp. 371–377, 2001, doi: 10.1016/S0263-8223(01)00112-X.

[15] T. K. Hwang, C. S. Hong, and C. G. Kim, “Probabilistic deformation and strength prediction for a filament wound pressure vessel,” *Compos. Part B Eng.*, vol. 34, no. 5, pp. 481–497, 2003, doi: 10.1016/S1359-8368(03)00021-0.

[16] B. Gangil, L. Ranakoti, S. Verma, T. Singh, and S. Kumar, “Natural and Synthetic Fibers for Hybrid Composites,” in *Hybrid Fiber Composites: Materials, Manufacturing, Process Engineering*, Wiley-VCH Verlag GmbH & Co. KGaA, 2020. doi: 10.1002/9783527824571.ch1.

[17] A. Ticoalu, T. Aravinthan, and F. Cardona, “A review of current development in natural fiber composites for structural and infrastructure applications,” in *Southern Region Engineering Conference*, SREC2010-F1-5, 2010, pp. 1–5.

[18] E. R. K. Chandrathilaka, S. K. Baduge, P. Mendis, and P. S. M. Thilakarathna, “Structural applications of synthetic fibre reinforced cementitious composites : A review on material properties , fire behaviour , durability and structural performance,” *Structures*, vol. 34, no. August, pp. 550–574, 2021, doi: 10.1016/j.istruc.2021.07.090.

[19] S. V Joshi, L. T. Drzal, A. K. Mohanty, and S. Arora, “Are natural fiber composites environmentally superior to glass fiber reinforced composites ?,” *Compos. Part A Appl. Sci. Manuf.*, vol. 35, pp. 371–376, 2004, doi: 10.1016/j.compositesa.2003.09.016.

[20] Z. Xia, Y. Chen, and F. Ellyin, “A meso / micro-mechanical model for damage progression

in glass- fiber / epoxy cross-ply laminates by finite-element analysis," *Compos. Sci. Technol.*, vol. 60, pp. 1171–1179, 2000, doi: 10.1016/S0266-3538(00)00022-1.

[21] S. K. Golla and P. Prasanthi, "Prediction of Micromechanical Behavior of Fiber (Glass / Basalt) Reinforced Polymer Composites," *Int. Res. J. Eng. Technol.*, vol. 3, no. January 2017, 2016.

[22] R. Potluri, K. Supriya, and G. V. V. N. G. Vittal, "Effect of boron carbide particles inclusion on the mechanical behaviour of S2-Glass fiber based polyester composites," *Mater. Today Proc.*, vol. 5, no. 9, pp. 20257–20267, 2018, doi: 10.1016/j.matpr.2018.06.397.

[23] J. N. Panda, E. Y. Orquera, A. A. Mohanty, and P. Egberts, "Tribo-corrosion inhibition of AISI 4715 steel pipe carrying hydraulic fracturing fluid," *Tribol. Int.*, vol. 161, 2021, doi: 10.1016/j.triboint.2021.107066.

[24] D. Zhou *et al.*, "The experiment study to assess the impact of hydrogen blended natural gas on the tensile properties and damage mechanism of X80 pipeline steel," *Int. J. Hydrogen Energy*, vol. 6, 2020, doi: 10.1016/j.ijhydene.2020.11.267.

[25] A. Royani, S. Prifiharni, and G. Priyotomo, "Corrosion Behavior of Low Carbon Steel Pipe in Condensate Environment," *TRENDS Sci.*, vol. 19, no. 3, pp. 1–11, 2022, doi: 10.48048/tis.2022.2072.

[26] A. H. Alamri, "Localized Corrosion and Mitigation Approach of Steel Materials Used in Oil and Gas Pipelines -An overview," *Eng. Fail. Anal.*, p. 104735, 2020, doi: 10.1016/j.engfailanal.2020.104735.

[27] M. Sun, H. Zhao, X. Li, J. Liu, and Z. Xu, "New evaluation method of failure pressure of steel pipeline with irregular-shaped defect," *Appl. Ocean Res.*, vol. 110, 2021, doi: 10.1016/j.apor.2021.102601.

[28] R. Potluri, K. J. Paul, and B. M. Babu, "Effect of Silicon Carbide Particles Embedmenton the properties of Kevlar Fiber ReinforcedPolymer Composites," *Mater. Today Proc.*, vol. 5, no. 2, pp. 6098–6108, 2018, doi: 10.1016/j.matpr.2017.12.215.

[29] S. Jiang, F. Sun, H. Fan, and D. Fang, "Fabrication and testing of composite orthogrid sandwich cylinder," *Compos. Sci. Technol.*, vol. 142, pp. 171–179, 2017, doi: 10.1016/j.compscitech.2017.02.009.

[30] J. S. Yang *et al.*, "Influence of manufacturing defects on modal properties of composite

pyramidal truss-like core sandwich cylindrical panels," *Compos. Sci. Technol.*, vol. 147, pp. 89–99, 2017, doi: 10.1016/j.compscitech.2017.05.007.

[31] J. Battaglia, M. Saboul, J. Pailhes, A. Saci, A. Kusiak, and O. Fudym, "Carbon epoxy composites thermal conductivity at 77K and 300K Carbon epoxy composites thermal conductivity at 77 K and 300 K," *J. Appl. Phys.*, vol. 223516, 2014, doi: 10.1063/1.4882300.

[32] A. Mohajerani *et al.*, "Amazing types, properties, and applications of fibres in construction materials," *Materials (Basel).*, vol. 12, no. 16, pp. 1–45, 2019, doi: 10.3390/ma12162513.

[33] Y. Shireesha, G. Nandipati, and K. Chandaka, "Properties of Hybrid Composites And Its Applications: A Brief Review," *Int. J. Sci. Technol. Res.*, vol. 8, no. 8, pp. 335–341, 2019.

[34] A. Ashothaman, J. Sudha, and N. Senthilkumar, "A comprehensive review on biodegradable polylactic acid polymer matrix composite material reinforced with synthetic and natural fibers," *Mater. Today Proc.*, vol. xxxx, no. xxxx, 2021, doi: 10.1016/j.matpr.2021.07.047.

[35] M. Alhijazi, Q. Zeeshan, Z. Qin, B. Safaei, and M. Asmael, "Finite Element Analysis of Natural Fibers Composites: A Review," *Nanotechnol. Rev.*, vol. 9, no. 1, pp. 853–875, 2020, doi: 10.1515/ntrev-2020-0069.

[36] G. Habbar, A. Maizia, A. Hocine, M. H. Dhaou, and R. João, "Micromechanical Analysis of a Bio-Sandwich Application for Cylinder under Pressure," *Compos. Sci.*, vol. 6, no. 69, 2022, doi: https://doi.org/10.3390/jcs6030069.

[37] A. Lotfi, H. Li, D. V. Dao, and G. Prusty, "Natural fiber–reinforced composites: A review on material, manufacturing, and machinability," *J. Thermoplast. Compos. Mater.*, vol. 34, no. 2, pp. 238–284, 2021, doi: 10.1177/0892705719844546.

[38] A. R. G. de Azevedo *et al.*, "Natural fibers as an alternative to synthetic fibers in reinforcement of geopolymer matrices: A comparative review," *Polymers (Basel).*, vol. 13, no. 15, p. 2493, 2021, doi: 10.3390/polym13152493.

[39] H. E. BALCIOĞLU, "Flexural Behaviors of Sandwich Composites Produced Using Recycled and Natural Material," *Mugla J. Sci. Technol.*, vol. 4, no. 1, pp. 64–73, 2018, doi: 10.22531/muglajsci.421813.

[40] S. N. A. Safri, M. T. H. Sultan, M. Jawaid, and K. Jayakrishna, "Impact behaviour of hybrid composites for structural applications: A review," *Compos. Part B Eng.*, vol. 133,

pp. 112–121, 2018, doi: 10.1016/j.compositesb.2017.09.008.

[41] M. Zwawi, "A review on natural fiber bio-composites, surface modifications and applications," *Molecules*, vol. 26, no. 2, 2021, doi: 10.3390/molecules26020404.

[42] A. Atmakuri, A. Palevicius, A. Vilkauskas, and G. Janusas, "Review of Hybrid Fiber Based Composites with Nano Particles — Material Properties and Applications," *Polymers (Basel).*, vol. 12, no. 2088, 2020, doi: 10.3390/polym12092088.

[43] E. Le Bourhis and F. Touchard, "Mechanical Properties of Natural Fiber Composites," *Encycl. Mater. Compos.*, pp. 0–27, 2021.

[44] M. Asim *et al.*, "A review on pineapple leaves fibre and its composites," *Int. J. Polym. Sci.*, vol. 2015, p. 16, 2015, doi: 10.1155/2015/950567.

[45] L. Li, D. K. Pratihar, and S. Chakrabarty, *Advances in Materials and Manufacturing Engineering*. 2020. doi: 10.1007/978-981-15-1307-7.

[46] N. Al-Azad, M. F. M. Asril, and M. K. M. Shah, "A Review on Development of Natural Fibre Composites for Construction Applications," *J. Mater. Sci. Chem. Eng.*, vol. 09, no. 07, pp. 1–9, 2021, doi: 10.4236/msce.2021.97001.

[47] A. Karimah *et al.*, "A review on natural fibers for development of eco-friendly bio-composite: characteristics, and utilizations," *J. Mater. Res. Technol.*, vol. 13, pp. 2442–2458, 2021, doi: 10.1016/j.jmrt.2021.06.014.

[48] G. Pramudi, W. W. Raharjo, D. Ariawan, Ubaidillah, and Z. Arifin, "Utilization of Bamboo Fiber in the Development of Environmentally Friendly Composite – A Review," *IOP Conf. Ser. Mater. Sci. Eng.*, vol. 1096, no. 1, p. 012038, 2021, doi: 10.1088/1757-899x/1096/1/012038.

[49] E. A. O. Al-Bahadly, "THE MECHANICAL PROPERTIES OF NATURAL FIBER COMPOSITES," Swinburne University of Technology, 2013.

[50] M. Nurazzi, A. Khalina, and D. Laila, "A Review : Fibres , Polymer Matrices and Composites SCIENCE & TECHNOLOGY," no. October, 2017.

[51] M. Yasir *et al.*, "Green composites and their contribution toward sustainability : A review," *Results Eng.*, vol. 11, no. April, p. 100263, 2021, doi: 10.1177/09673911211009372.

[52] Y. Djebloun, M. Hecini, T. Djoudi, and B. Guerira, "Experimental determination of elastic

modulus of elasticity and Poisson's coefficient of date palm tree fiber," *J. Nat. Fibers*, vol. 16, no. 3, pp. 357–367, 2019, doi: 10.1080/15440478.2017.1423256.

[53] A. H. Roslan and M. Hassan, "Mechanical properties of bamboo reinforced epoxy sandwich structure composites," *Int. J. Automot. Mech. Eng.*, vol. 12, pp. 2882–2892, 2015, doi: 10.15282/ijame.12.2015.7.0242.

[54] P. Peças, H. Carvalho, H. Salman, and M. Leite, "Natural fibre composites and their applications: A review," *J. Compos. Sci.*, vol. 2, no. 66, pp. 1–20, 2018, doi: 10.3390/jcs2040066.

[55] H. Jariwala and P. Jain, "A review on mechanical behavior of natural fiber reinforced polymer composites and its applications," *J. Reinf. Plast. Compos.*, vol. 38, no. 10, pp. 441–453, 2019, doi: 10.1177/0731684419828524.

[56] G. Habbar, A. Hocine, A. Maizia, and A. Bezazi, "Failure analysis of biocomposite sandwich pipe under internal pressure – Application for high pressure gas transportation pipelines MEDGAZ," *Int. J. Press. Vessel. Pip.*, vol. 202, no. January, p. 10, 2023, doi: 10.1016/j.ijpvp.2023.104891.

[57] Y. G. Thyavihalli Girijappa, S. Mavinkere Rangappa, J. Parameswaranpillai, and S. Siengchin, "Natural Fibers as Sustainable and Renewable Resource for Development of Eco-Friendly Composites: A Comprehensive Review," *Front. Mater.*, vol. 6, no. September, pp. 1–14, 2019, doi: 10.3389/fmats.2019.00226.

[58] P. Wambua, J. Ivens, and I. Verpoest, "Natural fibres: Can they replace glass in fibre reinforced plastics?," *Compos. Sci. Technol.*, vol. 63, no. 9, pp. 1259–1264, 2003, doi: 10.1016/S0266-3538(03)00096-4.

[59] I. Mokhtar, M. Y. Yahya, M. R. A. Kadir, and M. F. Kambali, "Effect on Mechanical Performance of UHMWPE/HDPE-Blend Reinforced with Kenaf, Basalt and Hybrid Kenaf/Basalt Fiber," *Polym. - Plast. Technol. Eng.*, vol. 52, no. 11, pp. 1140–1146, 2013, doi: 10.1080/03602559.2013.798814.

[60] M. R. Sanjay, G. R. Arpitha, L. L. Naik, K. Gopalakrishna, and B. Yogesha, "Applications of Natural Fibers and Its Composites : An Overview," *Sci. Res. publihing*, vol. 7, pp. 108–114, 2016, doi: http://dx.doi.org/10.4236/nr.2016.73011.

[61] M. Cihan, "Experimental and Numerical Investigation on the Mechanical and Dynamic Performance of Flax/E-glass Hybrid Composites," UNIVERSITY OF SOUTHAMPTON.

[62] S. Z. Rogovina, E. V Prut, and A. A. Berlin, “Composite Materials Based on Synthetic Polymers Reinforced with Natural Fibers,” *Polym. Sci.*, vol. 61, no. 4, pp. 417–438, 2019, doi: 10.1134/S0965545X19040084.

[63] K. Shaker, Y. Nawab, and M. Jabbar, “Bio-composites: Eco-friendly Substitute of Glass Fiber Composites,” *Handb. Nanomater. Nanocomposites Energy Environ. Appl.*, vol. 1, no. 4, pp. 151–176, 2021, doi: 10.1007/978-3-030-36268-3_108.

[64] A. Ali *et al.*, “Hydrophobic treatment of natural fibers and their composites—A review,” *J. Ind. Text.*, vol. 47, no. 8, pp. 2153–2183, 2016, doi: 10.1177/1528083716654468.

[65] Z. Y. Zheng, Y. Li, and W. D. Yang, “Absorption properties of natural fiber-reinforced sandwich structures based on the fabric structures,” *J. Reinf. Plast. Compos.*, vol. 32, no. 20, pp. 1561–1568, 2013, doi: 10.1177/0731684413488461.

[66] S. D. Salman, “Partial replacement of synthetic fibres by natural fibres in hybrid composites and its effect on monotonic properties,” *J. Ind. Text.*, vol. 51, no. 2, pp. 258–276, 2021, doi: 10.1177/1528083719878843.

[67] M. Rafiquzzaman and S. and J. Naim, “Study on Mechanical Properties of Pineapple-Glass Fiber Based Polymer Composites,” *Int. J. Mech. Eng. Autom.*, vol. 4, no. 3, pp. 83–88, 2017.

[68] J. Odusote and A. T. Oyewo, “Mechanical Properties of Pineapple Leaf Fibre Reinforced Polymer Composites for Application as Prosthetic Socket,” *J. Eng. Technol.*, vol. 7, no. 1, pp. 24–32, 2016, doi: 10.21859/jet-06011.

[69] F. E. El-Abbassi, M. Assarar, R. Ayad, A. Bourmaud, and C. Baley, “A review on alfa fibre (Stipa tenacissima L.): From the plant architecture to the reinforcement of polymer composites,” *Compos. Part A Appl. Sci. Manuf.*, vol. 128, no. June 2019, p. 105677, 2020, doi: 10.1016/j.compositesa.2019.105677.

[70] A. Merzoug, B. Bouhamida, Z. Sereir, A. Bezazi, A. Kilic, and Z. Candan, “Quasi-static and dynamic mechanical thermal performance of date palm/glass fiber hybrid composites,” *J. Ind. Text.*, vol. 0, no. 0, pp. 1–23, 2020, doi: 10.1177/1528083720958036.

[71] E. Mahdi, D. Ochoa, A. Vaziri, and E. Eltai, “Energy absorption capability of date palm leaf fiber reinforced epoxy composites rectangular tubes,” *Compos. Struct.*, vol. 224, p. 111004, 2019, doi: 10.1016/j.compstruct.2019.111004.

[72] M. Alhijazi, M. Asmael, B. Safaei, Q. Zeeshan, and M. Asmael, “Modeling and simulation

of the elastic properties of natural fiber-reinforced thermosets," *Polym. Compos.*, vol. 42, no. 7, pp. 1–10, 2021, doi: 10.1002/pc.26075.

[73] R. Dragonetti, M. Napolitano, L. Boccarusso, and M. Durante, "A study on the sound transmission loss of a new lightweight hemp/bio-epoxy sandwich structure," *Appl. Acoust.*, vol. 167, no. 107379, 2020, doi: 10.1016/j.apacoust.2020.107379.

[74] N. Elzayady and E. Elghandour, "Fracture Resistance of Composite Structurs From Hemp Bio-Fibers," *J. Adv. Eng. Trends*, vol. 40, no. 2, pp. 137–147, 2021, doi: 10.21608/jaet.2020.44308.1059.

[75] A. V Kiruthika, "A review on physico-mechanical properties of bast fibre reinforced polymer composites," *J. Build. Eng*, vol. 9, no. 1, pp. 91–99, 2016, doi: 10.1016/j.jobe.2016.12.003.

[76] N. Sgriccia, M. C. Hawley, and M. Misra, "Characterization of natural fiber surfaces and natural fiber composites," *Compos. Part A*, vol. 39, pp. 1632–1637, 2008, doi: 10.1016/j.compositesa.2008.07.007.

[77] A. Srikavi and M. Mekala, "Characterization of Sunn hemp fibers as a substitute for synthetic fibers in composites and various applications," *Ind. Crops Prod.*, vol. 192, no. November 2022, p. 116135, 2023, doi: 10.1016/j.indcrop.2022.116135.

[78] M. S. Mahzabin *et al.*, "Behaviour of kenaf fibre reinforced composite," *IOP Conf. Ser. Mater. Sci. Eng*, vol. 513, no. 1, 2019, doi: 10.1088/1757-899X/513/1/012006.

[79] N. Sapiai, A. Jumahat, and J. Mahmud, "Mechanical properties of functionalised CNT filled kenaf reinforced epoxy composites," *Mater. Res. Express*, vol. 5, 2018.

[80] A. Sailesh, R. Arunkumar, and S. Saravanan, "Mechanical Properties and Wear Properties of Kenaf - Aloe Vera - Jute Fiber Reinforced Natural Fiber Composites," *Mater. Today Proc.*, vol. 5, no. 2, pp. 7184–7190, 2018, doi: 10.1016/j.matpr.2017.11.384.

[81] A. E. Ismail, U. Tun, and H. Onn, "Kenaf fiber reinforced composites tubes as energy absorbing structures," *Int. J. Mech. Mechatronics Eng.*, vol. 16, no. 1, pp. 49–53, 2016.

[82] D. Tholibon *et al.*, "Kenaf Fiber Composites: A Review on Synthetic and Biodegradable Polymer Matrix," *J. Kejuruter.*, vol. 31, no. 1, pp. 65–76, 2019, doi: 10.17576/jkukm-2019-31(1)-08.

[83] D. E. Kari, A. Benmounah, A. Bezazi, B. Bezzazi, and B. Baali, "Evaluation of

circumferential properties of Jute / Epoxy tubes manufactured by filament winding based on the fiber orientation.," *J. Mater. Eng. Struct.*, vol. 8, pp. 459–468, 2021.

[84] M. Yasir *et al.*, "Experimental and numerical characterization of tensile property of jute/carbon fabric reinforced epoxy hybrid composites," *SN Appl. Sci.*, vol. 2, no. September 2019, p. 577, 2020, doi: https://doi.org/10.1007/s42452-020-2403-2.

[85] S. S. Hamza, A. E. Bin Ismail, M. Y. Yaakob, and S. M. AL Absi, "Influence of geometrical shape on the crashworthiness performance of tubular jute mat/epoxy composite specimens," *Int. J. Mech. Mechatronics Eng.*, vol. 20, no. 2, pp. 1–12, 2020.

[86] T. V. Popat and A. Y. Patil, "A Review on Bamboo Fiber Composites," *IRE Journals*, vol. 1, no. 2, pp. 54–72, 2017.

[87] L. CoDyre and A. Fam, "Axial Strength of Sandwich Panels of Different Lengths with Natural Flax-Fiber Composite Skins and Different Foam-Core Densities," *J. Compos. Constr.*, vol. 21, no. 5, p. 04017042, 2017, doi: 10.1061/(asce)cc.1943-5614.0000820.

[88] R. Mahjoub, J. M. Yatim, A. R. Mohd Sam, M. Raftari, A. R. M. Sam, and M. Raftari, "Characteristics of continuous unidirectional kenaf fiber reinforced epoxy composites," *Mater. Des*, vol. 64, no. September, pp. 640–649, 2014, doi: 10.1016/j.matdes.2014.08.010.

[89] R. Sangamesh, N. Kumar, K. S. Ravishankar, and S. M. Kulkarni, "Mechanical Characterization and Finite Element Analysis of Jute-Epoxy Composite," *MATEC Web Conf.*, vol. 144, pp. 1–6, 2018, doi: 10.1051/matecconf/201714402014.

[90] S. Boria, E. Raponi, F. Sarasini, J. Tirillò, and L. Lampani, "Green sandwich structures under impact: Experimental vs numerical analysis," *Procedia Struct. Integr.*, vol. 12, pp. 317–329, 2018, doi: 10.1016/j.prostr.2018.11.084.

[91] X. Wang, Y. C. Zhang, and H. L. Dai, "Critical strain for a locally elliptical delamination near the surface of a cylindrical laminated shell under hydrothermal effects," *Compos. Struct*, vol. 67, no. 4, pp. 491–499,, doi: 10.1016/j.compstruct.2004.02.008.

[92] J. M. Lifshitz and H. Dayan, "Filament-wound pressure vessel with thick metal liner," *Compos. Struct.*, vol. 32, no. 1–4, pp. 313–323, 1995, doi: 10.1016/0263-8223(95)00089-5.

[93] S. K. Mondal and M. W. Uddin, "Stresses at the junctions of axisymmetric shells under axially varying load," *Int. J. Press. Vessel. Pip*, vol. 75, no. 10, pp. 727–733,, doi:

10.1016/S0308-0161(98)00015-5.

[94] M. Menshykova and I. A. Guz, “Stress analysis of layered thick-walled composite pipes subjected to bending loading,” *Int. J. Mech. Sci*, vol. 88, no. March, pp. 289–299,, doi: 10.1016/j.ijmecsci.2014.05.012.

[95] I. A. Guz, M. Menshykova, and J. K. Paik, “Thick-walled composite tubes for offshore applications : an example of stress and failure analysis for filament-wound multi-layered pipes,” *Ships Offshore Struct.*, vol. 5302, 2015, doi: 10.1080/17445302.2015.1067019.

[96] T. Wang, M. Menshykova, O. Menshykov, and I. Guz, “Failure analysis of multi-layered thick-walled composite pipes subjected to torsion loading,” *Mater. Sci. Forum*, vol. 1047, pp. 25–30, 2021, doi: 10.4028/www.scientific.net/MSF.1047.25.

[97] M. Xia, H. Takayanagi, and K. Kemmochi, “Analysis of multi-layered filament-wound composite pipes under internal pressure,” *Compos. Struct.*, vol. 53, pp. 483–491, 2001, doi: 10.1016/S0263-8223(01)00061-7.

[98] T. Wang, O. Menshykov, and M. Menshykova, “Modelling and Optimal Design of Thick-Walled Composite Pipes under In- Service Conditions,” *IOP Conf. Ser. Mater. Sci. Eng.*, no. 936, 2020, doi: 10.1088/1757-899X/936/1/012046.

[99] S. Jansma, P. Cloos, and E. van der Stok, “TESTING SPOOLABLE REINFORCED FLEXIBLE PIPES AND LINER MATERIAL FOR HIGH-PRESSURE HYDROGEN TRANSPORT,” in *the 20th Plastic Pipes Conference*, Amsterdam, Netherlands: Elsevier Ltd, 2020, pp. 1–10. doi: 10.1088/1757-899X/936/1/012046.

[100] B. Nghiep, “DAMAGE MODELING OF LAMINATED COMPOSITES USE OF MULTILAYER VOLUME ELEMENTS,” *Compos. Scirnce Technol.*, vol. 58, no. 6, pp. 891–905, 1998, doi: 10.1016/S0266-3538(97)00196-6.

[101] M. Z. Kabir, “Finite element analysis of composite pressure vessels with a load sharing metallic liner,” *Compos. Struct*, vol. 49, no. 3, pp. 247–255, 2000, doi: 10.1016/S0263-8223(99)00044-6.

[102] W. Hufenbach, C. Holste, and L. Kroll, “Vibration and damping behaviour of multi-layered composite cylindrical shells,” *Compos. Struct.*, vol. 58, no. 1, pp. 165–174, 2002, doi: 10.1016/S0263-8223(02)00025-9.

[103] A. Hocine, F. K. Achira, and H. Ghouaouala, “Coupled structural / thermal analysis of cylindrical part of multilayered composite vessel,” *Adv. Mater. Res.*, vol. 445, pp. 589–

594, 2012, doi: 10.4028/www.scientific.net/AMR.445.589.

[104] H. Wang, M. Duan, C. An, and J. Su, "Lumped parameter thermal analysis of multilayered composite pipe with MicroPCM particles," *Compos. Struct.*, vol. 260, p. 113495, 2021, doi: 10.1016/j.compstruct.2020.113495.

[105] A. Hocine, A. Bezazi, L. Boubakar, A. Benamar, and A. Kondratas, "Multilayer tubular composite reinforced by a liner : behaviour under pressure loading simulation," *Mechanika*, vol. 5, no. 55, 2005.

[106] L. Zu, J. Wang, and S. Li, "Analysis of multi-layered thick-walled filament- wound hydrogen storage vessels," *Int. J. Hydrogen Energy*, vol. 39, no. 36, pp. 21083–21096, 2014, doi: 10.1016/j.ijhydene.2014.10.075.

[107] F. Laurin, N. Carrère, and J. F. Maire, "A multiscale progressive failure approach for composite laminates based on thermodynamical viscoelastic and damage models," *Compos. Part A Appl. Sci. Manuf*, vol. 38, no. 1, pp. 198–209,, doi: 10.1016/j.compositesa.2006.01.018.

[108] E. Mahdi and E. Eltai, "Development of cost-effective composite repair system for oil/gas pipelines," *Compos. Struct.*, vol. 202, no. April, pp. 802–806, 2018, doi: 10.1016/j.compstruct.2018.04.025.

[109] A. B. M. Supian, S. M. Sapuan, M. Y. M. Zuhri, E. S. Zainudin, and H. H. Ya, "Hybrid reinforced thermoset polymer composite in energy absorption tube application: A review," *Def. Technol*, vol. 14, no. 4, pp. 291–305,, doi: 10.1016/j.dt.2018.04.004.

[110] M. Z. M. Yusoff, "The Properties of Environmentally-Friendly Sandwich Structures," University of Liverpool, 2015.

[111] M. Brebu, "Environmental Degradation of Plastic Composites with Natural Fillers — A Review," *Polymers (Basel).*, vol. 12, 2020, doi: 10.3390/polym12010166.

[112] A. Lotfi, H. Li, D. V. Dao, and G. Prusty, "Natural fiber – reinforced composites : A review on material , manufacturing , and machinability," *J. Thermoplast. Compos. Mater.*, vol. 1, no. 47, 2019, doi: 10.1177/0892705719844546.

[113] E. A. Simbana, P. E. Ordonez, Y. F. Ordonez, V. H. Guerrero, M. C. Mera, and E. A. Carvaja, *Hand book of natural fibers// Abaca: cultivation, obtaining fi bre and potential uses*. 2020. doi: 10.1016/B978-0-12-818398-4.00008-6.

[114] D. B. Dittenber and H. V. S. Gangarao, “Critical review of recent publications on use of natural composites in infrastructure,” *Compos. Part A*, vol. 43, pp. 1419–1429, 2012, doi: 10.1016/j.compositesa.2011.11.019.

[115] S. M. Sapuan, M. M. Harussani, and E. Syafri, “A short review of recent engineering applications of natural fibres,” *IOP Conf. Ser. Earth Environ. Sci*, vol. 1097, no. 1, 2022, doi: 10.1088/1755-1315/1097/1/012033.

[116] R. D. S. . Campilho, *Natural fiber composites*, Crc Press., vol. 49, no. 2. London, UK; New York, 2016.

[117] M. Rouway, M. Nachtane, M. Tarfaoui, and N. Chakhchaoui, “Mechanical Properties of a Biocomposite Based on Carbon Nanotube and Graphene Nanoplatelet Reinforced Polymers : Analytical and Numerical Study,” *J. Compos. Sci.*, vol. 5, no. 234, 2021, doi: https://doi.org/10.3390/jcs5090234.

[118] K. L. Pickering, M. G. A. Efendy, and T. M. Le, “A review of recent developments in natural fibre composites and their mechanical performance,” *Compos. Part A*, pp. 98–112, 2015, doi: 10.1016/j.compositesa.2015.08.038.

[119] R. Latif, S. Wakeel, and N. Z. Khan, “Surface treatments of plant fibers and their effects on mechanical properties of fiber-reinforced composites : A review,” *J. Reinf. Plast. Compos.*, no. October, 2018, doi: 10.1177/0731684418802022.

[120] D. G. Devadiga, K. S. Bhat, and G. T. Mahesha, “Sugarcane bagasse fiber reinforced composites: Recent advances and applications,” *Cogent Eng.*, vol. 7, no. 1, 2020, doi: 10.1080/23311916.2020.1823159.

[121] S. R. D. Petroudy, *3-Physical and mechanical properties of natural fibers*. Elsevier Ltd, 2017. doi: 10.1016/B978-0-08-100411-1.00003-0.

[122] Ş. Yıldızhan, A. Çalık, M. Özcanlı, and H. Serin, “Bio-composite materials : a short review of recent trends , mechanical and chemical properties , and applications,” *Eur. Mech. Sci.*, vol. 2, no. September, pp. 83–91, 2018.

[123] S. N. Rabiatutadawiah Ramli, S. H. S. Siti Hajar, and Z. Mustafa, “The effect of alkaline treatment and fiber length on pineapple leaf fiber reinforced poly lactic acid biocomposites,” *J. Teknol.*, vol. 79, no. 5–2, pp. 111–115, 2017, doi: 10.11113/jt.v79.11293.

[124] P. P. Das *et al.*, “Moving towards the era of bio fibre based polymer composites,” *Clean.*

Eng. Technol., vol. 4, no. 3, p. 100182, 2021, doi: 10.1016/j.clet.2021.100182.

[125] K. Lau, P. Hung, M. Zhu, and D. Hui, "Properties of natural fi bre composites for structural engineering applications," *Compos. Part B J.*, vol. 136, pp. 222–233, 2017, doi: 10.1016/j.compositesb.2017.10.038.

[126] B. K. Tan, Y. C. Ching, S. C. Poh, and L. C. Abdullah, "A Review of Natural Fiber Reinforced Poly (Vinyl Alcohol) Based Composites : Application and Opportunity," *Polymers (Basel).*, vol. 7, pp. 2205–2222, 2015, doi: 10.3390/polym7111509.

[127] C. Chen *et al.*, "Properties and Applications of Bamboo Fiber — A Current-State-of-the Art," *J. Renew. Mater*, vol. 10, no. 3, 2022, doi: 10.32604/jrm.2022.018685.

[128] V. Kavitha and Aparna, "A Review on Banana Fiber and Its Properties," *Asian J. Pharm. Res. Dev.*, vol. 9, no. 3, pp. 118–121, 2021.

[129] N. Poonia, N. Arya, and Pooja, "Banana fiber: A review," *Int. J. Educ. Manag. Stud*, vol. 10, no. 2, pp. 144–146, 2020.

[130] M. Y. Khalid *et al.*, "Natural fiber reinforced composites: Sustainable materials for emerging applications," *Results Eng.*, vol. 11, no. July, p. 100263, 2021, doi: 10.1016/j.rineng.2021.100263.

[131] R. Malkapuram, V. Kumar, Y. S. Negi, and Y. Singh Negi, "Recent development in natural fiber reinforced polypropylene composites," *J. Reinf. Plast. Compos*, vol. 28, no. 10, pp. 1169–1189, 2009, doi: 10.1177/0731684407087759.

[132] M. C. Branciforti, A. L. Marinelli, M. Kobayashi, J. D. Ambrosio, M. R. Monteiro, and A. D. Nobre, "Wood polymer composites technology supporting the recovery and protection of tropical forests: The amazonian phoenix project," *Sustainability*, vol. 1, no. 4, pp. 1431–1443, 2009, doi: 10.3390/su1041431.

[133] O. Faruk, A. K. Bledzki, H. Fink, and M. Sain, "Biocomposites reinforced with natural fibers : 2000 – 2010," *Prog. Polym. Sci.*, vol. 37, no. 11, pp. 1552–1596, 2012, doi: 10.1016/j.progpolymsci.2012.04.003.

[134] E. Lichtfouse, *Sustainable Agriculture Reviews 42- Hemp Production and Applications*. 2020. doi: ISBN 978-3-030-41383-5 ISBN 978-3-030-41384-2 (eBook) https://doi.org/10.1007/978-3-030-41384-2.

[135] S. M. Asaduzzaman and G. M. S. Islam, "Using Jute Fiber to Improve Fresh and Hardened

Properties of Concrete," *J. Nat. Fibers*, vol. 20, no. 2, 2023, doi: 10.1080/15440478.2023.2204452.

[136] G. A. Khan, N. D. Yilmaz, and K. Yilmaz, "Okra Fibers : Potential Material for Green Biocomposites," in *Green Energy and Technology book series (GREEN)*, 2017, pp. 261–284. doi: 10.1007/978-3-319-49382-4.

[137] P. Navaneethakrishnan, S. Subramaniam, and R. Rajasekar, "Characterization of natural fiber and composites − A review," *J. Reinf. Plast. Compos.*, vol. 32, no. 19, pp. 1457–1476, 2013, doi: 10.1177/0731684413495322.

[138] M. Midani and N. Saba, *Date Palm Fiber Composites Processing, Properties and Applications*. 2020. doi: 10.1007/978-981-15-9339-0.

[139] H. El-mously, M. Midani, E. Atef, and E. A. Darwish, "Date Palm Byproducts in Fibers, Textiles and Composites," in *Materials Horizons: From Nature to Nanomaterials*, 2023, pp. 103–128. doi: 10.1007/978-981-99-0475-4_4.

[140] F. Jiang, D. Yan, J. Lin, H. Kong, and Q. Yao, "Implantation of multiscale silk fi bers on poly (lactic acid) fi brous membrane for biomedical applications," *Mater. Today Chem.*, vol. 21, p. 100494, 2021, doi: 10.1016/j.mtchem.2021.100494.

[141] K. M. Babu, *11 - Silk fibres – structure, properties and applications*. Elsevier Ltd, 2020. doi: Silk fibres – structure, properties and applications.

[142] F. Allafi *et al.*, "Advancements in Applications of Natural Wool Fiber: Review," *J. Nat. Fibers*, vol. 19, no. 2, pp. 497–512, 2022, doi: 10.1080/15440478.2020.1745128.

[143] N. M. N. Le *et al.*, "Grafting of wool fibers through disulfide bonds: An advanced application of S-protected thiolated starch," *Int. J. Biol. Macromol.*, vol. 147, pp. 473–481, 2020, doi: 10.1016/j.ijbiomac.2020.01.075.

[144] E. Mahdi, A. M. S. HAMOUDA, B. B. SAHARI, and Y. A. KHALID, "Effect of Material and Geometry on Crushing Behaviour of Laminated Conical Composite Shells," *Appl. Compos. Mater.*, vol. 9, pp. 265–290, 2002, doi: 10.1023/A:1019695903534.

[145] P. Lehtiniemi, K. Dufva, T. Berg, M. Skrifvars, and P. Järvelä, "Natural fiber-based reinforcements in epoxy composites processed by filament winding," *J. Reinf. Plast. Compos*, vol. 30, no. 23, pp. 1947–1955, 2011, doi: 10.1177/0731684411431019.

[146] M. F. M. Alkbir, S. M. Sapuan, A. A. Nuraini, and M. R. Ishak, "Effect of geometry on

crashworthiness parameters of natural kenaf fibre reinforced composite hexagonal tubes," *Mater. Des.*, vol. 60, pp. 85–93, 2014, doi: http://dx.doi.org/10.1016/j.matdes.2014.02.031.

[147] S. Misri, M. R. Ishak, S. M. Sapuan, and Z. Leman, "Filament Winding Process for Kenaf Fibre Reinforced Polymer Composites," in *Manufacturing of Natural Fibre Reinforced Polymer Composites*, S. I. P. Cham, Ed., 2015, pp. 369–383. doi: 10.1007/978-3-319-07944-8_18.

[148] A. B. M. Supian, S. M. Sapuan, M. Y. M. Zuhri, E. S. Zainudin, H. H. Ya, and H. N. Hisham, "Effect of winding orientation on energy absorption and failure modes of filament wound kenaf / glass fibre reinforced epoxy hybrid composite tubes under intermediate-velocity impact (IVI) load," *J. o f Mater. Res. Technol.*, vol. 10, pp. 1–14, 2020, doi: 10.1016/j.jmrt.2020.11.103.

[149] I. M. De Rosa *et al.*, "Post-impact mechanical characterisation of E-glass/basalt woven fabric interply hybrid laminates," *Express Polym. Lett.*, vol. 5, no. 5, pp. 449–459, 2011, doi: 10.3144/expresspolymlett.2011.43.

[150] M. R. Ricciardi, I. Papa, V. Lopresto, A. Langella, and V. Antonucci, "Effect of hybridization on the impact properties of flax/basalt epoxy composites: Influence of the stacking sequence," *Compos. Struct.*, vol. 214, pp. 476–485, 2019, doi: 10.1016/j.compstruct.2019.01.087.

[151] Z. Wang, B. Chen, C. Guedes Soares, and C. G. Soares, "Analytical study on the upheaval thermal buckling of sandwich pipes," *Mar. Struct*, vol. 85, no. 103245, 2022, doi: 10.1016/j.marstruc.2022.103245.

[152] X. Castello and S. F. Estefen, "Adhesion effect on the ultimate strength of sandwich pipes," *Proc. Int. Conf. Offshore Mech. Arct. Eng. - OMAE*, 2006, doi: 10.1115/OMAE2006-92481.

[153] X. Castello and S. F. Estefen, "Sandwich Pipes for Ultra Deepwater Applications," *OFFSHORE Technol. Conf.*, 2008, doi: 10.4043/19704-ms.

[154] K. Arjomandi and F. Taheri, "A new look at the external pressure capacity of sandwich pipes," *Mar. Struct.*, vol. 24, pp. 23–42, 2011, doi: 10.1016/j.marstruc.2010.12.001.

[155] X. Liu, C. Zhou, F. Wan, H. F. Tian, W. Chen, and F. Guan, "The difference of dent characteristics between the inner and outer tubes of sandwich pipes under lateral loading,"

Ocean Eng., vol. 271, no. 113726, 2023, doi: 10.1016/j.oceaneng.2023.113726.

[156] H. Zhu and H. Fan, "Manufacturing and testing of CFRC sandwich cylinder with zero-Poisson ' s-ratio Kevlar meta-honeycomb core layer," *Compos. Sci. Technol.*, vol. 230, 2022, doi: https://doi.org/10.1016/j.compscitech.2022.109774.

[157] H. Wang, Y. Chen, Z. Xi, L. Song, X. Kong, and X. Shen, "Forced vibration of sandwich pipes with zero Poisson's ratio honeycomb core under moving pressure," *Int. J. Press. Vessel. Pip.*, vol. 202, no. May 2022, 2023, doi: 10.1016/j.ijpvp.2022.104876.

[158] M. Xia, K. Kemmochi, and H. Takayanagi, "Analysis of filament-wound fiber-reinforced sandwich pipe under combined internal pressure and thermomechanical loading," *Compos. Struct.*, vol. 51, no. 3, pp. 273–283, 2001, doi: https://doi.org/10.1016/S0263-8223(00)00137-9.

[159] M. Xia, H. Takayanagi, and K. Kemmochi, "Bending behavior of filament-wound fiber-reinforced sandwich pipes," *Compos. Struct.*, vol. 56, pp. 201–210, 2002, doi: https://doi.org/10.1016/S0263-8223(01)00181-7.

[160] R. Rafiee and F. Reshadi, "Simulation of functional failure in GRP mortar pipes," *Compos. Struct.*, vol. 113, no. 1, pp. 155–163, 2014, doi: 10.1016/j.compstruct.2014.03.024.

[161] H. Bakaiyan and E. Ameri, "Thermomechanical analysis of filament-wound sandwich pipes under combined internal pressure and temperature gradient," in *Mechanics of Nano, Micro and Macro Composite Structures*, Torino, 2012, pp. 1–2.

[162] J. C. Hastie, M. Kashtalyan, and I. A. Guz, "Analysis of filament-wound sandwich pipe under combined internal pressure and thermal load considering restrained and closed ends," *Int. J. Press. Vessel. Pip.*, vol. 191, no. 104350, 2021, doi: 10.1016/j.ijpvp.2021.104350.

[163] M. W. . ROSENOW, "Wind angle effects in glass fibre- reinforced polyester filament wound pipes," *Composites*, vol. 15, no. 2, pp. 144–152, 1984.

[164] L. Varga, A. Nagy, and A. Kovacs, "Design of CNG tank made of aluminium and reinforced plastic," *Composites*, vol. 26, no. 6, pp. 457–463, 1995, doi: 10.1016/0010-4361(95)90918-P.

[165] P. M. Wild and G.W.Vickers, "Analysis of filament-wound cylindrical shells under combined centrifugal , pressure and axial loading," *Compos. Part A*, vol. 28, pp. 47–55,

1997, doi: https://doi.org/10.1016/S1359-835X(96)00093-0.

[166] M. Xia, K. Kemmochi, and H. Takayanagi, “Analysis of filament-wound sandwich pipe under internal pressure,” *Adv. Compos. Mater.*, vol. 9, no. 3, pp. 223–239, 2000, doi: https://doi.org/10.1163/15685510051033403.

[167] L. Parnas and N. Katırcı, “Design of fiber-reinforced composite pressure vessels under various loading conditions,” *Compos. Struct.*, vol. 58, pp. 83–95, 2002, doi: 10.1016/S0263-8223(02)00037-5.

[168] D. Chapelle and D. Perreux, “Optimal design of a Type 3 hydrogen vessel: Part I - Analytic modelling of the cylindrical section,” *Int. J. Hydrogen Energy*, vol. 31, no. 5, pp. 627–638, 2006, doi: 10.1016/j.ijhydene.2005.06.012.

[169] S. Kobayashi, T. Imai, and S. Wakayama, “Burst strength evaluation of the FW-CFRP hybrid composite pipes considering plastic deformation of the liner,” *Compos. Part A Appl. Sci. Manuf.*, vol. 38, no. 5, pp. 1344–1353, 2007, doi: 10.1016/j.compositesa.2006.10.011.

[170] J. Y. Zheng and P. F. Liu, “Elasto-plastic stress analysis and burst strength evaluation of Al-carbon fiber/epoxy composite cylindrical laminates,” *Comput. Mater. Sci.*, vol. 42, no. 3, pp. 453–461, 2008, doi: 10.1016/j.commatsci.2007.09.011.

[171] A. Ghouaoula, A. Hocine, D. Chapelle, F. Karaachira, and M. L. Boubakar, “ANALYTICAL PREDICTION OF DAMAGE IN THE COMPOSITEPART OF A TYPE-3 HYDROGEN STORAGE VESSEL,” *Mech. Compos. Mater.*, vol. 48, no. 1, pp. 77–88, 2012, doi: 10.1007/s11029-012-9253-y.

[172] D. Chapelle, A. Hocine, S. Carbillet, and M. L. Boubakar, “Analysis of intermetallic swelling on the behavior of a hybrid solution for compressed hydrogen storage - Part II: Finite element method simulation,” *Mater. Des.*, vol. 36, pp. 459–469, 2012, doi: 10.1016/j.matdes.2011.11.056.

[173] S. Misri, M. R. Ishak, S. M. Sapuan, and Z. Leman, “The effect of winding angles on crushing behavior of filament wound hollow kenaf yarn fibre reinforced unsaturated polyester composites,” *Fibers Polym.*, vol. 16, no. 10, pp. 2266–2275, 2015, doi: 10.1007/s12221-015-5447-y.

[174] A. Hocine, A. Maizia, M. Chérifi, and D. Chapelle, “A contribution of the reliability based approach for cylindrical composite of sensitivity analytical design,” *Adv. Mater. Process.*

Technol., vol. 3, no. 3, pp. 428–437, 2017, doi: 10.1080/2374068X.2017.1336883.

[175] I. Y. Sulu and S. Temiz, "Failure and stress analysis of internal pressurized composite pipes joined with sleeves," *J. Adhes. Sci. Technol.*, vol. 4243, pp. 1–17, 2017, doi: 10.1080/01694243.2017.1385376.

[176] A. Ghouaoula, A. Hocine, D. Chapelle, M. L. Boubakar, and M. Hadj Meliani, "Analytical prediction of behaviour of damaged composite tubular structures under quasi-static pressure," *Struct. Integr. Life*, vol. 18, no. 2, pp. 143–148, 2018.

[177] A. Hocine, A. Maizia, A. Ghouaoula, and H. Dehmous, "Reliability Prediction of Composite Tubular Structure Under Mechanical Loading by Finite Element Method," *J. Fail. Anal. Prev.*, vol. 18, no. 6, pp. 1439–1446, 2018, doi: 10.1007/s11668-018-0536-z.

[178] A. MAIZIA, A. HOCINE, A. GHOUAOULA, M. H. MELIANI, S. Mechanics, and M. Physics, "Numerical simulation of failure probability prediction : Application to cylindrical part of type III CNG storage vessel," *Recl. Mécanique*, vol. 001, pp. 245–253, 2018, doi: 10.5281/zenodo.1490511.

[179] F. Wang and L. Han, "Analytical behavior of carbon steel-concrete-stainless steel double-skin tube (DST) used in submarine pipeline structure," *Mar. Struct.*, vol. 63, no. September 2018, pp. 99–116, 2019, doi: 10.1016/j.marstruc.2018.09.001.

[180] A. Ghouaoula, A. Hocine, M. H. Meliani, A. Maizia, and R. Suleiman, "Reliability Analysis of Type III Gas Storage Vessel Under Pressure Loading," *J. Fail. Anal. Prev*, vol. 19, no. 2, pp. 445–452, 2019, doi: 10.1007/s11668-019-00616-y.

[181] A. Hocine, A. Maizia, A. Ghouaoula, and J. E. P. C. Ribeiro, "Deterministic Analysis for Creep Behavior of Damaged Composite Tubular Structure," *J. Fail. Anal. Prev.*, vol. 20, no. 6, pp. 1858–1863, 2020, doi: 10.1007/s11668-020-00994-8.

[182] A. Zubail, A. Traidia, M. Masulli, K. Vatopoulos, T. Villette, and I. Taie, "Carbon and energy footprint of nonmetallic composite pipes in onshore oil and gas flowlines," *J. Clean. Prod.*, vol. 305, p. 127150, 2021, doi: 10.1016/j.jclepro.2021.127150.

[183] B. N. Nguyen, H. S. Roh, D. R. Merkel, and K. L. Simmons, "A predictive modeling tool for damage analysis and design of hydrogen storage composite pressure vessels," *Int. J. Hydrogen Energy*, vol. 46, no. 39, pp. 20573–20585, 2021, doi: 10.1016/j.ijhydene.2021.03.139.

[184] D. V. V Patel, J. Daftary, P. Talekar, and V. M. M. Bhojawala, "Analysis of discontinuity

stress at shell and elliptical head juncture using theory of beam on elastic foundation," *Mater. Today Proc*, no. xxxx, 2023, doi: 10.1016/j.matpr.2023.06.019.

[185] P. Jasion and K. Magnucki, "Strength and elastic buckling of a sandwich cylindrical pressure vessel with dished heads," *Int. J. Press. Vessel. Pip.*, vol. 205, p. 105002, 2023, doi: 10.1016/j.ijpvp.2023.105002.

[186] Y. Luo, W. Jiang, and Q. Zeng, "High accuracy and efficiency calculation model for predicting the reduction of residual stress on large pressure vessels by ultrasonic impact surface treatment," *Eng. Reports*, pp. 1–16, 2023, doi: 10.1002/eng2.12662.

[187] A. HOCINE, "ANALYSE ET MODELISATION D'UNE SOLUTION HYBRIDE DE STOCKAGE D'HYDROGENE HAUTE PRESSION," Université des Sciences Technologiques d'Oran Mohamed BOUDIAF Faculté, 2008.

[188] M. R. Sheikhi and S. Gürgen, "Anti-impact design of multi-layer composites enhanced by shear thickening fluid," *Compos. Struct*, vol. 279, p. 114797, 2022, doi: 10.1016/j.compstruct.2021.114797.

[189] A. Hocine, D. Chapelle, M. L. Boubakar, A. Benamar, and A. Bezazi, "Experimental and analytical investigation of the cylindrical part of a metallic vessel reinforced by filament winding while submitted to internal pressure," *Int. J. Press. Vessel. Pip.*, vol. 86, no. 10, pp. 649–655, 2009, doi: 10.1016/j.ijpvp.2009.06.002.

[190] M. H. Elgohary, M. I. El-Geuchy, H. M. Abdallah, and S. S. Sayed, "Stress analysis of multi-layered composite cylinders subjected to various loadings," *IOP Conf. Ser. Mater. Sci. Eng.*, vol. 1172, no. 1, p. 012005, 2021, doi: 10.1088/1757-899x/1172/1/012005.

[191] R. Ansari, F. Alisafaei, and P. Ghaedi, "Dynamic analysis of multi-layered filament-wound composite pipes subjected to cyclic internal pressure and cyclic temperature," *Compos. Struct.*, vol. 92, no. 5, pp. 1100–1109, 2010, doi: 10.1016/j.compstruct.2009.09.058.

[192] I. De Paula *et al.*, "Flexural behavior of sandwich panels combining curauá fiber-reinforced composite layers and autoclaved aerated concrete core," *Constr. Build. Mater.*, vol. 286, p. 122890, 2021, doi: 10.1016/j.conbuildmat.2021.122890.

[193] J. C. Hastie, I. A. Guz, and M. Kashtalyan, "Effects of thermal gradient on failure of a thermoplastic composite pipe (TCP) riser leg," *Int. J. Press. Vessel. Pip.*, vol. 172, pp. 90–99, 2019, doi: 10.1016/j.ijpvp.2019.03.027.

[194] J. C. Hastie, M. Kashtalyan, and I. A. Guz, “Failure analysis of thermoplastic composite pipe (TCP) under combined pressure, tension and thermal gradient for an offshore riser application,” *Int. J. Press. Vessel. Pip.*, vol. 178, 2019, doi: 10.1016/j.ijpvp.2019.103998.

[195] J. C. Hastie, I. A. Guz, and M. Kashtalyan, “Structural integrity of deepwater composite pipes under combined thermal and mechanical loading,” *Procedia Struct. Integr.*, vol. 28, pp. 850–863, 2020, doi: 10.1016/j.prostr.2020.11.053.

[196] M. Moyo and R. Velmurugan, “QUASI-STATIC AXIAL CRUSHING PERFORMANCE OF JUTE / GLASS HYBRID COMPOSITE TUBES,” 2015.

[197] O. A. Afolabi, K. Kanny, and T. P. Mohan, “Investigation of mechanical characterization of hybrid sandwich composites with syntactic foam core for structural applications,” *Compos. Adv. Mater.*, vol. 32, pp. 1–14, 2023, doi: 10.1177/26349833221147539.

[198] G. Rajamurugan, A. E. A. Ismail, A. Othman, A. E. A. Ismail, G. Rajamurugan, and A. E. A. Ismail, “Quasi-static axial crushes on woven jute/polyester AA6063T52 composite tubes,” *IOP Conf. Ser. Mater. Sci. Eng.*, vol. 342, no. 1, 2018, doi: 10.1088/1757-899X/342/1/012064.

[199] Y. He, M. A. Vaz, and M. Caire, “Stress and failure analyses of thermoplastic composite pipes subjected to torsion and thermomechanical loading,” *Mar. Struct.*, vol. 79, no. 103024, 2021, doi: 10.1016/j.marstruc.2021.103024.

[200] H. Bakaiyan, H. Hosseini, and E. Ameri, “Analysis of multi-layered filament-wound composite pipes under combined internal pressure and thermomechanical loading with thermal variations,” *Compos. Struct.*, vol. 88, no. 4, pp. 532–541, 2009, doi: 10.1016/j.compstruct.2008.05.017.

[201] K. Foroutan, A. Shaterzadeh, and H. Ahmadi, “Nonlinear static and dynamic hygrothermal buckling analysis of imperfect functionally graded porous cylindrical shells,” *Appl. Math. Model.*, vol. 77, pp. 539–553, 2020, doi: 10.1016/j.apm.2019.07.062.

[202] X. Y. Zhang, Y. Peng, Y. J. Xie, and X. F. Li, “Hygrothermoelastic response of a hollow cylinder based on a coupled time-fractional heat and moisture transfer model,” *Zeitschrift fur Angew. Math. und Phys.*, vol. 70, no. 1, pp. 1–21, 2019, doi: 10.1007/s00033-018-1047-1.

[203] T. Ye, G. Jin, and S. Gao, “Three-dimensional hygrothermal vibration of multilayered cylindrical shells,” *Compos. Struct.*, vol. 201, no. 18, pp. 867–881, 2018, doi:

10.1016/j.compstruct.2018.06.055.

[204] C. B. Azevedo, J. H. S. Almeida, H. F. Flores, F. Eggers, and S. C. Amico, “Influence of mosaic pattern on hygrothermally-aged filament wound composite cylinders under axial compression,” *J. Compos. Mater.*, vol. 54, no. 19, pp. 2651–2659, 2020, doi: 10.1177/0021998319899144.

[205] T. Srinivasan, G. Suresh, P. Ramu, R. Vignesh, A. V. Harshan, and K. P. Vignesh, “Effect of hygrothermal ageing on the compressive behavior of glass fiber reinforced IPN composite pipes,” *Mater. Today Proc.*, vol. 45, no. xxxx, pp. 1354–1359, 2021, doi: 10.1016/j.matpr.2020.06.102.

[206] M. Soleimani, R. Gholami, A. Alijani, and R. Ansari, “An analytical solution for dynamics of cyclic thermomechanically loaded multi-layered filament-wound composite pipes in hygrothermal environment,” *Thin-Walled Struct.*, vol. 193, 2023, doi: 10.1016/j.tws.2023.111242.

[207] X. Li, “Parametric resonances of rotating composite laminated nonlinear cylindrical shells under periodic axial loads and hygrothermal environment,” *Compos. Struct.*, vol. 255, p. 112887, 2021, doi: 10.1016/j.compstruct.2020.112887.

[208] Y. Pan, L. Iorga, and A. A. Pelegri, “Numerical generation of a random chopped fiber composite RVE and its elastic properties,” vol. 68, pp. 2792–2798, 2008, doi: 10.1016/j.compscitech.2008.06.007.

[209] A. Benabbes, L. Siad, L. Dormieux, and W. K. Liu, “A homogenization approach to the yield strength of spherical powder compacts,” *AIP Conf. Proc.*, vol. 1252, no. 1, pp. 681–688, 2010, doi: 10.1063/1.3457621.

[210] M. Porfiri and N. Gupta, “Composites : Part B Effect of volume fraction and wall thickness on the elastic properties of hollow particle filled composites,” *Compos. Part B*, vol. 40, no. 2, pp. 166–173, 2009, doi: 10.1016/j.compositesb.2008.09.002.

[211] S. Migneault, A. Koubaa, F. Erchiqui, A. Chaala, K. Englund, and M. P. Wolcott, “Application of micromechanical models to tensile properties of wood-plastic composites,” *Wood Sci. Technol.*, vol. 45, no. 3, pp. 521–532, 2011, doi: 10.1007/s00226-010-0351-5.

[212] A. Al-fatlawi, K. Jármai, and G. Kovács, “Optimal design of a fiber-reinforced plastic composite sandwich structure for the base plate of aircraft pallets in order to reduce

weight," *Polymers (Basel).*, vol. 13, no. 5, 2021, doi: 10.3390/polym13050834.

[213] Y. Feng, B. Jia, X. Wang, M. Zhang, and Z. Zhu, "Research on microscopic properties of TiBw/TC4 composites for drilling process," *Materials (Basel).*, vol. 12, no. 13, 2019, doi: 10.3390/ma12132112.

[214] D. S. Craveiro and M. A. R. Loja, "An assessment of thick nanocomposite plates' behavior under the influence of carbon nanotubes agglomeration," *J. Compos. Sci.*, vol. 5, no. 2, pp. 1–32, 2021, doi: 10.3390/jcs5020041.

[215] A. Kriwet and M. Stommel, "Arbitrary-reconsidered-double-inclusion (ARDI) model to describe the anisotropic, viscoelastic stiffness and damping of short fiber-reinforced thermoplastics," *J. Compos. Sci.*, vol. 4, no. 2, 2020, doi: 10.3390/jcs4020037.

[216] A. Ramsaroop and K. Kanny, "Using MATLAB to Design and Analyse Composite Laminates," *Engineering*, vol. 02, no. 11, pp. 904–916, 2010, doi: 10.4236/eng.2010.211114.

[217] L. Farines, "Evaluation du potentiel restant de structures composites verre /époxy soumises à des sollicitations de fatigue," L'U.F.R des sciences et techniques de l'université de Franche-Comté, Besançon, 2007.

[218] L. M. Benzeggagh and M.Kenane, "MEASUREMENT OF MIXED-MODE DELAMINATION FRACTURE TOUGHNESS OF UNIDIRECTIONAL GLASS/EPOXY COMPOSITES WITH MIXED-MODE BENDING APPARATUS," *Compos. Sci. Technol.*, vol. 56, no. 4, pp. 439–449, 1996, doi: https://doi.org/10.1016/0266-3538(96)00005-X.

[219] F. Lachaud, B. Lorrain, L. Michel, and R. Barriol, "Experimental and numerical study of delamination caused by local buckling of thermoplastic and thermoset composites," *Compos. Sci. Technol.*, vol. 58, no. 5, pp. 727–733, 1998, doi: 10.1016/S0266-3538(97)00153-X.

[220] C. K. Yong, Y. C. Ching, C. H. Chuah, and N. S. Liou, "Effect of fiber orientation on mechanical properties of kenaf-reinforced polymer composite," *BioResources*, vol. 10, no. 2, pp. 2597–2608, 2015, doi: 10.15376/biores.10.2.2597-2608.

[221] X. XU, "Cellulose Fiber Reinforced Nylon 6 or Nylon 66 composites," School of Polymer, Textile and Fiber Engineering,Georgia Institute of Technology December, 2008.

[222] B. Mohammed, "EFFET SIMULTANE DE LA TEMPERATURE ET DE L'HUMIDITE

SUR LA DURABILITE DES TUBES EPAIS EN COMPOSITES A MATRICES POLYMERES," l'Université des Sciences et de la Technologie d'Oran "Mohamed Boudiaf," 2013.

[223] P. Surathi and V. M. Karbhari, "Hygrothermal effects on durability and moisture kinetics of fiber-reinforced polymer composites," *California. Dept. Transp. Div. Eng. Serv.*, no. FHWA/CA/ES-07/01, 2006, [Online]. Available: https://rosap.ntl.bts.gov/view/dot/27688

[224] R. M. Guedes, *Creep and fatigue in polymer matrix composites*, 2011th ed. Woodhead Publishing, 2019. doi: 10.1016/C2017-0-02292-9.

[225] C. H. Shen and G. S. Springer, "Moisture Absorption and Desorption of Composite Materials," *J. Compos. Mater.*, vol. 10, no. 1, pp. 2–20, 1976, doi: 10.1177/002199837601000101.

[226] Y. Weitsman, "Moisture in Composites: Sorption and Damage," in *Composite Materials Series , Elsevier*, vol. 4, Elsevier Science Publishers B.V., 1991, pp. 385–429. doi: 10.1016/B978-0-444-70507-5.50013-5.

[227] F. Mili, A. Lekrine, L. Bouyaya, and F. Bourouis, "Effect of Climatic Factor on the Mechanical Behaviour Of Aeolian Blades: Application of Hybrid Composite Materials," *J. Fundam. Appl. Sci.*, vol. 2, no. 1, pp. 23–34, 2010, doi: 10.4314/jfas.v2i1.3.

[228] Levent AYDIN, "DESIGN OF DIMENSIONALLY-STABLE LAMINATED COMPOSITES SUBJECTED TO HYGRO-THERMO-MECHANICAL LOADING BY STOCHASTIC OPTIMIZATION METHODS," Izmir Institute of Technology, 2011.

[229] R. Younes, A. Hallal, F. Fardoun, and F. Hajj, "Comparative Review Study on Elastic Properties Modeling for Unidirectional Composite Materials," *Compos. Their Prop.*, 2012, doi: 10.5772/50362.

[230] J.-M. Berthelot, *Mécanique des Matériaux et Structures Composites*. Le Mans, France, 2010. [Online]. Available: www.editions.lavoisier.fr

[231] G. A. ELRAOUF and D. ALI, "Contribution à la modelisation des structures tri-couche par la théorie locale," KASDI MERBAH OUARGLA.

[232] S. W. Tsai and E. M. Wu, "A General Theory of Strength for Anisotropic Materials," *J. Compos. Mater.*, vol. 5, no. 1, pp. 58–80, 1971, doi: https://doi.org/10.1177/002199837100500106.

[233] R. Imen, S. Wadhah, and B. Y. Rached, “Identification de la loi de comportement des matériaux composites à fibres organiques (Stipa Tenacissima L) [Identification of the behaviour law of organic fibre composite materials],” vol. 31, no. 6, pp. 37–42, 2017.

[234] ANSYS, *Ansys 18.1, help, Element Reference, Element Library, SOLID186.* 2015.

[235] E. J. Barbero, *Finite element analysis of viscoplastic composite materials and structures*, Second., vol. 3, no. 1. 2014. doi: 10.1080/10759419608945852.

[236] Cytec, “Technical Data Sheet APC-2-PEEK Thermoplastic Polymer,” *www.cytec.com*, 2016, [Online]. Available: https://www.cytec.com/sites/default/files/datasheets/APC-2_PEEK_031912-01.pdf

[237] S. Rajole, K. S. Ravishankar, and S. M. Kulkarni, “Performance study of jute-epoxy composites / sandwiches under normal ballistic impact,” *Def. Technol.*, vol. 16, no. 4, pp. 947–955, 2020, doi: 10.1016/j.dt.2019.11.011.

[238] S. Timmerberg *et al.*, “Hydrogen from renewables : Supply from North Africa to Central Europe as blend in existing pipelines – Potentials and costs,” *Appl. Energy*, vol. 237, pp. 795–809, 2020, doi: 10.1016/j.apenergy.2019.01.030.

[239] “Alibaba.com.” Accessed: Feb. 12, 2024. [Online]. Available: https://www.alibaba.com/

ANNEX A

ANNEX A:

1- QUASI STATIC LOADING

1.1- Analytical analysis

$$\begin{Bmatrix} D^{(1)} \\ D^{(2)} \\ D^{(2)} \\ E^{(1)} \\ E^{(2)} \\ E^{(3)} \\ E^{(4)} \\ \varepsilon_0 \\ \gamma_0 \end{Bmatrix} = \begin{bmatrix} d_{11} & 0 & 0 & 0 & e_{11} & 0 & 0 & 0 & a_{11} & a_{12} \\ d_{21} & d_{22} & 0 & 0 & e_{21} & e_{22} & 0 & 0 & a_{21} & a_{22} \\ 0 & d_{32} & d_{33} & 0 & 0 & e_{32} & e_{33} & 0 & a_{31} & a_{32} \\ 0 & 0 & d_{43} & d_{44} & 0 & 0 & e_{43} & e_{44} & a_{41} & a_{42} \\ d_{51} & d_{52} & 0 & 0 & e_{51} & e_{52} & 0 & 0 & a_{51} & a_{52} \\ 0 & d_{62} & d_{63} & 0 & 0 & e_{62} & e_{63} & 0 & a_{61} & a_{62} \\ 0 & 0 & d_{73} & d_{74} & 0 & 0 & e_{73} & e_{74} & a_{71} & a_{72} \\ 0 & 0 & 0 & d_{84} & 0 & 0 & 0 & e_{84} & a_{81} & a_{82} \\ d_{91} & d_{92} & d_{93} & d_{94} & e_{91} & e_{92} & e_{93} & e_{94} & a_{91} & a_{92} \\ d_{01} & d_{02} & d_{03} & d_{04} & e_{01} & e_{02} & e_{03} & e_{04} & a_{01} & a_{02} \end{bmatrix}^{-1} \begin{Bmatrix} -P_0 \\ 0 \\ 0 \\ 0 \\ 0 \\ 0 \\ 0 \\ 0 \\ 0 \\ 0 \end{Bmatrix} \quad (65)$$

Where :

$$d_{11} = \left(\bar{C}_{23}^{(1)} + \beta^{(1)}\bar{C}_{33}^{(1)}\right) r_0^{\beta(1)-1},$$
$$e_{11} = \left(\bar{C}_{23}^{(1)} - \beta^{(1)}\bar{C}_{33}^{(1)}\right) r_0^{-\beta(1)-1},$$
$$a_{11} = \bar{C}_{33}^{(1)} + \alpha_1^{(1)}\left(\bar{C}_{23}^{(1)} + \bar{C}_{33}^{(1)}\right), \quad (66)$$

$$a_{12} = \left(\left[C_{36}^{(1)}\right] + \alpha_2^{(1)}(\bar{C}_{23}^{(1)} + 2\bar{C}_{33}^{(1)}\right) r_0.$$

$$\mathrm{d}_{21} = \mathrm{r}_1^{\beta(1)},$$
$$\mathrm{d}_{22} = -\mathrm{r}_1^{\beta(2)},$$
$$\mathrm{e}_{21} = \mathrm{r}_1^{-\beta(1)},$$
$$\mathrm{e}_{22} = -\mathrm{r}_1^{-\beta(2)}, \quad (67)$$
$$a_{21} = \left(\alpha_1^{(1)} - \alpha_1^{(2)}\right) r_1,$$
$$\mathrm{a}_{22} = \left(\alpha_2^{(1)} - \alpha_2^{(2)}\right) \mathrm{r}_1^{\,2}.$$

$$\mathrm{d}_{32} = \mathrm{r}_2^{\beta(2)},$$
$$\mathrm{d}_{33} = -\mathrm{r}_2^{\beta(3)},$$

$$
\begin{aligned}
e_{32} &= r_2^{-\beta(2)}, \\
e_{33} &= -r_2^{-\beta(3)}, \\
a_{31} &= \left(\alpha_1^{(2)} - \alpha_1^{(3)}\right) r_2, \\
a_{32} &= \left(\alpha_2^{(2)} - \alpha_2^{(3)}\right) r_2^2.
\end{aligned} \tag{68}
$$

$$
\begin{aligned}
d_{43} &= r_2^{\beta(2)}, \\
d_{44} &= -r_3^{\beta(4)}, \\
e_{43} &= r_3^{-\beta(3)}, \\
e_{44} &= -r_3^{-\beta(4)}, \\
a_{41} &= \left(\alpha_1^{(3)} - \alpha_1^{(4)}\right) r_3, \\
a_{42} &= \left(\alpha_2^{(2)} - \alpha_2^{(4)}\right) r_3^2.
\end{aligned} \tag{69}
$$

$$
\begin{aligned}
d_{51} &= \left(\bar{C}_{23}^{(1)} + \beta^{(1)} \bar{C}_{33}^{(1)}\right) r_1^{\beta(1)-1}, \\
d_{52} &= \left(\bar{C}_{23}^{(2)} + \beta^{(2)} \bar{C}_{33}^{(2)}\right) r_1^{\beta(2)-1}, \\
e_{51} &= \left(\bar{C}_{23}^{(1)} - \beta^{(1)} \bar{C}_{33}^{(1)}\right) r_1^{-\beta(1)-1}, \\
e_{52} &= \left(\bar{C}_{23}^{(2)} - \beta^{(2)} \bar{C}_{33}^{(2)}\right) r_1^{-\beta(2)-1}, \\
a_{51} &= \left(\bar{C}_{13}^{(1)} - \bar{C}_{13}^{(2)}\right) + \alpha_1^{(1)} \left(\bar{C}_{23}^{(1)} + \bar{C}_{33}^{(1)}\right) - \alpha_1^{(2)} \left(\bar{C}_{23}^{(2)} + \bar{C}_{33}^{(2)}\right), \\
a_{52} &= \left[\left(\bar{C}_{36}^{(1)} - \bar{C}_{36}^{(2)}\right) + \alpha_2^{(1)} \left(\bar{C}_{23}^{(1)} + 2\bar{C}_{33}^{(1)}\right) - \alpha_2^{(2)} \left(\bar{C}_{23}^{(2)} + 2\bar{C}_{33}^{(2)}\right)\right] r_1.
\end{aligned} \tag{70}
$$

$$
\begin{aligned}
d_{62} &= \left(\bar{C}_{23}^{(2)} + \beta^{(2)} \bar{C}_{33}^{(2)}\right) r_2^{\beta(2)-1}, \\
d_{63} &= -\left(\bar{C}_{23}^{(3)} + \beta^{(3)} \bar{C}_{33}^{(3)}\right) r_1^{\beta(3)-1}, \\
e_{62} &= \left(\bar{C}_{23}^{(2)} - \beta^{(2)} \bar{C}_{33}^{(2)}\right) r_2^{-\beta(2)-1}, \\
e_{63} &= -\left(\bar{C}_{23}^{(3)} - \beta^{(3)} \bar{C}_{33}^{(3)}\right) r_2^{-\beta(3)-1}, \\
a_{61} &= \left(\bar{C}_{13}^{(2)} - \bar{C}_{13}^{(3)}\right) + \alpha_1^{(2)} \left(\bar{C}_{23}^{(2)} + \bar{C}_{33}^{(2)}\right) - \alpha_1^{(3)} \left(\bar{C}_{23}^{(3)} + \bar{C}_{33}^{(3)}\right), \\
a_{62} &= \left[\left(\bar{C}_{36}^{(2)} - \bar{C}_{36}^{(3)}\right) + \alpha_2^{(2)} \left(\bar{C}_{23}^{(2)} + 2\bar{C}_{33}^{(1)}\right) - \alpha_2^{(3)} \left(\bar{C}_{23}^{(3)} + 2\bar{C}_{33}^{(2)}\right)\right] r_2.
\end{aligned} \tag{71}
$$

2- CYCLIC LOADING

$$\begin{Bmatrix} D^{(1)} \\ D^{(2)} \\ D^{(2)} \\ E^{(1)} \\ E^{(2)} \\ E^{(3)} \\ E^{(4)} \\ \varepsilon_0 \\ \gamma_0 \end{Bmatrix} = \begin{bmatrix} d_{11} & 0 & 0 & 0 & e_{11} & 0 & 0 & 0 & a_{11} & a_{12} \\ d_{21} & d_{22} & 0 & 0 & e_{21} & e_{22} & 0 & 0 & a_{21} & a_{22} \\ 0 & d_{32} & d_{33} & 0 & 0 & e_{32} & e_{33} & 0 & a_{31} & a_{32} \\ 0 & 0 & d_{43} & d_{44} & 0 & 0 & e_{43} & e_{44} & a_{41} & a_{42} \\ d_{51} & d_{52} & 0 & 0 & e_{51} & e_{52} & 0 & 0 & a_{51} & a_{52} \\ 0 & d_{62} & d_{63} & 0 & 0 & e_{62} & e_{63} & 0 & a_{61} & a_{62} \\ 0 & 0 & d_{73} & d_{74} & 0 & 0 & e_{73} & e_{74} & a_{71} & a_{72} \\ 0 & 0 & 0 & d_{84} & 0 & 0 & 0 & e_{84} & a_{81} & a_{82} \\ d_{91} & d_{92} & d_{93} & d_{94} & e_{91} & e_{92} & e_{93} & e_{94} & a_{91} & a_{92} \\ d_{01} & d_{02} & d_{03} & d_{04} & e_{01} & e_{02} & e_{03} & e_{04} & a_{01} & a_{02} \end{bmatrix}^{-1} \times \begin{Bmatrix} -(P_m + P_a \sin(2\pi ft)) \\ 0 \\ 0 \\ 0 \\ 0 \\ 0 \\ 0 \\ 0 \\ 0 \\ 0 \end{Bmatrix} \quad (72)$$

LIST OF PUBLICATIONS AND COMMUNICATIONS

LIST OF PUBLICATIONS AND COMMUNICATIONS

1- LIST OF PUBLICATIONS

[1]. G. Habbar, A. Maizia, A. Hocine, M. H. Dhaou, and R. João, “Micromechanical Analysis of a Bio-Sandwich Application for Cylinder under Pressure,” *Compos. Sci.*, vol. 6, no. 69, 2022, doi: https://doi.org/10.3390/jcs6030069.

[2]. G. Habbar, A. Hocine, A. Maizia, and A. Bezazi, “Failure analysis of biocomposite sandwich pipe under internal pressure – Application for high pressure gas transportation pipelines MEDGAZ,” vol. 202, no. January, 2023, doi: 10.1016/j.ijpvp.2023.104891.

[3]. A. Maizia, G. Habbar, M. Bettayeb, A. Hocine, and O. Bouledroua, “Mechanical behavior analysis of corroded pipelines used to transport hydrogen,” in *All Sciences Proceedings*, 29-31 july , Konya, Turkey, 2023, pp. 395–399.

2- LIST OF COMMUNICATIONS

2.1- International Communications

[1]. A. MAIZIA, G. HABBAR, A. GHOUAOULA, A. HOCINE, and J. RIBEIRO, “Behaviour analysis of glass/epoxy fiber and bio-source fibers used in sandwich plates,” in 2 nd international seminar on Industrial engineering and applied mathematics (ISIEAM’22), 23-24 October,2022, SKIKDA, Algeria.

[2]. . G. HABBAR, A. MAIZIA, A. HOCINE, and J. RIBEIRO, “Mechanical Behavior Prediction Of Composite Multilayered Jute/Epoxy Pipe Under Internal Pressure,” in 3. INTERNATIONAL MARMARA SCIENTIFIC RESEARCH AND INNOVATION CONGRESS, 19-20 NOVEMBER 2022, İSTANBUL/ TURKEY.

[3]. G. HABBAR, A. Hocine, A. Maizia, J. Ribeiro, and M. H. Dhaou, “Behavior prediction of Pineapple leaf fiber/epoxy multilayered pipes under internal pressure,” in 1st International Conference on Materials Sciences and Technology (MatScience-2022), 13-15 December, 2022, Khenchela/Algeria.

[4]. M. Bettayeb, A. Bezazi, P. N. B. D. Reis, A. Hocine, G. Habbar, B. Baali, et al. “EXPERIMENTAL ANALYSIS OF COMPOSITE PIPE SPECIEMS UNDER

FLEXULAR LOADING, 9-11 JULY, 2023," in V.INTERNATIONAL ISTANBUL CURRENT SCIENTIFIC RESEARCH CONGRESS, Istanbul/Turkey.

[5]. M. Bettayeb, A. Bezazi, P. N. B. D. Reis, A. Hocine, G. Habbar, and B. Baali, "Development, elaboration and characterization of composite tubes intended for hydrogen transport," *5th International Conference on Applied Engineering and Natural Sciences.*10-12 July 2023. Konya/Turkey.

[6]. G. HABBAR, A. HOCINE, A. MAIZIA, A. BEZAZI, M. BETTAYEB, J. RIBEIRO, O. BOULEDROUA et al., "Analytical failure analysis of bio/synthetic sandwich pipe under pressure," in *5th International Conference on Applied Engineering and Natural Sciences. 10-12 July 2023* , Konya/Turkey. doi: 10.59287/as-abstracts.1239.

[7]. A. Maizia, G. Habbar, M. Bettayeb, A. Hocine, A. Bezazi, and O. Bouledroua, "Mechanical behavior analysis of corroded pipelines used to transport hydrogen," in 1st International Conference on Modern and Advanced Research. 29-31 July 2023, Konya/Turkey.

[8]. G. HABBAR, A. HOCINE, A. MAIZIA, A. BEZAZI, M. BETTAYEB, J. RIBEIRO, et al., "Stress And Failure Analysis Of Sandwich Pipes Intended For Transporting Hydrogen And Oil," in *2. INTERNATIONAL TRAKYA SCIENTIFIC RESEARCH CONGRESS , 12-13 AUGUST 2023*, EDİRNE/ TURKEY..

[9]. G. HABBAR, A. MAIZIA, A. HOCINE, and J. RIBEIRO, "Renewable Hydrogen Transportation Safety Analysis Using Composite Sandwich Pipes Under Fire Risk," in 3. INTERNATIONAL MEDITERRANEAN SCIENTIFIC RESEARCH AND INNOVATION CONGRESS, 26-27 AUGUST 2023., ANTALYA /TURKEY.

[10]. A. MAIZIA, G. HABBAR, A. GHOUAOULA, A. LOUZA, A. HOCINE, and A. BEZAZI, "The Impact of Corrosion Outer Defects on the Reliability of Hydrogen Pipeline Transport Systems," in 2nd International Conference on Contemporary Academic Research ICCAR 2023, 4-5 November, 2023, Konya/ Turkey.

[11]. A.Ghouaoula, A.Maizia, G.Habbar, and A.Hocine, "Evaluation of damage in glass/epoxy composite tube laminate," in ICME'23 The first international congress on mechanical engineer.15-16 November 2023, Constantine/ Algeria.

[12]. A. LOUZA, A. Hocine, A. Maizia, A. Levent, and G. HABBAR, "The Impact of The Stacking Sequence on the Behavior of Composite Hydrogen Storage Vessel type IV," in *The 5th International Seminar on Advanced Mechanical Technologies "'SITMA 2024'", April 29 & 30, 2024*, Tlemcen, Algeria, 2024.

2.2- National Communications

[1]. G. HABBAR, A. HOCINE, A. MAIZIA, and J. RIBEIRO, "Analytical Prediction of the Behaviour of Jute/Epoxy Pipes under Internal Pressure," in 1st National Conference on Science & Technology, 27-28 JUNE, 2022, Mascara/ Algeria.

[2]. G. HABBAR, A. MAIZIA, A. HOCINE, and J. RIBEIRO, "REVIEW OF MICROMECHANICAL ANALYSIS OF BIOCOMPOSITE SANDWICH STRUCTURES," in 1st National Conference on Science & Technology, 1st NCST22, 27-28 JUNE, 2022, Mascara/ Algeria.

[3]. A. MAIZIA, G. HABBAR, A. GHOUAOULA, and A. HOCINE, "Analysis of the thermomechanical behavior of a sandwich panel based on natural fibers," in 1st National Conference on Science & Technology, 27-28 JUNE, 2022, Mascara/ Algeria.

[4]. G. HABBAR, A. HOCINE, A. MAIZIA, A. GHOUAOULA, and J. RIBEIRO, "Safety analysis of renewable hydrogen transmission by composite sandwich pipe under fire," in The first National Seminar on Green hydrogen for the Algerian Industrial Sector (INSGH-AI'2022), 23 -28 July, 2022, Algiers.

[5]. A. MAIZIA, G. HABBAR, A. GHOUAOULA, A. HOCINE, and M. HADJMELIANI , "Behavior of a composite high-pressure hydrogen storage vessel: A review," in *The first National Seminar on Green hydrogen for the Algerian Industrial Sector (INSGH-AI'2022),* 23 -28 July, 2022, Algiers.

[6]. A. MAIZIA, A. GHOUAOULA, G. HABBAR, A. HOCINE, and M. HADJMELIANI, "Experimental study of a composite material used in the repair of pressure-corroded pipelines.," in *The first National Seminar on Green hydrogen for the Algerian Industrial Sector (INSGH-AI'2022),* 23 -28 July, 2022, Algiers.

[7]. A. GHOUAOULA, A. MAIZIA, G. HABBAR, and A. HOCINE, “Analyse du comportement mécanique d’un réservoir de stockage d’hydrogène type III,” in *The first National Seminar on Green hydrogen for the Algerian Industrial Sector (INSGH-AI’2022),* 23 -28 July, 2022, Algiers.

[8]. G. HABBAR, H. Abdelkader, R. João, M. Abdelhakim, and G. A. Elhamid, “Micro and macro mechanical behavior predictions of biocomposites pipes under pressure,” in THE SECOND DOCTORAL SYMPOSIUM ON TECHNOLOGY PROCESS, MECHANICAL AND ELECTRICAL ENGINEERING (DST°02-2022), 26 -27 October, 2022, Chlef/Algeria.

[9]. G. HABBAR, A. HOCINE, A. MAIZIA, and J. RIBEIRO, “The effect of volume fraction on Alfa fiber epoxy mechanical properties,” in the sixth student’s symposium on engineering application of mechanics, “Environment and Socio Economic impact” (SSENAM’6-2022), 30 th Nov & 1 st Dec 2022, Chlef/Algeria, pp. 7823–7830.

[10]. G. HABBAR, A. HOCINE, A. MAIZIA, and J. RIBEIRO, “A comparative failure investigation of sandwich pipelines destined for hydrogen gas transportation,” in The Third Doctoral Symposium on Technology: Process, Mechanical and Electrical Engineering DST’03-2023, 02 - 03 December, 2023, Chlef/ Algeria.